Understanding Early Transcriptional Events in *Staphylococcus aureus* Infection

Implications for Vaccine Design

A thesis submitted in fulfilment of the requirements for the degree of

Doctor of Philosophy in Clinical Medicine

Claudia Lindemann

“Our doubts are traitors, and make us lose the good we oft might win, by fearing to attempt”

W. Shakespeare

Acknowledgements

First and foremost, I would like to thank my supervisor Dr. David Wyllie for the interesting insight into research he has granted me through this unique project and through working in his research group. His indefatigable support has convinced me that even audacious experiments and projects can be made a success.

Secondly, I would like to thank my co-supervisor Dr. Daniel Wilson for his outstanding advice on various situation occurring in "academic life" and giving me an insight into the art of writing.

Thirdly, I would like to thank all the scientists, who have contributed to this project and who made it possible. Firstly, for their help with various analyses, Dr Julius Müller and Dr Adaikalavan Ramasamy, without whom the computational analysis would have simply been impossible to manage. Dr Nicola Ternette for her expertise and guidance in proteomics and for her help with the secretome experiments. The High Throughput Genomics Facility, Oxford (in particular Paolo Piazza and Amy Trebes) for their help and guidance in everything from RNA quality assessment over cDNA library preparation to RNA sequencing; for providing their facilities and knowledge and, above all, their patience. The British Heart Foundation Experimental Magnetic Resonance Unit, Oxford for the MRI images and the Oxford Centre for Histological Research for preparation and scanning of the histological slides.

Furthermore, I would like to thank our collaborators from the University of Würzburg for the collaboration in the *rsp* project and the scientific discussions.

Last but certainly not least, I would like to say a huge “Thank you” to the entire *S. aureus* group: Dr Pauline van Diemen, Dr Yuko Yamaguchi, Dr Claire Powers, Ritu Mann-Nuettel, Elizaveta Elshina and in particular Elizabeth Allen and Amy Flaxman. Not only did you make the working atmosphere in this group awesome – you showed me what real team spirit means and that in science we cannot just find competitors around us but true friends.

I would also like to thank the Vactrain project for making this experience possible. These last years were a unique experience and would not have been the same without the EU Commission frame-work of courses, support, funding and – of course – people.

The University of Oxford I would like to thank for eventually accepting me as a student. My stay here has introduced me to truly outstanding individuals – inside and outside my project- and many of them I met thanks to this university’s well organised system.

I’d like to thank the Linacre College, Oxford, for providing me with accommodation, food, entertainment and countless numbers of friends during this course. I am particularly grateful for the chance of rowing in its Boat Club, of which I have made extensive and most enjoyable use.

Die letzten Zeilen dieser Seite möchte ich den Menschen widmen, ohne die nichts von alldem möglich gewesen wäre: meiner Familie. Ohne Euren Rückhalt wäre ich heute nicht die Person, die ich bin. Ich verdanke Euch alles!

Esa página deseo dedicar a las dos personas más importantes de mi vida. Aunque su entrada a mi vida fue recientemente, ella no fuera la misma sin ustedes. Lalo y Diego, mi “chiquitín”: Gracias por todo! Ustedes son mi luz y mi esperanza. *Los amo!*

Table of Contents

Abstract

Understanding Early Transcriptional Events in Staphylococcus aureus Infection - Implications for Vaccine Design

Staphylococcus aureus remains an important pathogen, which, due to its capability to develop antimicrobial resistance, imposes an increasing threat to human health. Developing preventive means to decrease disease burden is a major aim. However, the development of an *S. aureus* vaccine, which would be one strategy to achieve such goals, has been complicated through limited understanding of the bacterium's pathogenic mechanisms. This work uses four approaches to address these limitations: Firstly, a reproducible RNA sequencing based method for the determination of gene transcription by *S. aureus in vivo* during mammalian infection. Secondly, examination of the impact of the bacterial transcription regulator "Rsp*"* on the bacterium, which shows that mutations in this gene have profound functional and transcriptional impacts. Thirdly, by examining the *in vivo* transcription of multiple *S. aureus* strains during infection, proposing a "core *in vivo* transcriptome" of induced genes under the conditions tested. Some of these genes are known to be involved in pathogenesis, others are not completely characterised and may represent suitable vaccine antigens. Finally, this work addresses limited understanding of *S. aureus* pathogenesis through defining transcriptional changes *in vivo*, which are induced by an altered immune response in immunised hosts. Together, this body of work contributes to the understanding of *S. aureus* pathogenesis and provides candidate antigens for future vaccine development.

Claudia Lindemann, Linacre College, Michaelmas Term 2017

List of Figures

List of Tables

List of Abbreviations

A

agr	*accessory gene regulator*
α-MEM	*Alpha Minimum Essential Media*
AMP	*Adenosine Monophosphate*
AraC	*Arabinose operon type C regulator*

B

bp	*base pairs*

C

C3(a/b)	*C3 protein of the complement cascade and its decomposition proteins C3a and C3b*
C4(a/b)	*C4 protein of the complement cascade and its decomposition proteins C4a and C4b*
C5(a/b**)**	*C5 protein of the complement cascade and its decomposition proteins C5a and C5b*
cDNA	*complimentary Deoxyribonucleic Acid*
CFU	*Colony Forming Unit*
CI	*Confidence Interval*

CID *Collision induced*

Ct value *Number of Real Time PCR cycles*

D

DMSO *Dimethyl sulfoxide*

DNA *Deoxyribonucleic acid*

DNase *Deoxyribonuclease*

DTT *Dithiothreitol*

E

E. coli *Escherichia coli*

EDTA *Ethylenediaminetetraacetic acid*

F

F_c region *Fragment, crystallisable (tail region of an antibody)*

FDR *False Discovery Rate*

G

GSEA *Gene Set Enrichment Analysis*

H

HBA *Horse Blood Agar*

I

ID_{50}	*Inhibitory Dose 50 (dose of an inhibitory compound at which 50% activity is detected)*
IgG1	*Immunoglobulin G subclass 1*
IgM	*Immunoglobulin M*
IsdA	*Iron surface determinant A*
IsdB	*Iron surface determinant B (V710 vaccine antigen, was tested as in clinical trials by Merck)*
IV	*intravenous*

K

kDa	*kilodalton*

L

log_2	*Binary logarithm*

M

M	*molar*
MAC	*Membrane Attack complex*
MBL	*Mannose – Binding – Lectin*
mg	*milligram*

µg	*microgram*
MHC	*Major Histocompatibility Complex*
MHz	*megahertz*
min	*minutes*
ml	*millilitre*
mm	*millimetre*
mM	*millimolar*
µm	*micrometer*
µM	*micromolar*
msec	*milliseconds*
mT	*millitesla*
MRI	*Magnetic Resonance Imaging*
mRNA	*messenger Ribonucleic Acid*

N

ncRNA	*non-coding Ribonucleic Acid*
ng	*nanogram*
nm	*nanometer*

O

OD	*Optical Density*
P	
Patient P	*First patient within a carriage study to develop a bloodstream infection caused by the carriage strain containing an rsp mutation*
Patient S	*Second bloodstream infection patient with an rsp mutation separating the carried and the infection strain*
PBS	*Phosphate buffered saline*
PCA	*Principal Component Analysis*
PCR	*Polymerase Chain Reaction*
PFA	*Paraformaldehyde*
pg	*picogram*
P. mirabilis	*Proteus mirabilis*
Q	
QC	*Quality Control*
R	
RDD	*RDD buffer (Qiagen)*
RLT	*RLT buffer (Qiagen)*
RNA	*Ribonucleic Acid*
RNase	*Ribonuclease*

RNA-seq	*Ribonucleic Acid Sequencing*
RNasin	*Ribonuclease inhibitor (Promega)*
RPE	*RPE buffer (Qiagen)*
rpm	*revolutions per minute*
RPMI	*Roswell Park Memorial Institute medium*
rRNA	*ribosomal Ribonucleic Acid*
Rsp	*"repressor of surface proteins", a S. aureus transcription factor*
Rsp^+	*strain expressing the rsp gene*
Rsp^-	*strain not expressing functional Rsp through a mutation*
rsp	*gene encoding the Rsp protein*
RT	*Room Temperature*
RW1	*RW1 buffer (Qiagen)*

S

S. aureus	*Staphylococcus aureus*
SATMD	*S. aureus Transcriptomic Meta Database*
sscDNA	*single stranded complimentary Deoxyribonucleic Acid*
SSR42	*a long non coding Ribonucleic Acid of S. aureus*

T

TSB	*Tryptic Soy Broth*
TRIS	*tris(hydroxymethyl)aminomethane*

U

UGN	*University of Oxford guidelines for biological health and safety*
USA300	*Staphylococcus aureus strain, also called USA300 FPR3757*
USA300 JE2	*USA300 cured of plasmids*
USA300 NE1304	*USA300 JE2 with transposon mutation in the rsp gene*

V

V710	*Vaccine from Merck (S. aureus IsdB protein formulation with alum)*

W

WGS	*Whole Genome Sequencing*

Introduction

Staphylococcus aureus – commensal or pathogen?

S. aureus is a gram-positive bacterium, which is commonly found on the skin and in the nares of mammals, including humans (1). In some humans, *S. aureus* is permanently present in the interiors of the nose and can be isolated from the nares (2, 3). If *S. aureus* is present in the nose, this state is referred to as "colonisation" or "carriage", and it is asymptomatic for the so-called "carrier". However, *S. aureus* cannot just colonise but also infect the human host and cause a variety of diseases such as skin infections, pneumonia or sepsis (4, 5). Very often human carriers are infected by their own colonising *S. aureus* strain (6). The carriers risk of experiencing a staphylococcal infection is higher than that of non-carriers (7). Yet, *S. aureus* carriers have a lower chance of lethal outcome when suffering from an *S. aureus* infection (5, 8), but the reason for this is unknown.

The pathology of S. aureus infections

S. aureus can cause a variety of infections in different tissues of the human host (Fig. 1) (5). Soft tissue and skin infection caused by this bacterium is common and dangerous, as skin infection can progress to bacteraemia and sepsis (9). Numbers of community acquired infections have increased (9, 10) and due to a high mortality rate, bacterial sepsis is being studied intensively (11).

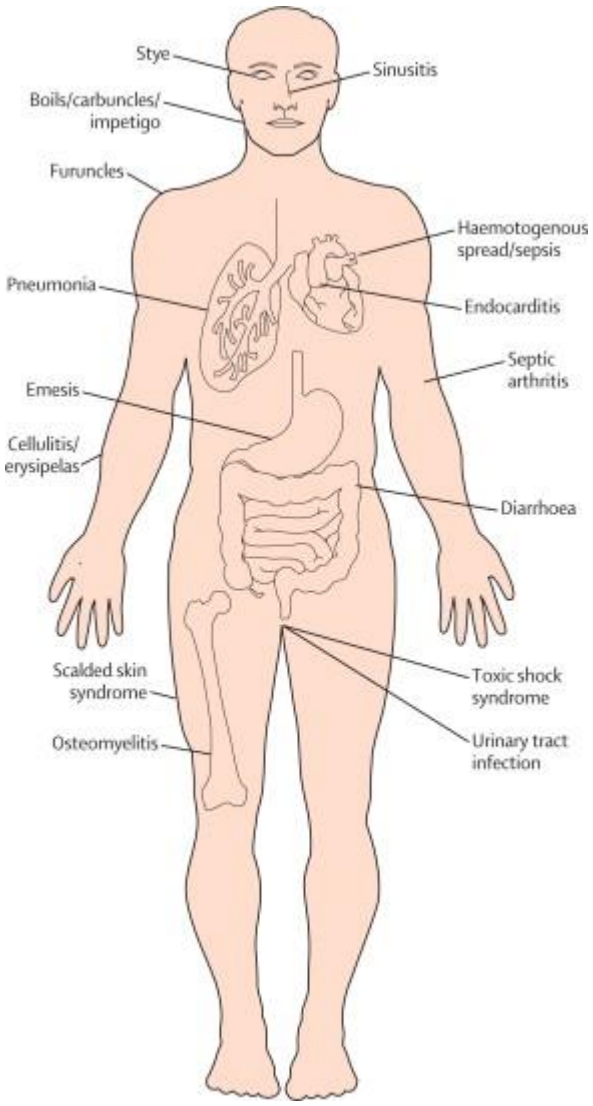

Figure 1: Diversity in *S. aureus* infection

Figure adapted from Wertheim *et al.*, 2005. (5).

Some mechanisms of pathogenesis of *S. aureus* infection have been identified such as different strategies to attack the host tissue and defend itself against the immune response (12, 13): *S. aureus* can produce a range of toxins that lyse host cells (Fig. 2) and thereby breaking and trespassing barriers and leukocyte defences. Furthermore, *S. aureus* can lyse erythrocytes, which enables the bacterium to access iron-containing molecules during infection (14).

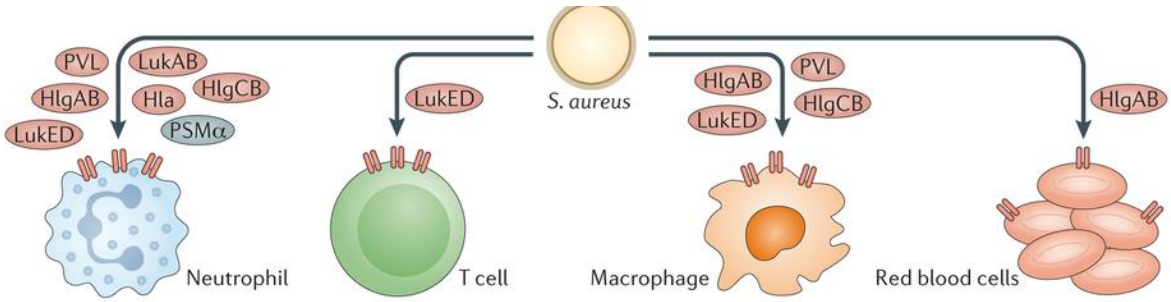

Figure 2: **Toxins of *S. aureus***

S. aureus toxins (red) and small cytotoxic molecules (grey) with some of their cellular targets (12). The figure was adapted from Thammavongsa *et al.,* 2015.

S. aureus has also developed ways of evading innate immune recognition: Through secreted and surface proteins, the bacterium can manipulate chemotaxis and phagocytosis in various manners (15). One specific way of influencing the innate immune response is by skewing complement system activation (12).

The complement system, as part of the innate immune response, has three ways of detecting gram-positive bacteria, activating a common pathway that leads to opsonisation (16). Activation of the complement cascade also leads to release of pro-inflammatory anaphylatoxins (C3a, C4a and C5a). Some staphylococcal proteins can affect the complement cascade. An overview of where and how staphylococcal proteins affect complement activation is shown in Figure 3.

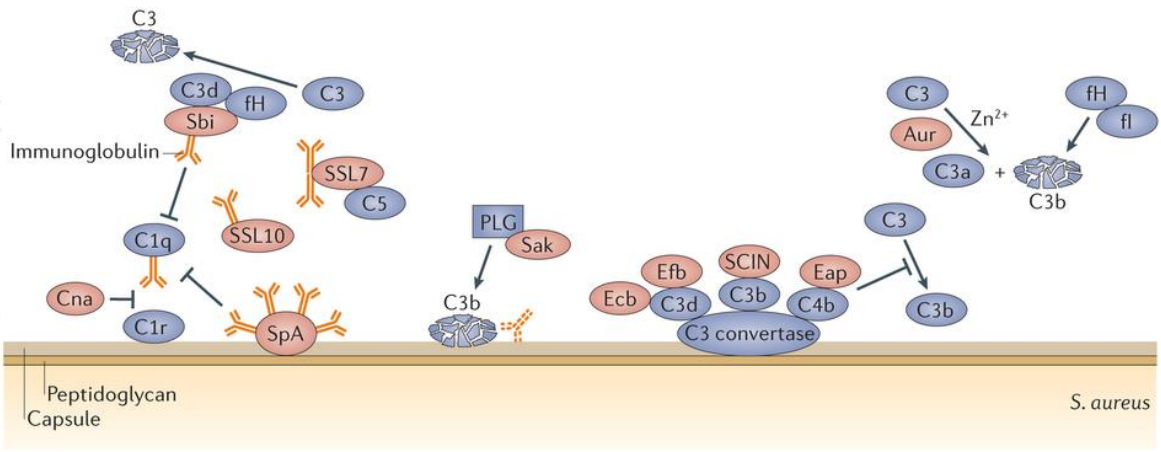

Figure 3: Complement modulators of *S. aureus*

S. aureus proteins (red) and the complement cascade proteins (blue), which they modulate (12). The figure was adapted from Thammavongsa *et al.,* 2015.

If despite the plethora of phagocytosis subversion strategies, *S. aureus* is taken up by neutrophils, it is not necessarily killed within the phagocyte. Rather, this bacterium has developed various strategies to resist phagolysosomes and survive intracellularly (Fig. 4, (17-21)).

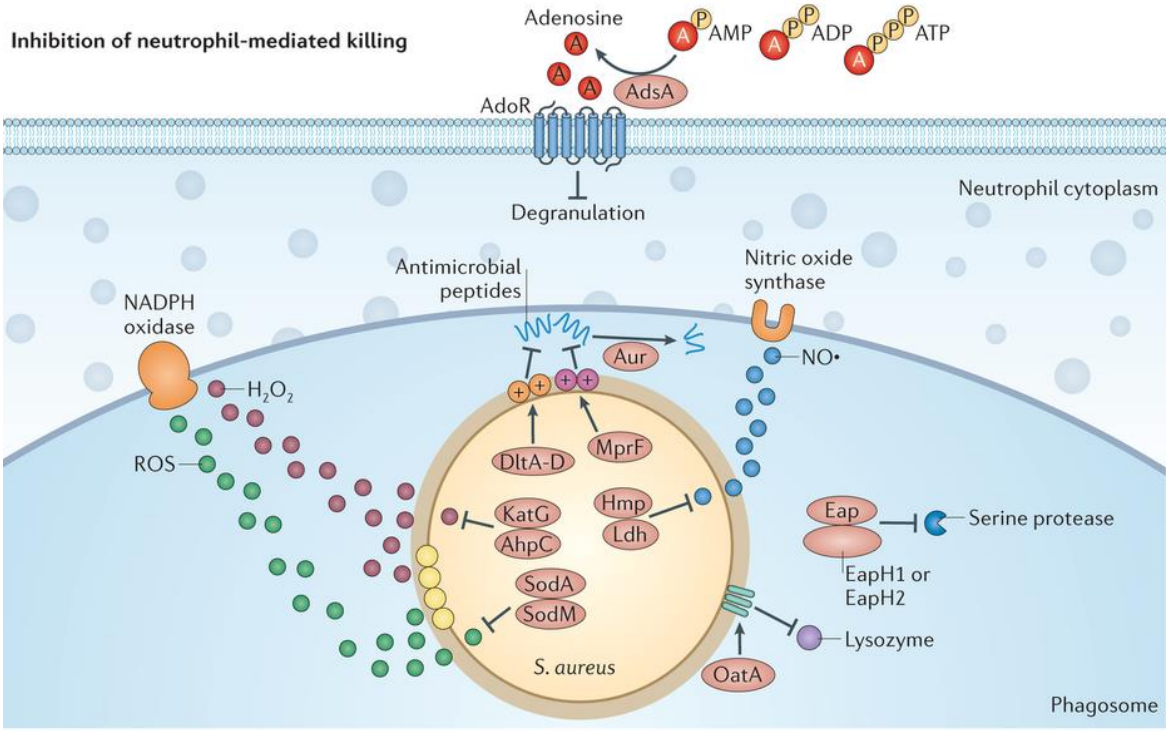

Figure 4: Inhibition of neutrophil-mediated killing

S. aureus phagocytic killing inhibition proteins (red) and their targets (12). The figure was adapted from Thammavongsa *et al.,* 2015.

It has become evident recently that intracellular *S. aureus* resembles an infection reservoir protected from antimicrobials and the host defence (22). If antimicrobials reach intracellular and extracellular bacteria, the infection is eliminated (23).

Current treatments

The high clinical (24) and economic (25) burdens of *S. aureus* infections make the bacterium an important pathogen. *S. aureus* is now a leading cause of sepsis and bacteriaemia (26), diseases which are associated with high mortality (27) and there is a need for treatment options. The standard of care is preventive treatment of populations at high risk such as invasive surgery patients. If a bacterial blood infection occurs, a prolonged intravenous therapy with a combination of antibiotics is recommended (28). However, preventive and therapeutic measures often fail due to antimicrobial resistance of the pathogen (29). In order to reduce antibiotic exposure and therefore chances of resistance development, infection prevention using other means would be a feasible alternative. A vaccine preventing *S. aureus* bloodstream infections is highly desirable. Yet, no effective vaccine has been licensed (30).

Challenges in vaccine development

Major efforts have been made over the last two decades to develop and license an effective *S. aureus* vaccine. Various active and passive immunisation strategies were tested in clinical trials – without success (31). Several explanations for these failures have been hypothesized: First of all the broad range of infections caused by *S. aureus* makes it necessary to focus on one particular infection, as there are differences in the mechanism of pathogenesis between for example pneumonia and

sepsis (32). Thus, the targeted infection needs to be specified for each vaccine and this must be considered in the design of clinical trials. Second, murine models have failed to predict vaccine efficacy so far (33) and no reliable model to assess immunisation is available until today. Third, the focus has been on generating antibody mediated protection as observed in mouse models. In humans, however, generation of antigen specific antibodies did not correlate with any protection (34). Instead, a stronger focus on cell-mediated protection has been suggested (35). Last but not least, *S. aureus* possesses multiple virulence factors, many of which have similar functions. Some of these contribute to immune evasion and hamper development of an adaptive immune response during infection (36). Due to the complexity of infection, it has been suggested that multiple antigens might be required in a vaccine formulation (30). The selection of the antigens is a challenge, as it is not clear which virulence factors *S. aureus* produces are essential to establish and maintain disease. The focus should therefore be on studying bacteria isolated from infection sides and to identify, which antigens are expressed during the state of infection *in vivo.*

Experimental Chapters

Chapter 1: Repressor of surface proteins (Rsp) – an *S. aureus* transcription regulator influencing acute infection

This chapter describes the phenotypic differences observed in *S. aureus rsp* mutants. Bacterial growth, behaviour in a murine sepsis model, changes in transcription and protein recognition as well as differential host immune recognition are studied.

Chapter 2: Development of an assay to measure bacterial transcriptomes *in vivo*

The development of an extraction method for bacterial RNA from murine tissue is described. RNA quality control, cDNA library generation and RNA Sequencing are standardised. A transcriptome for *S. aureus* strain Newman is characterised.

Chapter 3: Application of an *in vivo* transcriptomic assay to study clinical isolates

The effects of *in vivo* conditions on gene transcription of three *S. aureus* strains are presented and the effect of the mutation of the transcription factor Rsp on gene expression *in vivo* is assessed.

Chapter 4: The influence of vaccination on the bacterial *in vivo* transcriptome

Gene expression in bacteria infecting immunised mice is compared to bacterial transcription in mock-vaccinated mice.

Ethical Framework

Animal studies were approved under the Animal (Scientific Procedures) Act 1986 (Project license 30/2825) and by the University of Oxford Animal Care and Ethical Review Committee, conforming to Directive 2010/63/EU of the European Union. Patient P isolates were obtained during participation in a study of *S. aureus* carriage in Oxfordshire. This study was approved by Oxfordshire Research Ethics Committee B (approval reference 08/H0605/102 granted September 2, 2008) and obtained individual written consent from all participants. Patient S isolates were collected from routine clinical samples. Ethical approval for sequencing *S. aureus* isolates from routine clinical samples and linkage to patient data without individual patient consent in Oxford and Brighton in the U.K. was obtained from Berkshire Ethics Committee (10/H0505/83) and the U.K. National Information Governance Board (8-05(e)/2010). Venepuncture of healthy volunteers was performed according to the University of Oxford guidelines for Biological Health and Safety (UGN S1/95).

Chapter 1:

Repressor of surface proteins (Rsp) – an *S. aureus* transcription regulator influencing acute infection

1.1 Introduction

1.1.1 Natural Mutations of Transcription Regulators can separate invasive from non-invasive *S. aureus* Strains

At present, the determinants of *S. aureus* virulence are not fully understood. Several secreted and surface proteins have been characterised as "virulence" factors, among them adhesins (12), nucleases (37, 38), complement control proteins (39-41), and multiple toxins (42-44), which all interfere with host immune function. Cytotoxic proteins induce lysis in various cells, extending from epithelial cells to leukocytes (12, 32, 45). Cytotoxic protein secretion is associated with lethality in some animal disease models (44, 46-48) and some staphylococcal lineages, such as *S. aureus* USA300, display high levels of toxin secretion, which may be linked to *S. aureus'* evolutionary success (44, 49).

The colonizing *S. aureus* strain of a human carrier represents a reservoir for infection (4, 32). Interestingly, bacterial isolates from blood often differ from those from the nares to the extent that they exhibit decreased cytotoxicity (50) and reduced haemolysis (51). As invasive and carried isolates are usually closely related genetically (6), mutations could be a possible explanation for these observed differences in cytotoxicity. When mutations are found in transcription regulators, the effect on the bacterial phenotype can be of a large dimension as seen in the major *accessory gene regulator* (*agr*), which influences *S. aureus* cytotoxicity. *agr* is mutated in a proportion of bacteria recovered from human sites of infection (52-54). The invasive *agr* mutants show prolonged intracellular residence due to attenuated cytotoxicity and delay in initiation of host cell death (55-57).

However, genes other than *agr* might control the induction of cytotoxic attenuation. One transcription regulator for such a role was suggested by a study of a patient with long-term nasal *S. aureus* carriage and functional *agr* gene (58). Within the studied patient, an invasive bacterial isolate with reduced cytotoxicity evolved through a loss-of-function mutation. The gene affected, *rsp*, encodes an AraC-family type transcriptional regulator. The occurrence of this genetic change accompanied the progression from carriage to bacteraemia (58).

1.1.2 *rsp* Mutants are isolated from the Human Bloodstream

In a *S. aureus* carriage study (58), a participant, designated P, was identified as an *S. aureus* carrier. 15 month after joining the study, P (from here on called "Patient P") was admitted to hospital with a *S. aureus* bloodstream infection. Bacterial isolates recovered from this patient's bloodstream differed by a small number of mutations from the nasal ancestor, previously isolated during the study (Fig. 5). One mutation caused a premature stop codon in the *S. aureus* transcription regulator *rsp* (58). Subsequently, another patient (Patient S) with bloodstream infection was identified in the same hospital. A nasal swab was taken after admission and in this case the bloodstream isolate differed from the nasal one by only one mutation (Fig. 5), located in the DNA binding region of the *rsp* gene (Fig. 6). This non - synonymous mutation in the helix - turn - helix motive (A204P) is predicted to abrogate DNA binding.

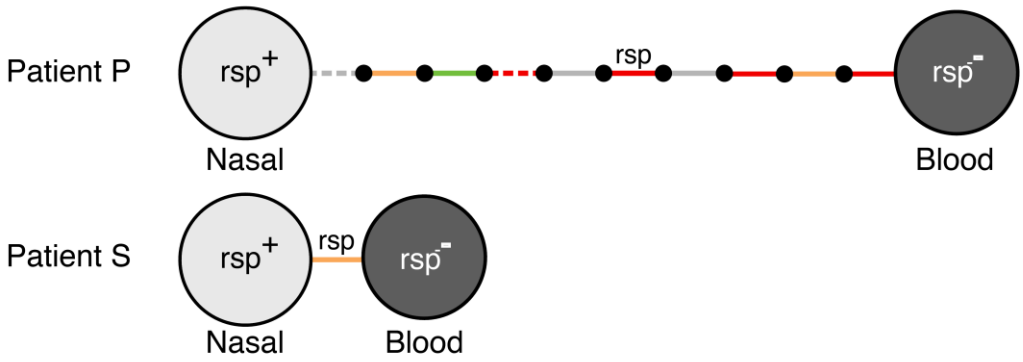

Figure 5: Genetic differences between invasive blood and nasal carriage isolates

Schematic illustrating genomic comparisons of two bloodstream isolates (Patient P and S) with their respective carried nasal strains. Isolates are represented by light (nasal/Rsp^{+}) and dark (blood/Rsp^{-}) grey circles. Intergenic (grey), synonymous (green), non-synonymous (orange), nonsense (red) mutations are represented by solid and dashed lines, respectively. Small black circles represent hypothetical intermediate genotypes. The ordering of mutations along the branch in Patient P is arbitrary. Only a single mutation (A204P) in the whole genome (including the accessory genome) separated the bacteraemic from the carriage isolate in Patient S. Dr. Daniel Wilson kindly provided this figure (59).

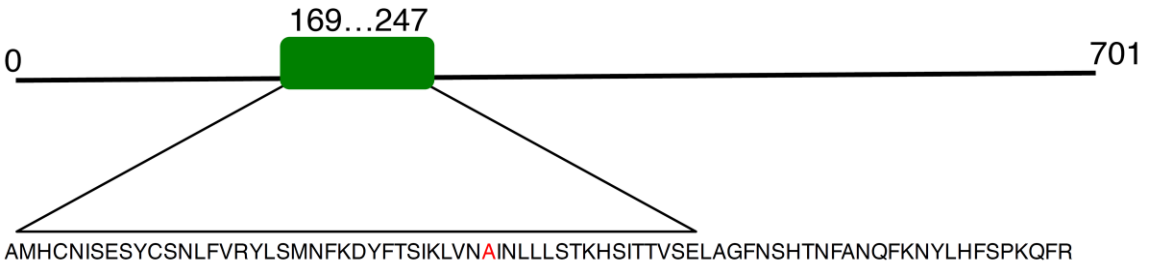

Figure 6: A single nucleotide exchange in the *rsp* gene causes a non-synonymous mutation

Rsp contains a helix turn helix domain (amino acids 169-247). The observed substitution in the Patient S Rsp^{-} isolate (indicated in red) occurs in the centre of this domain, substituting an alanine with a proline and is thereby predicted to disrupt the three dimensional structure of the DNA binding region. Dr Bernadette Young kindly provided this figure.

To assess relatedness of these strains, the Illumina next generation sequencing output from Patients S and P was mapped to the USA300 FPR3757 reference. In silico multilocus sequence (MLST) typing showed these strains to be of different sequence types (STs) (USA300: ST-8; isolates from patient S: ST-59; isolates from patient P: ST-15) and a pairwise distance matrix confirmed USA300, Patient P and Patient S isolates their differences (Table 1).

Table 1: Pairwise SNP distance matrix between the isolates studied

Isolate	P, Blood	P, Nasal	S, Blood	S, Nasal	USA300
P, Blood	0	10	35,852	35,868	15,330
P, Nasal	10	0	35,987	35,999	15,309
S, Blood	35,852	35,987	0	1	37,953
S, Nasal	35,868	35,999	1	0	37,978
USA300	15,330	15,309	35,953	37,978	0

S. aureus is a diverse organism with multiple deep evolutionary branches (60), of which these isolates are derived from three different branches and no evolutionary relationship exists (Fig. 7).

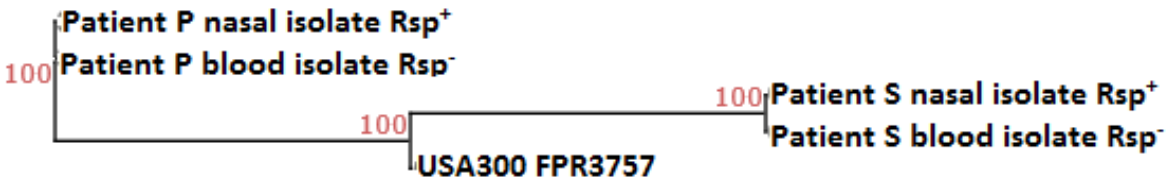

Figure 7: Phylogenetic tree showing genetic relationship of *S. aureus* strains

Phylogenetic dendrogram calculated with sequences of the isolates the *S. aureus* strains USA300 FPR3757, Patient S and Patient P using maximum likelihood approach. Dr. David Wyllie kindly provided this figure.

1.1.3 Experimental Approach

The aim of this chapter is to investigate the effect of *rsp* mutation on the *S. aureus* phenotype *in vitro* and in disease models *in vivo*. First, bacterial growth in broth and human blood is assessed. In a murine mouse model, lethality, clinical symptoms and bacterial capability of abscess formation is compared between *rsp* mutants and wild types. As Rsp is annotated a transcription regulator, effects of *rsp* mutation on transcription and secreted protein expression are characterised *in vitro*. Subsequently, identified phenotypical changes are confirmed using enzyme activity determination in two enzymes (D-lactate dehydrogenase (ddh) and urease (ure)), which are upregulated in the transcriptome of the *rsp* mutant when compared with its wild type. Finally, differential recognition of the *rsp* mutant *S. aureus* by the human complement system is quantified in an *in vitro* complement activation assay.

1.2 Research Questions and Objectives

1.2.1 Research Questions

1. Does *rsp* mutation in clinical isolates affect bacterial growth or survival *in vivo*?
2. Does *rsp* mutation alter sepsis and renal abscess development in the host? Does *rsp* mutation change host survival?
3. How is global gene expression affected by the mutation of the transcription regulator *rsp*? How is the secreted proteome altered by r*sp* mutation?
4. Are phenotypic differences indicated by transcriptomic and proteomic studies confirmable through other independent assays?
5. Does a *S. aureus rsp* mutant interact with the immune system differently than a *S. aureus* with wild type *rsp*?
6. Which differentially expressed proteins could make novel potential vaccine antigens and why?

1.2.2 Research Objectives

1. To test effects of *rsp* mutation on *S. aureus* growth
2. To test Rsp-dependent effects on *S. aureus* sepsis development in mice
3. To characterize the differential transcription profile of *rsp* mutants
4. To classify protein expression changes depending on Rsp
5. Determine alterations in host immune recognition of *rsp* mutants
6. Find Rsp regulated antigens which could make potential new vaccine candidates

1.3 Materials & Methods

1.3.1 Reagents, Materials and Enzymes

Table 2: Name, supplier and catalogue number of reagents, materials and enzymes

Reagent	Supplier	Catalogue Number
Sodium deoxycholate (SDC)	Sigma Aldrich	D6750
Acetonitrile LC-MS CHROMASOLV®	Sigma Aldrich	34967
β - Mercaptoethanol , Molecular Biological Grade	Calbiochem	444203
Chloroform, ACS spectrophotometric grade, ≥99.8%	Sigma Aldrich	366919
Dimethyl sulphoxide (DMSO), sterile	Sigma Aldrich	D2650
Ethanol, pure, Molecular Biology Grade	Sigma-Aldrich	E7023
Formic acid for mass spectrometry	Sigma Aldrich	94318
HyClone, RNase free water, Molecular Biology Grade	GE Healthcare	SH30538.02
Hydrochloric Acid (HCl) [1M]	Sigma Aldrich	71763-1L
L-glutamine sterile solution [200 mM]	Sigma Aldrich	G-7513
Methanol, pure, ACS reagent	Sigma Aldrich	32213
Paraformaldehyde (PFA), 16 % w/v aqueous solution, methanol free	Alfa Aesar	43368
Phosphate Buffered Saline (PBS), liquid, sterile	Sigma Aldrich	D-8537
RNA Screen Tape Sample Buffer	Agilent	5067-5577
RNA Screen Tape Sample Ladder	Agilent	5067-5578
RNAprotect Bacteria Reagent	Qiagen	76506
RNaseZap RNase Inhibitor surface decontamination solution	Invitrogen	AM9780
RPMI 1640 Medium	Sigma Aldrich	R5886
Trishydroxymethylaminomethane (TRIS), ACS reagent	Sigma-Aldrich	252859
Tryptic Soy Broth (TBA), culture media	Oxoid	BO0369
Urea 40% solution	Oxoid	SR0020
Urea Broth Base (Christensen's medium)	Oxoid	CM0071
α-MEM (Minimal essential medium)	Gibco/life technologies	41061-029
Material	**Supplier**	**Catalogue Number**
3-kDa Amicon Ultra-15 Centrifugal Filter Unit with Ultracel-3 membrane	Millipore	UFC900308
Turbo DNA free DNase I kit	Ambion	AM1907
Flat bottom 96-well plate (Nunc Microwell)	Thermo Fisher Scientific	161093

Gas permeable Moisture Barrier Imaging Sealer	4titude	4ti-0516/96
Horse Blood Agar Plates (HBA)	Oxoid	PB0114
Lactate Dehydrogenase Colorimetric Assay	Amplite	13809
Qubit® RNA BR Kit	Thermo Fisher Scientific	Q10210
RNA Screen Tape	Agilent	5067-5576
RNase-free DNase Set	Qiagen	79254
RNeasy Midi Kit	Qiagen	75144
Sep-Pak C18 Plus Short Cartridge	Waters	WAT020515
TRIS-EDTA (TE) buffer	Qiagen	19046
Vivaspin 4-Maximum, 5 kDa	Satorius	VS0413
Wieslab® complement system screen	Invitech/EuroDiagnostics	ED-COMPL300
Enzyme	**Supplier**	**Catalogue Number**
Lysostaphin, >500 units/mg	Sigma-Aldrich	L7386 – 1MG
Proteinase K, 2ml, >600mAU	Qiagen	19131
Trypsin, Sequencing Grade, frozen (20 µg)	Promega	V511C

1.3.2 Clinical Samples

S. aureus strains were isolated from two patients (hereafter called "Patient P" and "Patient S") with concomitant nasal carriage and bloodstream infection by our collaborators (Dr. Bernadette Young, Dr. Daniel Wilson). They recruited Patient P to a longitudinal study, in which they monitored asymptomatic carriage among adults attending general practices in Oxfordshire, U.K., and Patient P developed an *S. aureus* bloodstream infection 15 months after joining the study (58). The second patient, Patient S, was treated for a *S. aureus* bloodstream infection at a hospital in Oxfordshire, with a nasal swab subsequently taken as part of routine surveillance. In both cases, our collaborators performed microbiological processing and whole genome sequencing (WGS) as described (58).

1.3.3 Bacterial Strains

All bacterial strains in this thesis are listed in Table S1 (Supplementary). From Patient P we selected one nasal culture isolate (isolate reference number C1360, "Patient P nasal") and one blood culture isolate (isolate reference number C1158, "Patient P blood"). The blood isolate differs by ten single-nucleotide variants, including a premature stop codon in the arabinose type C (AraC)-family transcriptional regulator *rsp* (61) Both isolates belong to lineage ST-15 with a sequence similarity of 99.5% to the MSSA476 strain (62). Patient P isolates carry two copies of a 20.7-kb plasmid that is 99.9% similar to the MSSA476 pSAS plasmid and that contained a region homologous to the staphylococcal transposon Tn552 (58).

From Patient S (lineage ST-59) we selected one nasal isolate (isolate C24365, "Patient S nasal") and one blood isolate (isolate C24366, "Patient S blood"). The blood isolate differed by a single (Alanine to Proline) point mutation in the helix-turn-helix domain of *rsp,* predicted to disrupt DNA binding of the transcriptional regulator. Genetic analysis of Patient S' accessory genome revealed presence of toxins and adhesins encoded in the strain (a comprehensive list can be found in Table S2 in the supplementary).

In both cases, the nasal isolates exhibited the *rsp* wild type (Rsp^{+}) and the blood isolates non-synonymous mutations (Rsp^{-}). In addition, we obtained from the Nebraska Transposon Mutant Library wild type (JE2) (63) and *rsp* insertional transposon mutant (NE1304) strain of *S. aureus* USA300 FPR3757. *S. aureus* USA300 is a highly virulent and cytotoxic strain (lineage ST-8, (64)). An overview of all strains used and their genetic relationship can be found in Table 3.

Table 3: Genetic differences of strains

Name of strain	Name of mutated strain	Number of mutations
USA 300 JE2 Rsp^+	USA300 NE1304 Rsp^-	1 (transposon insertion mutation)
Patient P nasal Rsp^+	Patient P blood Rsp^-	10 (3 intergenic, 2 non-synonymous, 1 synonymous and 4 nonsense)
Patient S nasal Rsp^+	Patient S blood Rsp^-	1 (non-synonymous)

For isolates P and S, we identified homologues of the 2604 proteins in *S. aureus* USA300 FPR3757 (NCBI accession NC_007793.1) proteins by comparison with Velvet assemblies of strains from P and S . Overall 2,411 homologues were found in either P or S genomes (homologue databases have been published previously: (59), http://www.pnas.org/content/113/22/E3101.abstract?tab=ds, Supplementary Dataset S5).

1.3.4 Bacterial Culture Conditions

Bacteria were grown on HBA (Oxoid), overnight (12 – 16 hours) at 37°C. Liquid bacterial cultures were grown aerobically by inoculating 10 ml of Tryptic Soy Broth (TSB, Oxoid), and incubating overnight (18 hours) at 37°C with shaking (180 revolutions per minute (rpm)).

1.3.5 Bacterial Growth Curves

S. aureus strains were grown overnight (18 hours) in TSB at 37°C with shaking at 180 rpm. The culture was diluted in TSB (series of 1:10 to 1:100000) and growth curves determined measuring optical density (OD) at 600 nm in triplicates over 20 hours in a 48 well plate. Absorbance was measured every 15 minutes in an automated fashion using a CLARIOstar Microplate reader (BMG Labtech).

1.3.6 *Ex vivo* Human Blood Survival Assay

This assay was developed based on internal protocols and a published method (65).

S. aureus strains were grown overnight as described in section 1.3.3. Bacteria were pelleted and washed using 3000 xg for 10 min. The pellet was taken up in 10 ml RPMI 1640 containing 1 % (v/v) L-Glutamine (1 M). The bacterial suspensions were diluted 1:10 (4 x 10^8 CFU/ml) and 1:1000 (4 x 10^6 CFU/ml). The bacterial inocula were plated on HBA for CFU enumeration.

For the human blood samples, 42 ml of whole blood (EDTA Vacutainers, BD Biosciences) were taken from three healthy volunteers. Bacterial suspension was added to anticoagulated blood to a final concentration of either 1 x 10^8 or 1 x 10^6 CFU/ml and incubated for 1, 3 or 24 hours at 37 °C, 130 rpm shaking. After incubation, samples were spun at 14000 xg for 10 min. Deionized sterile water was added to the pellet to lyse blood cells and release intracellular bacteria. The sample was mixed, spun and the supernatant plated on HBA to enumerate bacterial survival.

1.3.7 Murine intravenous Infection (Sepsis) Model

Female Balb/c, mice aged six weeks, were obtained from Taconic Biosciences Inc. (Denmark) and housed in individually filtered cages on a regular diet in groups of six. All mice used in murine experiments were confirmed to be *S. aureus* free by stool sampling and plating, followed by microbial colony identification. At eight weeks, mice were inoculated intravenously (IV) in the lateral tail vein with 0.1 ml bacterial suspensions in PBS at a dose of 5x10^6 CFU/mouse. Weight and clinical score/survival was monitored using a scoring system based on published work (66, 67) included in Supplementary Table S3. Mice were sacrificed 3 hours, two or three

days post infection with terminal anaesthesia using Isoflurane followed by confirmation of death through dislocation of the neck. Blood, livers, spleens and kidneys were taken for bacterial enumeration (for post mortem two days post infection only right kidneys were used for enumeration and left kidneys for histopathological analysis of bacterial abscesses). Viable *S. aureus* per gram of tissue/ml of blood were enumerated by spreading serially diluted aliquots of homogenized tissue (GentleMACS M-tubes, Miltenyi Biotec) using an Autoplate Spiral Plating System (Advanced Instruments) on HBA (Oxoid). Plates were incubated for 24 hours at 37°C, and colonies were counted using an automated counter (QCount Colony Counter, Quadrachem).

1.3.8 Magnetic Resonance Imaging Analysis of infected Murine Kidneys

Murine renal histopathology was analysed using a described MRI based approach (68). Kidneys were harvested two days post intravenous infection and stored in 4 % paraformaldehyde (PFA, Sigma Aldrich). The British Heart Foundation Experimental Magnetic Resonance Unit (BMRU, Oxford) performed sample preparation and scanning. In short, kidneys were removed from PFA and soaked in a gadolinium-based contrast agent (Omniscan, GE Healthcare) at a concentration of 0.5 mmol/ml for 24 hours. Afterwards, kidneys were mounted in a 28 mm glass tube and embedded in 1% agarose (Iberose, Web scientific) containing 2mM gadolinium contrast agent. Imaging was carried out on a 9.4 T (400 MHz) MR system (Varian Inc., Palo Alto) comprising a horizontal magnet (bore size 210 mm), a VNMRS Direct DriveTM console and an actively shielded gradient system (1000 mT/m, rise

time 130 msec, od 115 mm, id 60 mm). Image analysis was performed as described (68) to obtain abscess volumes and numbers.

1.3.9 Histopathology of infected murine Kidneys

Kidneys were embedded in wax, three 5 μM sections were taken through the long (sagittal) axis of each kidney at approximately 15 %, 35 % and 50% renal thickness. The slides were stained with haematoxylin and eosin in the Oxford Centre for Histological Research (OCHRE), John Radcliffe Hospital, Oxford. Images were scanned using a Hamamatsu C600 Nanozoomer slide scanner and visualised with ImageScope (Aperio) software. Abscesses were defined as areas of focal neutrophil infiltration.

1.3.10 Bacterial Ribonucleic Acid (RNA) Extraction and Quality Assessment

Bacterial messenger RNA (mRNA) from overnight cultures (prepared as described in section 1.3.3) was extracted using the RNeasy Protect Bacteria Kit (Qiagen) according to the manufacturer instructions (protocol 4) and treated with DNase I (DNAfree kit, Ambion) to remove remaining DNA. The concentration of the RNA was determined via fluorometry using the Qubit Fluorometer RNA BR Kit (Invitrogen). Quality and quantity of the RNA were examined by analysis on Tapestation (Agilent Technologies).

1.3.11 Complementary Deoxyribonucleic Acid (cDNA) Library Preparation and Ribonucleic Acid (RNA) Sequencing

When required, bacterial messenger RNA (mRNA) was enriched using the Universal Ribozero bacterial rRNA Depletion Kit (Epicentre) followed by Next Ultra Directional Library Preparation Kit for Illumina (NEB). The High Throughput Genomics Facility, Wellcome Trust Centre for Human Genomics (Oxford, UK), executed the Library preparation and sequencing. RNA adapter was ligated to the 5'-phosphate of the RNA. First-strand cDNA was generated using an oligo(dT)-primer and M-MLV reverse transcriptase. Using a high-fidelity DNA polymerase, cDNA (NEBNext® Q5® Hot Start HiFi PCR Master Mix) was amplified to 20-30 ng/µl by PCR.

The cDNA was sequenced on HiSeqTM 2000 (Illumina) yielding 100 bp paired end reads. Adapters were removed and reads trimmed to 70 bp using Trimmomatic (69) and only reads exceeding a mean base quality of 5 (Phred/Q quality score) within all sliding windows of 5 bp were mapped to the *S. aureus* USA300 FPR3757 genome (NCBI accession NC_007793.1). Read mapping was conducted using Bowtie2 ((70), settings were set to “no mismatches allowed”, “end-to-end alignment reads only” in the sensitive mode) and only paired and concordant alignments were considered further. To quantify per-gene read counts, htseq (71) was used counting only reads with an alignment quality of greater than 10 in mode ‘union’.

1.3.12 Sample Preparation for secreted Proteome (Secretome) Analysis

Bacterial strains were grown overnight (18 hours) in both, TSB (Oxoid) and in α-MEM (alpha Minimum Essential Media, Life Technologies), in parallel. Bacteria were pelleted from cultures by centrifugation (10000 xg, 20 min, 4°C) and

supernatants aspirated. Proteins were precipitated from the supernatant with methanol/chloroform precipitation. Protein pellets were re-solubilized in 6 M urea solution in 0.1 M TRIS (pH 7.8). After 20 min resolubilization, dithiothreitol (DTT) (20 mM in 0.1 M TRIS) and iodoacetamide were added (40 mM) and incubated for 20 min at room temperature to alkylate cysteines. The DTT treatment was repeated with 40 mM DTT to consume remaining alkylation reagent. Samples were diluted with water to a final concentration of 1 M urea in the solution, then 0.2 µg trypsin was added for overnight digestion. Salts were removed from the sample using a C18 Sep-Pak column (Light, Waters), washed with buffer A (2% Acetonitrile, 0.1% formic acid in water) and eluted with buffer B (98% Acetonitrile, 0.1% formic acid in water). Purified peptides were dried using a vacuum manifold before re-suspension in Buffer A.

1.3.13 Liquid Chromatography Tandem Mass Spectrometry

This work was performed by Dr Nicola Ternette (Nuffield Department of Medicine, Oxford) as part of a collaboration. She separated peptides on a Dionex Ultimate 3000 UPLC system (Thermo Scientific) supplemented with a 50 cm x 75 µm Acclaim PepMap RSLC column. A 2 µm particle size with a linear gradient from 2-35% buffer B (5% DMSO, 0.1% formic acid in acetonitrile) into buffer A (5% DMSO, 0.1 % formic acid in water) was used. The flow rate was 250 nl/min (at approx. 600 bar) for 60 min. Peptides were introduced to a TripleTOF 5600 mass spectrometer (AB Sciex) by electrospray ionization. Collision induced (CID) fragmentation using ramped collision energy was induced on the 30 most abundant ions per full mass spectrometry.

1.3.14 Mass Spectrometry Data Analysis

Data analysis was performed together with Dr Nicola Ternette. Data (wiff-files) was converted to MASCOT generic files using ProteinPilot (72). Sequence interpretation of mass spectrometry spectra was performed with PEAKS (73) using bacterial-backbone specific databases as described previously (59), together with (in all cases) all 74,380 UniProt entries for the soybean plant (*Glycine max,* NCBI taxon id 3847). This was included to control for soybean protein detection in bacterially-conditioned tryptic soy broth. The probability score threshold was defined by decoy database searches implemented in the regarding search engines at a general false discovery rate of 1%. For *S. aureus* USA300, the protein database used contained all 2604 annotated proteins of the USA300 FPR3757 strain (NCBI accession NC_007793.1). For isolates P and S, we identified homologues of the 2604 proteins in *S. aureus* USA300 by comparison of USA300 FPR3757 proteins with Velvet assemblies of whole genome sequencing of strains from P and S using the NCBI Blast+ Suite 2.2.6 tblastn program. The single best hit with an e-value < 10^{-5} and a similar amino acid: query length ratio of > 0.7 was retained and considered to be a homologue of the USA300 predicted protein used as a query. Overall 2,411 homologues were found in either P or S genomes (homologue databases have been published previously: http://www.pnas.org/content/113/22/E3101.abstract?tab=ds, (59), Supplementary Dataset S5). Abundances were computed from the top 3 peptides shared by all gene homologs in NC_007793.1, and genomes P and S. Although not strictly count data, the decoupling of mean and variance in the negative binomial distribution assumed by DESeq2 enabled us to model differential secreted protein abundance in an identical manner to the transcript abundances by discretizing the abundance. This

assisted direct comparison between the results of the transcriptomic and proteomic analyses.

1.3.15 Secreted Proteins in Tryptic Soy Broth and Alpha Minimum Essential Medium (α-MEM)

Proteins in the supernatants of stationary phase cultures of USA300, Patient P and S bacterial backgrounds were grown in both TSB (Oxoid) and α-MEM (Life Technologies), a protein-free media, and analysed using mass spectrometry (1.3.10 – 1.3.12). The means of two biological replicates were determined. Proteins not detected were considered to have an abundance of zero. Spearman's rank correlation coefficient was computed between different isolates and growth buffers (TSB and α-MEM), and visualized using the corrplot package in R 3.1.11 for Linux.

1.3.16 Urease enzymatic Activity Assay

In vitro activity of bacterial urease was measured for USA300, Patient P and S backgrounds. Christensen's media urease assay was carried out according to manufacturer's instruction. *Proteus mirabilis* was used as a positive control and *Escherichia coli* (both clinical isolates, identified by the Department of Microbiology, John Radcliffe Hospital, Oxford) as a negative control for the presence of urease activity. Growth media was prepared by adding Urea Broth Base (Oxoid) and sterile urea solution (SR0020, Oxoid) to distilled water. *P. mirabilis, E. coli,* and *S. aureus* (USA300, Patient S, Patient P) were grown overnight (200 rpm shaking, 37 °C) in the media and optical density measured every 10 minutes. To

control for absorption bias through bacterial growth, plates were spun (3000 xg, 10 min) and the supernatant used for measurements. A spectrum from 430 nm (phenol red absorbance peak at pH 6.5) to 560 nm (phenol red absorbance peak at pH 8.2) was measured. pH elevation through ammonia release as a result of urea hydrolysis indicates urease activity (pH > 8.1). No change in colour is expected for urease negative strains.

1.3.17 D-lactate Dehydrogenase (Ddh) Activity Assay

Activity of D-lactate dehydrogenase (Ddh) was measured in the overnight culture supernatants of samples from the genetic background USA300, Patient P and S. Bacteria were grown for 18 hours in α-MEM (life technologies), spun down (3000 xg, 10 min, 4 °C). Culture supernatants were filtered (0.22 µm pore size) and concentrated (up to 40x) using a 3 kDa filter column (4700 xg, 1.5 hour, 4 °C). Ddh activity was measured using a colorimetric assay (Amplite) according to the manual (Amplite™ Colorimetric D-Lactate Dehydrogenase Assay Kit). In this assay, NAD^+ is added to the sample and NADH concentration measured through a chromogenic sensor (absorption at A_{575nm}/A_{605nm}) over two hours. Its concentration correlates to Ddh activity in the samples and was calculated using a standard curve with known activity.

1.3.18 Complement Activation Assay

Serum complement activation was assessed in vitro using the Wieslab® Complement System Screen (Euro Diagnostica). Supernatants from bacterial overnight cultures of *S. aureus* USA300 JE2, Patient P and S backgrounds were filtered (pore size: 0.22 μm) and concentrated (3 kDa Amicon Ultra Spin Column). Total protein concentrations in the supernatants were normalised across all strains.

A consented healthy volunteer was bled using SST II Vacutainers (BD Biosciences), the blood coagulated (60 min, room temperature (RT)) and the serum separated by centrifugation (3000 xg, 5 min). Serum and bacterial supernatant at different concentrations were incubated for 15 min (RT) to permit interaction of serum proteins with bacterial complement inhibitors.

The instructions of the manufacturer's protocol were followed. The assay assesses induced activation of the complement cascade *in vitro* through activators of specific pathways coated on a plate. The concentration of Membrane-Attack Complex (MAC) was measured colorimetrically.

1.3.19 Statistical Analysis

The activities of urease (Chapter 1, [1.3.16]) and D-lactate dehydrogenase (Chapter 1, [1.3.17]) were compared strain by strain using a Student's t-test test. For data where no normality could be assumed, a non-parametric test was performed. This was the case for abscess volume and counts (Chapter 1, [1.3.8]), bacterial tissue load, infection severity score and animal weight comparisons in murine experiments

(Chapter1, [1.3.7]). Survival curves were analysed using a log-rank test (Mantel-Cox). GraphPad 6 was used for the above mentioned analysis.

Correlation between the proteomes detected in the two media compared was assessed using a Spearman's rank correlation (Chapter 1, [1.3.15]), which, unlike Pearson's correlation, does not make assumptions about linearity of the correlation and is more robust to outliers.

Regression models were used for bacterial growth curve comparison (Chapter 1, [1.3.5]), *ex vivo* blood survival assay (Chapter 1, [1.3.6]) and the comparison of complement activation (Chapter 1, [1.3.18]). R was used for regression models, apart from the complement activation comparison, where an inhibition curve for the effect transmitted by the different bacterial supernatants was plotted using GraphPad 6. Values were normalized and non-linear regression (variable slope) applied.

Differential transcript abundance analysis [1.3.11] was performed by Dr Julius Müller (Jenner Institute Bioinformatics Core, Oxford) using the DESeq2 package v.1.5.9 (74) in R, as described previously (59). Significant effects were identified using the Bayesian Wald test in DESeq2 (75) and transcripts with low counts were filtered out to improve power (76). The Benjamini-Hochberg adjustment of the *p*-values was employed to obtain an expected false discovery rate (FDR) of 10% (77).

1.4 Results

1.4.1 *rsp* Mutation does not alter Bacterial Growth *in vitro*

Mutations in the *S. aureus* transcription regulator *rsp* are found in clinical blood isolates (58). To test, whether *rsp* mutants grow at a different pace than wild type bacteria, growth of *rsp* mutants (Rsp^-) and wild type (Rsp^+) was compared *in vitro*. It appears that bacterial strains (Patient P, Patient S and USA300 (Chapter 1, [1.3.2])) grow independent of their *rsp* status in culture (Fig. 8). There is no evidence that growth rates differed (normalized growth rate of wild type relative to mutant was 107 % using non-linear regression (95% CI 79 – 147 %)).

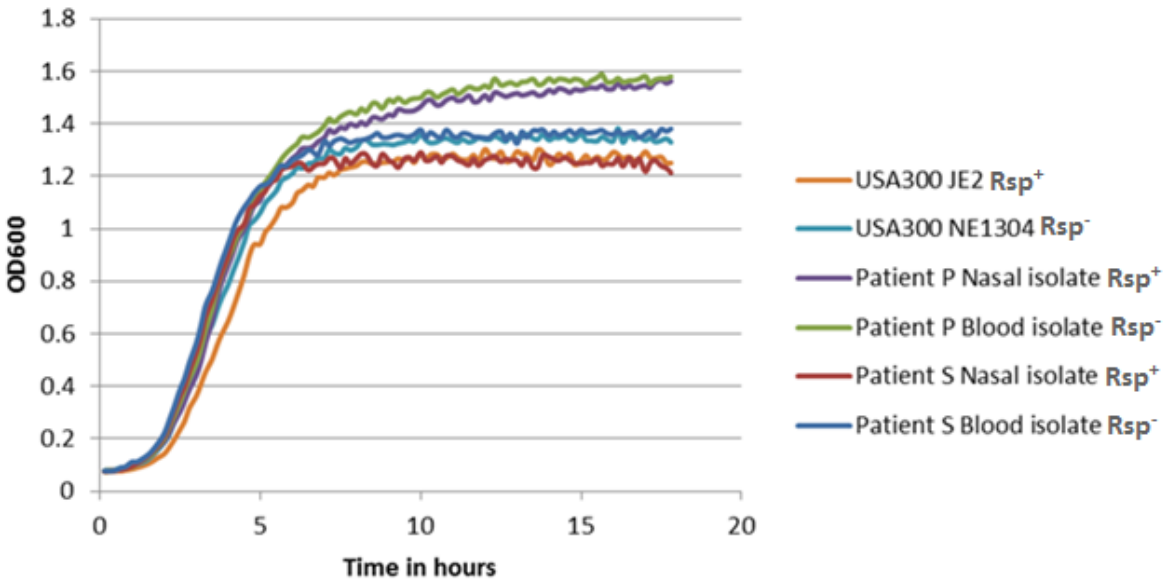

Figure 8: The impact of *rsp* mutation on bacterial growth

Cultures of USA300 (JE2 Rsp+ orange, NE1304 Rsp^- light blue), Patient P (nasal isolate Rsp^+ purple, blood isolate Rsp^- green) and Patient S (nasal isolate Rsp^+ red, blood isolate Rsp^- blue) [all strains described in 1.3.3] were diluted 1:100 in TSB, incubated and optical density (OD_{600}) measured over time [Method described in 1.3.5]. Non-linear regression was used to compare the growth curves of Rsp^- to Rsp^+ strains.

1.4.2 *rsp* Mutation does not affect Bacterial Survival in Human Blood

To test whether survival of *S. aureus rsp* mutants differs to wild type in human blood, bacterial growth was compared *ex vivo* in human blood (Fig. 9). After inoculating strains USA300, Patient P or S into human blood from three healthy donors, bacterial survival was measured at three time points (1h, 3h and 24h) [1.3.6].

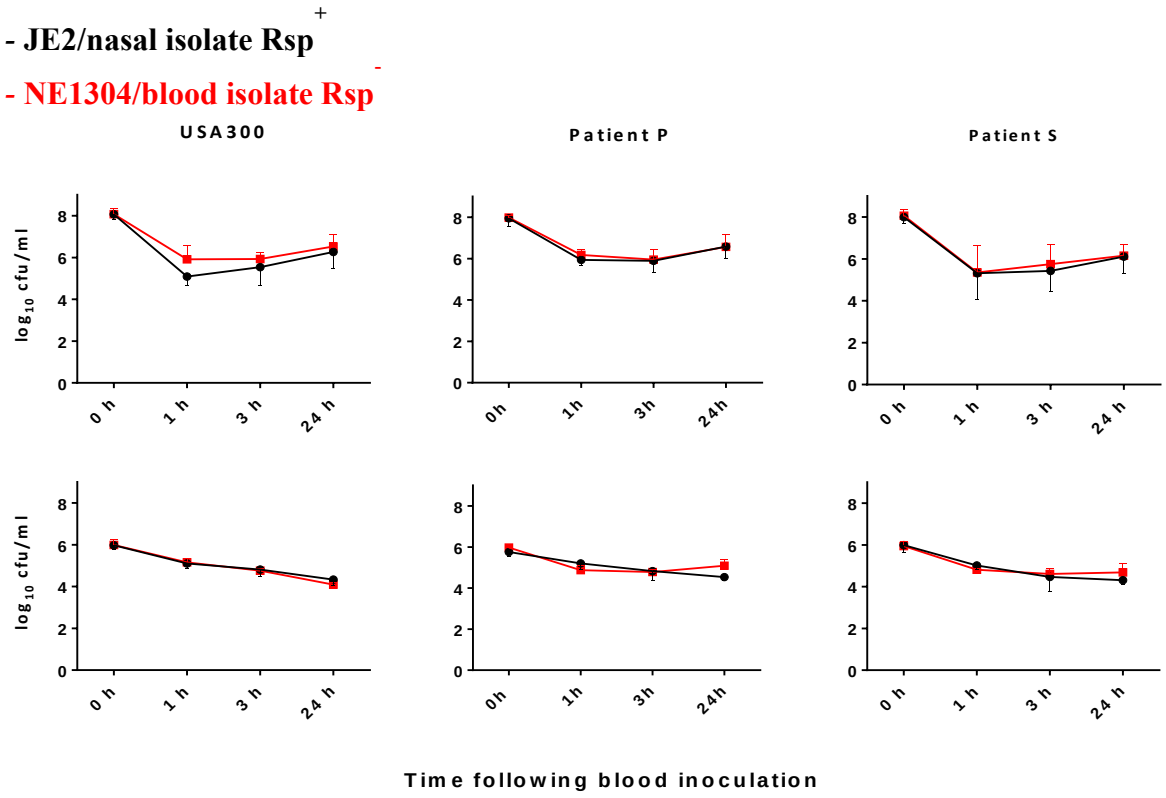

Figure 9: *S. aureus* Rsp⁻ vs Rsp⁺ survival in human blood in three different strains

Ex vivo blood survival between *rsp* mutant (USA300 JE2 Rsp⁻, Patient P Rsp⁻ and S Rsp⁻ blood isolates: **black** lines) and wild type bacteria (USA300 NE1304 Rsp⁺, Patient P Rsp⁺ and S Rsp⁺ nasal isolates: **red** lines) [Strains described in 1.3.3]. High inocula (10^8 CFU/ml blood, top row) and low inocula (10^6 CFU/ml blood, bottom row) were used and numbers of colony forming units (CFU) across three time points (1, 3, 24 hours) counted. Results shown were obtained from three independent experiments [Method described in 1.3.6]. Statistical significance was determined by general linear modelling, considering counts at each time point as a function of *rsp* genotype and genetic background of the organism.

There was no significant difference in CFU in whole blood after inoculation and incubation between *rsp* mutants and wild types in strains USA300, Patient P and Patient S (Fig. 9). Thus, bacterial survival e*x vivo* in human blood is Rsp independent under the conditions tested.

1.4.3 Repressor of surface proteins (Rsp) is required for Lethality in murine Infection

As *rsp* mutants were isolated from the bloodstream, I investigated whether *rsp* mutation altered progression of experimental *S. aureus* infection, using an established murine sepsis model (78), in which abscesses form following intravenous administration of *S. aureus (*Chapter 1, [1.3.6]). USA300 *rsp* mutant and wild type strains were used for infection and lethality monitored (Fig. 10).

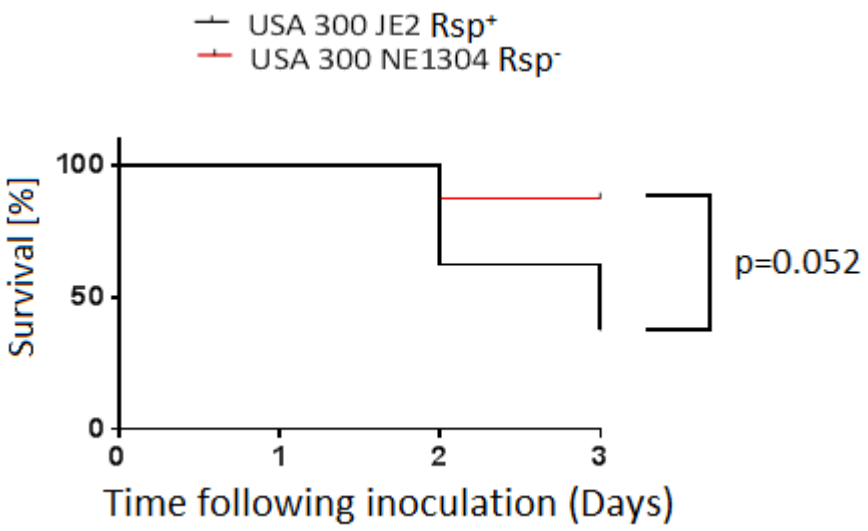

Figure 10: Survival of mice after IV infection with Rsp$^-$ or Rsp$^+$ *S. aureus.*

Murine survival in percentage from challenge with *S. aureus* USA300 JE2 Rsp$^+$ (black line) or its *rsp* mutant NE1304 Rsp$^-$ (red line) [Strains described in 1.3.3; Method described in Section 1.3.7] was compared. Results shown were obtained by combining two independent experiments (total of 16 mice per group). Differences were assessed using a log-rank (Mantel-Cox) test.

Lethality in this model is lower in *rsp* mutant infected mice than in the wild type infected mice (Fig. 10, p=0.052).

During infection, disease symptoms were measured and clinical severity scores (66, 67) determined. In general, a high clinical severity score (>7) indicates a very sick mouse. Starting from day two post infection, clinical severity scores increased in the mice infected with wild type bacteria (Rsp^+) when compared to the group infected with the *rsp* mutant (Rsp^-) (Fig. 11, p=0.039/p=0.002 Day2/3 post infection).

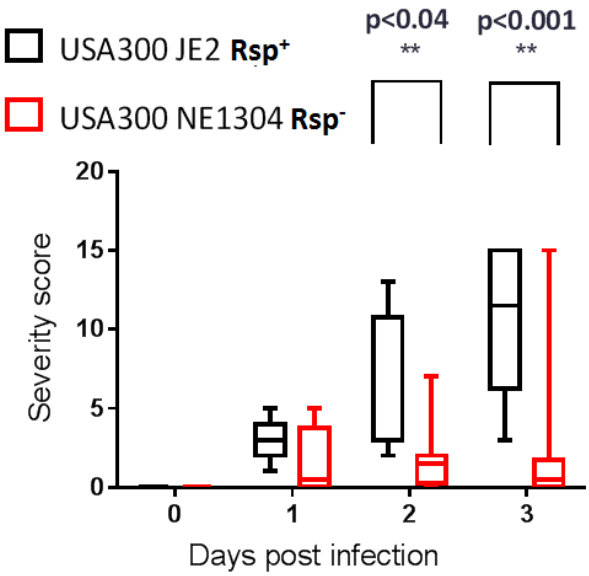

Figure 11: Illness scores of USA300 Rsp^+ and Rsp^- IV infected mice over three days

Illness scores of mice infected intravenously with *S. aureus* USA300 JE2 Rsp^+ (black) or USA300 NE1304 Rsp^- (red) [Strains described in Section 1.3.3; Method described in Section 1.3.7]. Day "0" represents day of challenge and scores were determined twice daily (66, 67). Animals with a score higher than seven were sacrificed and considered "endpoint". These animals were arbitrarily given illness scores of 15. Differences were assessed using multiple t-tests with eight mice per group.

Mice infected with *rsp* mutant *S. aureus* USA300 NE1304 developed fewer disease symptoms (Fig. 11) than *rsp* wild type USA300 JE2 infected mice and were less likely to succumb to the infection.

Mice challenged with *rsp* wild type bacteria (Rsp^+) also lost less weight when compared to mice challenged with *rsp* mutants (Rsp^-) (Fig. 12; day 2 difference, p=0.01; data is shown for USA300 representatively) until day 2.

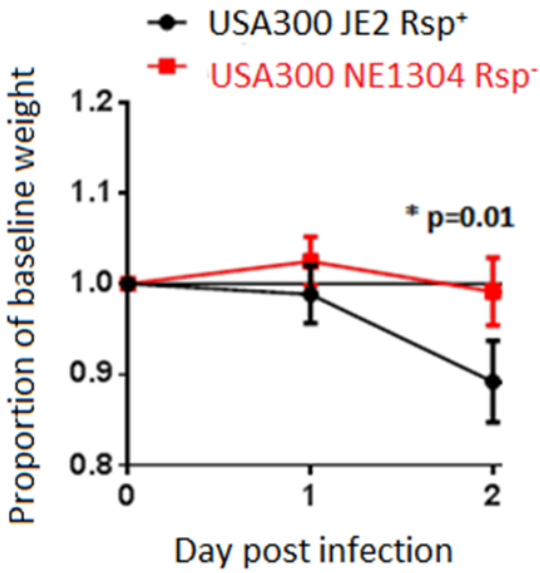

Figure 12: **Weight proportions of mice after IV infection from day 0 (day of challenge)**

The straight grey line shows the start weight of each animal, normalized to "1". The black line shows the proportional development of weight of USA300 JE2 Rsp^+ challenged mice, the red line of USA300 NE1304 Rsp^- challenged mice [Strains described in 1.3.3; Method described in Section 1.3.7]. At day 2, some animals had reached the humane endpoint. Weight deviations after infection were assessed using a non-parametric test (Mann-Whitney).

Day 3 post infection weights could not be compared due to differences in group size caused by animals, which had reached a humane endpoint on day 2 post infection. These results show that Rsp influences bacterially induced lethality *in vivo*, and that mortality occurred in the first days after experimental infection (Fig, 10). It also indicates that *rsp* mutation decreases disease symptoms and weight loss early after infection (Fig. 11 and 12) in the used disease model.

1.4.4 Murine Kidney Abscess Formation is not regulated by Repressor of surface proteins (Rsp)

A common way of assessing bacterial infectivity in the murine sepsis model is quantifying tissue bacterial loads *post mortem*. After intravenous inoculation, *S. aureus* disseminates within the murine host and viable bacteria can be detected at high levels in the liver, spleen and kidney (79).

In addition, 24 – 48 hours post infection of the murine bloodstream, *S. aureus* commences to form abscesses in the murine kidney (80). These abscesses can be analysed regarding their quantitative load of viable bacteria in the kidney tissue, as well as in respect of their structure, size and number. In order to capture bacterial load during early dissemination and at early abscess formation, I quantified viable bacteria within liver, spleen and kidney at 3 hours and 48 hours post infection.

The observed differences in lethality (Chapter 1, [1.4.3, Fig. 10]), suggest that bacterial load in the mice infected with *rsp* mutants (Rsp^-) would be altered compared to *rsp* wild type (Rsp^+). Three hours after injection of the USA300 JE2 strain (Rsp^+), or its *rsp* insertion mutant (Rsp^-), viable bacteria were detectable in multiple tissues. Both bacterial strains had high concentrations in liver and spleen, but low renal concentrations (Fig. 13). Patient P and S infected mice exhibit equal distribution of bacterial loads to USA300 infected mice (data not shown). By 48 hours, both wild type and *rsp* mutant bacteria infected mice presented increased bacterial load compared to 3 hours post infection. No significant difference for any of the tissues investigated was observed at either time point (Mann-Whitney test).

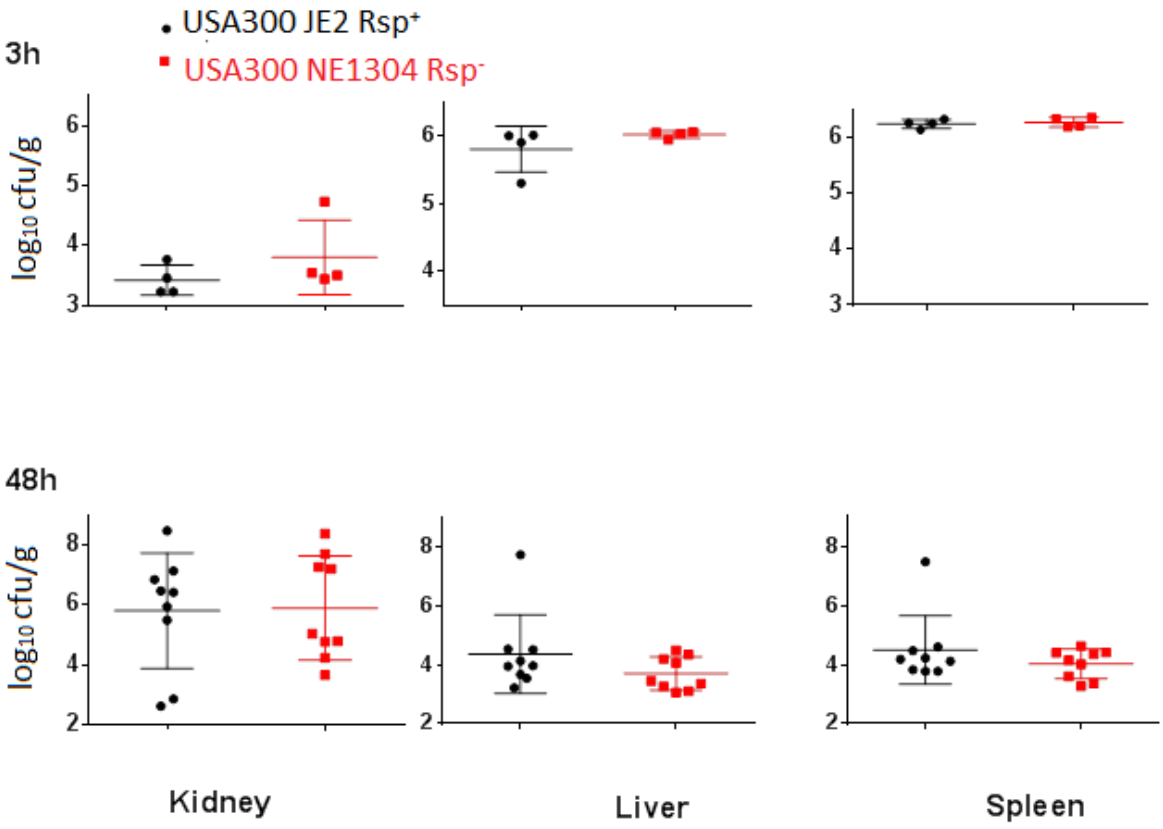

Figure 13: Bacterial counts in kidney, liver and spleen after IV infection.

Mice were infected with either *S. aureus* USA300 JE2 Rsp$^+$ or USA300 NE1304 Rsp$^-$ and murine tissues (kidneys, liver and spleen) harvested 3 or 48 hours post infection. Shown is the number of colony forming units (CFU) per gram tissue 3 hours (upper graphs, 4 mice per group) and 48 hours (lower graphs, 8 mice per group) post infection [Strains are described in 1.3.3, Method described in Section 1.3.7]. Groups were compared using a Mann-Whitney test.

In brief, bacterial loads appear to be similar in all three tested tissues, indicating that there is no Rsp-dependent effect on bacterial tissue load in murine sepsis (Fig. 13).

Another way of comparing bacterial infectivity is to determine renal abscess numbers, volume and architecture. Classically, this is done using histopathological tissue staining. However, volume determination of abscesses using this method is not completely reliable, as histological analysis is only two-dimensional. Recently, a method for renal abscess quantification has been published (68). Here, both methods were applied – MRI for abscess quantification and volume determination, histological analysis for structural comparison. Groups of nine mice were injected with either *rsp* mutant (Rsp^-) or wild type (Rsp^+) of all three strains (USA300, Patient P or Patient S). 54 kidneys – 27 obtained from *rsp* wild type and 27 from mutant infected mice - were analyzed. Comparable to the bacterial loads in the tissue (Fig. 13), the numbers and volumes of renal abscesses identified were also similar in all three strains (Fig. 14A+B; Mann-Whitney test, p=0.522/p=0.555, respectively).

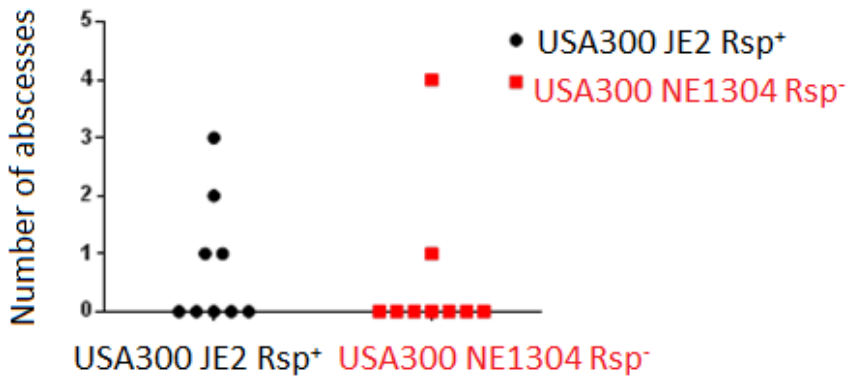

Figure 14: Number of renal abscesses 48 hours post infection in infected mice

A: 48 hours post IV infection [Method described in Sections 1.3.7, 1.3.8 and 1.3.9], numbers of abscesses were quantified in mice infected with *S. aureus* USA300 NE1304 Rsp^- (red) and USA300 JE2 Rsp^+ (black). Groups consisted of nine mice and were compared using a Mann-Whitney test (p = 0.522).

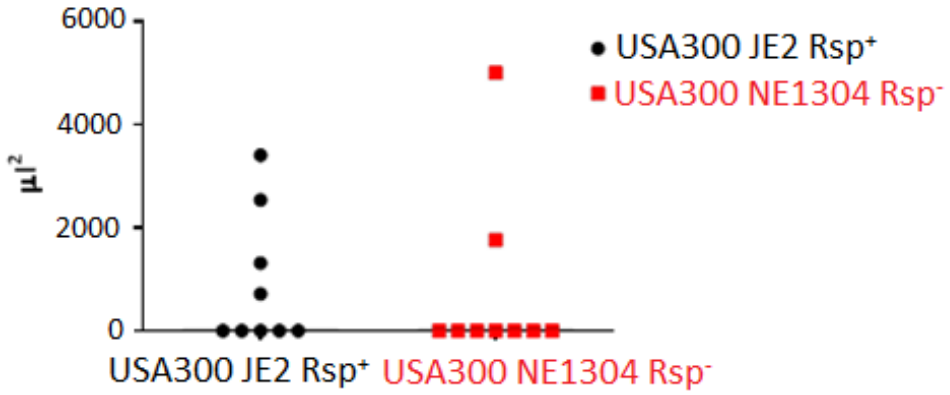

Figure 14:

B: Volumes [μ^2] of renal abscesses 48 hours post infection in mice infected with *S. aureus* USA300 NE1304 Rsp^- (red) and USA300 JE2 Rsp^+ (black) [Methods described in Sections 1.3.7, 1.3.8 and 1.3.9]. Groups consisted of nine mice and were compared using a Mann-Whitney test (p = 0.555).

S. aureus renal abscesses display increase in neutrophil influx as a structural characteristic and in both, *rsp* wild type and mutant infected kidneys, abscesses were formed with no differences in numbers (Figure 14A) and volumes (Figure 14B). The architecture of renal abscesses appeared similar, as visible in histopathological slides (Fig. 15). No two abscesses were in the same location within the kidney, making direct comparison difficult. However, both strains cause lesions with high neutrophil influx. Taken together, these results conclude that bacterial dissemination from the blood, survival or proliferation in murine tissues is not Rsp-dependent.

A

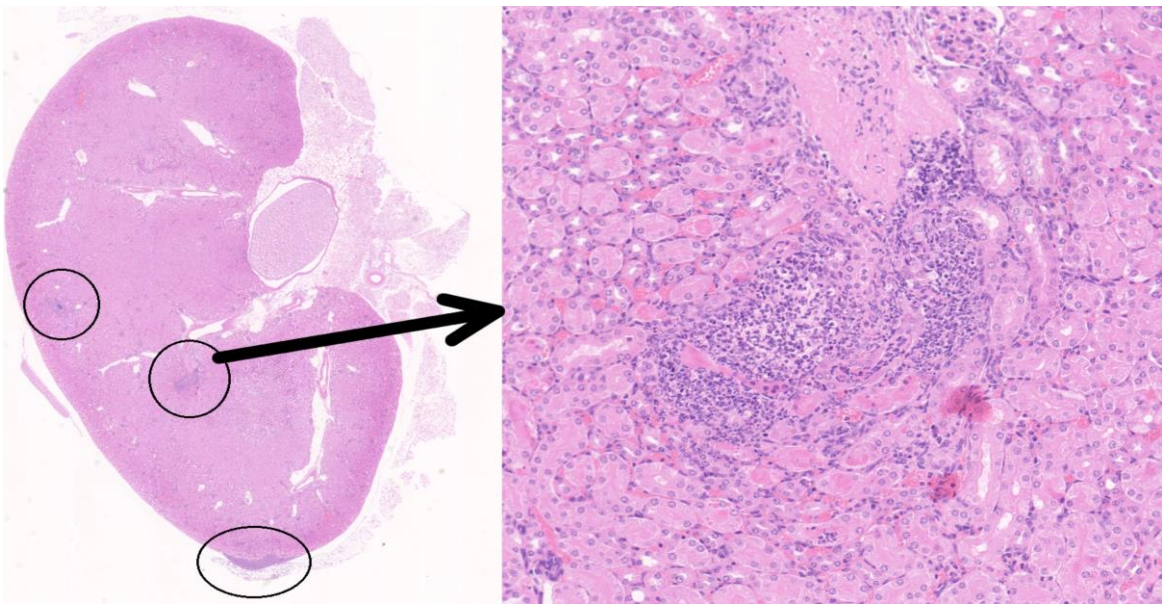

B

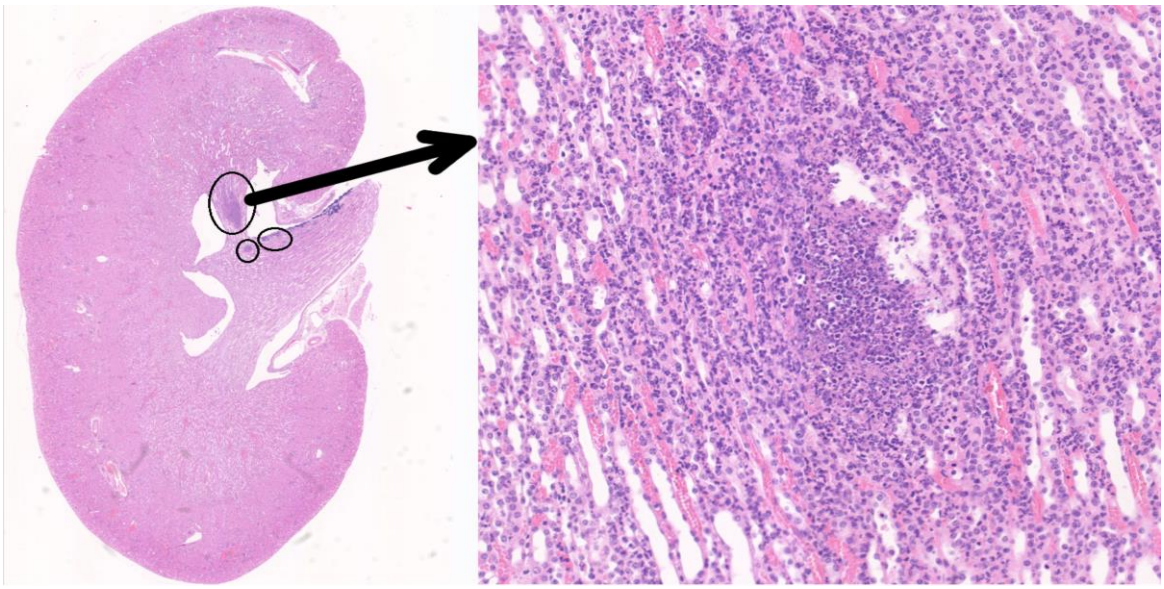

Figure 15: Histology of Rsp^{+} and Rsp^{-} infected kidneys 48 hours post infection

Areas demonstrating neutrophil enrichment in a haematoxylin and eosin stain were counted as abscess [Methods described in section 1.3.7 – 1.3.9]. **A**, A representative histological image of a kidney infected with USA300 JE2 (Rsp^{+}) shows formation of 3 abscesses. On the right: 14x magnification of one of the USA300 JE2 (Rsp^{+}) abscesses. **B**, USA300 NE1304 (Rsp^{-}) infected kidney. On the right: 14x magnification of one of the USA300 NE1304 (Rsp^{-}) abscesses

1.4.5 Repressor of surface proteins (Rsp) is a Regulator of *S. aureus* Immune Modulators and Toxins

The spontaneous evolution of *rsp* loss-of-function mutations found in human bloodstream infections (58), and the *rsp* mutants capability to survive *ex vivo* in human blood [Chapter 1, 1.4.3], demonstrate that *S. aureus rsp* mutants are not avirulent in man. However, this observation raises questions as to whether, in the absence of *rsp*, *S. aureus* might elaborate an alternative set of virulence proteins other than toxins. Rsp is a transcription regulator; hence, I analysed differential transcription between wild type strains and *rsp* mutants in three genetic backgrounds of *S. aureus* isolates (USA300, Patient P and Patient S).

In USA300, Patient P and Patient S strain backgrounds [detailed description of strains in Section 1.3.3], transcription in stationary phase differed between blood isolated mutants (Rsp^-) and nasally isolated wild type (Rsp^+) isolates in about 30% of the 2368 genes present in all three strains across the *S. aureus* genome (Fig. 16). Effects of *rsp* mutation on gene transcription were determined estimating effects per-gene from RNA-seq data as published previously (59). Transcription was similar across genetic backgrounds (ρ between 0.67 to 0.79). 584 genes were upregulated through *rsp* mutation in all three backgrounds, 327 genes showed an Rsp-dependent decrease in transcription in all three strains (Figures 17 and 18), but strain specific Rsp-dependency in gene expression is also found. A complete list of the Rsp-mediated effects on each gene has been published (http://www.pnas.org/content/113/22/E3101.abstract?tab=ds , Supplementary S2, (59)).

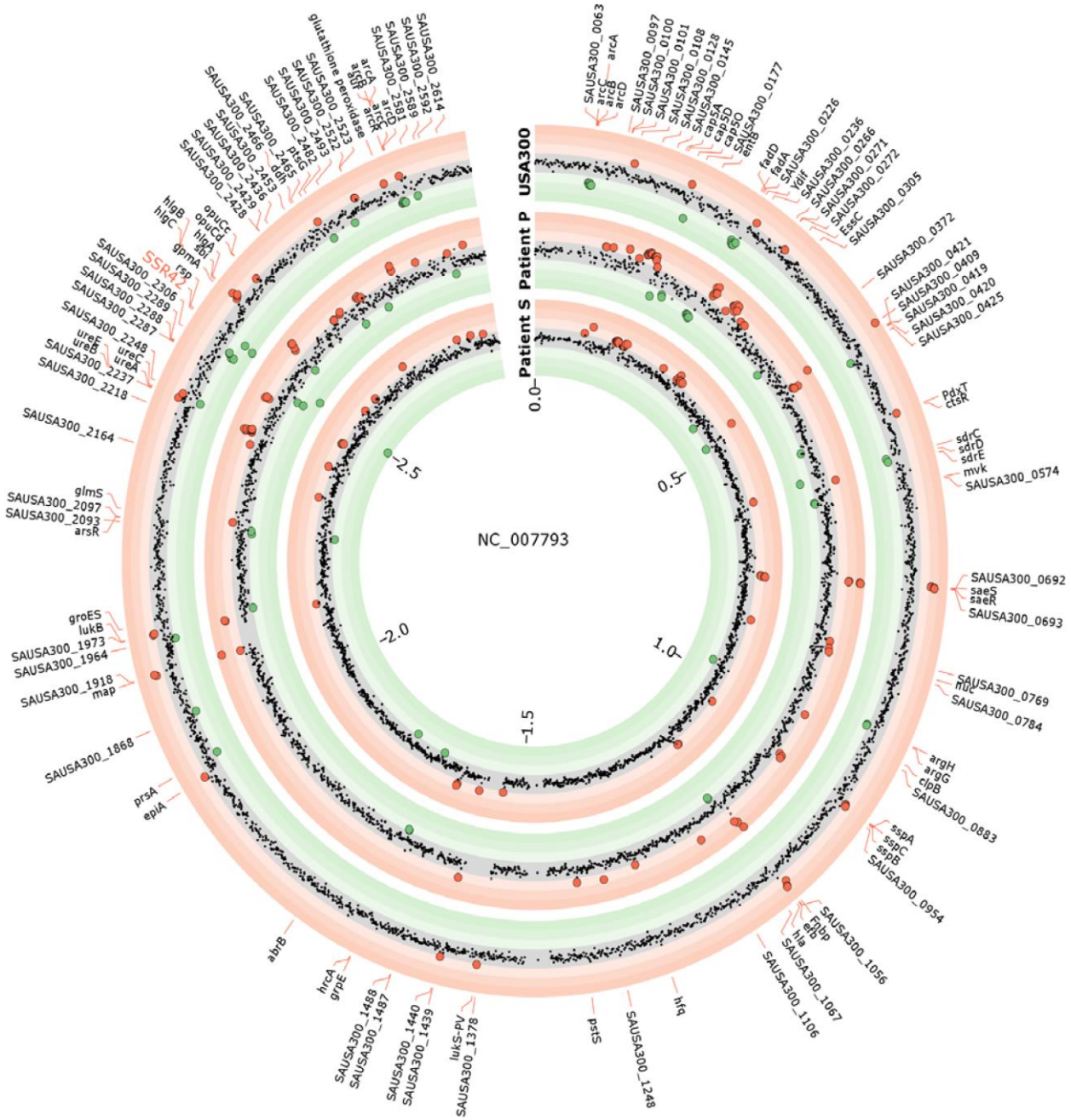

Figure 16: The effect of *rsp* mutation on *S. aureus* transcription

Gene expression (in two replicates) in stationary growth phase. Transcripts were mapped against the USA300 JE2 genome (NC_007793). Red rings indicate significant $\log_2$ fold upregulation, green rings significant repression by the mutant (Rsp^-) relative to the wild type (Rsp^+) within each strain background (outer ring: USA300, central ring: Patient P, and inner ring: Patient S) [Strains are described in 1.3.3]. Differential gene expression was analysed using the DESeq2 package in R [Method described in 1.3.19]. The most affected non-coding RNA SSR42 is labelled in red letters. Dr. Julius Müller kindly provided this figure.

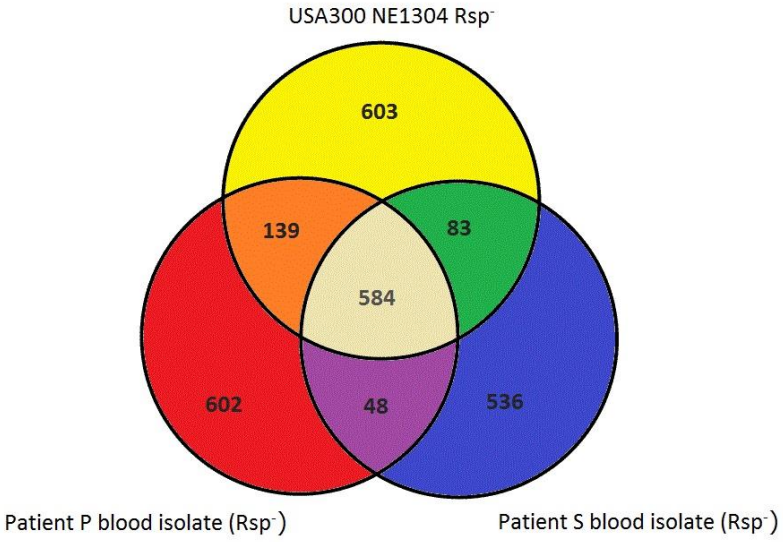

Figure 17: Upregulated genes in Rsp$^-$ strains when compared to Rsp$^+$ strains

Gene expression of USA300 NE1304 Rsp$^-$, Patient P and S blood isolates (Rsp$^-$) was compared to expression in *rsp* wild type strains USA300 JE2 Rsp$^+$, Patient P and S nasal isolates (Rsp$^+$), respectively. Numbers of upregulated genes specific to each strain and strain overlapping are displayed.

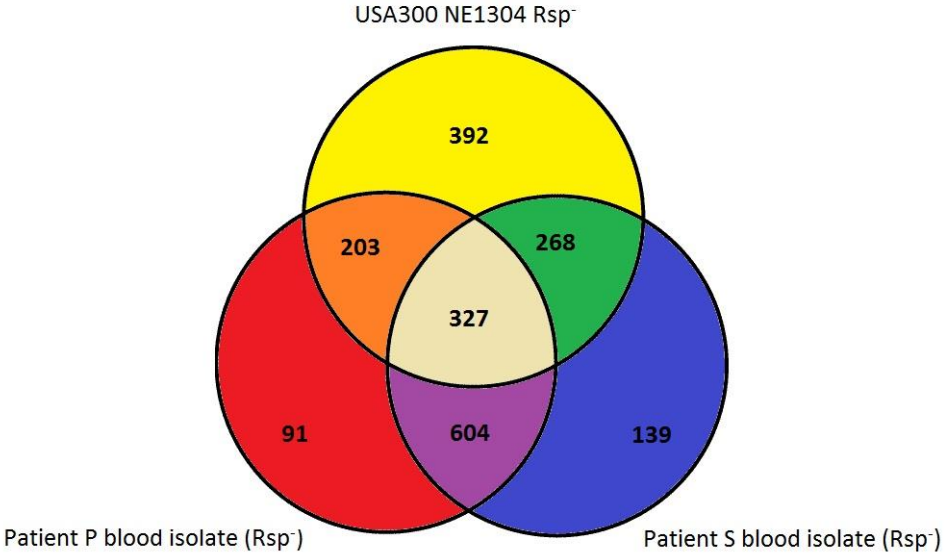

Figure 18: Downregulated genes in Rsp$^-$ strains when compared to Rsp$^+$ strains

Gene expression of USA300 NE1304 Rsp$^-$, Patient P and S blood isolates (Rsp$^-$) was compared to expression in *rsp* wild type strains USA300 JE2 Rsp$^+$, Patient P and S nasal isolates (Rsp$^+$), respectively. Numbers of downregulated genes specific to each strain and strain overlapping are displayed.

Among the genes upregulated in *rsp* mutants (Table S4), we see enrichment for genes involved in pathogenesis (Figure 19). For instance, *map* (2.6 fold-change), an immunomodulatory molecule (81), *nuc* (1.74 fold-change), a nuclease capable of lysing Neutrophil Extracellular Traps (37), the immunoglobulin-binding protein *sbi* (82) (2.33 fold-change), and capsule biosynthesis genes (≥ 2 fold-change), whose product impedes phagocytosis (83) are also highly upregulated. Genes influenced by Rsp also include reported complement inhibitors such as extracellular proteases *sspABC* (84) (≥ 1.74 fold-change), the extracellular fibrinogen binding protein *efb* (85) (4.23 fold-change), complement regulator binding protein *sdrE* (86) (≥ 1.87 fold-change) and the protease aureolysin *aur* (87) (2.3 fold-change). Genes associated with adhesion to squamous cells and colonization were found to be downregulated (*sdrCD* (88) (0.55 and 0.85 fold-change respectively). The largest change in gene transcription was observed in the long non-coding RNA SSR42 (89), which was not expressed in Rsp-deficient strains.

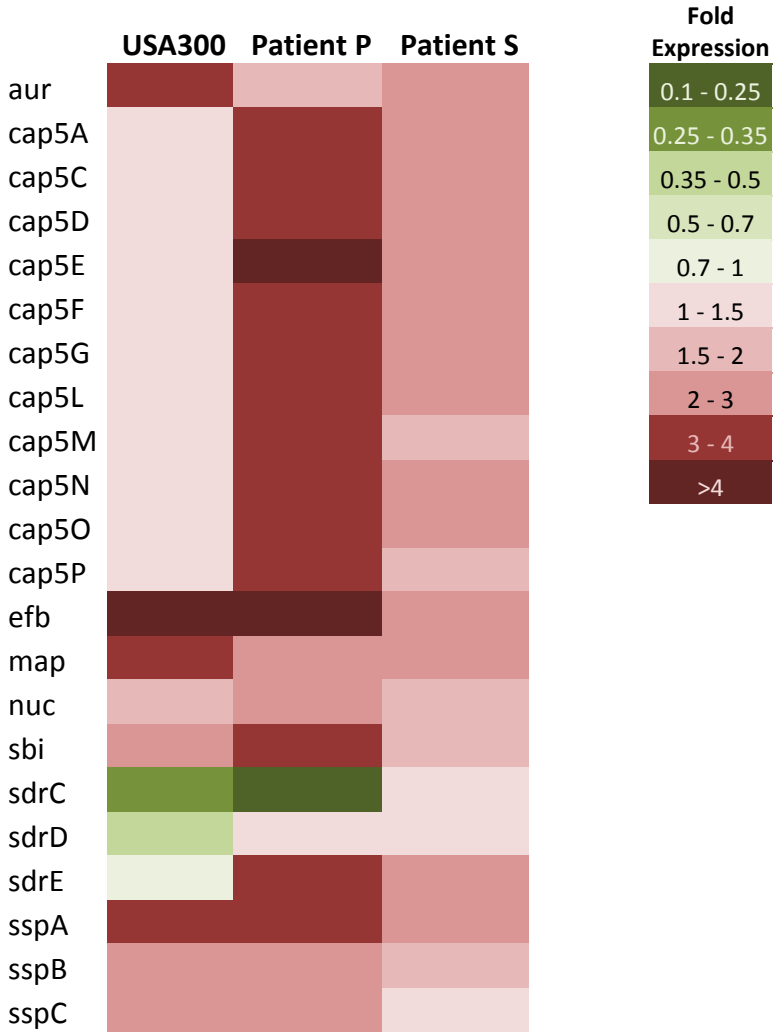

Figure 19: Heatmap of genes affected by *rsp* mutation *in vitro*

Downregulated (green) and upregulated (red) genes in USA300 NE1304 (Rsp^-), Patient P and S blood isolates (Rsp^-) when compared to *rsp* wild types USA300 JE2 (Rsp^+), Patient P and S nasal isolates (Rsp^+), respectively.

1.4.6 Repressor of surface proteins (Rsp) influences the Abundance of Secreted Proteins

Rsp affects gene transcription of many secreted proteins (published data: http://www.pnas.org/content/113/22/E3101.abstract?tab=ds, Supplementary Dataset S4, (59)). Hence, I tested whether the effect of Rsp on transcripts was detectable at protein level in the supernatant of bacterial cultures. First, I compared detection sensitivity in two culture media: TBA, a complex growth media of variable composition, and αMEM, a defined protein-free growth media (Fig. 20).

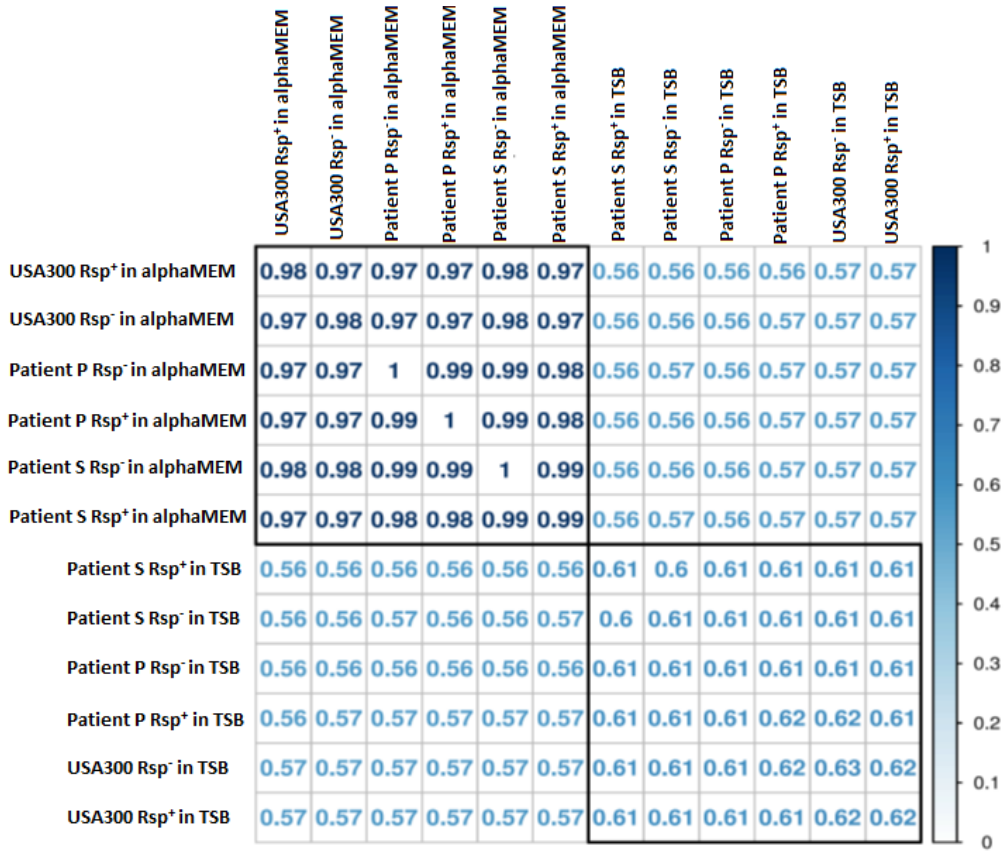

Figure 20: Secreted proteome of three strains and their corresponding *rsp* mutants

Supernatants of stationary phase bacterial cultures (USA300, Patient P and S) [strains described in 1.3.3] grown in either TSB or αMEM [Method described in Section 1.3.12 -15]. In total, 651 of the 2,604 *S. aureus* proteins were identified in the supernatant. Numbers shown reflect proportion of detected proteins. "1" reflects detection of all 651 proteins.

Growth in αMEM enhanced sensitivity of protein detection over growth in TBA (Fig. 20) and was used for the proteome analysis. Differences between the secreted proteome of *rsp* mutants (Rsp^-) and their respective wild types (Rsp^+) in the USA300, Patient P and Patient S lineages were present and similar. A high proportion (113/636, 18%) of the proteins in the supernatant of any of the strains analysed was affected by *rsp* mutation (published data: Supplementary Dataset S4, http://www.pnas.org/content/113/22/E3101.abstract?tab=ds, (59)). Immune evasion proteins such as nuclease (*nuc*, (37)) and the extracellular fibrinogen binding protein (*efb*, (85)) were found in higher abundance in the Rsp^- supernatants compared with the Rsp^+ supernatants, confirming the tendency indicated by the RNA Sequencing results. However, toxins (α- haemolysin Hla, γ- haemolysin components HlgA-C, the Panton-Valentine Leucocidin LukS, and LukAB (also known as LukGH (43)) had decreased abundances in Rsp^- organisms, as did the neutrophil chemotaxis inhibitor CHIPS (*chs* gene product) (Fig. 21A, are shown for USA300 NE130 Rsp^- representatively). This indicates that there is concordance between mRNA and protein levels of an Rsp induced effect for some proteins but not others.

Subsequently, I compared secreted protein abundances with intracellular RNA levels in stationary phase (Fig. 21B) and some proteins showed increased abundancy as their upregulated gene expression had indicated, while others were less abundant as their decreased levels of detected mRNA had predicted. For a subset of genes, including the toxins *hla*, *luk*B, and *hlg*B, stationary phase RNA abundance increased in *rsp* mutants while protein levels decreased in them.

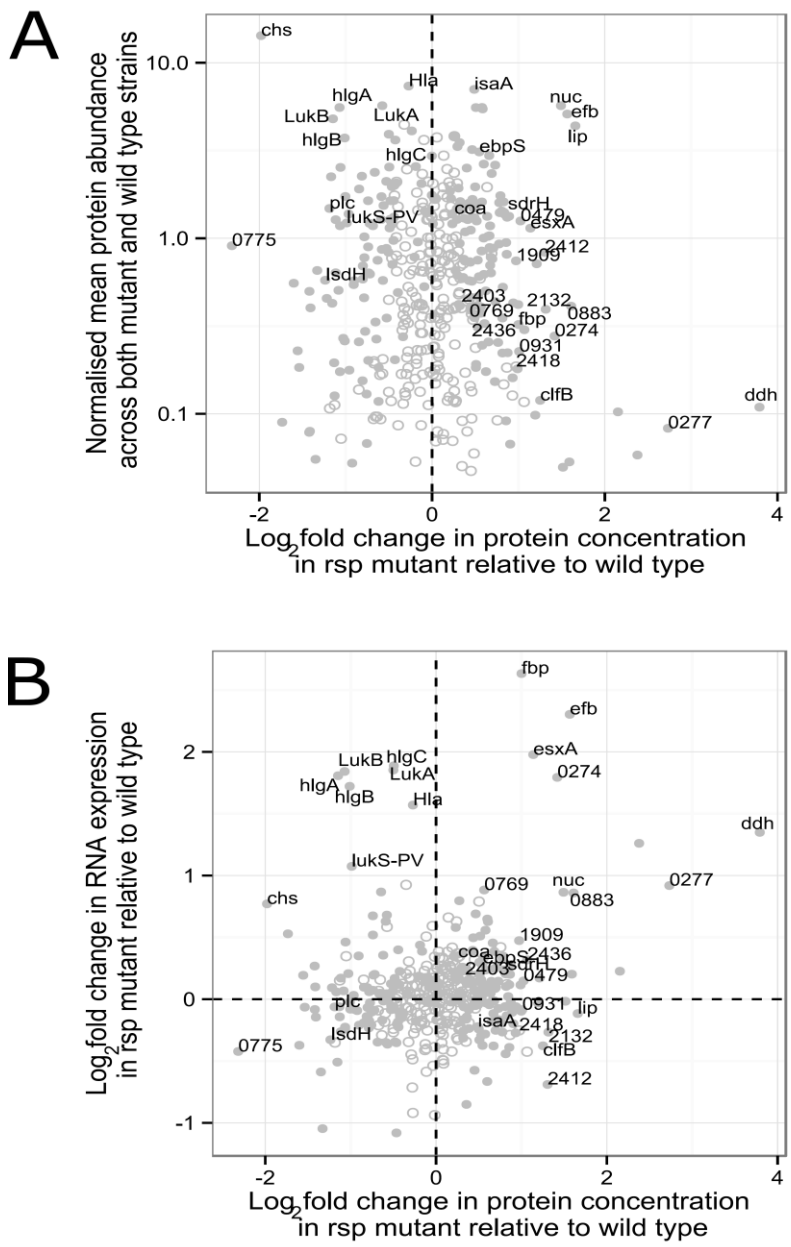

Figure 21: Secretome versus transcriptome in the stationary growth phase of *S. aureus* USA300

Fold change in secreted protein concentration of *S. aureus* USA300 NE1304 Rsp^- relative to *S. aureus* USA300 JE2 Rsp^+ (x-axis) is compared to **A**) protein abundance and **B**) fold change of RNA expression (y-axis) at the same time point [Methods described in 1.3.10 -15 and 1.3.19]. Each dot represents a gene/the protein it encodes; numbers denote locus identifiers, e.g. 0274 refers to SAUSA300_0274. Open circles indicate that the effect of Rsp is not significant (q>0.05) for this gene/protein, whereas closed symbols indicate that the effect of Rsp is significant on that gene/protein. The dotted lines indicate where *rsp* mutation has no effect (59).

In Figure 21 (B) the upper right quadrant identifies genes, which are increased in RNA as well as protein level. The upper left quadrant shows genes with increased RNA expression, but lower levels of protein in stationary phase. Some toxins, including Hla, HlgA, HlgC, and LukB fall into this category. Thus, Rsp has pleiotropic effects on the bacteria, inducing some virulence factors (such as toxins) and significantly reducing the concentrations of others known to be involved in pathogenesis and complement evasion, including the ESAT-6 homologue EsxA, nuclease (37) and the complement control protein Efb (85).

Finally, when looking at genes which were >2-fold upregulated or downregulated, there is a divergence between the extent of protein and gene expression. Only a few up- or downregulated secreted proteins are being up- or downregulated at gene expression level to the same extent (Figure 22 below).

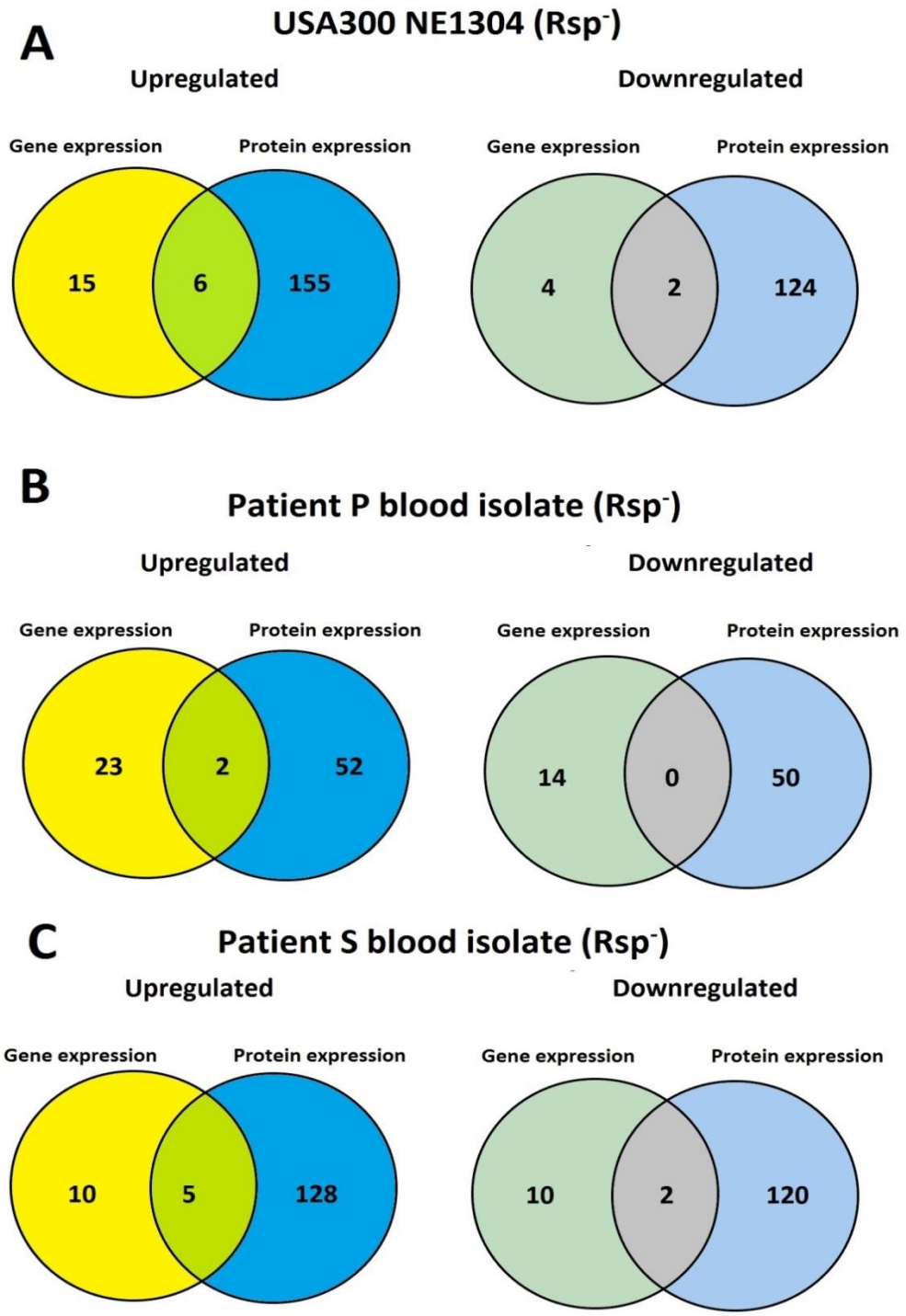

Figure 22: Comparison of gene and protein expression in three *rsp* mutants *in vitro*

Number of genes which are upregulated (>2-fold upregulation, left diagram) or downregulated (>2-fold downregulation, right diagram) in gene and protein expression *in vitro* in **A** USA300 NE1304 (Rsp$^-$) **B** Patient P blood isolate (Rsp$^-$) and **C** Patient S blood isolate (Rsp$^-$) when compared with their respective *rsp* wild types. [Methods described 1.3.10 – 1.3.15 and 1.3.19; Strains described in 1.3.3]

1.4.7 *S. aureus rsp* mutants show increased Urease Activity

Rsp influences gene expression as well as protein abundance in *S. aureus*, as quantified through mRNA (Chapter 1, [1.4.5]) and protein analysis (Chapter 1, [1.4.6]). To test whether these altered protein levels would eventually lead to changes in enzymatic activity of expressed enzymes depending on bacterial *rsp* status, I performed kinetical assays on two secreted *S. aureus* enzymes.

The heterotrimeric urease, has been described as a virulence factor in *S. aureus* and other pathogens (90). Its transcripts' (*ureABC*) proportions are increased in *rsp* mutants *in vitro.* Urease catalyses the hydrolysis of urea to ammonium and carbonic acid that leads to the release of carbon dioxide. Its activity can be measured through changes in the pH of the media caused by the dissolved ammonium (Fig. 23).

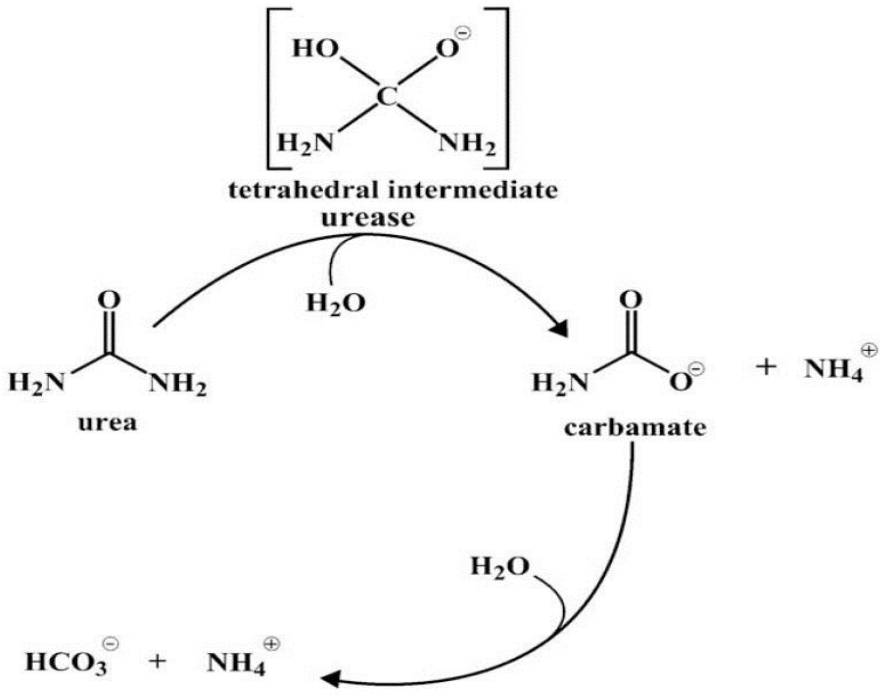

Figure 23: Hydrolysis of urea to carbon acid and ammonium, catalysed by urease.

This figure was adapted from Konieczna *et al.*, 2012 (90).

Christensen's urease assay medium contains urea and phenol red to indicated urea dependent pH elevation. Christensen's media without urea was used as a control for each test strain (*S. aureus* USA300, Patient P and Patient S) and control strain (urease-positive: *P. mirabilis*, urease-negative: *E. coli*) (Fig. 24A-D).

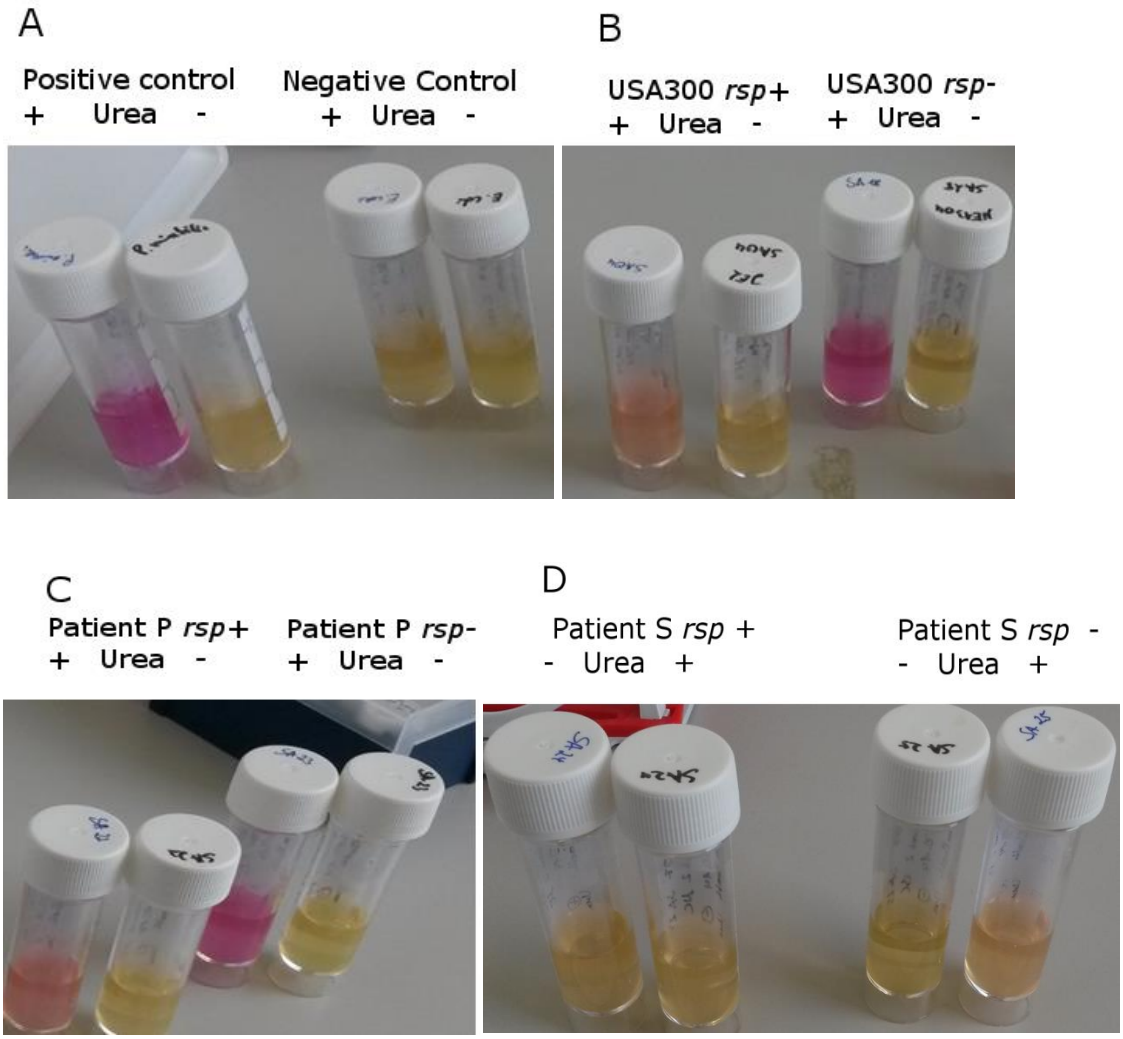

Figure 24: Urease activity assay

Photos show overnight cultures grown in Christensen's media [Method described in Section 1.2.16]. For every strain a sample incubation tube (left) is compared with a control tube without urea (right) of **A** *P. mirabilis* and *E. coli*, **B** USA300 JE2 Rsp^+ (left) and USA300 NE1304 Rsp^- (right), **C** Patient P nasal isolate (Rsp^+) (left) and blood isolate (Rsp^-) (right) and **D** Patient S nasal isolate (Rsp^+) (left) and blood isolate (Rsp^-) (right).

When grown overnight in Christensen's broth, all three *rsp* mutants (USA300 NE1304 Rsp^-, Patient P blood isolate Rsp^- and Patient S blood isolate Rsp^-) showed a urea dependent higher pH than their respective *rsp* wild types (USA300 JE2 Rsp^+, Patient P nasal isolate Rsp^+ and Patient S nasal isolate Rsp^+) (Fig. 24A-D). The positive control (Fig. 24A) indicates the colour change observed in media containing urease positive bacteria. For *S. aureus* USA300 (Fig. 24B), the *rsp* negative wild type exhibits only small urea dependent colour change overnight. In comparison, the *rsp* mutant culture was of pink colour, indicating a high pH (>7.3). Patient P background samples (Fig. 24C) show a similar Rsp-dependent change in urease activity. In the Patient S background (Fig. 24D) there is also an increase of urease activity in *rsp* mutants compared to wild type Patient S, but the difference is much smaller and the baseline urease activity not-detectable using this method. Therefore, the absorbance of the broth was measured (A_{560}), where phenol red has its maximum absorbance for pH >7.3, after sterile filtration (Fig. 25). The negative control (yellow bars, *E. coli* culture) showed an absorbance around A_{560} = 0.25 in presence of urea, the positive control around A_{560} = 1.1. USA300 Rsp^+ shows absorbance values close to the negative control, whereas USA300 Rsp^- absorbance is almost level with the positive control (green bars, Student's t-test: p-value<0.001). In Patient P (blue bars) basal urease activity of Patient P Rsp^+ is higher than USA300 Rsp^+. However, an Rsp-dependent increase in urease activity is observed in Patient P as well (Student's t-test: p-value<0.001). In Patient S (red bars), the effect of Rsp on the urease activity is small, but statistically significant (Student's t-test: p-value <0.001).

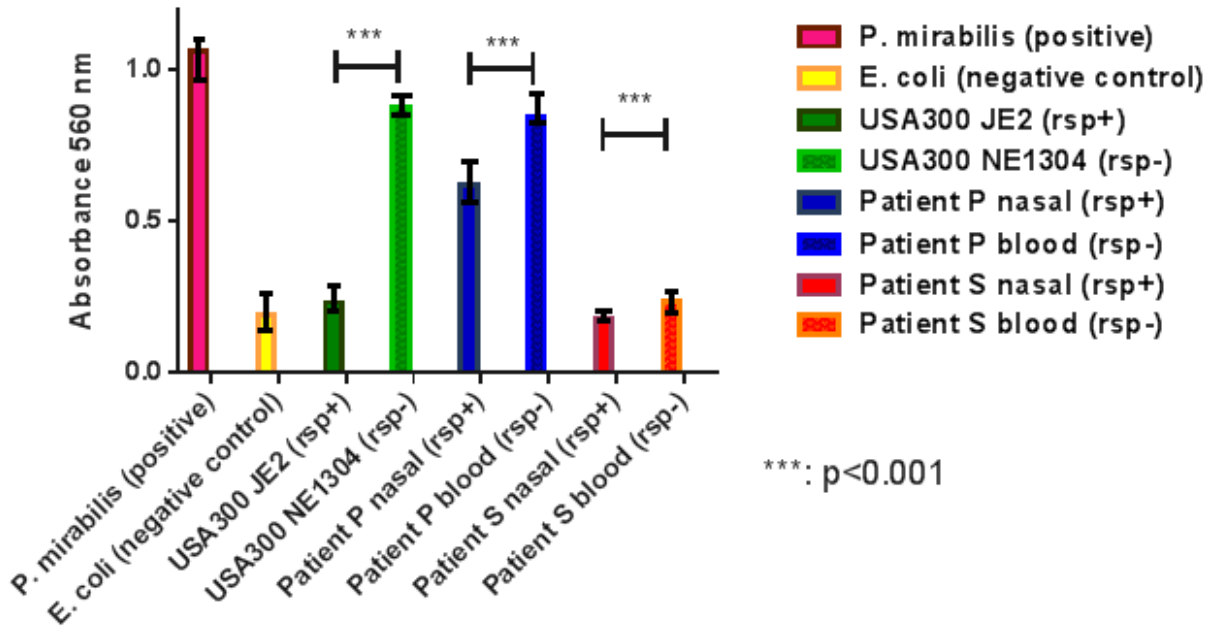

Figure 25: Urease activity assay: Absorbance at 560 nm

Absorbance at 560 nm of Christiansen's broth with urea after overnight growth of *P. mirabilis* (pink bar), *E. coli* (yellow), *S. aureus* USA300 (green), *S. aureus* Patient P (blue) and *S. aureus* Patient S (red) [Strains described in 1.3.3; Method described in 1.3.16]. Differences from three independent experiments were assessed using a Student's t-test (USA300: p = 0.0000002, Patient P: p = 0.0000005, Patient S: p = 0.0001), error bars showing the standard error are displayed for each value.

In conclusion, an Rsp-dependent effect on urease activity *in vitro* is observed in all three *S. aureus* strains, but the extent of this effect depends on the genetic background.

1.4.8 Rsp-dependent D-lactate Dehydrogenase Activity in Culture

In *rsp* mutants, some secreted proteins were found in increased abundance in the supernatant (Chapter 1, [1.4.6, Fig. 21]). The protein with highest change in concentration was D-lactate dehydrogenase (Ddh). Ddh is one of three lactate dehydrogenases (Ldh1, Ldh2 and Ddh) in *S. aureus* (91) and it catalyses the NAD^+/NADH dependent balance reaction between lactate and pyruvate. Lactate-dehydrogenases in *S. aureus* have been reported to play a crucial role in the $NO^\bullet$ radical response, enabling the bacteria to maintain redox homeostasis in environments with high nitrosative stress such as within phagocytes (92).

In order to determine differences in Ddh activity between *rsp* mutants (Rsp^-) and wild type (Rsp^+), I compared sterile filtered supernatants from three genetic backgrounds: USA300, Patient P and Patient S (Fig. 26). Rsp^- culture supernatant displayed significantly higher enzyme activity in all 3 strains ($p=0.026$, $p=0.012$ and $p=0.043$, respectively).

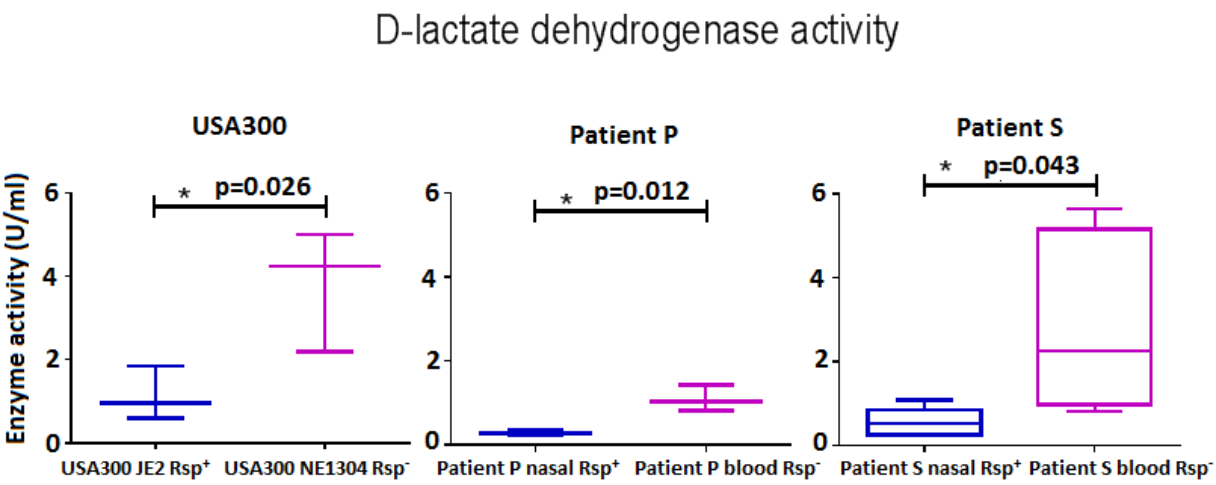

Figure 26: Ddh activity assay

Boxplot showing Ddh activity in bacterial culture supernatants (Units/ml) for Rsp^+ (blue) and Rsp^- (purple) in USA300 (left), Patient P (centre) and Patient S (right) [Strains described in 1.3.3; Method described in 1.3.17]. *p*-values were calculated using a Student's t-test [Method described in 1.3.17].

Mutation of *rsp* leads to increased abundance of D-lactate dehydrogenase (Chapter 1, [1.4.6, Fig. 21]) and to increased enzymatic activity (Fig. 26). The effect size of the mutation on the activity was dependent on the strain, like previously observed. Patient P Rsp^+ showed lower levels of Ddh activity than USA300 Rsp^+ and Patient S Rsp^+ (Patient P Rsp^+: 0.25 U/ml compared to USA300 Rsp^+: 1.1 U/ml, Patient S Rsp^+: 0.9 U/ml). However, the factor by which enzyme activity increased in *rsp* mutants was similar in all three strains, between 3 to 5 (USA300 Rsp^-: x3.3, Patient P Rsp^-: x3.9 and Patient S Rsp^-: x5.4).

1.4.9 Repressor of surface proteins affects Complement Activation *in vitro*

rsp mutation changes the outcome of *S. aureus* intravenous infection (Chapter 1, [1.4.3]). Lethality and disease symptoms in the intravenous infection model are reduced for mice infected with Rsp^- strains and this indicates potentially altered interaction with the immune system. As differential lethality is observed early after infection (2-3 days) in mice previously unexposed to *S. aureus*, I hypothesized that detection of Rsp^- *S. aureus* by the innate immune system might be altered.

In an *in vitro* assay, I tested the inhibitory effect of bacterial supernatant from Rsp^- and Rsp^+ strains on serum complement activation. After incubation of serum with the supernatants, capability of activation of all three pathways was tested (Chapter 1, [1.3.18]). For the three strains tested (USA300, Patient P and Patient S) there was no difference found between Rsp^- and Rsp^+ strain capacity to inhibit complement activation via the classical pathway (Fig. 27A-C). The ID_{50} resulting from the inhibitor dose-response curves allowed statistical comparison resulting in no significance (Table 4). Activation of the MBL pathway was indifferent for serum incubated with USA300 and Patient P Rsp^- or Rsp^+ serum (Fig. 28A-C). However, decrease of complement activation in the Patient S strain was found in Patient S blood isolate (Rsp^-) compared to Patient S nasal isolate (Rsp^+), but this effect was strain dependent (Table 4), as it is only observed in one strain. Yet, when testing the *in vitro* activation of complement system via the alternative pathway (Fig. 29A-C), Rsp^- strain supernatant exhibit reduced capability of inhibiting initiation of the cascade across all three strains compared with Rsp^+ supernatant. ID_{50} values for Rsp^- are significantly higher than Rsp^+ (Table 4).

Table 4: ID_{50} values and 95% confidence intervals for fold concentration of bacterial supernatant required for inhibition of serum complement activation

Pathway	Strain	Rsp+/-	ID_{50}	95% CI
Classical	USA300	+	9.18	8.43 - 9.92
		-	10.40	9.44 – 11.36
	Patient P	+	19.50	14.06 – 23.45
		-	13.16	11.14 – 15.18
	Patient S	+	8.14	7.04 – 9.60
		-	9.86	8.78 – 10.94
Lectin (MBL)	USA300	+	7.71	6.94 – 8.47
		-	9.39	8.58 – 10.20
	Patient P	+	10.70	8.75 – 12.64
		-	11.53	10.31 – 12.76
	Patient S	+	6.74	5.02 – 8.47
		-	10.10	9.35 – 10.86
Alternative	USA300	+	0.69	0.65 – 0.72
		-	1.51	1.43 – 1.58
	Patient P	+	0.95	0.90 – 1.01
		-	2.54	1.88 – 3,19
	Patient S	+	0.66	0.63 – 0.70
		-	0.93	0.84 – 1.03

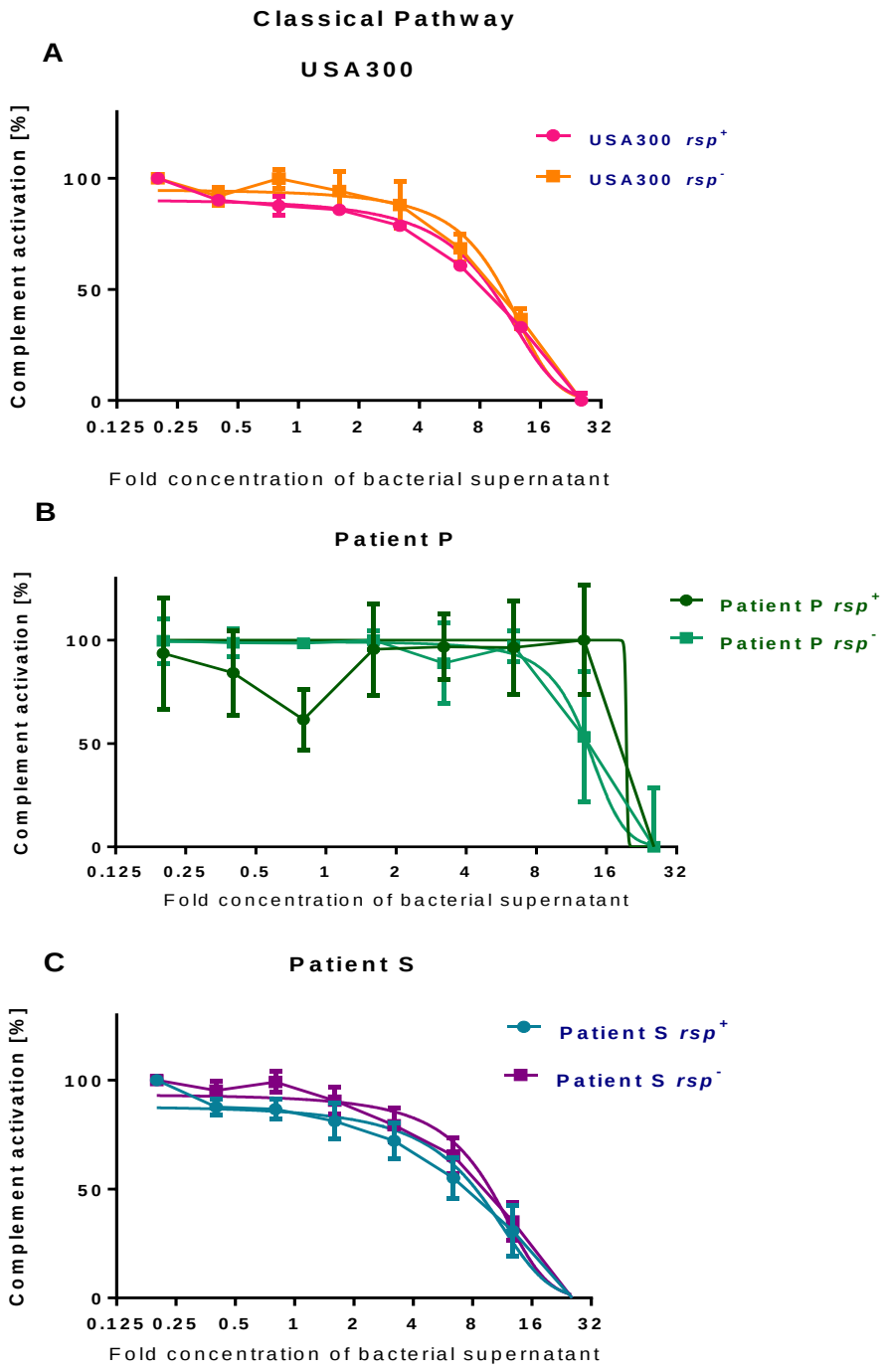

Figure 27: Comparison of classical complement pathway activation by Rsp$^-$ and Rsp$^+$ *S. aureus* strains

Activation of serum complement classical pathway *in vitro* [y-axis: %] after incubation with bacterial supernatant from **A** USA300, **B** Patient P and **C** Patient S overnight cultures (x-axis: Fold concentration of bacterial supernatant) [Strains described in 1.3.3; Methods described in Sections 1.3.18-19].

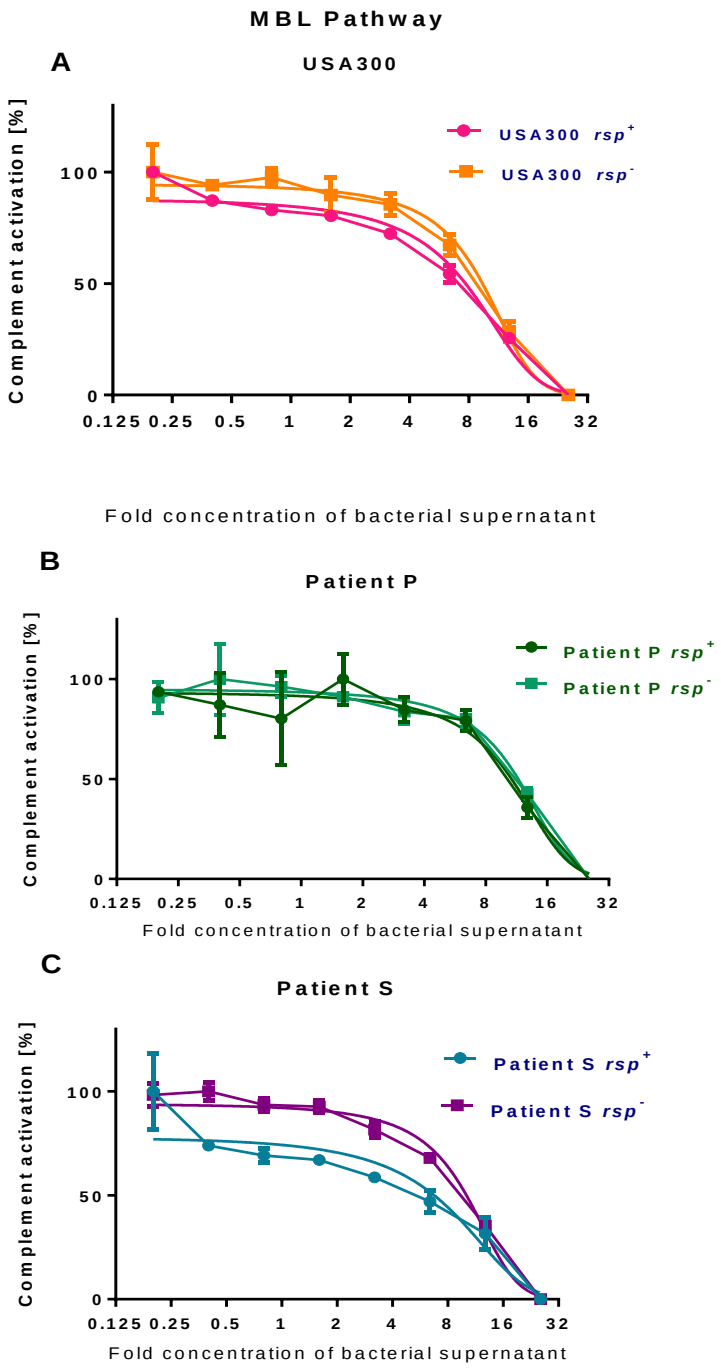

Figure 28: Comparison of Mannose-Binding-Lectin complement pathway activation by Rsp$^-$ and Rsp$^+$ *S. aureus* strains

Activation of serum complement MBL pathway *in vitro* [y-axis: %] after incubation with bacterial supernatant from **A** USA300, **B** Patient P and **C** Patient S overnight cultures (x-axis: Fold concentration of bacterial supernatant) [Strains described in 1.3.3; Methods described in Sections 1.3.18-19].

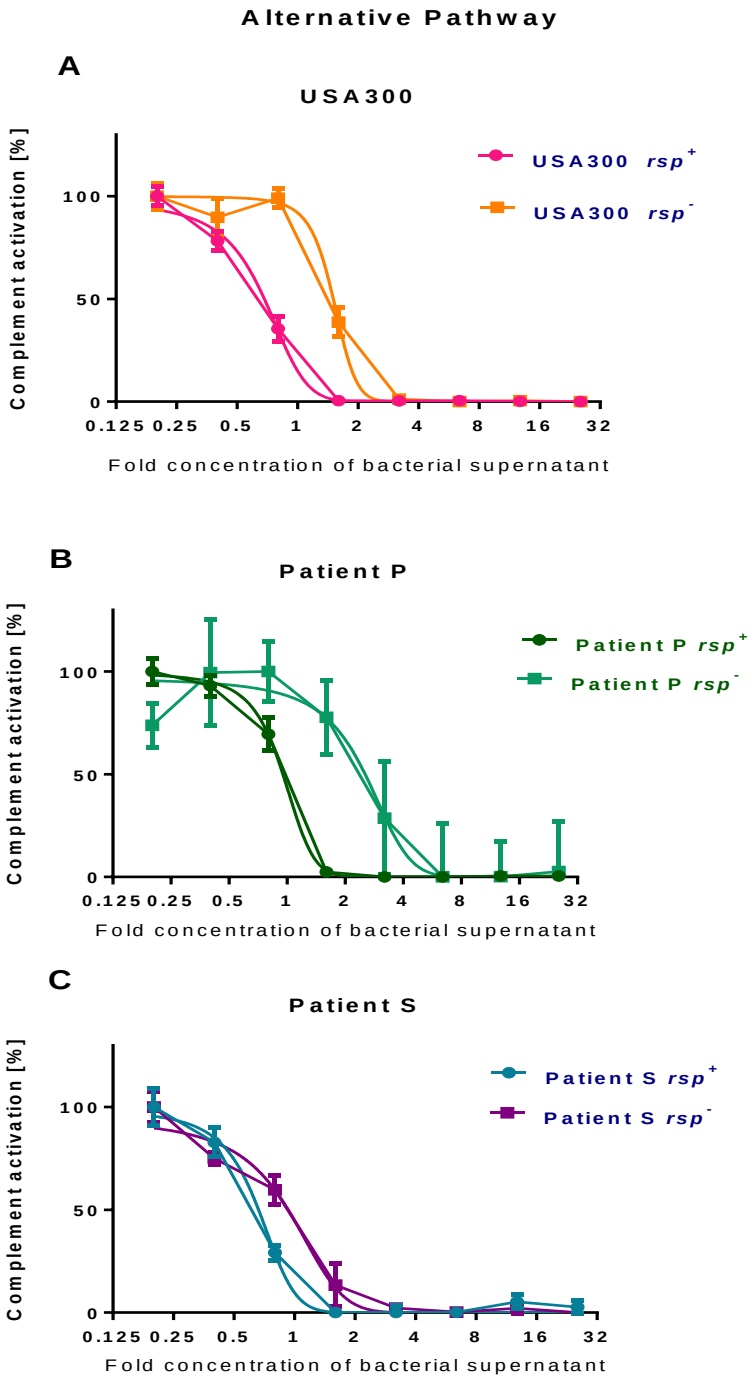

Figure 29: **Comparison of alternative complement pathway activation by Rsp$^-$ and Rsp$^+$ *S. aureus***

Activation of serum complement alternative pathway *in vitro* [y-axis: %] after incubation with bacterial supernatant from **A** USA300, **B** Patient P and **C** Patient S overnight cultures (x-axis: Fold concentration of bacterial supernatant) [Strains described in 1.3.3; Methods described in Sections 1.3.18-19].

1.4.10 Repressor of surface proteins (Rsp) regulated Antigens

Mutations in the transcription regulator *rsp* can be found in *S. aureus* bloodstream infections of patients with intact genes in their nasal strain (58). The bacterial phenotype displayed by Rsp$^-$ *S. aureus in vitro*, which was described in this chapter, might represent a phenotype favoured in bloodstream infections. As a result, extracellular or membrane-bound antigens presented in this state might be accessible to the host immune system. Enriched proteins in the exo-proteome analysis represent a pool of such antigens, as they might play a role in the establishment or maintenance of bloodstream infections, if they were expressed during infection, and would therefore make good vaccine targets for a sepsis preventing immunisation strategy. In addition, conservation across strains is important to assure a wide range of protection. Based on these criteria, six new antigens were proposed as new vaccine candidates (Table 5).

Table 5: **Rsp-repressed vaccine antigens**

Locus tag	Gene name
SAUSA300_0274	Membrane bound hypothetical protein
SAUSA300_0277	*ssaA*, putative staphyloxanthin biosynthesis protein
SAUSA300_0279	*esaA*, Type 7 secretion complex protein (partially transmembrane)
SAUSA300_0307	5'- nucleotidase
SAUSA300_0769	Putative lipoprotein
SAUSA300_2403	Putative lipoprotein

The student Ritu Mann-Nuettel, as part of her master project, tested the immunogenicity of the six proposed antigens, through detection of serum antibodies in 42 healthy volunteers (19 *S. aureus* carriers, 23 non-carriers). She expressed the proteins in *E. coli* and quantified recognition through immunoglobulins. Two ("SAUSA300__0277" and "SAUSA300_0307") out of the six antigens were recognised.

1.5 Discussion

In this study, I have shown that naturally occurring *rsp* mutants (58) in *S. aureus* with reduced cytotoxicity (50) cause altered disease symptoms and lethality in a murine infection model. The mutations in *rsp* execute global changes in gene expression and protein production, leading to differential enzyme activity. The Rsp-dependent phenotypic changes lead to altered interaction with the human complement system, while maintaining the ability to survive, proliferate and cause disseminated infection within the human body.

The transcription regulator Rsp (61), a member of the AraC family of transcriptional regulators, was mutated in bloodstream *S. aureus* isolates from patients, separating them genetically from their nasal *S. aureus* isolates. Previous studies have indicated, that Rsp plays a crucial role in biofilm suppression (61) and cytotoxicity (50) *in vitro*. Cytotoxicity of *S. aureus* is now commonly associated with bloodstream infection, for example through dysfunction of the transcription regulator *agr*, frequently found to be mutated in invasive disease leading to low cytotoxic strains (53, 54, 93). Here I investigated the behaviour of *rsp* mutants and observed no change of bacterial capability to grow in broth (Chapter 1, [1.4.1]) or *ex vivo* in human blood (Chapter 1, [1.4.2]). The indifferences of *in vitro* bacterial growth indicate that the phenomenon of *rsp* mutant isolation from human blood might not be due to growth advantages.

Despite not presenting altered growth, *rsp* mutants exhibit differences *in vivo*. When injected intravenously, mice infected with blood isolates (Rsp^-) develop less severe disease symptoms and weight loss during the first three days of infection compared

to mice infected with the respective nasal strains. Infected mice also succumb slower to infection (Chapter 1, [1.4.3]). These results were unexpected, as one would predict invasive bacterial strains to be more lethal than their colonizing counterparts in an invasive disease model. However, I observed that nasally isolated bacteria showed higher lethality than bacteria isolated from blood in the murine sepsis model. These results were confirmed by collaborators (group of Martin Fraunholz, University of Würzburg, Germany), who tested *rsp* mutants and wild types in a murine pneumonia model (59). While this study was underway, other research groups (group of Michael Otto, NIH Bethesda, United States of America and Min Li, Shanghai Jiao Tong University, China) performed independent experiments with *rsp* mutant strains of different genetic background (USA400 and USA500). They show an Rsp-dependent state of acute virulence in murine bacteraemia and reduced lethality in mice infected with Rsp^- *S. aureus* compared with Rsp^+ strains (94). They also demonstrate reduction of skin lesion size when *rsp* mutants are inoculated intradermally compared with intradermal inoculation of *S. aureus rsp* wild type. Their experiments provide further evidence that lethality and disease symptoms are affected in an Rsp-dependent manner. However, at this point the precise function of Rsp cannot be explained, yet.

In the murine sepsis model used, quantifying bacterial loads in murine tissue and abscess formation in kidneys are well-established ways of comparing bacterial infectivity (79). Due to the reduced weight loss, disease symptoms and lethality observed in murine intravenous infections through the *S. aureus rsp* mutant, less bacterial tissue load and abscess formation was expected. However, upon quantifying liver, renal and spleen load, no difference in bacterial tissue load

between Rsp^- and Rsp^+ *S. aureus* infected tissue was detected. In addition, Rsp^- and Rsp^+ strains were indifferent in their capability to form abscesses (Chapter 1, [1.4.4]), which was equal for blood isolated Rsp^- and nose isolated Rsp^+ strains in renal tissue of mice. These results imply that *rsp* mutation does not alter bacterial dissemination in the bloodstream or bacterial abscess formation in murine renal tissue. Bacterial numbers and differences in abscess formation or structure do not explain the changes in disease and lethality observed.

The phenotype *rsp* mutants exhibit *in vitro* and *in vivo* suggest major differences in the molecular phenotype of these bacteria. At gene expression level, RNA Sequencing shows differences across the whole bacterial genome at stationary growth phase (Chapter 1, [1.4.5]), in particular for toxins (α – and γ - haemolysins, leukocidins), adherence and immune evasion proteins (fibronectin binding protein, extracellular adhesion protein). An Rsp-dependent gene expression effect on a non-coding RNA, annotated SSR42, was found. Transcripts of this longest known ncRNA in *S. aureus* were absent when the *rsp* gene was mutated, raising the possibility that some of Rsp-dependent gene expression might be conferred through SSR42, as previously suggested (89). Synergy of SSR42-mediated effects with direct effects of Rsp itself, such the recently demonstrated binding of Rsp to the *agr* promoter, may also occur (94).

The expression differences described in this chapter were complemented and confirmed by collaborators using RNA Sequencing (in exponential phase) in addition to Real Time PCR (59). They show that Rsp-dependent gene expression is influenced by the bacterial growth phase, with the above mentioned toxins being down-regulated in the exponential and up-regulated in the stationary growth phase.

At protein level, some of the transcriptional differences were confirmed in the secreted proteome of stationary bacteria (Chapter 1, [1.4.6]). I found immune evasion factors as well as uncharacterised proteins in higher abundance in Rsp^- supernatant than in the Rsp^+ supernatant. However, toxin abundance was reduced in Rsp^- supernatant compared to Rsp^+. This discordance between transcript and protein levels suggests the existence of post-transcriptional control(s) (95) on toxin secretion. In addition to that, I measured activities for urease (Chapter 1, [1.4.7]) and D-lactate dehydrogenase (Chapter 1, [1.4.8]), which were both increased in Rsp^- when compared with Rsp^+, as predicted by increased gene expression and protein abundance in the previous experiments and thereby confirming the transcriptomic and proteomic results.

Collaborators confirmed altered toxin expression through functional assays and showed decreased haemolysis as well as diminished intra- and extracellular cytotoxicity in Rsp^- strains compared with Rsp^+ strains (59). Our collaborators also demonstrated that lower intracellular toxicity causes a delay in release of Rsp deficient bacteria from epithelial cells and neutrophils. Reduced intracellular toxicity might lead to differential host-pathogen interaction through prolonged intracellular persistance. Recently, the intracellular space was identified to be crucial for bacterial survival of *S. aureus* in bloodstream infection (23). In summary *S. aureus* might adopt an attenuated cytotoxic phenotype, mediated by Rsp, as described above. An attenuated cytotoxic phenotype prolongs intracellular residence (96-98), which permits effective dissemination of the organism with few initial disease symptoms of the host, followed by deep abscess establishment.

Furthermore, mice infected with *rsp* mutants display reduced disease symptoms. I therefore hypothesized altered interaction of Rsp^- strains compared with Rsp^+ strains with the host immune system. *S. aureus* possesses a variety of complement activation inhibitors: These include proteases (*sspABC* (84)), extracellular fibrinogen binding protein (*efb* (85)), surface protein SdrE (*sdrE* (86)) and aureolysin (*aur* (87)), which all showed elevated transcription and protein abundance in Rsp^- strains compared with Rsp^+ strains. Interestingly, no difference in inhibition of the cascade was found via Classical and Lectin (MBL) pathway activation, indicating, that the common pathway of the cascade (from C3 to the membrane attack complex) is not affected. However, reduced capability of Rsp^- strains compared with Rsp^+ strains to inhibit Alternative pathway activation suggests diminished inhibition by its supernatant. Proteins such as Sbi, which has been reported to induce futile complement consumption (99), avoiding C3b deposition on the bacterial surface and thereby escaping recognition, might influence this observation. On the other hand, increased complement activation and recognition of the bacterial cell might improve the bacteria's chances to reach an intracellular niche, in which *rsp* mutants persist longer (59).

In addition, our collaborators found *rsp* transcription induced by hydrogen peroxide (59), which is produced by neutrophils *in vivo* upon stimulation. This suggests a model in which Rsp fulfils an environment-sensing role: on encountering phagocytes, it initiates a specific response that consists of virulence factors that target phagocyte functions, including α and γ haemolysins, *luk*AB (l*uk*GH) and the Panton-Valentine leucocidin. In contrast, Rsp-defective strains have a non-cytotoxic

phenotype with increased complement recognition and prolonged intracellular residence.

Taken together, these results provide evidence that an *S. aureus* regulatory system involving the Rsp transcription regulator can be subject to loss-of-function mutation, separating invasive from non-invasive strains in some patients, and that these mutants display attenuated lethality in the initial stages of experimental infection compared with wild type, but still invade deep tissues causing severe disease. Rsp loss-of-function has wider significance as an example of how within-host bacterial evolution affects key regulatory pathways, thus influencing disease progression and clinical outcome. Therefore, genes influenced by Rsp might make suitable vaccine candidates (1.4.10). It has been proposed, that a suitable *S. aureus* vaccine should contain multiple antigens with different functionalities (covering immune evasion, adhesion and nutrient acquisition proteins) (100). Under these aspects, the proposed antigens need to be assessed regarding their molecular function, their role in virulence and their suitability as a vaccine component.

Chapter 2:
Development of an assay to measure the bacterial transcriptome *in vivo*

2.1 Introduction

2.1.1 From *in vitro* to *in vivo* assays for Discovery of new Therapeutics

There is a constant need for development of new therapeutics and infection prevention. In *S. aureus* infection, the lack of new antibiotics discovery combined with increased antimicrobial resistance development poses a threat to human health (29). Employing assays, which imitate infection conditions to monitor bacterial adaptation to the host in drug discovery has become a recent trend. Such assays can offer new mechanistic insights into pathogenesis and might reveal new therapeutic targets. Thus, for staphylococcal infections, efforts have been made to mimic infection conditions or take samples from infected tissue directly and to characterize bacterial behaviour *in vivo* (14, 101-104).

2.1.2 Tailoring modern Sequencing Technologies to *in vivo* Settings

Next Generation RNA Sequencing (RNA-Seq) has some advantages over Microarray transcription analysis: It allows detection of novel transcripts and avoids bias which might be introduced through probe hybridization (105, 106). RNA-Seq has also been found to provide better estimates of absolute transcripts levels (107) and to show higher sensitivity towards changes in genes with low transcript abundance (108, 109). Hence, it represents a good way of studying the bacterial transcription response *in vivo*. RNA-Seq has been employed to study several types of *S. aureus* gene expression responses *in vivo* (e.g. in nasal carriage (110), joint (111) and skin infection (112)). However, to date no RNA-Seq obtained *in vivo* transcriptome for *S. aureus* has been reported for a murine sepsis model. *S. aureus* RNA has been isolated from infected murine kidneys after intravenously induced sepsis, but

although RNA was obtained in sufficient quantities for microarray analysis, no RNA Sequencing was performed (113). It is difficult to obtain *in vivo* RNA without large amounts of mammalian RNA in tissue samples: the high mammalian to bacterial ratio causes low proportions of bacterial RNA to be present in the sample. Thus, following sequencing, alignment rates of reads mapping to the bacterial genome are low, making differential gene expression analysis difficult.

2.1.3 Experimental Approach

I established a method for bacterial RNA extraction from tissue of bacteraemic mice with a focus on obtaining a high bacterial to mammalian RNA ratio, together with quality control metrics in order to characterise the *S. aureus in vivo* transcriptome during sepsis. For this purpose, a variety of bacterial RNA preservation and extraction methods were compared using tissues from mice injected intravenously with *S. aureus*. Methods quantifying the mammalian to bacterial RNA ratio in the sample were established. Furthermore, the generation of cDNA libraries and sample sequencing was standardised. Then, a computational pipeline to verify quality of transcriptomes and their differences to *in vitro* transcriptomes was set up. Finally, differences in gene expression during infection compared with broth-grown bacteria were described.

2.2 Research Questions and Objectives

2.2.1 Research Questions

1. Is it possible to obtain bacterial RNA of sufficient quality for RNA sequencing from *S. aureus* from infected murine tissue?
2. How can the ratio between bacterial and mammalian RNA extracted from infected tissue be determined?
3. Can an "*in vivo*" transcriptome be characterised for *S. aureus* and what does the *in vivo* transcriptome look like during infection in a murine sepsis model?

2.2.2 Research Objectives

1. To develop a method for obtaining intact *S. aureus* RNA from infected tissues
2. To establish a quality control pipeline for RNA obtained from mammalian-bacterial mixed nucleic acid samples from infected tissues
3. To characterize an "*in vivo*" transcriptome of *S. aureus*

2.3 Materials & Methods

2.3.1 Reagents, Materials and Enzymes

Table 6: Name, supplier and catalogue number of reagents, materials and enzymes

Reagent	Supplier	Catalogue Number
β -Mercaptoethanol , molecular biological grade	Calbiochem	444203
Chloroform, ACS spectrophotometric grade, ≥99.8%	Sigma Aldrich	366919
DNase I reaction buffer	NEB	B0303S
dNTPs (from NEB Next Ultra Directional RNA Library Preparation Kit)	New England Biolabs	E7420
Ethanol, pure, Molecular Biology Grade	Sigma-Aldrich	E7023
HyClone, RNase free water, Molecular Biology Grade	GE Healthcare	SH30538.02
Master Mix , Brilliant III Ultra-fast SYBR Green qPCR	Agilent	600882
Master Mix , Kapa SYBR Fast qPCR	Kapa Biosystems	KK4601
Master Mix, Q5® High-Fidelity	New England Biolabs	M0492S
Phosphate Buffered Saline (PBS), liquid, sterile	Sigma Aldrich	D-8537
RNA Screen Tape Sample Buffer, High Sensitivity	Agilent	5067-5577
RNA Screen Tape Sample Ladder, High Sensitivity	Agilent	5067-5578
RNAlater® RNA Stabilisation Reagent	Qiagen	76104
RNAlater® Stabilisation Solution	Ambion	AM7020
RNAprotect Bacteria Reagent	Qiagen	76506
RNAsin Recombinant Ribonuclease Inhibitor	Promega	N2111
Triton-X100 1% solution	Thermo Fisher Scientific	HFH10
TRIzol® LS Reagent	Invitrogen	10296010
Tryptic Soy Broth (TBA), bottled culture media	Oxoid	BO0369
Material	**Supplier**	**Catalogue Number**
E-gel 96, 2% Agarose gel	Invitrogen	G700802
Horse Blood Agar Plates (HBA)	Oxoid	PB0114
Qubit® RNA High Sensitivity (HS) Assay Kit	Thermo Fisher Scientific	Q32852
Reverse Transcriptase, Super Script® II kit	Thermo Fisher Scientific	18064-022
RiboPureTM Bacteria RNA purification Kit	Ambion	AM1925

RNA Screen Tape, High Sensitivity Tape	Agilent	5067-5579
RNase-free DNase Kit	Qiagen	79254
RNeasy Midi Kit	Qiagen	75144
TRIS-EDTA (TE) buffer from Plasmid kit	Qiagen	19046
Turbo DNAfree DNase I kit	Ambion	AM1907
Enzymes	**Supplier**	**Catalogue Number**
DNase I grade II	Roche	10104159001
Lysostaphin, >500 units/mg	Sigma-Aldrich	L7386 – 1MG
Proteinase K, >600 mAU/ml	Qiagen	19131

2.3.2 Primers used for Polymerase Chain Reaction and Real Time – PCR

Table 7: List of primers.

Yellow background indicates *S. aureus* specific primers, blue background murine (*Mus musculus*) specific primer. "_F" indicates forward primer, "_R" reverse.

Primer name	*Target Gene*	*Primer Sequence (5' -3')*	*PCR Product Size*
*S.a. recA*_F	Recombinase A	GGGAGACACTCACGTTGGTTTAC	121 bp
*S.a. recA*_R	Recombinase A	AACTTTTTCACGAATTTGGTTGATG	121 bp
*S.a. rpoB*_F	RNA polymerase beta chain	GCGAACATGCAACGTCAAG	121 bp
*S.a. rpoB*_R	RNA polymerase beta chain	GACCTCTGTGCTTAGCTGTAATAGC	121 bp
*S.a. pta*_F	Phosphate acetyltransferase	AAAGCGCCAGGTGCTAAATTAC	121 bp
*S.a. pta*_R	Phosphate acetyltransferase	CTGGACCAACTGCATCATATCC	121 bp
*M.m. ACTB*_F	Actin beta subunit	CTCTGGCTCCTAGCACCATGAAGA	200 bp
*M.m. ACTB*_R	Actin beta subunit	GTAAAACGCAGCTCAGTAACAGTCCG	200 bp
*M.m. B2M*_F	Beta 2 MHC subunit	CTGCTACGTAACACAGTTCCACCC	241 bp
*M.m. B2M*_R	Beta 2 MHC subunit	CATGATGCTTGATCACATGTCTCG	241 bp
*M.m. HMBS*_F	Hydroxymethyl bilanesynthase	GAGTCTAGATGGCTCAGATAGCATGC	250 bp
*M.m. HMBS*_R	Hydroxymethyl bilanesynthase	CCTACAGACCAGTTAGCGCACATC	250 bp

2.3.3 Bacterial Strains and Cultivation

All bacterial strains used in this thesis are listed in Table S1 (Supplementary). In this chapter, *S. aureus* Newman was grown by selecting four single colonies of an HBA stock plate (Oxoid) to inoculate 10 ml of TSB in an incubation tube. Overnight cultures were prepared at 130 rpm shaking, 37°C overnight.

2.3.4 Murine Sepsis Model

Female BALB/c mice, eight weeks of age, were injected with *S. aureus* Newman intravenously through the lateral tail vein, with 10^7 CFU/mouse. An aliquot of each inoculum was treated with RNAprotect Bacteria (Qiagen) according to manufacturer's instructions. Weight and clinical disease scores of the mice were monitored throughout the experiment. Animals were sacrificed by cervical dislocation of the neck 1, 3 or 4 days post infection and permanent cessation of circulation confirmed.

2.3.5 Tissue Harvest and bacterial Ribonucleic Acid (RNA) Preservation

Murine spleens, kidneys and livers were harvested from infected and uninfected animals. Tissues from uninfected mice were used as controls, and processed contemporaneously in parallel with infected tissues. Spleens were submerged into RNAlater (Ambion) immediately after harvesting, to preserve RNA from being degraded. Right kidneys were used to enumerate bacterial load. Left kidneys and livers were visually inspected for superficial abscesses, which, if present, were removed carefully with a sterile scalpel and submerged into RNAlater (Ambion).

Livers without visible abscesses were not processed further, but right kidneys were sliced longitudinally (in a coronal plane) to enhance chemical penetration and quickly submerged into RNAlater. All tissues in RNA preservation reagent were left at 4 °C overnight, as recommended by the manufacturer. Left kidneys without visible abscesses were used to confirm successful infection and estimate bacterial titres by tissue homogenisation and plating o HBA (Oxoid).

2.3.6 Bacterial RNA Extraction from *in vitro* Samples

The RNA of *S. aureus* Newman broth-grown inocula was extracted following the manufacturer's protocol (RNeasy Midi Kit, Qiagen), using an on column DNase I digest step and a second post elution DNase incubation (DNAfree DNase Kit, Ambion) for one hour, 37 °C with shaking at 300 rpm.

2.3.7 Separation of mammalian and bacterial Cells from infected Tissue samples

In order to obtain bacterial RNA from infected tissues, mammalian cells in samples (kidneys, spleens, liver and kidney abscesses) were lysed using a tissue dissociator (gentleMACS) in M-tubes. This treatment does not affect cellular integrity of bacteria, as determined by plating of homogenates and assessement of viable counts. The suspensions, containing disrupted mammalian cells and intact bacteria, were filtered (40 μm cell strainer, BD Biosciences) and mammalian tissue debris removed by two centrifugation steps (3200 xg, 10 min at 4°C), thereby reducing the amount of mammalian nucleic acids present in the sample.

Bacterial cells were lysed at 37°C for 30 min using Lysostaphin (50 µg/ml, Sigma Aldrich, resuspended in TE buffer, Qiagen) and subsequently Proteinase K (Qiagen, 30 mAU/sample) for 10 min. To prevent degradation an RNase inhibitor was added (500 U/ml RNasin, Promega). For extraction of bacterial RNA from infected whole kidneys, mechanical cell disruption after enzymatic lysis was performed using Lysing Matrix B tubes (MP Biomedicals) on a FastPrep-24 device. RNA was purified using an RNeasy Midi Kit, as described above (Chapter 2, [2.3.5]).

2.3.8 Quantity and Quality Assessment of Ribonucleic Acid (RNA) - Generation of cDNA

Total RNA for *in vitro* and *in vivo* obtained samples, was quantified using the $OD_{260/280}$ ratio (NanoDrop, Thermo Scientific) and by fluorometric quantitation (Qubit Fluorometer, Thermo Fisher, RNA HS assay kit). The quality of bacterial RNA obtained was assessed using a Tapestation (Agilent Genomics) with the Agilent High Sensitivity RNA ScreenTape System kit according to manufacturer's instructions.

To standardize quantification of bacterial RNA within mixed samples of mammalian and bacterial RNA, *S. aureus* and murine RNA samples of known concentration were used to determine a calibration curve. cDNA was generated following the SuperScript II manual (Thermo Scientific) using random primers (New England Biolabs). Sample controls were not treated with reverse transcriptase. Presence or absence of cDNA in samples was confirmed using the respective species specific

primers (Chapter 2, [2.3.2]) and a Q5 PCR Master Mix (NEB) in a polymerase chain reaction (PCR) using a Thermocycler. Settings were as follows:

Segment 1:	Initial Denaturation 95°C (10:00 min)	1 cycle
Segment 2:	Denaturation 95°C (00:30 min)	
	Annealing 60°C (1:00 min)	40 cycles
	Elongation 72°C (1:00 min)	

The PCR product was detected on a SYBR Green containing 1% Agarose gel (E-gel 96, Invitrogen).

2.3.9 Real Time Polymerase Chain Reaction

Real Time PCR determined quantities of RNA in samples. Primers (Chapter 2, [2.3.2]) were tested for their specificity and efficiency according to the published Pfaffl method (114). Controls included samples without templates, with non-matching primers (*S. aureus* primers with murine cDNA and murine primers with bacterial cDNA) and RNA samples, which had not been reverse transcribed. Samples were prepared with master mixes Kapa SYBR Fast qPCR (Kapa) and SYBRIII Green (Agilent). The cycle settings were as described above with a third segment to measure the melting curve of amplified DNA as another control for primer specific DNA fragment amplification (Fig. 30).

2.3.10 Quantification of the bacterial Ribonucleic Acid Ratio

RNA samples with known concentration of *S. aureus* and *M. musculus* (mouse) RNA were used to prepare standards of mixed RNA samples with a range of concentrations (15 ng/µl to 0.15 pg/µl, in a sample to sample ratio from 1:1 to 1:10000). A standard curve for murine and bacterial RNA was calculated to determine concentration of mixed samples obtained from murine kidneys.

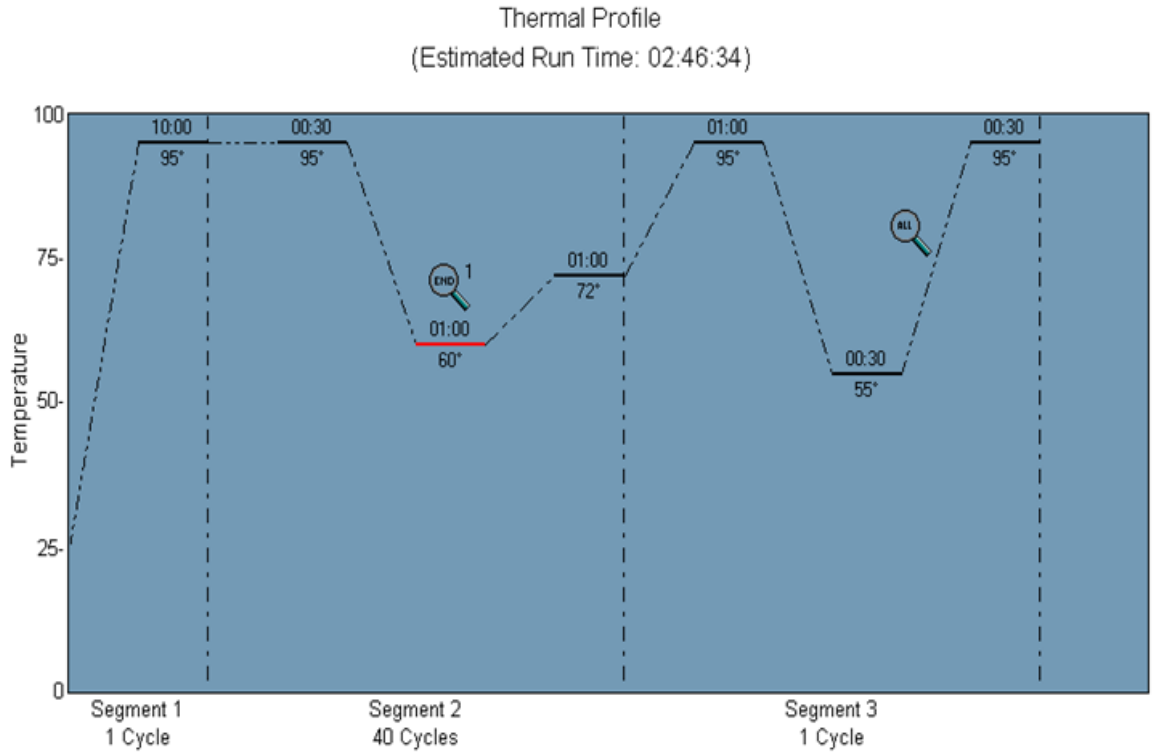

Figure 30: Diagram of conditions used for Real Time PCR

2.3.11 Preparation of cDNA Libraries and RNA Sequencing

mRNA was enriched using the Universal Ribodepletion Kit, Ribozero Gold Epidemiological (Epicentre) followed by Next Ultra Directional Library Preparation Kit for Illumina (NEB). The High Throughput Genomics Facility, Wellcome Trust Centre for Human Genomics (Oxford, UK), performed library preparation and sequencing. cDNA was sequenced on a HiSeq™ 2000 instrument (Illumina) yielding 100 bp paired end reads. Adapters were removed and reads trimmed to 80 bp using Trimmomatic (69), quality assessed with FastQC (http://www.bioinformatics.babraham.ac.uk/projects/fastqc/) and only reads exceeding a mean base quality of five within all sliding windows of 5 bp were mapped to the *S. aureus* Newman genome (DNA Database of Japan, accession number: AP009351). Read mapping was conducted using Bowtie2 (70) and only paired and concordant alignments which could be mapped to a single locus were considered further. Alignment quality scoring was carried out using the Picard package (http://picard.sourceforge.net): Only samples with high per gene counts (cut-off of at least 10 reads per gene in average) and alignment rate were used for further analysis. To quantify per-gene read counts, the htseq package in R (71) was applied in the setting, which allows counting reads with an alignment quality of greater than 10 in mode 'union' only.

2.3.12 Gene-by-Gene Expression Analysis

Differential transcript abundance analysis was performed together with Dr. Julius Müller using the DESeq2 package v.1.5.9 (74) in R. Significant effects were detected using the Bayesian Wald test in DESeq2, a screening procedure motivated by

Bayesian decision theory (75). Transcripts with low counts were filtered out to improve statistical power, as previously described (64) and the Benjamini-Hochberg adjustment of the *p*-values was employed to obtain an expected false discovery rate (FDR) of 10% (115).

2.3.13 Gene Set Enrichment Analysis

Enrichment of functional modules was tested by grouping genes according to their biological process involvement, molecular function or cellular compartment. Genes were assigned a functional group based on the *S. aureus* MRSA252 Ontology Database (www.biocyc.org), with gene mapping between *S. aureus* Newman (which was used for experimentation) and *S. aureus* MRSA252 via the Orthologue database (www.pathogenomics.sfu.ca/orthologuedb). A second database was constructed which assigned genes to a modules according to their transcriptional response under a series of published *in vitro* and *ex vivo* test conditions. Data from the SATMD (*S. aureus* Transcriptomic Meta Database) was used to do this. For example, if in some published work significantly up- and down- regulated genes were identified, the database noted the experimental condition and the gene response (e.g. 'up', 'down') associated with the response for each gene, e.g.

hla Schneider *et al.*, 2015, "up"

hlg Windsor *et al.*, 2012, "down"

hlg Wu *et al.*, 2014, "up"

2.3.14 Statistical Analysis

Transcriptomic changes at single gene level were assessed using a Bayesian Wald test (Chapter 2, [2.3.12]), assuming negative binomial distribution for the per gene read count. Correlation between transcriptomes was assessed using Pearson's correlation coefficient applied to the vectors of $\log_2$ fold changes derived from the DeSeq2 computation (Chapter 2, [2.3.12]). At an individual gene level, differential expression was considered significant if the *q*-value was below 0.05. A gene was considered upregulated if it reached > 2 fold change and downregulated if the fold change was < 0.5. A significantly upregulated gene is therefore a gene with > 2 fold change in expression and a *q*-value < 0.05 and a downregulated gene one with < 0.5 fold change in expression and a *q*-value < 0.05. These values were chosen to set strict cut-off parameters and identify large expression changes only.

Gene Set Enrichment Analysis (GSEA) was performed implementing a CERNO test (116) using the tmod package in R (Version 0.27, Weiner 3rd J, Domaszewska T. (2016) tmod: an R package for general and multivariate enrichment analysis. PeerJ Preprints 4:e2420v1 https://doi.org/10.7287/peerj.preprints.2420v1) to identify significant modules, based on the Fisher's method of combined probabilities:

$$f_{CERNO} = -2 \cdot \sum_{i=1}^{N} ln \frac{R_i}{N_{tot}}$$

Here, N is the number of genes in a given module, N_{tot} is the total number of genes and R_i is the rank of a gene (116).

The effect size was calculated via the area under the curve of the receiver operating characteristic curve (ROC). This curve is obtained by sorting genes according to

their *p*-value and then plotting the true positive rate (the gene in that position being a member of the module) against the false positive rate (the gene not being a member of the module). The script was developed with help of Dr Adaikalavan Ramasamy and Dr Julius Müller.

2.4 Results

2.4.1 Optimization of Ribonucleic Acid (RNA) Extraction from *S. aureus* infected Tissue

To date, no standardised method for extraction of bacterial RNA from infected tissue has been described for *S. aureus*. Accordingly, the first aim was to develop and optimise a method to obtain *S. aureus* transcripts from infected murine tissue samples (protocol and simplified flow chart, Supplementary Figure S1). Multiple steps had to be optimised, a process which is described below.

I selected commercial extraction methods for *S. aureus* Newman RNA from culture. I tested the RNeasy kit (Qiagen, after RNA preservation using RNAprotect Bacteria, Qiagen) after bacterial cell disruption with the Fastprep24 system (LysingMatrix B bead tubes, MP Biomedicals). Subsequently, samples were treated with DNaseI (DNAfree kit, Ambion). This same method was successfully employed on broth-grown bacteria and therefore, with an added tissue disruption step (GentleMACS, Miltenyi), tested on a sample containing murine tissue (kidney or spleen). To this, a known number of bacteria was added, imitating *S. aureus* infected tissue, using a spike/recovery approach. Recovery per bacterial cell was much lower (~1%, ~310 ng instead of ~35 μg in the absence of murine tissue) than of that achieved from the same number of bacteria in a broth. Hence, I compared three different extraction methods:

1. RNeasy midi kit 2. TRIzol reagent 3. RiboPure Bacteria kit

In this experiment, a low yield of total (mammalian and bacterial) RNA (9 % of broth extracted RNA from a similar number of bacterial CFU, Table 9) was obtained with RNeasy midi, which outperformed the other extractions (1 % of broth extracted RNA for the RiboPure and 2.5 % of broth extracted RNA for the TRIzol method, Table 9) in three experimental replicates. However, quality assessments (Chapter 2, [2.3.9, general flow through described in: Supplementary Figure S2]) showed that the RNA thus obtained was degraded and of insufficient quality for sequencing experiments.

After tissue disruption (M-tubes, GentleMACS, Miltenyi), lysed mammalian cells were separated from intact bacterial cells by centrifugation and filtration (40 µm) before bacterial cells were washed and lysed (LysingMatrixB bead tubes, Fastprep24, MP Biomedicals). This step increased the bacterial to mammalian RNA ratio, as quantified by Real Time PCR [2.3.10, Table 8], which was advantageous for subsequent RNA sequencing. It also increased overall RNA yields (19 % of yield compared to broth extracted RNA, Table 9) and reduced presence of degraded RNA.

Another important step for maintenance of RNA integrity was found to be the lysis of bacterial cells, during which addition of an RNase inhibitor (RNasin, Promega) prevented bacterial RNA degradation almost completely (Fig. 31).

Table 8: Ratios of bacterial to mammalian extracted RNA (infected murine tissue, values were taken from replicates within one experiment)

With additional LysingMatrixB bead step [S. aureus RNA : M. musculus RNA]	Without additional LysingMatrixB bead step [S. aureus RNA : M. musculus RNA]
1:5	1:1760
1:26	1:2381
1:85	1:4290
1:193	1:4312
1:112	1:6820

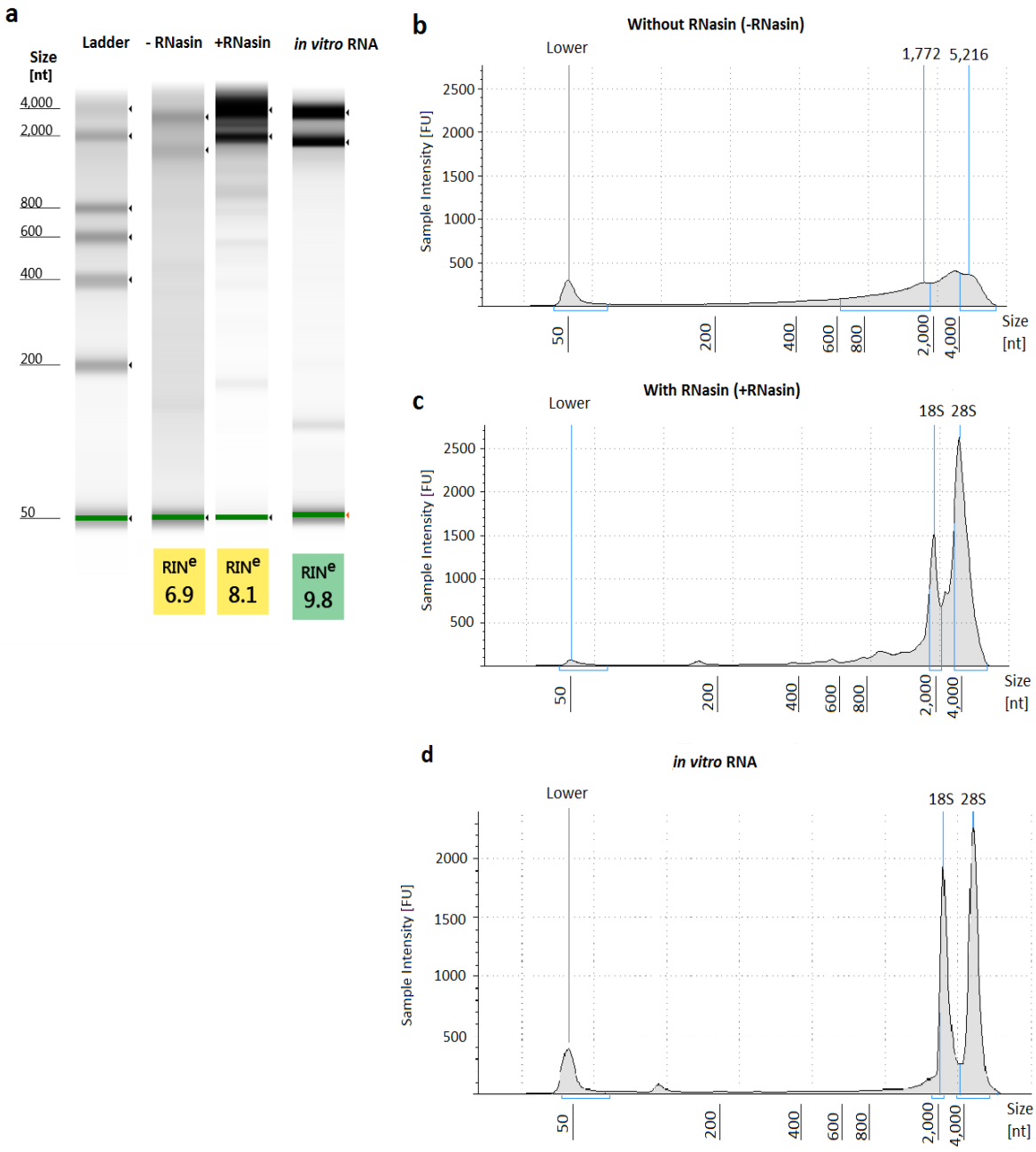

Figure 31: Tapestation assay of an *S. aureus* RNA

(**a**–**d**) TapeStation assay of total RNA obtained extracting *S. aureus* RNA with or without the use of RNasin and from *in vitro* RNA extraction: (**a**) gel image, (−) RNasin and (+) RNasin indicate library without and with use of RNasin during extraction, respectively. (**b**,**c,d**) Histogram representation of the results from panel **a**.

Using the combination of RNeasy columns with RNAse inhibitor mediated protection during bacterial lysis, I proceeded to extract RNA from infected renal and spleen tissue from mice. Yields were low compared to a tissue-bacteria mixture containing similar numbers of bacteria. Higher yields were obtained with bacterial RNA preservation using RNAlater (Ambion), which outperformed RNAlater (Qiagen) and RNAprotect Bacteria (Qiagen), especially when the tissue samples were sliced horizontally to improve tissue penetration of the preservative solution. However, RNA quantities extracted from these samples were still low (9 % of broth extracted yield, Table 9).

Improving mammalian tissue disruption, to release intracellular bacteria, by comparing disruption buffers (Table 9) increased the yield of RNA marginally (11 % of broth extracted RNA), when using 0.15 % Triton-X100 in PBS. Further experimentation indicated that, possibly through abscess structures and enhanced capsule formation within the tissues, lysis of bacterial cells was incomplete. Using bead tubes, as addition to two enzymatic lysis steps (Lysostaphin, Sigma Aldrich, and Proteinase K, Qiagen) re-established yields of around 20% (as compared to broth extracted RNA, Table 9). The application of other bacterial cell disruption methods (sonication, zirconia or glass bead tubes) did not result in any improvement. Finally, elongation of centrifugation and column elution steps, yielded reproducible total RNA yields of averages ranging between 0.5 – 10 µg with a range from 1 in 5 to 1 in 200 transcripts in each sample originating from bacteria [the ratio of bacterial transcripts to murine transcripts in each sample was calculated using Real Time PCR as described in 2.3.9]. Altogether, 20 conditions were tested (Table 9) in various combinations, until the final protocol (Supplementary Figure S1) was obtained.

Table 9: Conditions, reagents and yields of RNA extraction tested for optimisation of RNA *in vivo* extraction protocol

Yields are given as percentage of yield obtained from RNA extraction of broth grown bacteria of similar CFU, considered the yield of extraction from broth grown bacteria 100 %.

	Conditions	Reagents tested	Yield [%]
A	RNA preservation in tissue	RNAprotect Bacteria, Qiagen; RNAlater, Qiagen; RNAlater, Ambion	9 %
B	Tissue disruption buffer	TRIzol solution, Invitrogen; RLT buffer from RNeasy kit, Qiagen; PBS; PBS + Triton-X 100	11 %
C	Separation of mammalian cell debris from *S. aureus* cells	Centrifugation steps, intensity and duration; Filtration, 40 µm cell strainer, Fisher Scientific	19 %
D	RNA preservation during extraction	RNasin, Promega	23 %
E	Bacterial cell lysis	Mechanical: Lysing MatrixB + Fastprep24, MP Biomedicals; Glass beads + Bead Beater, Biospec; Zirconia Beads + Vortex, Ambion / Enzymatical: Lysostaphin, Sigma Aldrich; Proteinase K, Qiagen	20 %
F	Extraction methods	Column-based: RNeasy, Qiagen; RiboPure Bacteria, Ambion; In-solution: TRIzol, Invitrogen	9%
G	Elution time	Column elution buffer incubation time	27%

2.4.2 A Real Time Polymerase Chain Reaction (PCR) to quantify mammalian and bacterial Ribunucleic acid (RNA)

Fluorometric and optical density techniques were used to quantify total nucleic acid content of RNA samples obtained from infected murine tissue. However, RNA from infected murine tissues contains nucleic acids of mammalian and bacterial origin and the ratio between those cannot be determined using these approaches. Quality assessment technologies, such as Agarose gels, the Bioanalyzer or Tapestation (both Agilent Technologies), do not detect small proportions of intact nucleic acids in a sample (see Figure 31), which contains partially degraded RNA (117). In *in vivo* RNA samples from infected murine tissues, mammalian RNA is not preserved during extraction through presence of RNases in high concentrations immediately after tissue disruption (Fig. 31). Hence mammalian RNA degrades early during tissue disruption. This is intended to reduce mammalian RNA presence in these mixed samples, but makes quality assessment of bacterial RNA within the samples impossible using the above mentioned techniques.

For these two reasons, a new method needed to be developed, assuring bacterial RNA integrity in the sample, as it is critical to obtain accurate gene expression data (118), as well as to determine the composition ratio between bacterial and mammalian RNA. Real-Time PCR allows the bacterial : murine RNA ratio to be determined. Therefore, a protocol for *S. aureus* RNA quantification from murine tissue samples using Real Time PCR was developed.

Single stranded complementary DNA (cDNA) was generated, using the Superscript II Reverse Transcriptase (Invitrogen) (Chapter 2, [2.3.9]) using unmixed mouse and bacterial RNA of known concentration. Presence of cDNA was confirmed using PCR with three primer pairs for housekeeping genes of each, murine and bacterial, cDNA (Chapter 2, [2.3.2]). The amplification with all six primer pairs was successful. Cross-reactivity of all six primer pairs was tested by adding them to non-relevant cDNA (*S. aureus* primers to murine cDNA and murine primers to bacterial cDNA). No bands were detected in any case, excluding cross-reactivity of any of the primers with DNA from the other organism.

As cDNA first strand synthesis products and primers were adequate for PCR, conditions for Real Time PCR could be optimised. Two commercially available master mixes for Real Time PCR were tested (Brilliant III SYBR Green, Agilent; KaPa SYBR Fast qPCR, Kapa) with murine and bacterial cDNA and all six primers. Overall the Agilent Brilliant II SYBR Green Master Mix outperformed the Kapa Master Mix, as there were no amplification products detected in RNA-containing samples and water controls or wells, where cDNA had been combined with irrelevant primers (murine primers with bacterial DNA and vice versa) (Fig. 32). The signal intensity of Kapa master mix treated samples was also lower (Fig. 33) and the use of Kapa master mix was therefore discontinued.

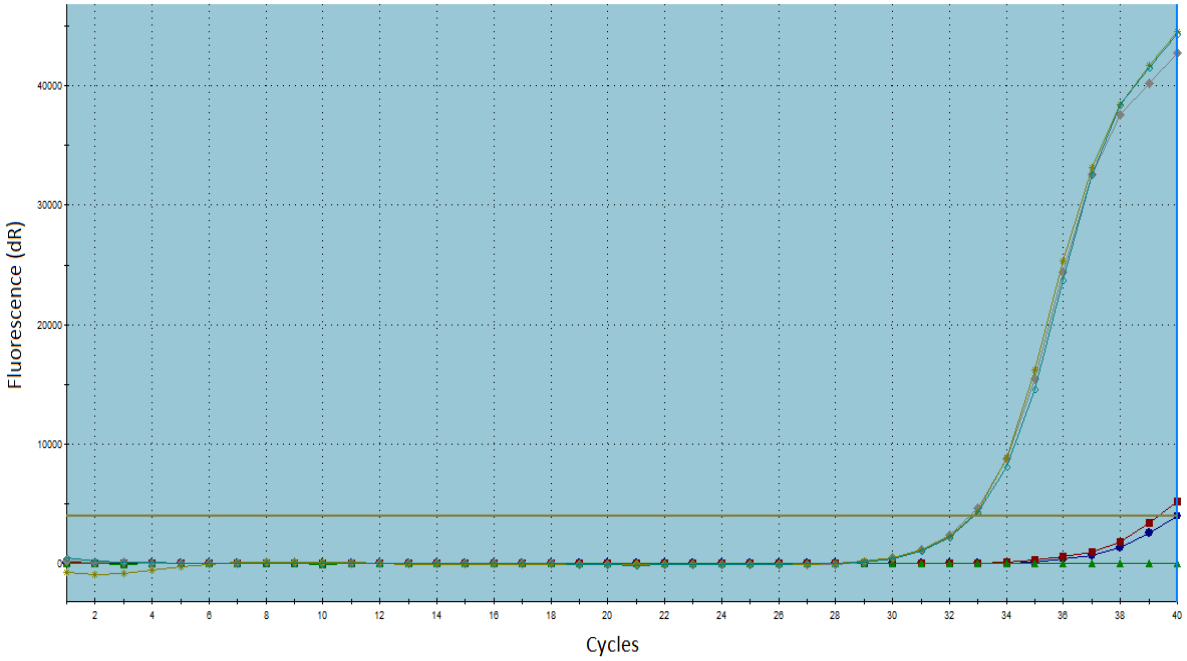

Figure 32: Real Time PCR curves of water controls

Curves of controls with Kapa Master Mix (orange, light blue).and with Agilent SYBR Green Master Mix (red, dark blue and green curves) [Method described in 2.3.10].

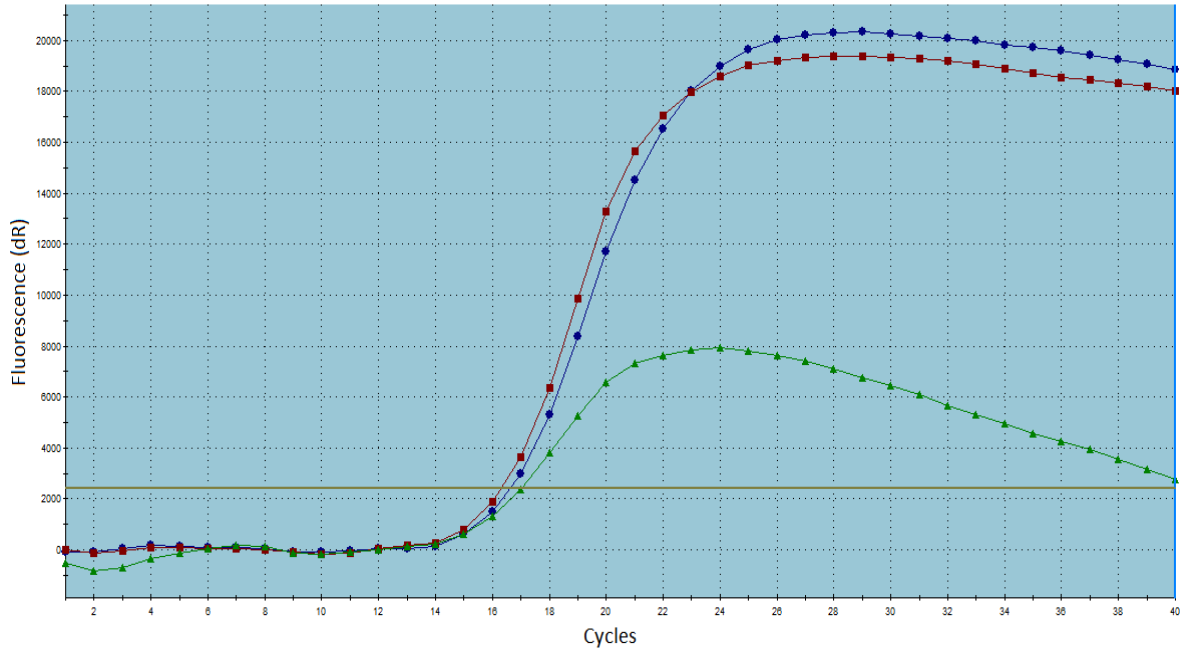

Figure 33: Real Time PCR curves of murine cDNA with different Master Mix

Curves of murine cDNA amplified with Agilent SYBR Green Master Mix (red and blue line) and Kapa Master Mix (green line) [Method described in 2.3.10].

After experimental conditions for Real Time PCR had been defined, primer specificity was assessed by measuring dissociation curves of cDNA amplification products with all six primer pairs, first mammalian or bacterial RNA samples speperately, then in mixed RNA samples. All six primer pairs resulted in product specific dissociation curves with clear amplitudes. However, the murine primer pairs for the hydroxymethyl bilanesynthase (HMBS) required a higher cycle number before its amplification product reached the detection limit (Fig. 34). Use of this primer pair was therefore discontinued.

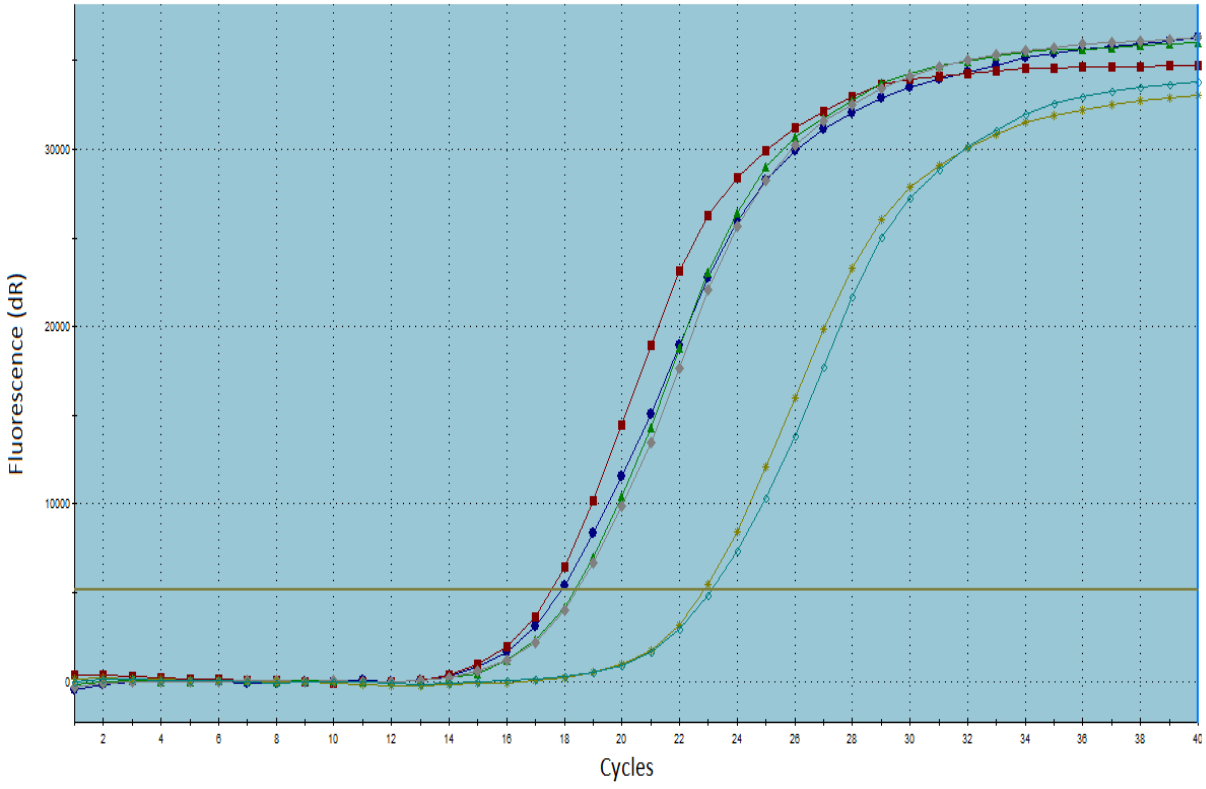

Figure 34: Real Time PCR curve of murine cDNA with different murine primers

Amplification of murine cDNA using B2M primers (red and blue curves), ACTB primers (grey and green curves) and HMBS primers (golden and light blue curves) [Method described in 2.3.10].

For the five remaining primer pairs (two murine and three bacterial) reproducibility was assessed across a set of three technical replicates using aliquots from the same RNA sample of known concentration. Here murine ACTB (Actin beta subunit) primers and bacterial rpoB (RNA polymerase beta chain) primers varied about 1-3 cycle numbers between experiments. Their use was therefore discontinued. The bacterial primers for pta (Phosphate acetyltransferase) had a consistently higher cycle threshold. As a conclusion the bacterial primers recA (recombinase A) and the murine primers B2M (Beta 2 MHC subunit) were chosen for further method development.

During Real Time PCR, constant amplification efficacy is required for reliable comparison of RNA quantities between samples. The amplicon specific efficacy can be determined by identifying the degree of linearity between samples, depending on concentration (114). A dilution series of murine and bacterial RNA was used (75 ng – 7.5 pg, 1:10 dilutions) and a curve plotted (Figures 35A and B).

A

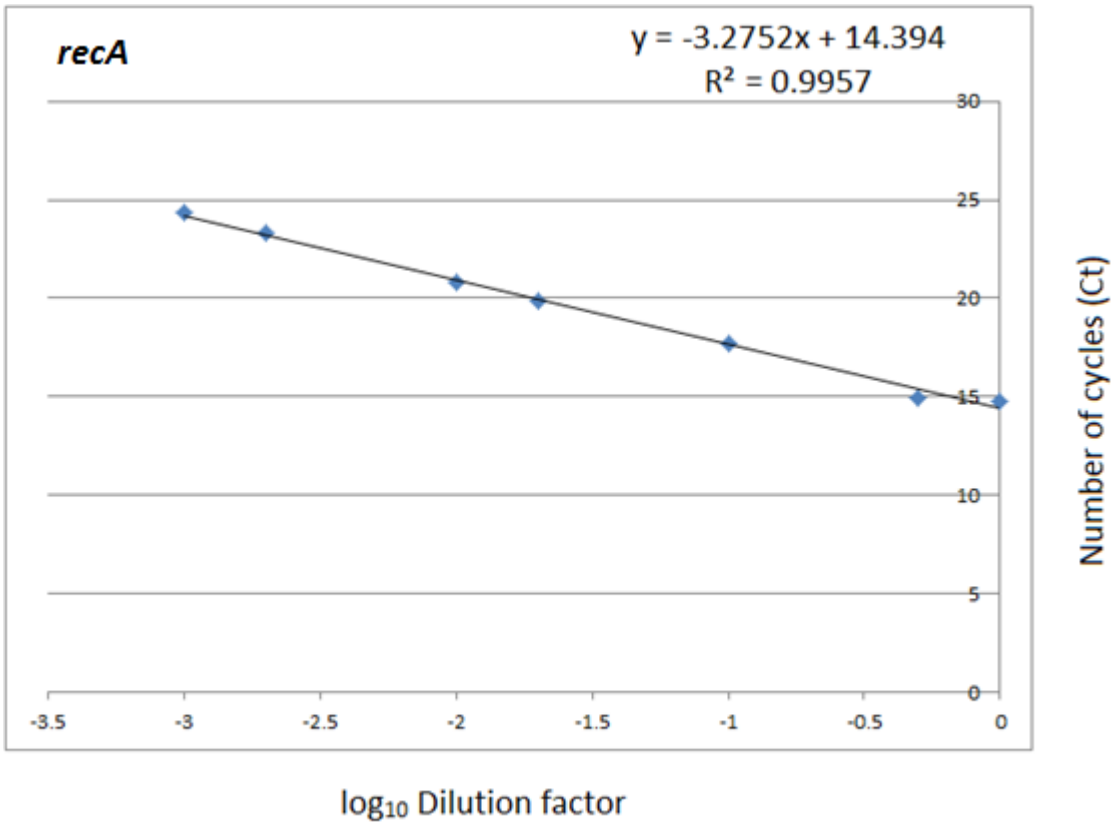

Figure 35: Standard curve for relation between RNA concentration and Ct value

A: Linear relation between bacterial RNA concentration and Ct value measured using Real Time PCR with recA bacterial primers. The linear curve equation and R^2 are given.

B

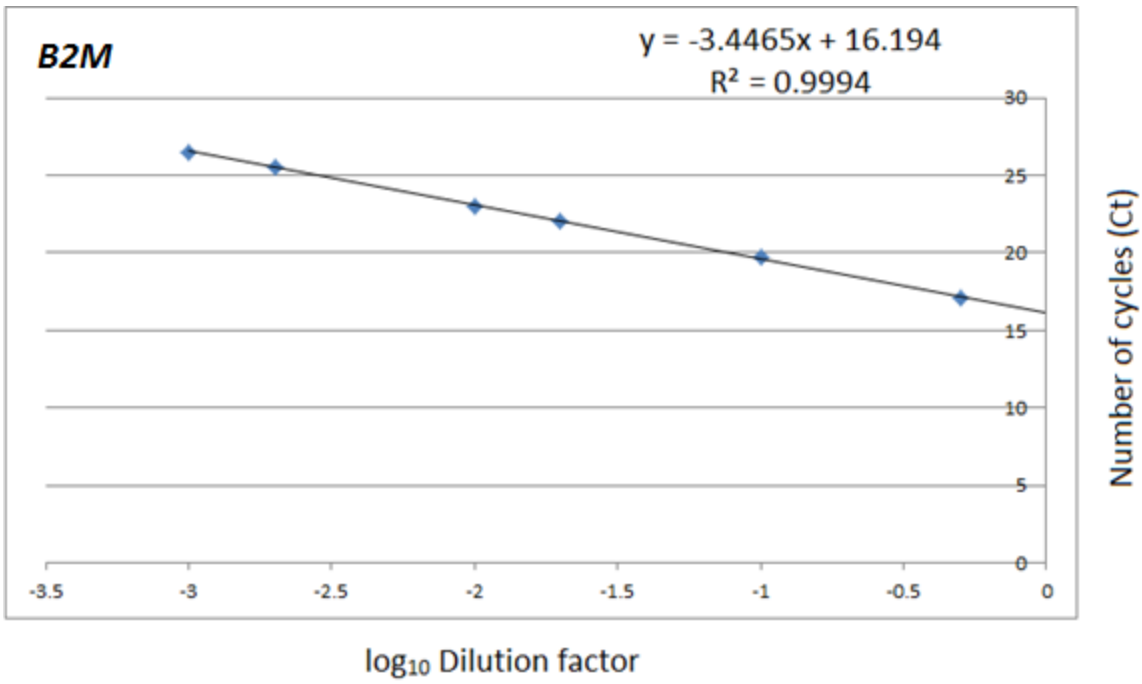

Figure 35B:

Linear relation between murine RNA concentration and Ct value measured using Real Time PCR with murine B2M primers. The linear curve equation and R^2 are given.

Efficacies were calculated using the following equation:

$$10^{-\frac{1}{Slope}} - 1 = E(\%)$$

Efficacy (E) for bacterial *recA* amplification was 95% and for murine *B2M* 102%. A primer efficacy between 95 – 105 % is recommended (114) and consequently, both primer pairs are suitable for this method.

In order to test a sample of RNA from mixed genetic origin, interference of murine RNA with bacterial RNA detection and vice versa must be excluded. I therefore tested if amplification specificity and efficacy were maintained when combining murine and bacterial nucleic acids. I mixed sscDNA of bacterial and murine origin (Table 10). There were no differences found in specificity and efficacy of detection. Next, the influence of mixing RNA before sscDNA generation was measured by repeating the before mentioned assays with mixing murine and bacterial samples. No differences were found in sensitivity, specificity and efficacy of nucleic acid quantification when compared to mixing murine and bacterial sscDNA (Table 10). Hence, the use of this protocol is adequate for determination of the ratio of bacterial to mammalian RNA in a mixed sample.

Table 10: Detection of bacterial sscDNA/RNA from a mixture with murine sscDNA/RNA in different ratios (1:1 to 1:10000) using qPCR

Ratio of bacterial RNA to murine RNA	Ct value
1:0 (15 ng:0 ng)	16
1:1 (15 ng:15 ng)	16
1:10 (1.5 ng: 15 ng)	19
1:100 (0.15 ng: 15 ng)	22
1:1000 (0.015 ng: 15 ng)	25
1:10000 (0.0015 ng: 15 ng)	29

The cut-off for a sample ratio of bacterial to murine RNA was set as 1:5000 transcripts. With a total anticipated sequence yield of 5×10^8 reads/sample, a sample with one bacterial read per 5000 murine reads would still result in 1×10^5 bacterial reads/sample. The average *S. aureus* genome encodes 2800 genes (119). Accordingly, the sample would produce an average depth of 35 reads per gene

(assuming identical expression of all genes), making it sensitive enough to detect large expression changes. However, for lower abundance transcript detection higher sequencing depth would be required. A common way to increase sequencing depth of RNA-Seq is depletion of ribosomal RNA transcripts, which make up to 95% of transcripts detected (115, 120). All cDNA libraries generated in this thesis were therefore rRNA-depleted (Fig. 36), as described in 2.3.11, using a commercial ribosomal RNA depletion kit Universal Ribodepletion Kit, Ribozero Gold Epidemiological (Epicentre).

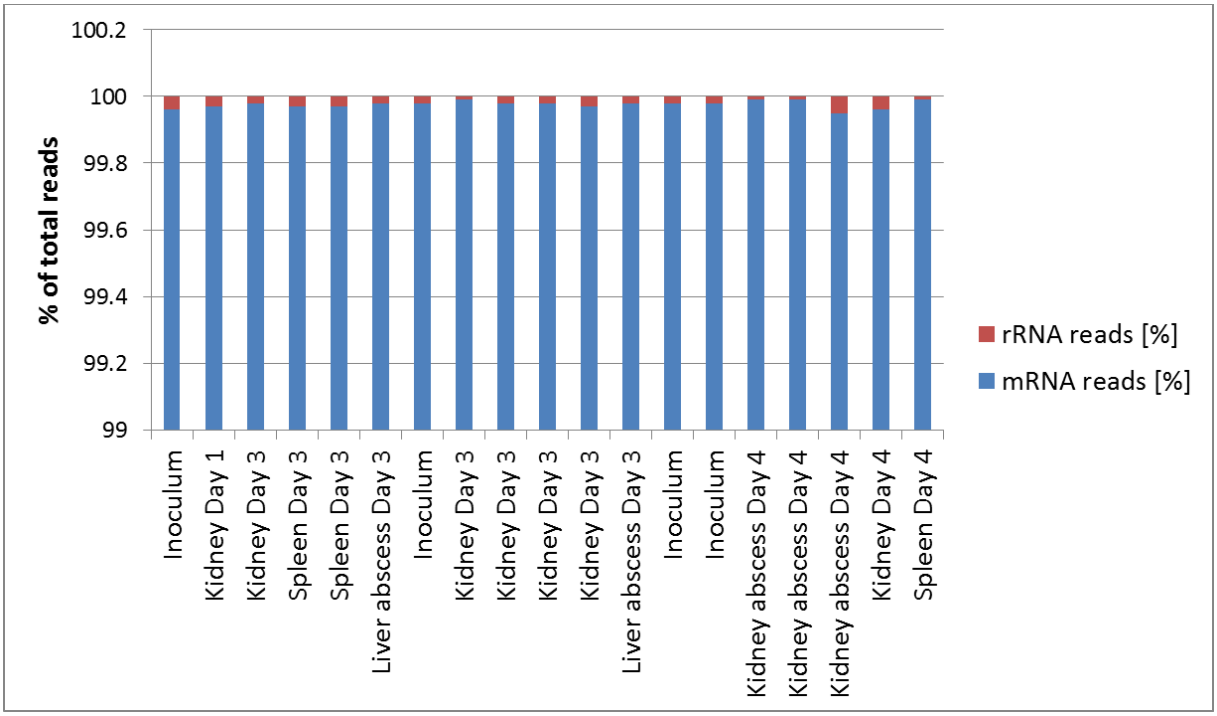

Figure 36: Proportion of rRNA in sequencing libraries

Percentages of mRNA (blue) and rRNA (red) in each generated RNA-Seq dataset from Inoculum (broth grown bacteria) or tissue (bacteria obtained from murine kidney, liver or spleen) after rRNA depletion using Universal Ribodepletion Kit, Ribozero Gold Epidemiological (Epicentre).

Though a minimum of 5 million aligned reads per library has been suggested sufficiently deep to sequence a bacterial transcriptome (121), the authors of this study stress that, for studies comparing gene expression between different strains and/or growth conditions, the importance of sequencing breadth outweighs depth. They propose including more biological replicates to increase transcriptome breadth, reducing the necessary amount of reads per sample to $4 – 6 \times 10^4$ or even $2.5 – 3 \times 10^4$ in the case of *V. cholerae* (121). Thus, the transcriptome of each condition or time point was defined as the joined transcriptome of at least three biological replicates to improve transcript detection and identification of transcriptional changes.

2.4.3 *In vivo* Transcriptomics: Evaluating the Assay Performance

After the establishment of an RNA *in vivo* extraction method (Chapter 2, [2.4.1]) with relevant quality controls (Chapter 2, [2.4.2]), samples which had passed the quality control threshold were used for cDNA library preparation. Libraries were prepared blinded and paired-end from samples obtained from three independent experiments. RNA sequencing was performed (100 bp read length) by the High Throughput Genomics Core Facility. Fifteen bacterial transcriptomes from *in vivo* sources (infected murine kidneys and spleens, superficial tissue abscesses) and, for comparison, four transcriptomes from *in vitro* broth grown bacterial inocula were obtained. Two control samples from uninfected tissue were also obtained (no bacterial RNA present). Each library had between 15 and 171 million reads (Fig. 37).

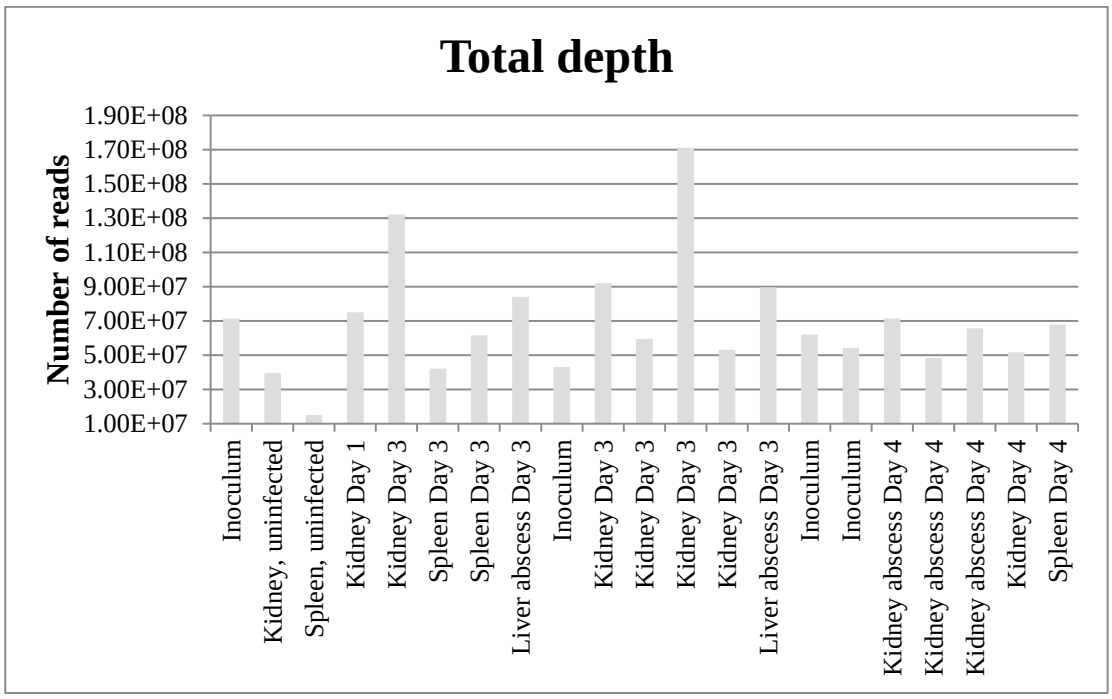

Figure 37: Total number of reads per library obtained after RNA Sequencing

Transcriptional reads before mapping for samples obtained *in vitro* (Inoculum) and *in vivo* (from infected and uninfected murine tissue) at different time points (Day 1, 3 and 4 post infection) are shown.

All samples were mapped to the *S. aureus* Newman genome (AP009351) using Bowtie2. Between 15 and 42 million reads could be mapped uniquely to the *S. aureus* Newman genome from broth grown inoculum samples. Due to the presence of murine RNA, fewer reads were mapped uniquely to the bacterial genome from *in vivo* samples, ranging widely from 3500 to 16 million reads (Table 11). Uninfected tissue samples (kidney and spleen), which were included to control for non-specific mapping, did not contain any reads that could be mapped to the bacterial genome.

Table 11: Number of uniquely mapped bacterial reads from cDNA libraries.

Samples were obtained from broth grown bacteria *in vitro* (Inoculum) and from bacteria from infected murine tissues (Kidney, Spleen, Liver) *in vivo* at different time points post infection (Day 1, 3 and 4). Reads obtained from uninfected murine tissues without bacteria (kidney and Spleen) are included as control.

Sample	Number of uniquely mapped bacterial reads
Inoculum	2.22E+07
Kidney, uninfected	0
Spleen, uninfected	0
Kidney Day 1	3.95E+03
Kidney Day 3	7.86E+04
Spleen Day 3	1.50E+03
Spleen Day 3	1.96E+05
Liver abscess Day 3	3.45E+05
Inoculum	2.96E+07
Kidney Day 3	5.77E+04
Kidney Day 3	3.52E+03
Kidney Day 3	4.57E+05
Kidney Day 3	3.23E+04
Liver abscess Day 3	4.53E+04
Inoculum	4.27E+07
Inoculum	3.79E+07
Kidney abscess Day 4	1.66E+07
Kidney abscess Day 4	6.67E+06
Kidney abscess Day 4	1.83E+07
Kidney Day 4	1.30E+07
Spleen Day 4	2.71E+04

Quality of the reads was assessed using FastQC (http://www.bioinformatics.babraham.ac.uk/projects/fastqc/), followed by adapter removal and trimming of the reads using Trimmomatic (69) as previously described (Chapter 2, [2.3.11]). Removing the ends of a read improves its quality, as it did for this set of samples (Fig. 38). The trimmed reads were then re-mapped against the *S. aureus* Newman genome.

A

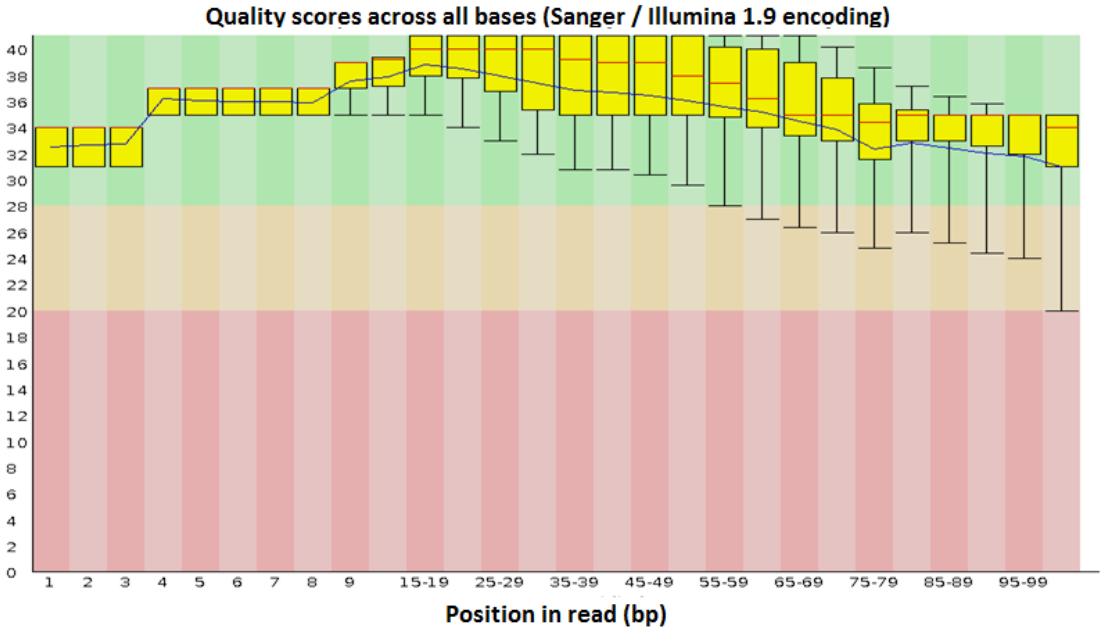

B

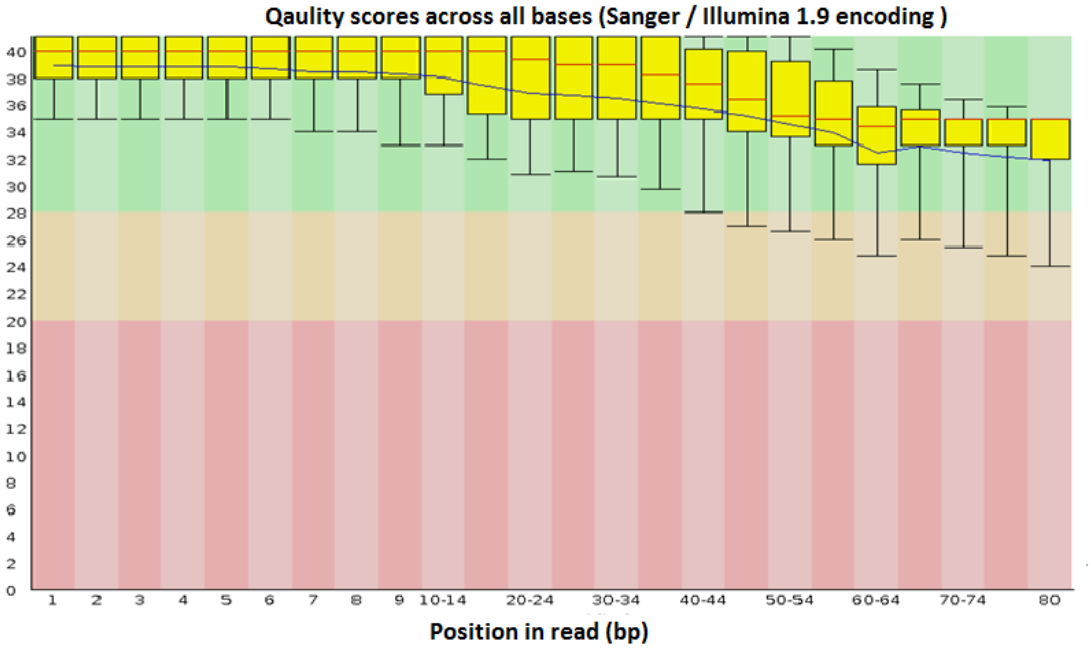

Figure 38: **Assessment of per base quality in an *in vivo* transcriptome sample**

Per base quality across transcriptomic reads of an *in vivo* sample harvested from infected tissue (kidney) mapped against *S. aureus* Newman before (A) and after (B) trimming [Strain described in 2.3.3; Method described in 2.3.11].

After quality-trimmed reads were mapped to the *S. aureus* Newman genome, alignment was controlled using the Picard package (http://picard.sourceforge.net). Samples with good alignment and high per gene counts (>35 average counts per gene) were used for per gene and gene set analysis (Fig. 39). Samples, which did not meet these criteria (Fig. 40) were excluded from subsequent analysis.

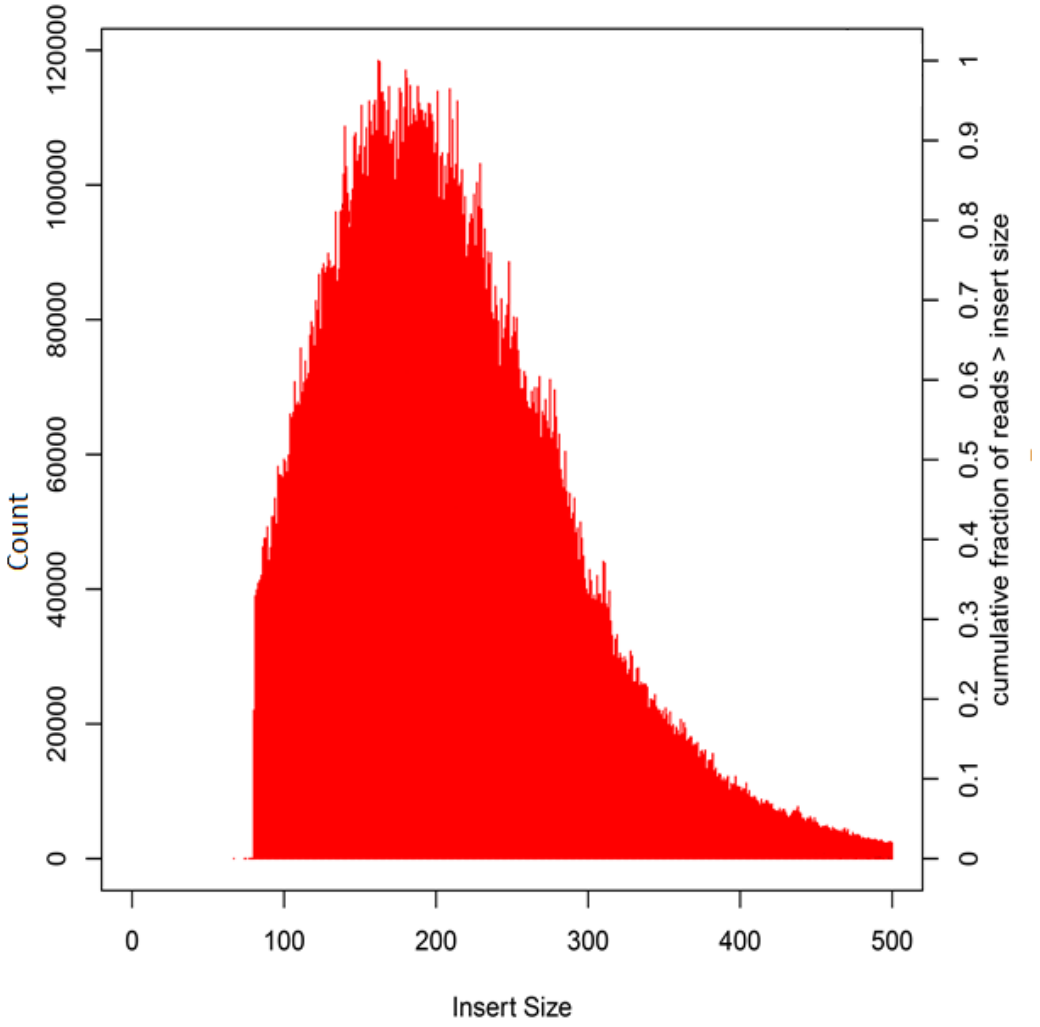

Figure 39: Insert sizes and per gene counts across a sample with high alignment rate

Distribution of insert sizes and per gene counts in a transcriptome library. In this sample, from 43.1 million total reads, 14.8 million reads were mapped and aligned (34.4 %).

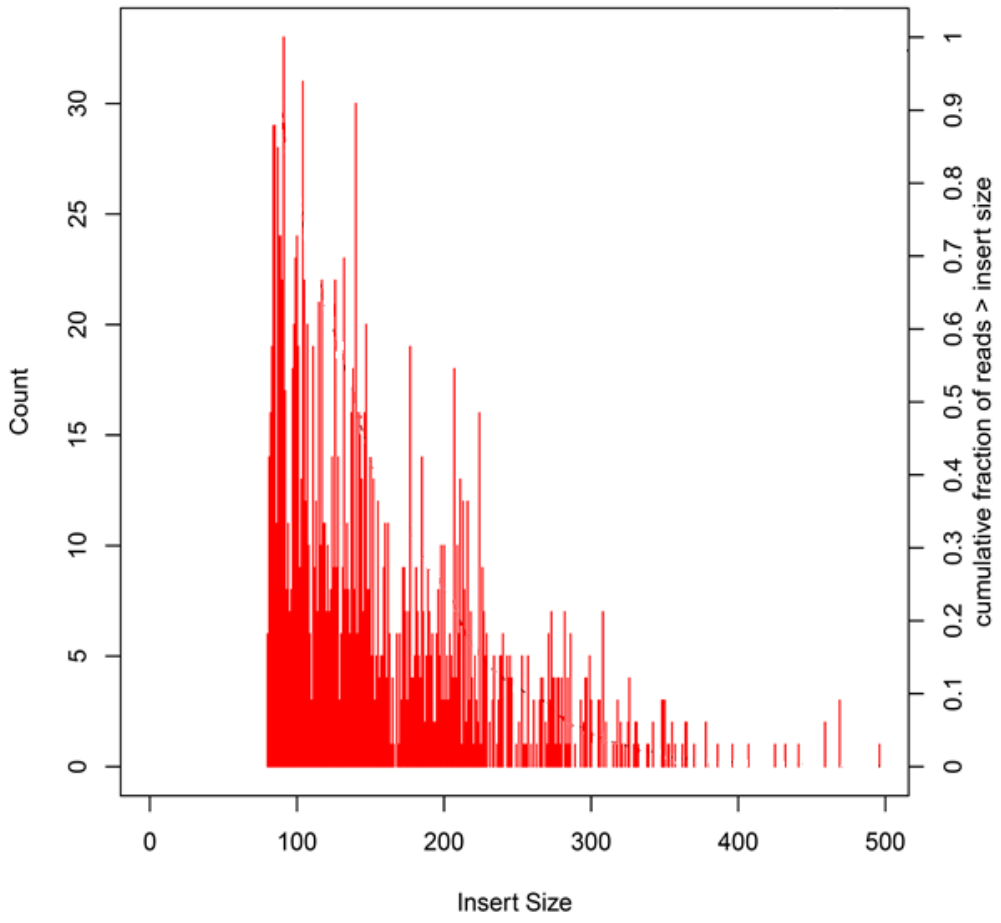

Figure 40: Insert sizes and per gene counts across a sample with low alignment rate.

Distribution of insert sizes and per gene counts in a transcriptome library. In this sample, from 75.1 million total reads, 3950 reads were mapped and aligned (0.005 %). This sample did not pass quality control, as the average per gene count did not exceed 35.

Of the total 21 samples sequenced, all four inocula samples passed quality control and were used as reference comparators for the *in vivo* transcriptomes. Two samples obtained from uninfected murine tissue contained no bacterial RNA and showed no alignment to the *S. aureus* genome. Two of the remaining fifteen *in vivo* samples failed quality control [2.3.9]. The first, obtained one day post infection, did not contain enough *S. aureus* RNA and the second, from three days post infection, had poor alignment to the bacterial genome (Figure 40). The remaining thirteen *in vivo* transcriptomes passed quality control according to the recommended cut-offs of the Picard (http://picard.sourceforge.net) and FastQC ((http://www.bioinformatics.babraham.ac.uk/projects/fastqc/) packages; thus eight samples from three days post infection and five from four days post infection were analysed further.

Thirteen samples, which originate from bacteria recovered from infected murine tissue were obtained in three independent experiments. The first two experiments ("Replicate 1" and "Replicate 2") were terminated three days post infection; the following experiment ("Replicate 3") was terminated four days post infection [Method is described in Section 2.3.4]. Correlation between the expression changes observed in these three experiments when comparing *in vivo* obtained bacteria to *in vitro* broth grown bacteria was assessed (Fig. 41).

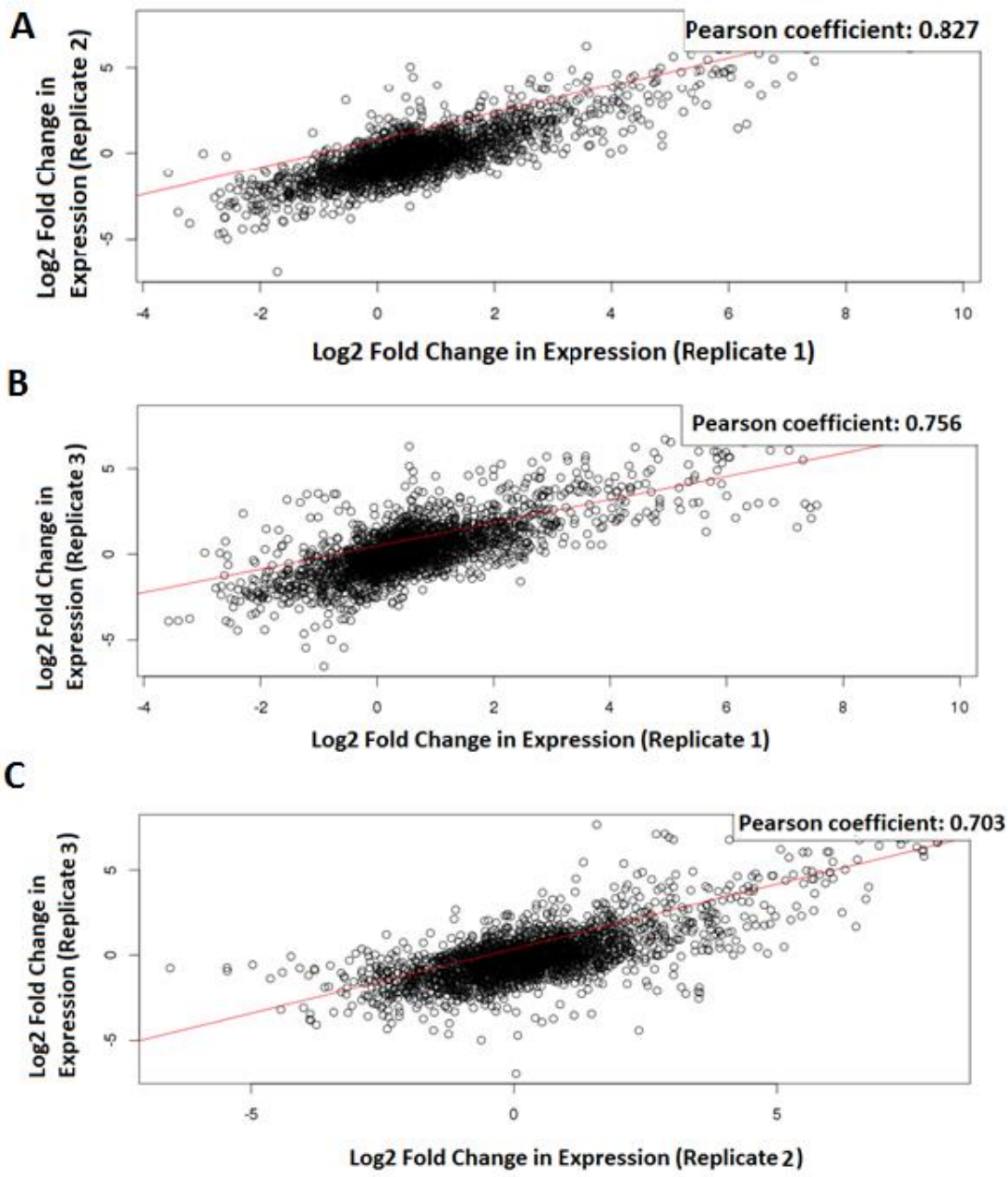

Figure 41: Expression correlation *in vivo* compared to *in vitro* in *S. aureus* Newman

Correlation of gene expression fold-changes *in vivo* during infection in *S. aureus* Newman when compared to *in vitro* between: **A** the first ("Replicate 1", x-axis, Day 3 post infection) and the second ("Replicate 2", y-axis, Day 3 post infection) experiment, **B** the first ("Replicate 1", x-axis Day 3 post infection) and the third ("Replicate 3", y-axis Day 4 post infection) experiment and **C** the second ("Replicate 2", x-axis, Day 3 post infection) and the third ("Replicate 3", y-axis, Day 4 post infection) experiment. The red line indicates regression. [Methods are described in Sections 2.3.4 – 2.3.12, statistical analysis in 2.3.14]

2.4.4 Confirming the *in vivo* transcriptomic Assay Reproducibility

To test for reproducibility between experiments, correlation of the three experiments was determined. First, Principal Component Analysis PCA was used to detect clustering of samples according to their tissue origin: Kidney, Spleen, Kidney abscess (all *in vivo*) and Inoculum (*in vitro*) bacterial transcripts were compared irrespective of the day they were harvested (Day 3/4 post infection). The two liver abscess samples did not align well with each other or with the other *in vivo* samples and were excluded from any further analysis. The *in vitro* group clusters away from the *in vivo* group. The former, *in vivo* originating samples, are influenced by both principal components one and two, while the latter, *in vitro* originating samples, are mostly affected by principal component two, clustering on the right of the graph (Fig. 42).

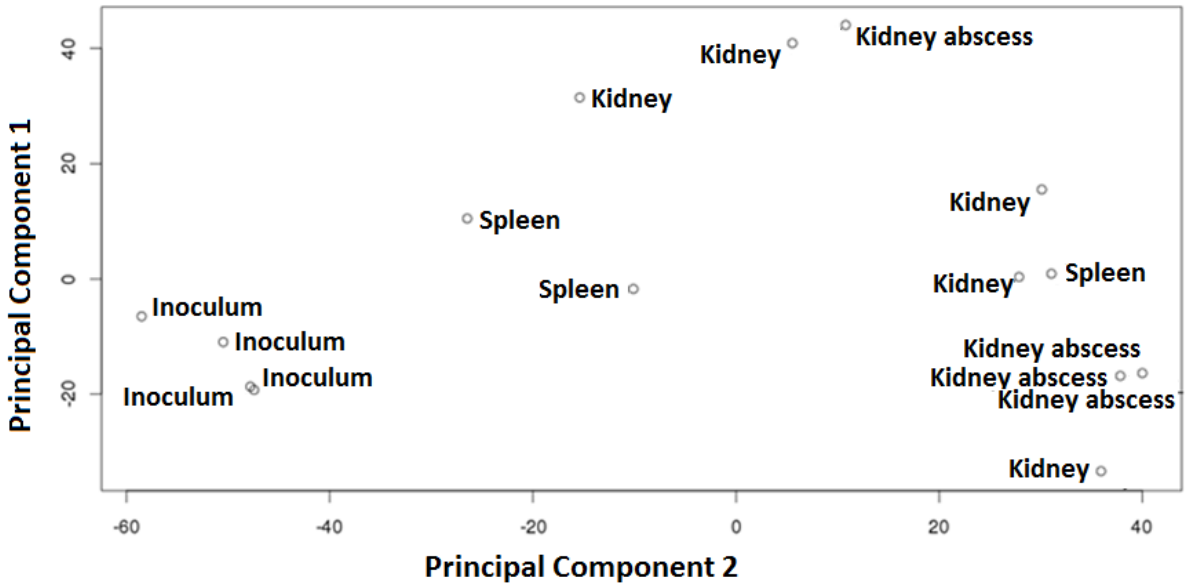

Figure 42: PCA of *S. aureus* transcriptomes *in vivo* from different tissues

Transcriptomes of *S. aureus* Newman from three experimental replicates of *in vivo* samples ("Spleen", "Kidney", "Kidney abscess") and *in vitro* samples ("Inoculum"). Samples are sorted according to their tissue origins [Method described in 2.3.4 – 2.3.12] and each dot represents one sample and is labelled with its origin. The x-axis shows the effect of principal component two, the y-axis principal component one.

As shown in Figure 42, bacterial transcripts from *in vivo* sources are distinct from *in vitro* originating RNA. Furthermore, spleen, kidney and abscess derived transcripts do not differ systematically when applying differential gene expression analysis on *in vivo* samples derived from kidney vs *in vivo* samples derived from spleens [2.3.11]. When gene-by-gene transcription was compared in whole kidneys with spleen or kidney abscesses, no differential transcription was identified. Consequently, they are all considered as "*in vivo*" originating samples and analysed disregarding their tissue origin.

Infected tissue samples were taken at different days post intravenous infection. However, extraction of bacterial RNA from tissue obtained one day after infection was not successful and tissue samples taken two days after infection also contained low bacterial quantities below the cut-off for succesfull RNA extraction ($<10^5$ CFU/g tissue). Low abundance of staphylococci in murine tissue two days post intravenous infection is common and has been reported (80). Therefore, tissues were harvested three and four days post infection and bacterial RNA extracted. Principal component analysis was used to assess the effect of the time of tissue harvest. An effect of the day of tissue harvesting on the bacterial transcriptome is seen (Fig. 43), separating bacterial transcriptomes recovered four days post infection from transcriptomes of three days post infection in a principal component 1 dependent manner. Samples obtained three days and four days post infection were therefore analysed separately.

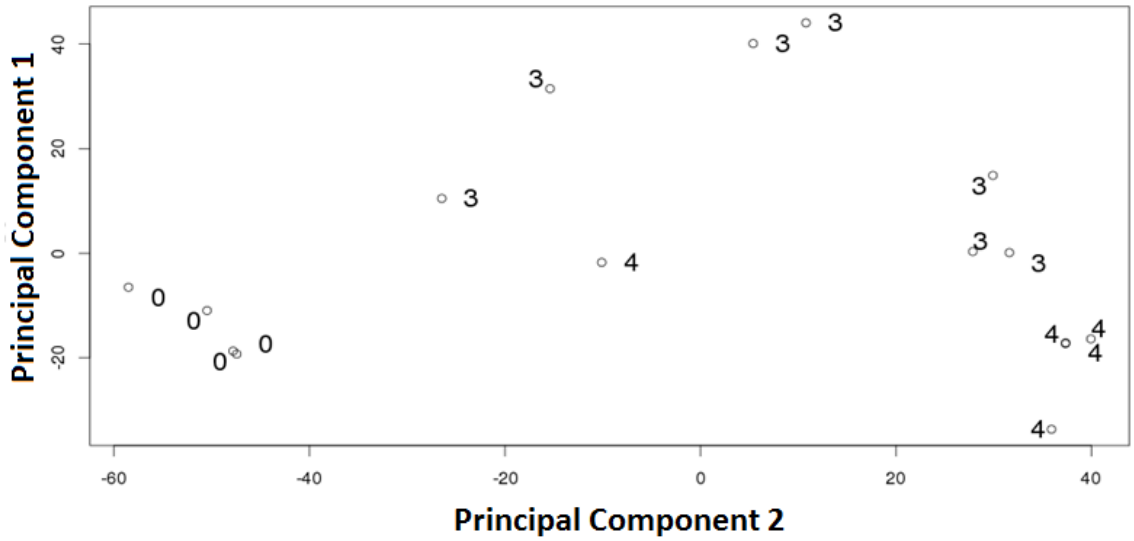

Figure 43: PCA of *S. aureus* Newman transcriptomes sorted by day of harvest

Effects of two principal components on *S. aureus* Newman transcriptomes *in vivo* and *in vitro* are displayed. "0" indicates *in vitro* derived bacterial transcriptomes from the inoculum used (Day 0), whereas "3" indicates samples derived three days post infection (Day 3) and "4" four days post infection (Day 4) [Methods described in 2.3.4 -2.3.12, statistical analysis in 2.3.14].

In order to compare the per-gene effect on the fold changes of *in vivo* samples compared to *in vitro* derived transcriptomes, the Pearson correlation between the two replicates obtained 3 days post infection was calculated. Log_2 fold changes were calculated using the DESeq2 package (74), and contrasts between *in vivo* derived bacterial transcriptomes and inoculum depicted (Fig. 44).

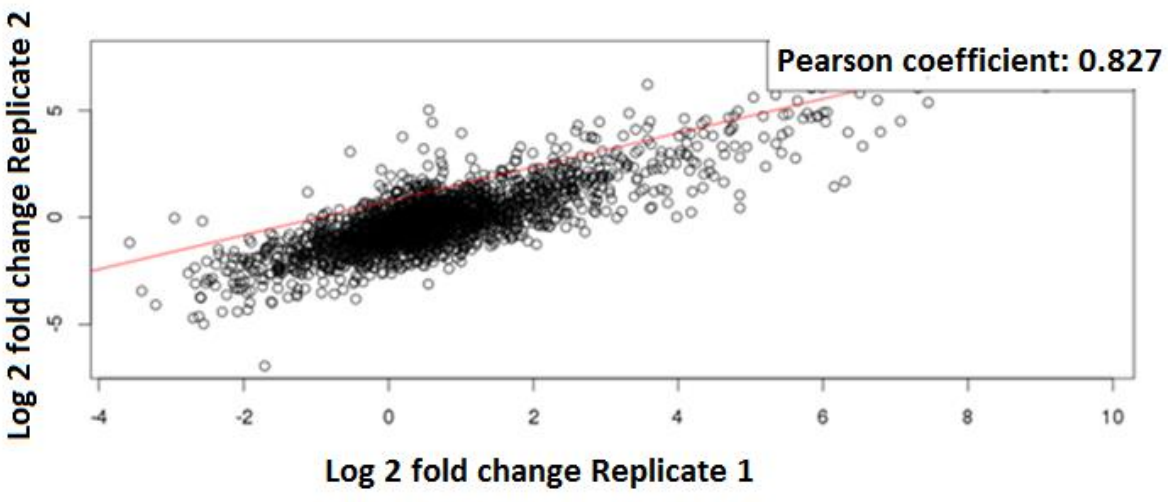

Figure 44: Correlation between two experimental replicates of *S. aureus* Newman *in vivo* transcriptomes

Comparison of log_2 fold changes *S. aureus* Newman transcriptomes *in vivo* three days post infection compared with *in vitro* in two independent experiments. [Methods are described in 2.3.4 – 2.3.12, statistical analysis in 2.3.14].

The Pearson coefficient was >0.82, indicating a high correlation between the replicates and demonstrating reproducibility of the technique. However, the range of log_2 fold changes in the first replicate is larger (-4 to 10) than in the second replicate (-5 to 5), indicating higher sensitivity of detection of transcriptional changes in Replicate 1.

To further validate the estimates of gene regulation obtained, and to assess generalisability of the findings, I compared gene expression described here with a published study exploring *S. aureus in vivo* transcription using a different extraction method and microarrays (113). There, *S. aureus* expression in a murine kidney and in a human cutaneous abscess was compared to *in vitro* transcription. In the following, I compare per gene effects in ten upregulated (Figure 45) and ten

downregulated (Figure 46) genes against the effect this study reports for bacterial expression in the murine kidney.

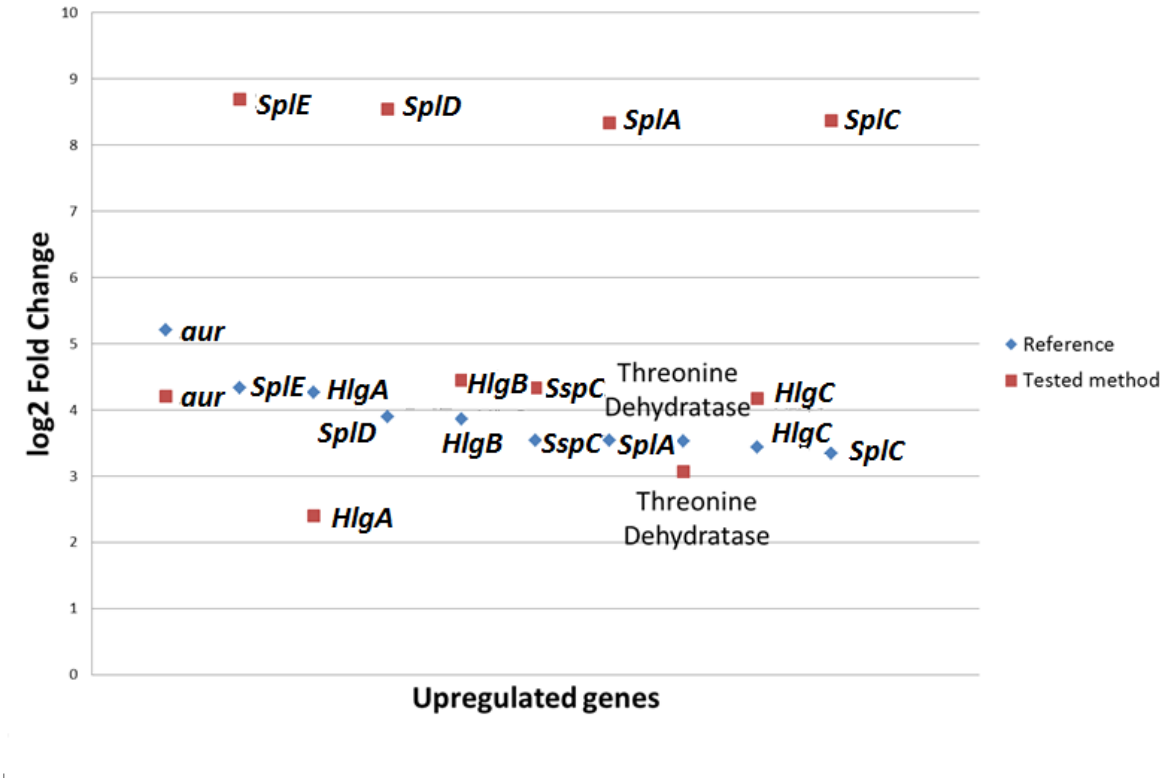

Figure 45: Log_2 fold change of upregulated genes in the tested and reference method

Log_2 fold change of 10 upregulated genes *in vivo* when compared with *in vitro* in *S. aureus* Newman in the method described in this thesis (red) and *S. aureus* USA300 in a published method (blue) (113). Genes are shown in an arbitrary order on the x-axis (Aureolysisn *aur*, Serine Protease *spl* (*splA, splC, splD, splE*), Gamma Haemolysin *hlg* (*hlgA, hlgB, hlgC*), Staphostatin (*sspC*) and Threonine Dehydratase).

Figure 45 shows that genes upregulated in the reference dataset were also upregulated in this experiment. Log_2 fold change values were comparable for the reference and experimental datasets; except, in the experimental dataset, serine protease Spl was more upregulated and the A subunit of gamma haemolysin less upregulated.

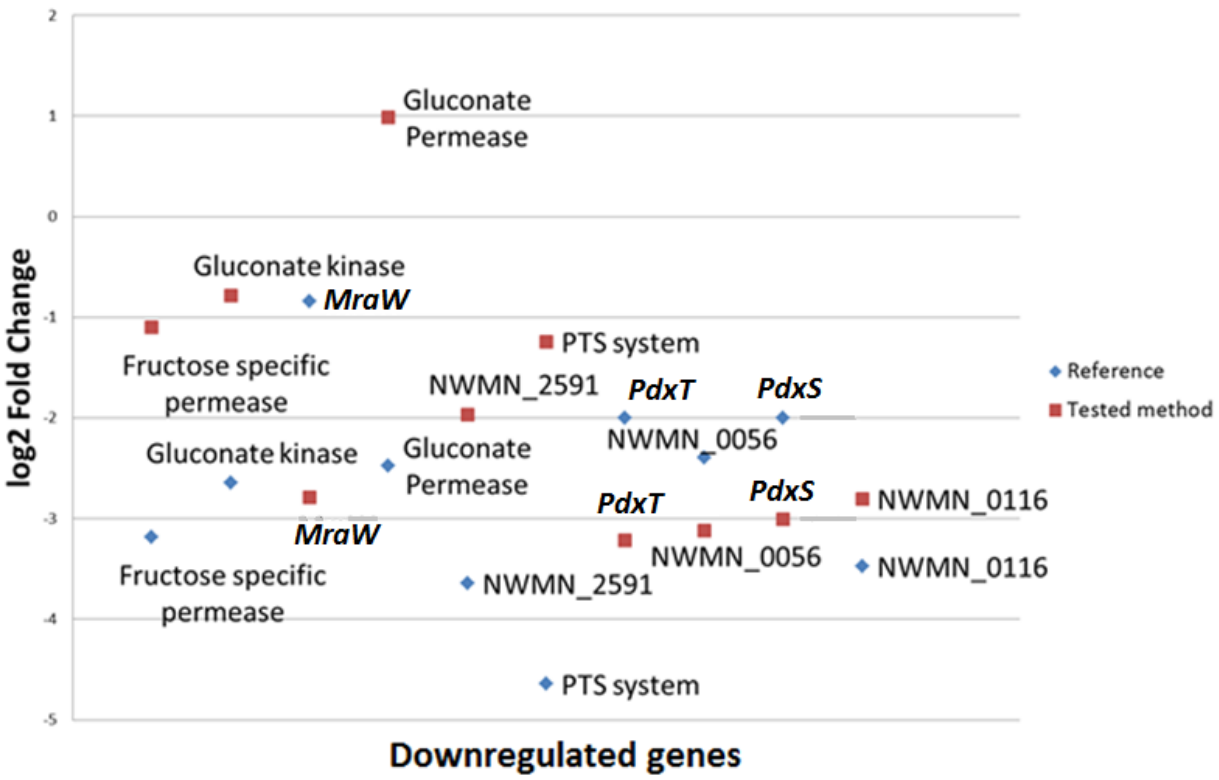

Figure 46: Log_2 fold change of downregulated genes in tested and reference method

Log_2 fold change of 10 downregulated genes *in vivo* when compared with *in vitro* in *S. aureus* Newman in the tested method (red) and *S. aureus* USA300 in a published method (blue) (113). Genes are shown in random order on the x-axis (Fructose specific permease, Gluconate kinase, S-adenosyl-methyltransferase *mraW*, Gluconate Permease, Hypothetical Protein NWMN_2591, PTS system, Glutamine Amidotransferase *pdxT*, Hypothetical Protein NWMN_0056, Pyridoxal Biosynthesis Lyase *pdxS*, Hypothetical Protein NWMN_0116).

Figure 46 shows that gene expression levels in downregulated genes are similar for 9 out of 10 chosen genes in the here described experiment when compared to the published results (113). Even though the extent of downregulation differs 1 to 2 log-fold between the methods, only gluconate permease is found upregulated in the tested method and downregulated in the published reference method. I concluded that, at least for these genes the observed gene expression is congruent with previously published data.

When log_2 fold changes for all genes described by the authors are plotted against log_2 fold changes found in this *in vivo* RNA-Seq experiment, we observe some correlation, as already described for the ten most up- and downregulated genes (Fig. 46). However, they correlate only in a moderate positive relationship (Pearson coefficient = 0.478), indicating differences between the results seen in the Microarray experiment using *S. aureus* USA300 FPR3757 versus results from this thesis' RNA Sequencing using *S. aureus* Newman (Fig. 47).

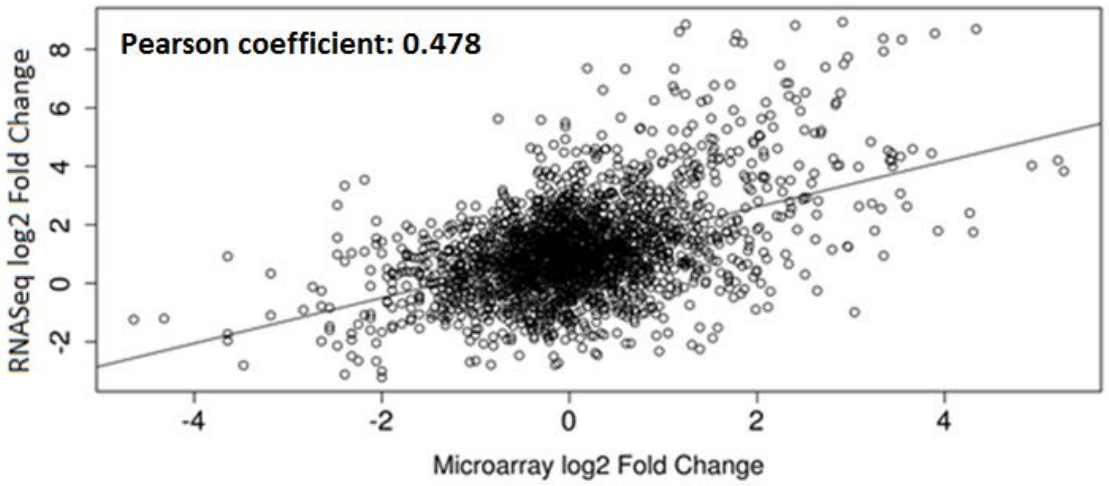

Figure 47: Comparison of RNA Sequencing results from *in vivo* transcriptome of *S. aureus* Newman and Microarray produced data of *in vivo* transcriptomes from *S. aureus* USA300

S. aureus transcriptomes *in vivo* compared with *in vitro* from USA300 generated by Microarray (113) (x-axis) in a reference and from *S. aureus* Newman generated by RNA-Seq (y-axis) [Methods are described in 2.3.4-2.3.12, analysis is described in 2.3.14].

2.4.5 The *in vivo* Transcriptome of *S. aureus* in a murine Infection Model

After the establishment of the method, six bacterial transcriptome samples obtained from infected tissues (murine spleen and kidney) were compared to four replicates of broth-grown inocula. First, the overall distribution of per gene counts, normalized to total counts per sample was assessed.

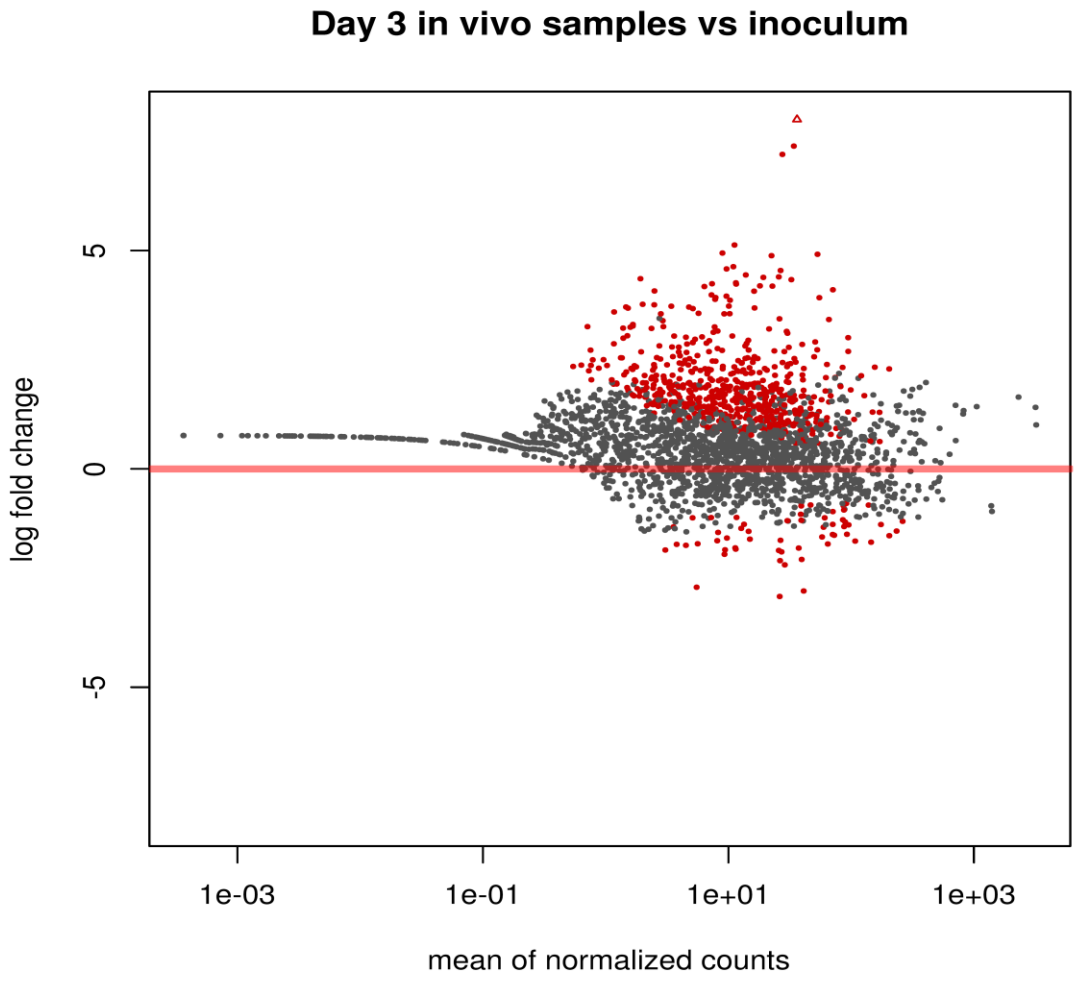

Figure 48: Mean normalized counts per gene in the *in vivo* transcriptome of *S. aureus* Newman when compared to *in vitro*

Mean normalized counts per gene (x-axis) against $\log_2$ fold change observed *in vivo* (y-axis) compared with *in vitro*. Grey dots indicate non-significant (FDR adjusted p-value > 0.05), red significant changes (FDR adjusted p-value =< 0.05) [Method described in 2.3.12].

The distribution of normalized per gene counts indicates that normalization was successful (Fig. 48) and most statistically significant changes in expression *in vivo* occur in upregulation of selected genes (Fig. 48, red dots).

I then looked at the distribution of up and downregulation of genes *in vivo,* considering a fold change of >=2 “upregulated” and a fold change of <= 0.5 “downregulated”. Plotting the per gene FDR corrected *p*-value (*q*-value) against the gene position in the bacterial genome (Fig. 49), I observed that significantly up- and downregulated genes *in vivo* were distributed across the entire genome with upregulated genes (755 genes), far outnumbering downregulated genes (72 genes). Furthermore, 117 genes annotated as encoding for “hypothetical proteins” were found with enriched mRNA levels *in vivo*.

Figure 49: Manhattan plot of *S. aureus* Newman *in vivo* transcriptome

(next page, vertical)

Manhattan plot of gene expression of *S. aureus* Newman *in vivo* during infection when compared to *in vitro*, showing the gene position in the bacterial genome (x-axis) against the $-\log_{10}$ *q*-value. Fold change (FC) is indicated by dot colour with red indicating a gene with upregulated and blue genes with downregulated gene expression. Labels show gene annotation: unlabelled dots are unannotated genes.

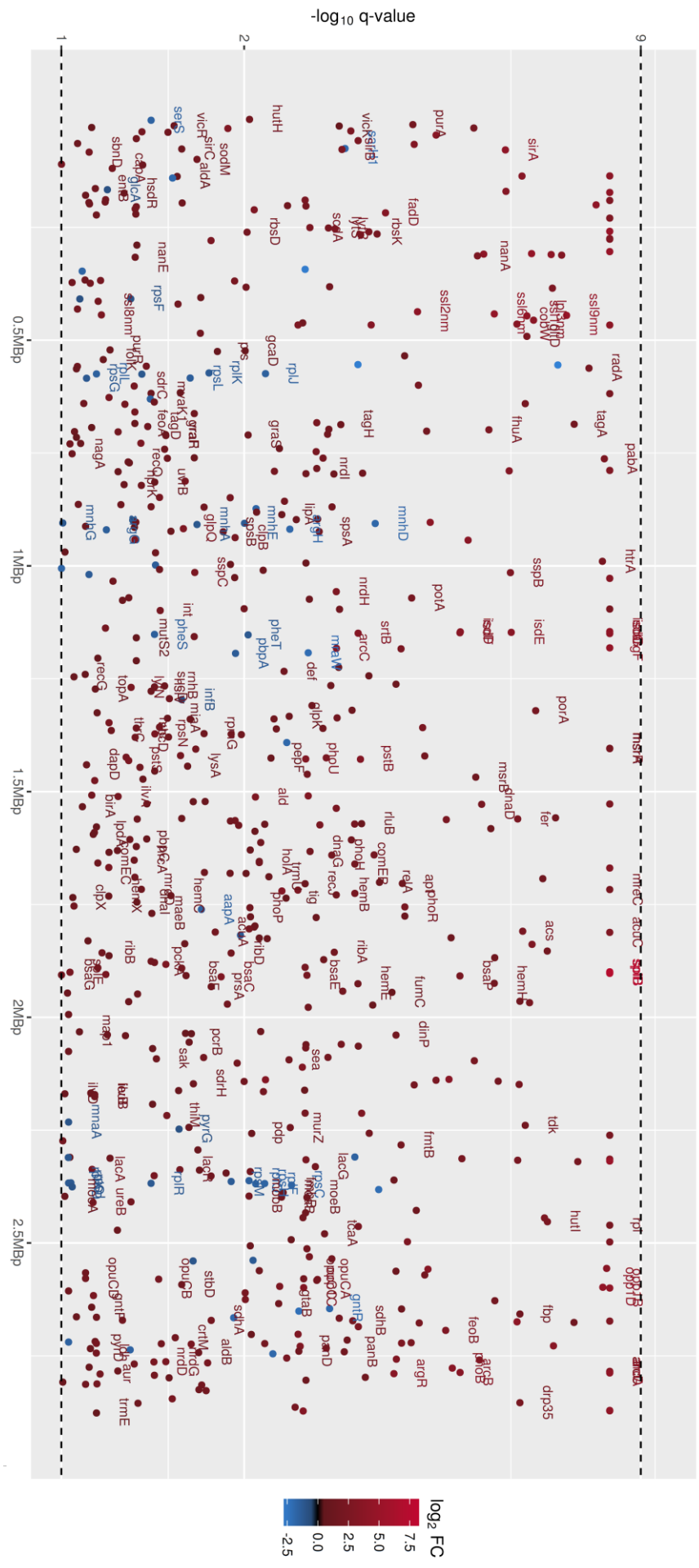
In vivo Day 3 p.i. vs Inoculum
-log10 q-value
log2 FC
-2.5
0.0
2.5
5.0
7.5
0.5MBp
1MBp
1.5MBp
2MBp
2.5MBp

Overall, more upregulated genes were detected than downregulated genes (Fig. 49). Among the twenty most upregulated genes (Table 12 and Fig. 50) in murine tissues *in vivo* compared to broth grown bacteria *in vitro* are toxins, leukotoxin LukED's subunits *lukD* and *lukE*, as well as all genes from the Spl serine protease operon (*splABCDEF*), which are reported to be virulence factors (122, 123). Further genes found fall into the category of iron uptake related proteins (siderophore biosynthesis protein *sbnA* and *sbnB*) and metabolic proteins (*adhE* bifunctional acetaldehyde-CoA/alcohol deydrogenase and diaminopimelate epimerase), indicating a metabolic shift to adapt to the new environment. The largest group, however, is the group of proteins with unknown function (Table 12).

Table 12: **Twenty upregulated genes in *S. aureus* Newman *in vivo***

Fold change expression change in *S. aureus* Newman *in vivo* compared with *in vitro.*

Gene	Product	Fold change	*p*-value (adjusted)
lukE	*lukE*, Leucocidin E subunit	557	7.46E-56
lukD	*lukD,* Leucocidin D subunit	498	7.67E-36
ssl14	Conserved hypothetical protein	481	9.31E-39
splF	*splF,* Serine protease F	474	1.23E-36
splE	*splE,* Serine protease E	452	7.91E-79
bsaA1	Lantibiotic precursor, epidermin	450	2.30E-58
splB	*splB,* Serine protease B	406	4.37E-42
splA	*splA,* Serine protease A	406	1.53E-87
splD	*splD,* Serine protease D	338	2.88E-41
splC	*splC,* Serine protease C	331	4.93E-49
ssl3	Hypothetical protein	316	1.85E-39
ssl13	Conserved hypothetical protein	297	5.31E-28
ssl12	Hypothetical protein, superantigen like	296	4.80E-47
sbnA	*SbnA,* Siderophore biosynthesis protein SbnA	227	2.26E-49
adhE	*adhE*, bifunctional acetaldehyde-CoA/alcohol dehydrogenase	212	4.21E-57
NWMN_2365	Hypothetical protein	196	5.04E-97
sbnB	*sbnB*, staphyloferrin B precursor, ornithine cyclodeaminase	192	1.14E-53
dapF	Diaminopimelate epimerase	185	3.99E-239
fmrO	Conserved hypothetical protein	144	2.05E-63
ssl5	*ssl5nm*, superantigen-like protein 5	141	6.47E-32

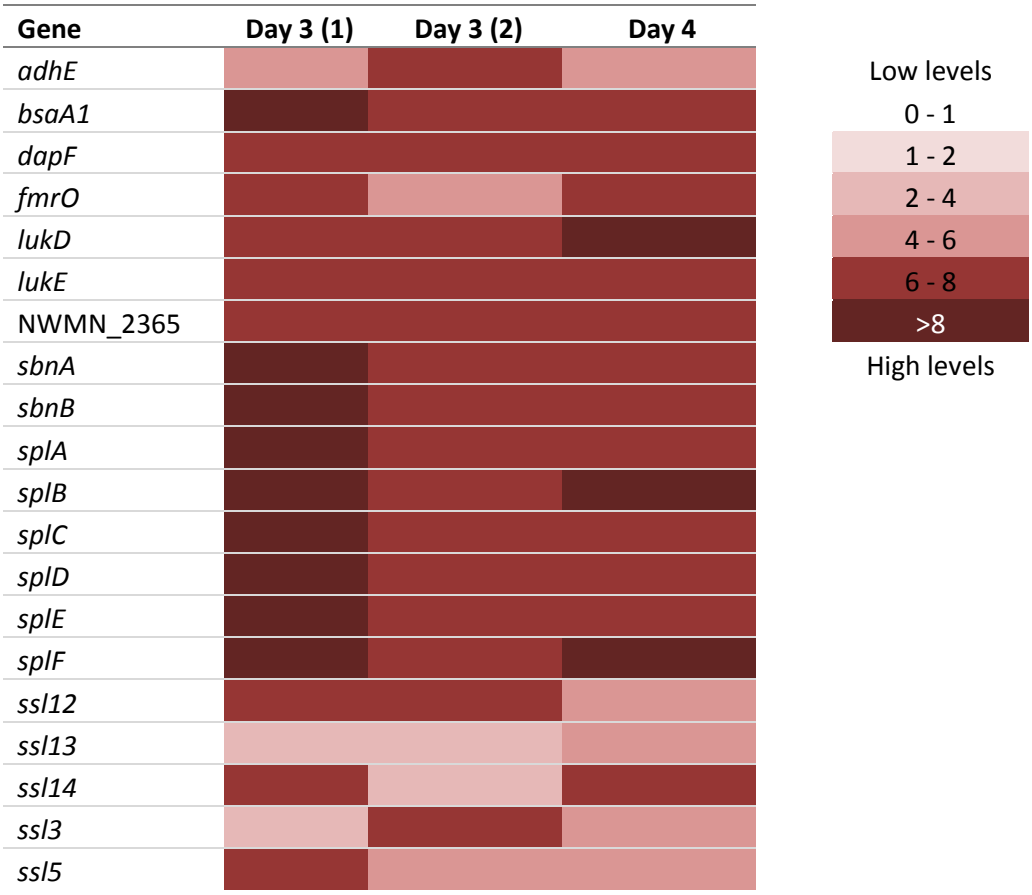

Figure 50: Upregulated genes during *in vivo* expression of *S. aureus* Newman

The expression of twenty genes from *S. aureus* Newman during infection in murine tissues three days (left column – "Day 3(1)" and on the central column its biological replicate "Day 3(2)") and four days post infection (right column – "Day 4") when compared with *in vitro* are displayed in a heat map. Levels of expression in each experiment were calculated by pooling samples from each experiment [Methods described in 2.3.3 – 2.3.2.3.12].

Figure 51: Volcano plot of *S. aureus* Newman *in vivo* transcriptome

(next page, vertical)

Volcano plot of $\log_2$ fold change (LFC) of *S. aureus* Newman *in vivo* transcriptome during infection (pooled spleen and kidney harvested on day 3 post infection) when compared with *in vitro* (inoculum), plotted against respective *q*-value, indicating upregulated genes (red) and downregulated genes (blue).

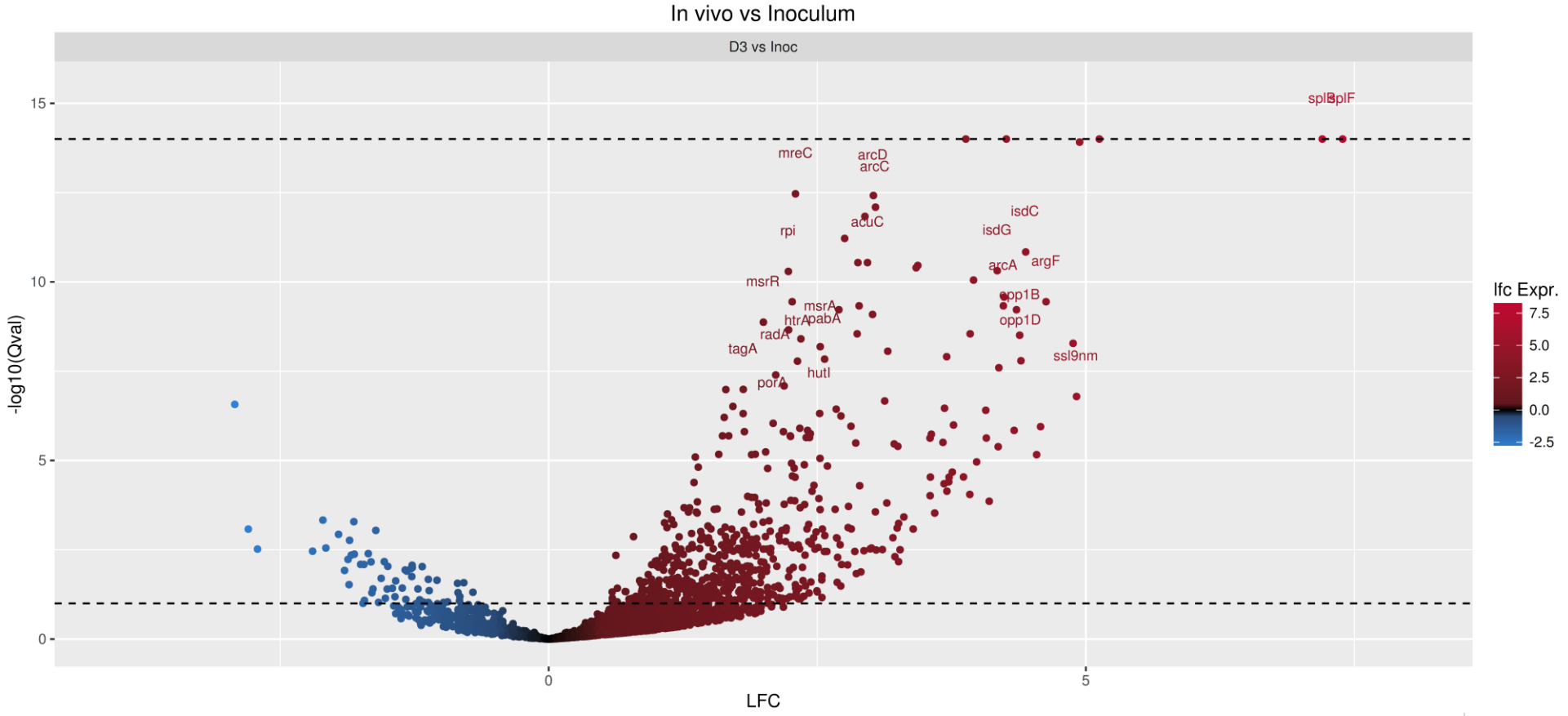
In vivo vs Inoculum
D3 vs Inoc
-log10(Qval)
LFC
lfc Expr.
7.5
5.0
2.5
0.0
-2.5
splB
splF
mreC
arcD
arcC
rpi
acuC
isdC
isdG
arcA
argF
msrR
msrA
htrA
pabA
radA
tagA
hutI
porA
opp1B
opp1D
ssl9nm

When looking at the twenty most downregulated genes (Table 13 and Fig. 52), the most dominant group (7 out of 20 proteins) is composed of proteins influencing the cellular metabolism (O-acetylserine dependent cystathionine beta-synthase, PdxS/T pyridoxal 5' -phosphate synthase, Sodium glutamate transporter, Sulfonate ABC transporter, Basic amino acid/polyamine antiporter, APA family and glucose uptake protein GlcU). Another large proportion is comprised of proteins of unknown function (Table 13). No toxins are found in this group, only a protein predicted to be associated with self-immunity through neutralisation of bacteriocins produced by *S. aureus* (CAAX amino protease) and another superantigen (ssl11nm).

Table 13: Twenty downregulated genes in *S. aureus* Newman *in vivo*

Gene	Product	Fold change	*p*-value (adjusted)
NWMN_0293	Hypothetical protein	**0.06**	1.82E-03
cysM	O-acetylserine dependent cystathionine beta-synthase	**0.10**	1.01E-02
pdxS	*pdxS,* Pyridoxal 5'-phosphate synthase subunit PdxS	**0.10**	1.01E-20
pdxT	*pdxT,* Pyridoxal 5'-phosphate synthase subunit PdxT	**0.11**	3.32E-22
NWMN_0294	Phage head protein	**0.11**	1.25E-03
NWMN_0298	Hypothetical protein	**0.12**	2.96E-02
NWMN_0907	Hypothetical protein	**0.12**	1.22E-03
ltrA	Hypothetical protein	**0.12**	2.17E-03
gltS	Sodium/glutamate symporter	**0.13**	1.05E-03
NWMN_1952	Hypothetical membrane protein	**0.13**	4.11E-03
NWMN_0300	Hypothetical protein	**0.13**	4.50E-02
tgt	Queuine tRNA-ribosyltransferase	**0.15**	1.89E-14
tauB	Sulfonate ABC transporter ATP-binding protein	**0.15**	1.92E-02
NWMN_0299	Phage tail protein	**0.16**	3.88E-02
NWMN_2500	Basic amino acid/polyamine antiporter, APA family	**0.17**	3.90E-08
pfoS/R	Hypothetical membrane protein	**0.18**	2.82E-04
glcU	*glcU,* Glucose uptake protein GlcU	**0.18**	2.13E-15
NWMN_0784	Hypothetical membrane protein	**0.18**	1.11E-05
NWMN_2215	CAAX amino protease	**0.18**	1.74E-03
ssl11	*ssl11nm*, superantigen like protein	**0.19**	1.99E-02

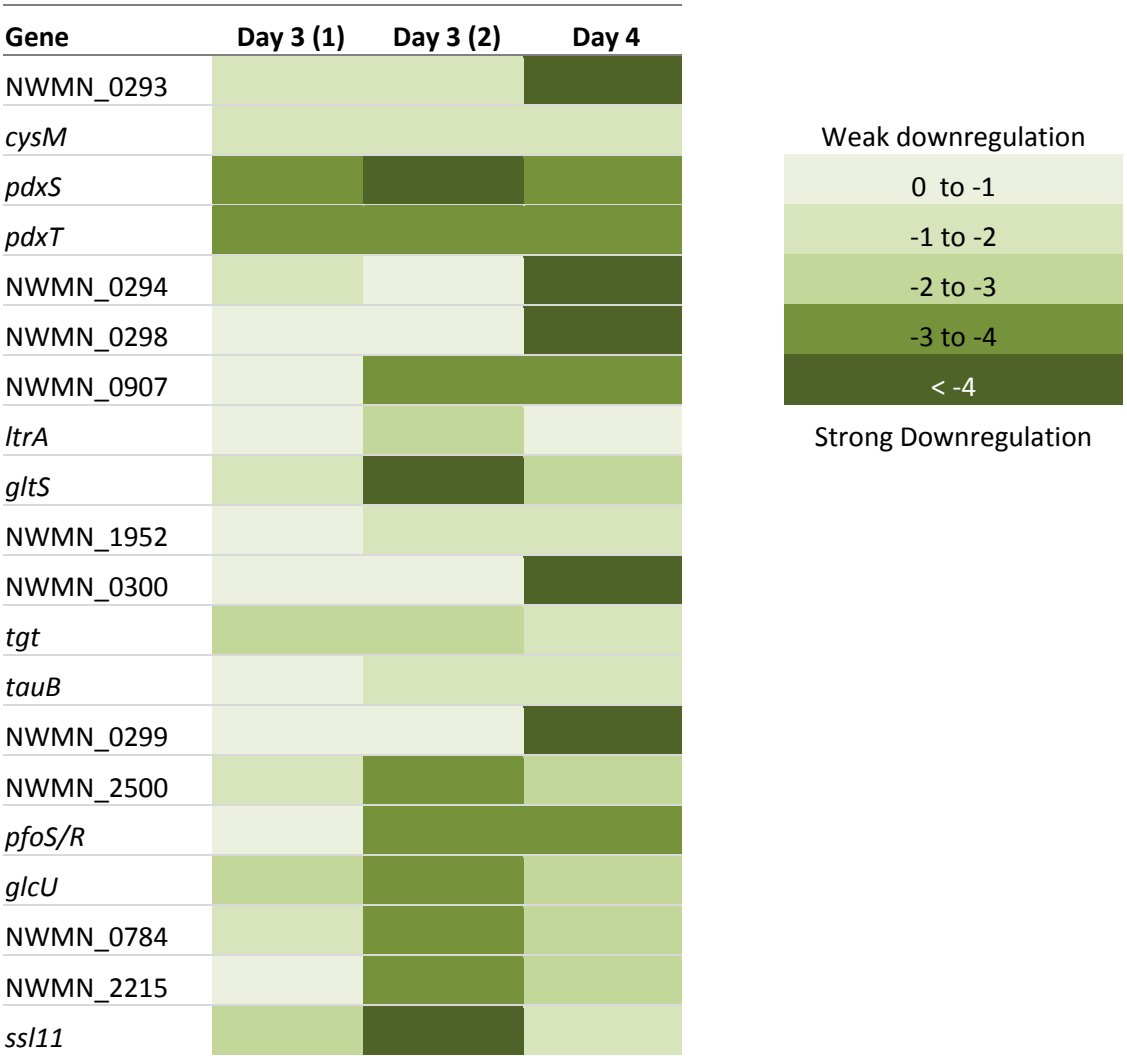

Figure 52: Downregulated genes during *in vivo* expression of *S. aureus* Newman in murine tissues

The expression of twenty genes from *S. aureus* Newman three days (left column – "Day 3(1)" and on the central column its biological replicate "Day 3(2)") and four days post infection (right column – "Day 4") are displayed in a heat map. Levels of expression in each experiment were calculated by pooling samples from one experiment [Methods described in 2.3.3 – 2.3.2.3.12].

2.4.6 Functional Profiling of the *in vivo* Transcriptome

Gene set enrichment analysis (GSEA) is a common way of detecting pathways and functionalities, which are affected by experimental conditions. For *S. aureus,* single genes are grouped according to their molecular function, their involvement in biological processes or their cellular location and each group of genes is analysed as a set [2.3.13].

In this experiment, gene clusters for biological processes indicated enrichment of genes relevant in the tricarboxylic acid cycle, the siderophore transmembrane transport/biosynthetic process and pathogenesis are upregulated (Fig. 53, per gene effects in modules Figures S3 – S4, Supplementary).

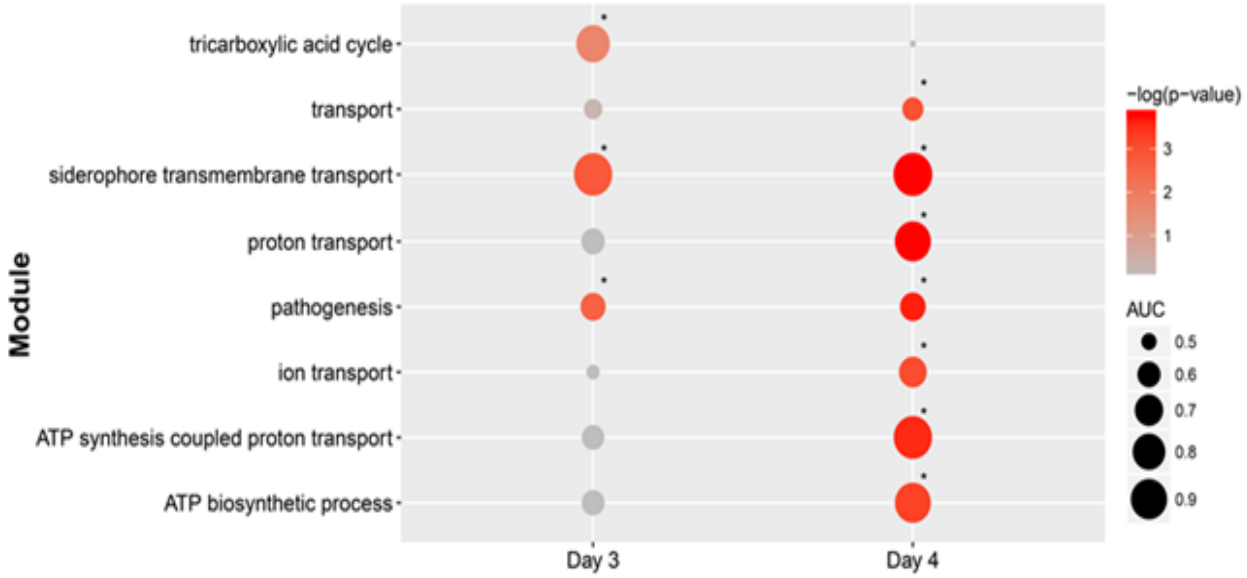

Figure 53: Gene set enrichment analysis for "Biological Process" modules
Genes grouped according to the predicted biological process they are involved in [Methods described in 2.3.13 and 2.3.14]. Effect size (Area under the curve (AUC) displayed as dot size) and significance (shade of red) per gene module are displayed for *in vivo* transcriptomes compared with *in vitro* transcription three (left column) and four days (right column) post infection when compared to *in vitro* broth grown bacteria. Day 4 results are displayed for comparative reasons only, demonstrating the transcriptomic variability over time. Significant modules are marked with "*" with a significant cut-off of q=0.05.

As demonstrated previously in Figure 43, *in vivo* effects on clustered gene modules are time-dependent and bacterial transcription four days post infection displayed a different profile compared with three days after infection (Fig 53).

Genes, which influenced the highly upregulated modules "siderophore transmembrane transport"", were also found to be most influential when they were grouped according to their function at molecular level in the module "siderophore transmembrane transporter activity" (Fig. 54).

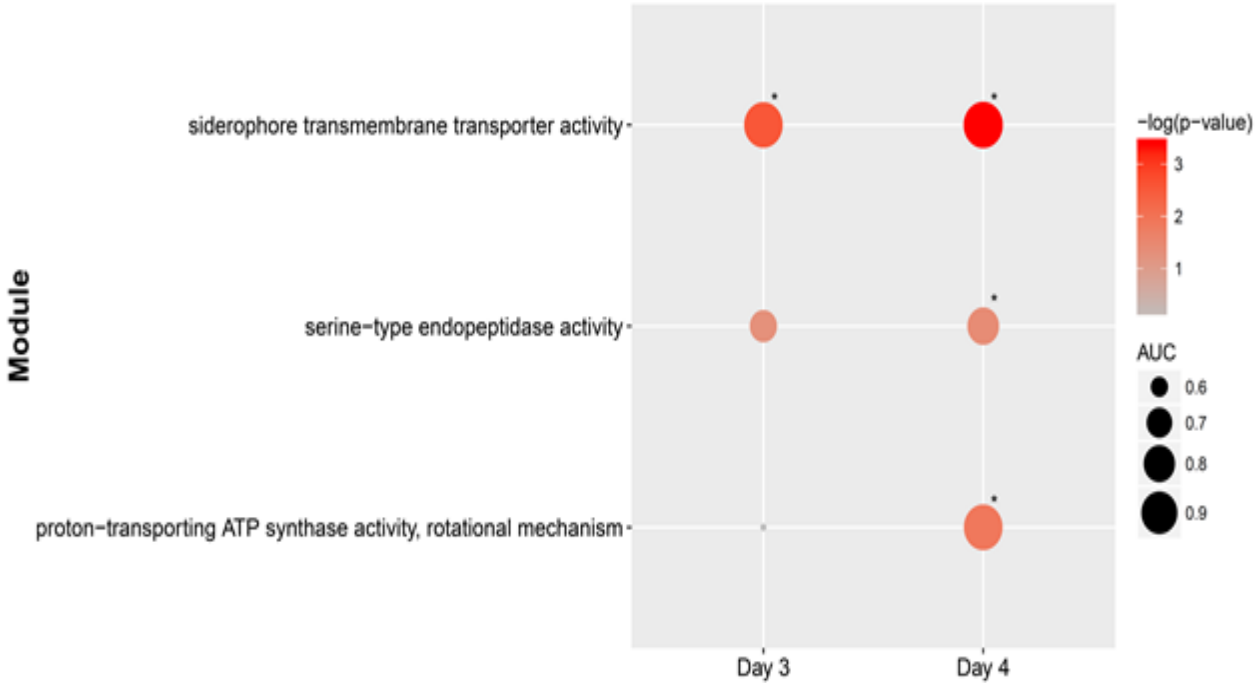

Figure 54: Gene set enrichment analysis for "Molecular Function" modules

Genes grouped according to their predicted molecular function [Methods described in 2.3.13 and 2.3.14]. The effect size (Area under the curve (AUC) displayed as dot size) and significance (shade of red) per gene module are displayed for *in vivo* transcriptomes compared with *in vitro* transcription three (left column) and four (right column) days post infection. The latter is displayed for comparative reasons only, demonstrating the transcriptomic variability over time. Significant modules are marked with "*"using a significant cut-off of q=0.05.

Now, when genes are grouped into modules according to their cellular location, the only significant trend found is an enrichment of *S. aureus* transcripts encoding for extracellular proteins (Fig. 55).

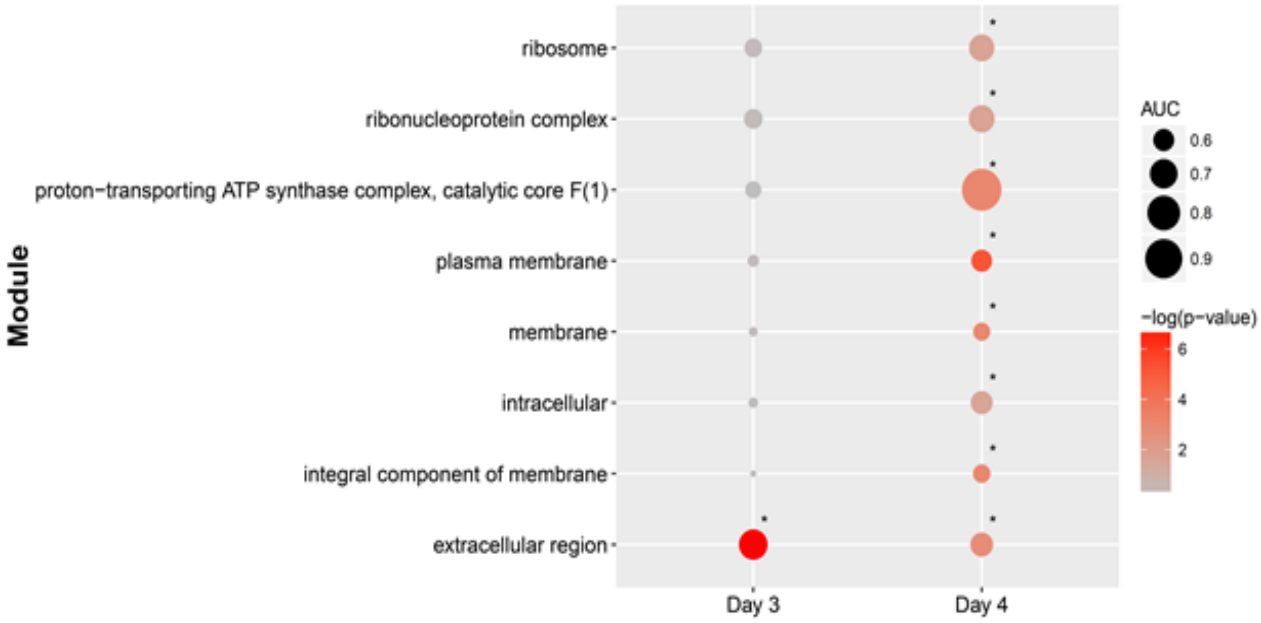

Figure 55: Gene set enrichment analysis for "Cellular Compartment" modules
Modules enriched *in vivo* when genes are grouped according to the cellular compartment. The effect size (Area under the curve (AUC) displayed as dot size) and significance (shade of red) per gene module are displayed for *in vivo* transcriptomes compared with *in vitro* transcriptomes three (left column) and four (right column) days post infection. Significant modules are marked with "*"using a significant cut-off of q=0.05.

.

Transcriptomic characterisation of experimental effects on *S. aureus*, such as exposure to antibiotics, environmental changes and genetic deletions has commonly been carried out using microarrays and RNA Sequencing *in vitro*. *S. aureus* Transcriptomic Meta Database (SATMD) is a database where these published results are collected. In order to identify common pathways up- and downregulated in murine tissues *in vivo* and in previously published conditions, genes were grouped into up- and down-regulated clusters according to their SATMD results (Method is described in 2.3.13). Gene set enrichment analysis resulted in a large overlap of genes found upregulated in various *in vitro* conditions (Fig. 56). One of the overlaps found is with the bacterial transcriptome when inside epithelial cells.

Figure 56: Gene set enrichment analysis of the *S. aureus in vivo* transcriptome using microarray effect based gene modules (upregulation)

(next page)

List of gene clusters upregulated *in vivo* when compared to *in vitro* when grouping genes in clusters according to the conditions under which they are found to be upregulated. [Methods described in 2.3.13 and 2.3.14]. The size of the circle represents the area under the curve (AUC) of the Receiver Operator Curve (ROC), the shade of blue indicates the adjusted *p*-value and significant modules are indicated with an asterisk.

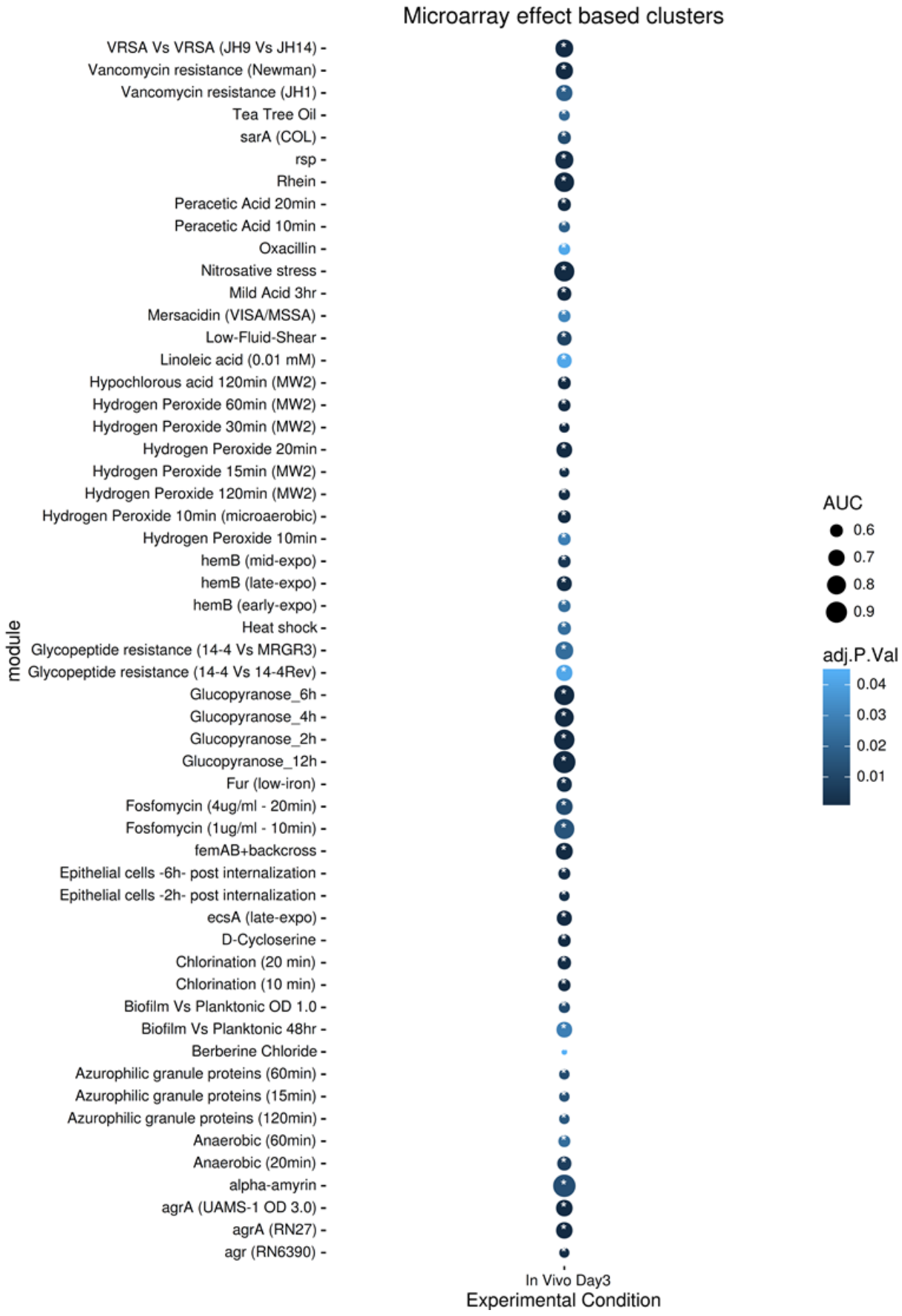
Microarray effect based clusters
VRSA Vs VRSA (JH9 Vs JH14)
Vancomycin resistance (Newman)
Vancomycin resistance (JH1)
Tea Tree Oil
sarA (COL)
rsp
Rhein
Peracetic Acid 20min
Peracetic Acid 10min
Oxacillin
Nitrosative stress
Mild Acid 3hr
Mersacidin (VISA/MSSA)
Low-Fluid-Shear
Linoleic acid (0.01 mM)
Hypochlorous acid 120min (MW2)
Hydrogen Peroxide 60min (MW2)
Hydrogen Peroxide 30min (MW2)
Hydrogen Peroxide 20min
Hydrogen Peroxide 15min (MW2)
Hydrogen Peroxide 120min (MW2)
Hydrogen Peroxide 10min (microaerobic)
Hydrogen Peroxide 10min
hemB (mid-expo)
hemB (late-expo)
hemB (early-expo)
Heat shock
Glycopeptide resistance (14-4 Vs MRGR3)
Glycopeptide resistance (14-4 Vs 14-4Rev)
Glucopyranose_6h
Glucopyranose_4h
Glucopyranose_2h
Glucopyranose_12h
Fur (low-iron)
Fosfomycin (4ug/ml - 20min)
Fosfomycin (1ug/ml - 10min)
femAB+backcross
Epithelial cells -6h- post internalization
Epithelial cells -2h- post internalization
ecsA (late-expo)
D-Cycloserine
Chlorination (20 min)
Chlorination (10 min)
Biofilm Vs Planktonic OD 1.0
Biofilm Vs Planktonic 48hr
Berberine Chloride
Azurophilic granule proteins (60min)
Azurophilic granule proteins (15min)
Azurophilic granule proteins (120min)
Anaerobic (60min)
Anaerobic (20min)
alpha-amyrin
agrA (UAMS-1 OD 3.0)
agrA (RN27)
agr (RN6390)
module
In Vivo Day3
Experimental Condition
AUC
0.6
0.7
0.8
0.9
adj.P.Val
0.04
0.03
0.02
0.01

When identifying groups of *S. aureus* genes, which are downregulated *in vivo* when compared to *in vitro* and which are downregulated in published datasets as well, similar clusters as for upregulation (Fig. 56), such as *agr, sarA,* leukocyte defence molecules and antibiotic exposure, are observed (Fig. 57), indicating a switch to common phenotypes on both sides of regulation. However, *S. aureus* metabolic pathways knockout strains (*mvaA/K1/S*), antibiotic resistance knockout strains (*vraT/vraS*) and cell wall synthesis proteins knockout strains (*murB/E/F*) also show downregulation of groups of genes as it is seen for *S. aureus in vivo* when compared to *in vitro.*

Figure 57: Gene set enrichment analysis of the *S. aureus in vivo* transcriptome using microarray effect based gene modules (downregulation)

(next page)

List of gene clusters downregulated *in vivo* in *S. aureus* Newman compared to *in vitro* when grouping genes in clusters according to the conditions under which they are found to be downregulated. [Methods described in 2.3.13 and 2.3.14]. The size of the circle represents the area under the curve (AUC) of the Receiver Operator Curve (ROC), the shade of blue indicates the adjusted *p*-value and significant modules are indicated with an asterisk.

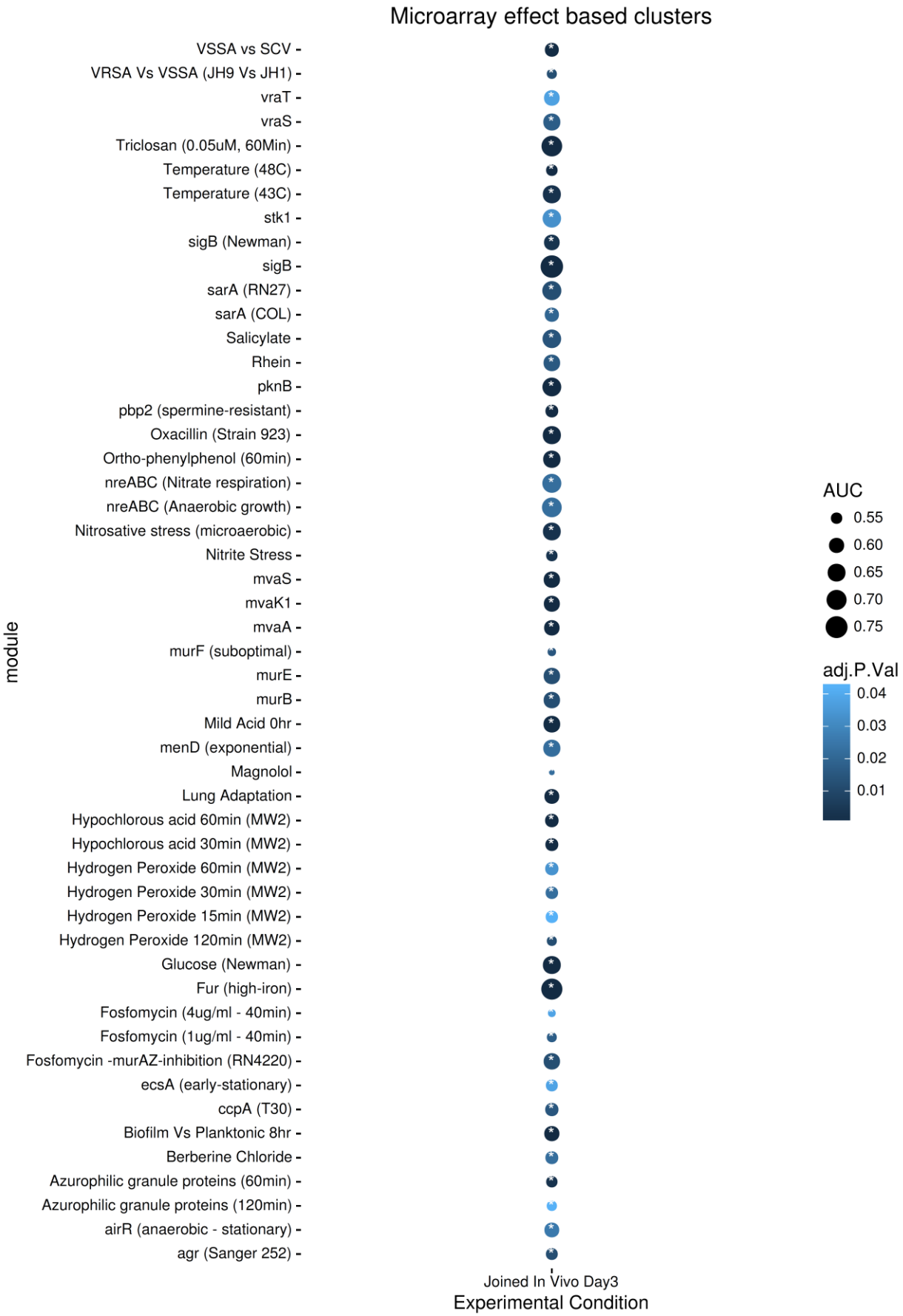
Microarray effect based clusters
VSSA vs SCV
VRSA Vs VSSA (JH9 Vs JH1)
vraT
vraS
Triclosan (0.05uM, 60Min)
Temperature (48C)
Temperature (43C)
stk1
sigB (Newman)
sigB
sarA (RN27)
sarA (COL)
Salicylate
Rhein
pknB
pbp2 (spermine-resistant)
Oxacillin (Strain 923)
Ortho-phenylphenol (60min)
nreABC (Nitrate respiration)
nreABC (Anaerobic growth)
Nitrosative stress (microaerobic)
Nitrite Stress
mvaS
mvaK1
mvaA
murF (suboptimal)
murE
murB
Mild Acid 0hr
menD (exponential)
Magnolol
Lung Adaptation
Hypochlorous acid 60min (MW2)
Hypochlorous acid 30min (MW2)
Hydrogen Peroxide 60min (MW2)
Hydrogen Peroxide 30min (MW2)
Hydrogen Peroxide 15min (MW2)
Hydrogen Peroxide 120min (MW2)
Glucose (Newman)
Fur (high-iron)
Fosfomycin (4ug/ml - 40min)
Fosfomycin (1ug/ml - 40min)
Fosfomycin -murAZ-inhibition (RN4220)
ecsA (early-stationary)
ccpA (T30)
Biofilm Vs Planktonic 8hr
Berberine Chloride
Azurophilic granule proteins (60min)
Azurophilic granule proteins (120min)
airR (anaerobic - stationary)
agr (Sanger 252)
module
Joined In Vivo Day3
Experimental Condition
AUC
0.55
0.60
0.65
0.70
0.75
adj.P.Val
0.04
0.03
0.02
0.01

To sum it up, gene expression *in vivo* is altered compared to *in vitro* and expression of groups of genes was found to be similar to previously published results (Fig. 56 and 57). The presented results demonstrate the extent of overlap of gene clusters identified *in vitro* affected by exposure to an *in vivo* environment. They indicate the complexity of factors causing these transcriptional changes, which are difficult to imitate to a sufficient extent *in vitro*. The presented method and analysis capture these changes and represent a future tool for effective *in vivo* transcriptional analysis of *S. aureus*.

2.5 Discussion

This chapter describes the development and optimization of an RNA extraction method (Chapter 2, [2.4.1]) and quality control (Chapter 2, [2.4.2]) for bacterial samples isolated from infected murine tissue. Crucial steps for obtaining sufficient RNA were preservation after tissue harvest, enrichment of bacterial cells, and the combination of two cell lysis methods (enzymatic and mechanical) to increase overall yield. Assessment of read quality, mapping to the *S. aureus* Newman genome and per gene counting showed that most samples were of high quality in all three aspects (Chapter 2, [2.4.3]). Continuation of a per-gene analysis with these qualitatively high samples resulted in reproducible (Chapter 2, [2.4.4]) *in vivo* transcriptomes for *S. aureus* during murine infection in the kidney and spleen. However, bacterial RNA yield was low, especially when extracting bacteria from murine tissue obtained one day post infection. With further technical improvements, total yield and total number of reads could be further increased, which might make profiling of bacterial expression at earlier time points than three days post infection possible and fewer biological replicates necessary. On the other hand, modern sequencing technologies, such as single-cell sequencing, could erase this problem as soon as they become applicable to prokaryotes, which, as of today, is under development (124). As it stands, the method is technically feasible, reproducible and delivers transcriptomes of sufficient quality for further analysis.

When looking at the effect of the environment during infection on *S. aureus* Newman gene expression at single gene level when compared with *in vitro* (Chapter 2, [2.4.5]), we can see that a large proportion of genes are affected in their expression (23.9% of 2676 annotated genes in the whole genome). These results indicate major differences in bacterial behaviour *in vivo* compared to overnight broth culture, clearly demonstrating that broth cultures are not a suitable medium to analyse or predict pathogenic behaviour of *S. aureus*. This was previously suspected through transcriptional changes observed in experiments mimicking infection conditions *in vitro* (14, 125) as well as seen in other experiments measuring *in vivo* transcriptional changes (104, 113). Genes for well-known and characterised proteins such as haemolytic toxins (Hlg, LukD) and virulence factors such as serine proteases (Spl) were found among the most upregulated during infection. These have been found to be upregulated in *in vivo* conditions previously (14, 126, 127). However, among the twenty most upregulated genes, seven encode unstudied hypothetical proteins. These might be important during infection and therefore interesting therapeutic targets, otherwise unrecognized.

The RNA extraction method presented in this chapter also allows the study of expression downregulation during infection in the sepsis model. Genes encoding proteins involved in the cell metabolism were among the most affected. This is expected as the availability of nutrients in the surrounding environment is drastically altered in tissue and blood compared to growth medium (128, 129). A proportion of genes affected (128/827 ~ 16%) encode unstudied proteins or membrane proteins, whose functions are unknown.

In short, downregulated genes are detected through this method giving it a wider application range, for example measuring the effects a mutation has on *in vivo* gene transcription.

When comparing per-gene effects in this experiment to published data of *in vivo S. aureus* transcription in murine kidney (113), we see some correlation (Chapter 2, [2.4.4, 2.4.5]) (Pearson: r=0.478). There might be several reasons for this variability: Firstly, the authors (113) used microarrays, which have a lower sensitivity and dynamic rang than RNA sequencing (130, 131). Secondly, the extraction method used for RNA purification varies from the method used in this thesis. Thirdly, they used different mouse (C57Bl/6) and bacterial (USA300) strains. Only genes present in both strains could be compared and strain specific variation might influence results in both cases.

Grouping of genes into gene sets according to their molecular function, cellular location or by experimental conditions that affected their gene transcription, allows a more holistic view of the transcriptomic dataset. In the *S. aureus* Newman *in vivo* transcriptome, the main biological processes affected during infection were iron-uptake and pathogenesis processes, as well as the citric acid cycle (Fig. 53/54) and extracellular proteins showed an increase in expression (Fig. 55). When categorizing genes according to environmental factors, which have been reported to alter their expression (using information published in the SATMD database), a variety of experimental conditions published affect gene expression in the same way as during infection in a murine kidney. From the conditions tested *in vitro,* anaerobic, acidic conditions and presence of leukocyte defence molecules (reactive oxygen species, nitrosative species and azurophilic granule proteins) gene expression profiles from

published microarray results show an overlap with *in vivo* expression described in this chapter (Fig. 56 and 57). Transcription regulators such as Agr and SarA are regulators known to be expressed *in vivo* (132-134). Finding genes, which these regulators affect, verifies the suitability of this technique to obtain and analyse RNA from *S. aureus in vivo*. The same applies to epithelial cell internalisation and lung adaptation (103, 125), which represent an *in vivo* state environment. Finding our recently described (59) transcription regulator Rsp among the enriched modules, supported our hypothesis about it being an important regulator during infection. Next, *hemB* mutants are small colony variants of *S. aureus* (135) and these variants can be isolated from infection after inoculation with a normal colony variant and thereby represent an *in vivo* infection adaptation. Iron uptake inhibition (mutation of the iron uptake regulator *fur* and glucopyranose treatment) also seemed to trigger similar gene upregulation as found *in vivo*, where free iron is scarce (128). Finding antibiotic treatments such as tea tree oil, alpha amyrin, lineolic acid oxacillin, mersacidin, D-cycloserine, berberine chloride and fosfomycin might indicate bacterial defence patterns, which are commonly activated in both states, *in vivo* and upon antimicrobial exposure (136-138).

In conclusion, the extraction method described in this Chapter permits the purification, processing and analysis of *S. aureus* RNA from murine tissues. The method yields samples with reduced mammalian RNA, which provide sufficient read depth per sample and allow reproducible profiling of the *in vivo* transcriptome of *S. aureus*. With this technology, bacterial responses during mammalian infection can be monitored. An interesting next step would be to test whether clinical isolates from patients can be investigated using this method, for example by comparing their

transcriptomic profiles to laboratory strains. This would enable us to identify gene transcription that differs, at the same time reveal which pathways are alike and perhaps study effects of genetic variation such as mutation in an *in vivo* setting.

Chapter 3:
Application of an *in vivo* transcriptomic assay to study clinical isolates

3.1 Introduction

Staphylococcus aureus adapts to different environments (139) through feedback systems (140-142) and transcriptional control mechanisms (143-146). As such, its transcription is highly dynamic and different in infection and *in vitro* culture, as microarray data have indicated genome wide transcriptional changes *in vivo* (113) and an RNA-Seq study during infection has shown in Chapter 2 of this thesis. However, the number of bacterial strains studied *in vivo* so far is limited, making the extent of strain specific *in vivo* variation uncertain. It is of interest, how invasive *S. aureus* strains, isolated from patients, adapt to the infection environment in the human host. Clinical pairs – *S. aureus* isolates obtained from the skin or nares and the infection site of the same patient – offer an opportunity for such comparisons.

3.1.1 Clinical Isolate Pairs allow comparative Studies

It has been proposed that invasive *S. aureus* isolates differ systematically from *S. aureus* isolates from the nares (50). Some invasive *S. aureus* isolates show genetic variation (58) and such mutants have been characterised *in vitro* to a certain extent (147). However, how such mutations affect transcription *in vivo*, a complex environment in which the regulatory machinery in the bacterium is stimulated by various factors, has not been studied.

3.1.2 Experimental Approach

This chapter characterises the impact of the infection environment *in vivo* on transcription in three genetic backgrounds: in two isolated from nasal populations in patients (Patient P and S) and the third in the *S. aureus* USA300 strain [for description of strains see section 1.3.3]. Consistency of response patterns is evaluated and results compared to the transcriptional adaptation previously described in *S. aureus* Newman. Commonly upregulated genes in all four genetic backgrounds during infection were identified.

In addition, Patient P and S invasive isolates (Rsp^-) from the bloodstream are studied, which both have a mutation in the transcription factor Rsp. I examine the effect of *rsp* mutation on *in vivo* transcription, comparing Patient P' and S' nasal isolates (Rsp^+) transcriptomes to Patient P' and S' invasive *rsp* mutants (Rsp^-). As a control, I compare the *S. aureus* USA300 JE2 (Rsp^+) *in vivo* transcriptome with a USA300 *rsp* transposon mutant (Rsp^-) *in vivo* transcriptome.

Based on the results of this chapter, I propose new potential *S. aureus* vaccine antigens.

3.2 Research Questions and Objectives

3.2.1 Research Questions

1. Can an *in vivo* transcriptome be characterised for *S. aureus* strains other than Newman and USA300, including those directly obtained from humans (like Patient P and Patient S)?
2. Which genes are upregulated and downregulated across several strains?
3. How does *rsp* mutation affect the *in vivo* transcriptome?
4. Are there genes regulated by Rsp during infection?
5. Are there antigens expressed and/or regulated by Rsp during infection which might make suitable vaccine candidates?

3.2.2 Research Objectives

1. To test if the developed method can be applied to clinical *S. aureus* isolates
2. To identify commonly upregulated genes in pathogenic strains during infection
3. To explore further application of the developed new method
4. To propose an *S. aureus* "*in vivo* core transcriptome" for four strains during infection
5. To characterize *in vivo* effects of *rsp* mutation
6. To propose new *in vivo* expressed vaccine antigen candidates

3.3 Materials & Methods

3.3.1 Reagents, Materials and Primers

Reagents and primers used in Chapter 3 of this work have been described in 2.3.1 and 2.3.2, respectively.

3.3.2 Bacterial Strains and Cultivation

All bacterial strains used in this thesis are listed in Table S1 (Supplementary). In this chapter, *S. aureus* bacterial strains described in Chapter 1 [1.3.3] were used: three Rsp^+ and three Rsp^- strains (genetical backgrounds: USA300, Patient S and Patient P). The bacterial strains were grown by selecting four single colonies from a HBA stock plate (Oxoid) to inoculate TSB. Overnight cultures of 10 ml in an incubation tube were prepared at 180 rpm shaking, 37°C for 18 hours.

3.3.3 Murine Sepsis Model

Eight-week-old female BALB/c mice were administered with *S. aureus* intravenously via the lateral tail vein, with bacterial suspensions of 5×10^6 CFU/mouse from the relevant strain. An aliquot of each inoculum was treated with RNAprotect Bacteria (Qiagen) according to manufacturer's instructions. Weight loss and clinical disease score were monitored throughout the experiment. Animals were sacrificed by cervical dislocation of the neck three days post infection and permanent cessation of circulation confirmed.

3.3.4 Bacterial RNA Extraction and General Quality Assessment

Murine kidneys were harvested and RNA preserved as described in section 2.3.5. Bacterial RNA was extracted from infected murine kidneys as described in sections 2.3.5 to 2.3.7 of Chapter 2. Quality and Quantity of obtained RNA was assessed as described in sections 2.3.8, 2.3.9 and 2.3.10 of Chapter 2 [Supplementary Figure S2 shows a flow chart depicting the process]. Preparation of cDNA libraries, RNA Sequencing and quality control of results were performed as described in section 2.3.11 of Chapter 2, apart from the rRNA removal kit (Ribozero) where "Ribozero Gold" was used instead of "Ribozero Gold epidemiological". Bacterial rRNA was therefore not depleted before sequencing. The reads for all three strain pairs were mapped against the USA300 FPR3757 genome (NCBI accession NC_007793.1) as described in Chapter 2 [2.3.11].

3.3.5 Computational Analysis

Gene-by-gene expression analysis was carried out as described in section 2.3.12. Samples from each respective strain *in vitro* and *in vivo* were compared. Furthermore, the effect of *rsp* mutations was assessed by comparing Rsp^- with Rsp^+ transcriptomes across all three genetic backgrounds. Gene set enrichment analysis (GSEA) was performed as described in section 2.3.13. Subcellular localisation prediction of proteins was carried out using "CELLO" ((148), http://cello.life.nctu.edu.tw/), LocTree 3 ((149), https://rostlab.org/services/loctree3/), PSORTb ((150), http://www.psort.org/psortb/) and LocateP ((151), http://www.cmbi.ru.nl/locatep-db/cgi-bin/locatepdb.py). These four bioinformatics tools use algorithms that predict folding and subcellular

transport of proteins based on their primary structure. If there was a discrepancy in subcellular prediction between any of the four, the location which was predicted by at least two programs was chosen.

3.3.6 Statistical Analysis

The statistical approach used in this chapter was described in Chapter 2 [2.3.14]. Differential expression was considered significant if the false discovery adjusted *p*-value (*q*-value) was below 0.05. A gene was termed 'upregulated' if it had an estimated fold change of larger than 2 and 'downregulated' if the estimated fold change was smaller than 0.5. Accordingly, a significantly upregulated gene is a gene with larger than two fold change expression and *q*-value smaller than 0.05.

3.4 Results

3.4.1 The Transcriptome of Clinical Isolates during Infection

How genetic background affects transcription *in vivo* in different *S. aureus* strains has not been studied, to date. To begin to address this, I have characterised the impact of infection on transcription *in vivo* when compared with *in vitro* broth grown bacteria in different genetic backgrounds.

The bacteria studied were isolated from two patients, denoted Patients P and S ((Patient P and S nasal isolates (Rsp^+) and Patient P and S blood isolates (Rsp^-)). As described in Chapter 1 [1.3.2], two variants were isolated from each of these patients, one from the nose and one from the bloodstream, and the variations altered the sequence of the coding sequence of the Rsp transcription factor. Additionally, the USA300 JE2 (Rsp^+) and USA300 NE1304 (Rsp^-) strains (Table S1) were studied in parallel. USA300 JE2 has been sequenced (Genbank: CP000255.1, *Staphylococcus aureus* subsp. aureus USA300_FPR3757). While these isolates do not encompass the whole diversity of *S. aureus* (Chapter 1, 1.1.2, Table 1), their study should allow the testing of a hypothesis that *S. aureus* transcription *in vivo* is strain dependent.

3.4.1.1 In vivo the majority of the annotated S. aures genome is transcribed differently compared with gene expression in vitro in different strains

In all three strains tested (USA300 JE2 (Rsp^+), nasal isolate Patient P (Rsp^+) and nasal isolate Patient S (Rsp^+)), transcription *in vivo* when compared with *in vitro* differs across a large proportion of the genome, similar to transcriptional changes observed *in vivo* in *S. aureus* Newman in Chapter 2. For the *S. aureus* strain USA300 JE2, the number of significantly downregulated genes (901) during infection compared with *in vitro* exceeds that of upregulated genes (858) *in vivo* (Fig. 58). The *in vivo* transcriptomes of the nasal Patient P and S strains also display expression changes (upregulated: 835/696; downregulated: 798/801 genes, Supplementary Figure S5/6, respectively).

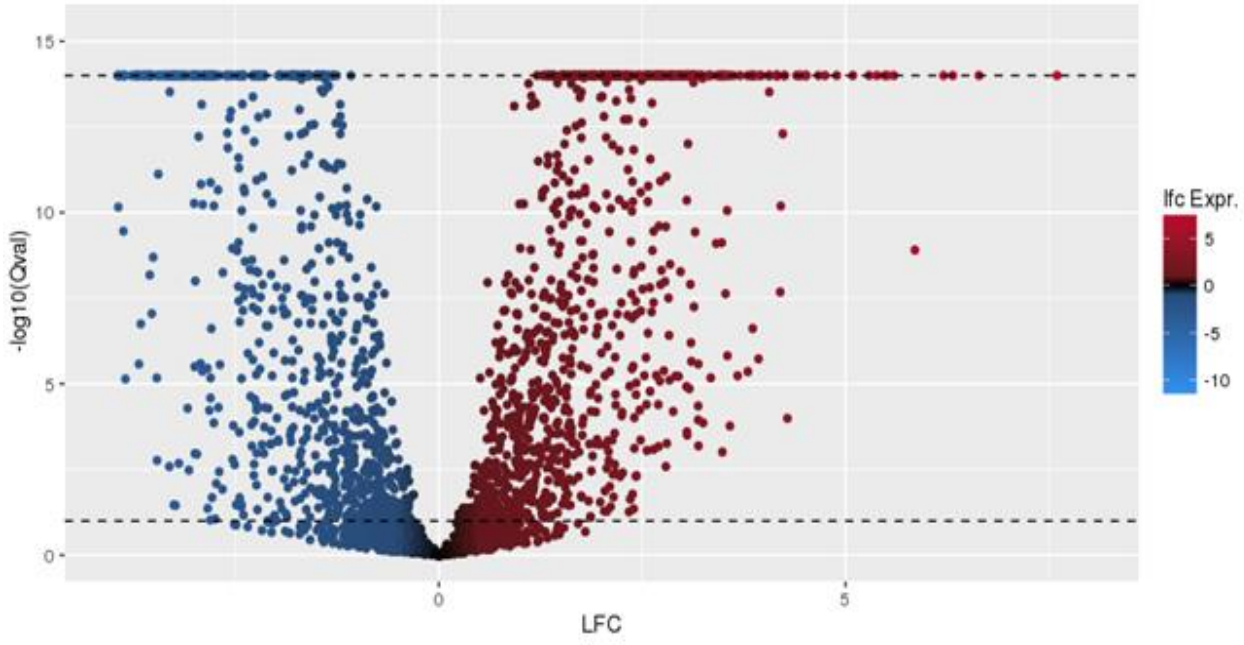

Figure 58: Volcano plot of the *S. aureus* USA300 JE2 *in vivo* transcriptome

Volcano plot of up- (red, on the right) and down- (blue, on the left) regulated genes in *S. aureus* USA300 JE2 during infection in murine tissues compared with broth grown bacteria [Method described in 3.3.3 – 3.3.5]. Log_2 fold change (LFC, x-axis) is plotted against the *q*-value ($-log_{10}$(Qval), y-axis). Genes with q-value<10^{-14} are plotted at q=10^{-14} to improve visibility of significantly affected genes.

3.4.1.2 In vivo transcriptomes of S. aureus USA300 and two nasal isolates correlate

I compared up- and downregulated genes across three strains (USA300 JE2, nasal Patient P and nasal Patient S) and the *in vivo* transcriptomes correlate in expression fold changes. High correlation of the *in vivo* gene expression profiles is found between USA300 and the nasal clinical isolate from Patient P (Pearson coefficient = 0.830, Fig. 59) and the two clinical strains from the nares of Patient P and S (Pearson coefficient = 0.821, Fig. 59). However, the correlation between USA300 and Patient S nasal isolate was only slightly lower (Pearson coefficient = 0.780, Fig. 59). Overall, the expression profiles of all three strains display similarities and a common trend.

A

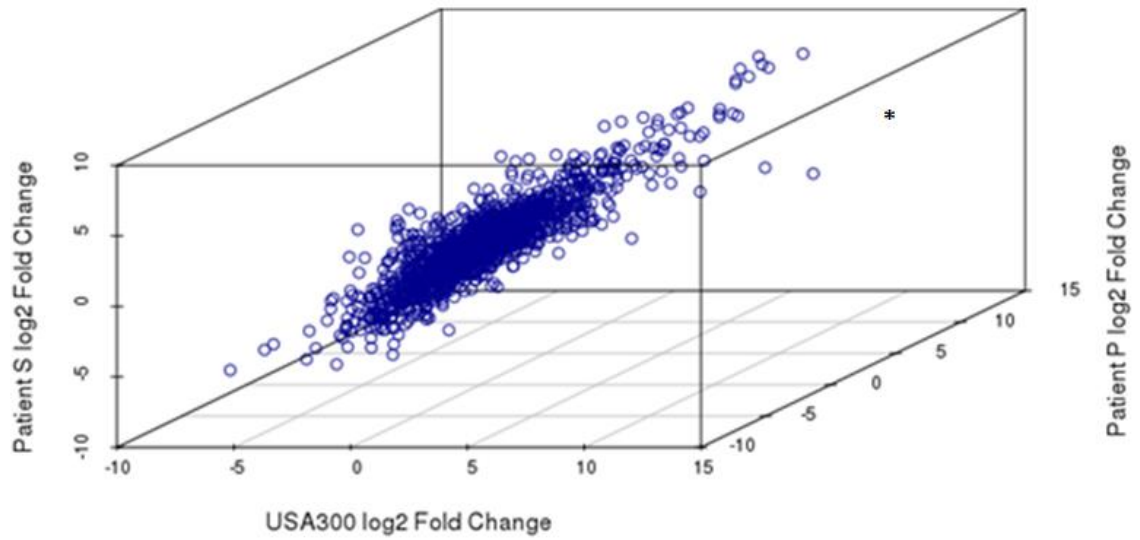

***Pearson coefficient: USA300/PatientP = 0.830, Patient P/PatientS = 0.821, USA300/PatientS = 0.780**

B

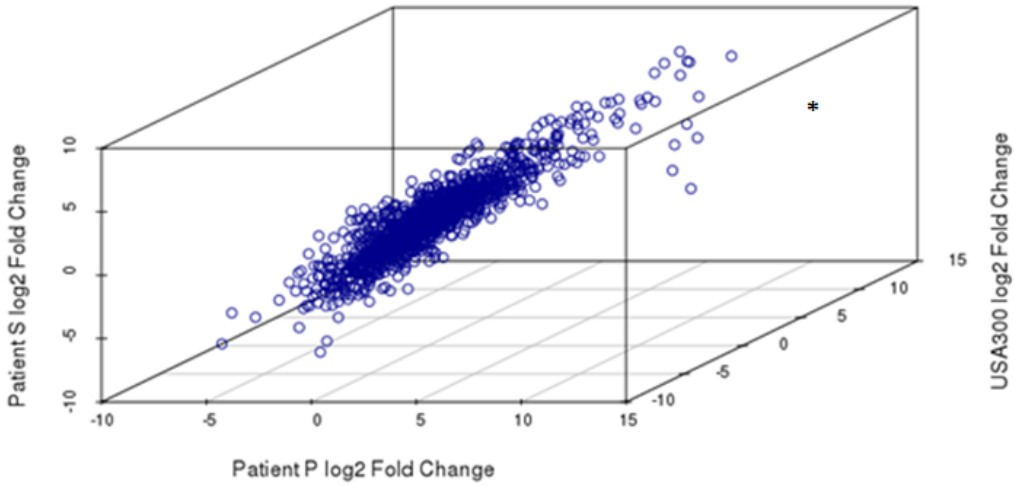

***Pearson coefficient: USA300/PatientP = 0.830, Patient P/PatientS = 0.821, USA300/PatientS = 0.780**

Figure 59: Correlation of USA300 and nasal isolate expression changes *in vivo*

A: Correlation of log_2 fold expression change in USA300 JE2 (Rsp^+) (x-axis), Patient P nasal isolate (Rsp^+) (y-axis) and Patient S nasal isolate (Rsp^+) (z-axis) *in vivo* in murine tissues compared with broth grown bacteria. **B:** A different angle (Patient P nasal isolate on the x-axis, USA300 on the y-axis), demonstrating correlation between expression in USA300, Patient P and S nasal isolate samples.

There are similarities when comparing the results in detail (Table 14): The iron uptake protein SbnC/F, Map and three hypothetical proteins are found among the strongest upregulated in all three strains. The two nasal isolates from Patient P and Patient S share eleven among their twenty most upregulated genes, despite their genetically different backgrounds. When comparing genes with high fold changes in expression, no gene, which is found to be upregulated in any of the strains, is downregulated in another and vice versa. However, some genes (*graD*, *kdpA*, *lucA/C* and *sbnA/B*) are not expressed in the clinical isolates (Fig. 60).

Table 14: Comparison of twenty upregulated genes *in vivo* in three strains

Genes, found in three *in vivo* transcriptomes of *S. aureus* USA300 and the nasal clinical isolates from Patient P and Patient S compared with the inoculum. Genes are ranked according to their expression fold change. Bold letters and the same coloured background indicate appearance of the identical gene in two or more strains (Protease, iron uptake, immune evasion, metal transport, non-metal transport, hypothetical). By contrast, genes with white background were only found to be differentially regulated in one strain.

Rank	*S. aureus* USA300	*S. aureus* Patient P	*S. aureus* Patient S
1	0815, *ear*	**1754, *splE***	**1920, *chs***
2	0118, Cys synthase A	1757, *splB*	**2413, Hypothetical**
3	**2412, Hypothetical**	1758, *splA*	**2412, Hypothetical**
4	1382, *lukS-PV*	**2413, Hypothetical**	**2414, Hypothetical**
5	**2413, Hypothetical**	**2414, Hypothetical**	**1754, *splE***
6	0119, Cyclodeaminase	**2412, Hypothetical**	**2407, Ni-transport**
7	2034, *kdpA*	**1920, *chs***	0223, Complement inhibitor
8	**0121, Putative**	**0121, Putative**	**2364, *sbi***
9	**0120, *sbnC***	1028, *isdB*	2408, Ni-transport
10	0122, *lucA/lucC*	1768, *lukD*	2409, Ni-transport
11	1381, *lukF-PV*	**1917, *map***	2520, Co-transport
12	**1920, chs**	**0120, *sbnC***	0424, Cobalamin synthesis
13	**2414, Hypothetical**	1769, *lukE*	**0120, *sbnC***
14	**0123, sbnF**	**0123, *sbnF***	**0123, *sbnF***
15	**1917, *map***	1759, Hypothetical	2406, Putative transporter
16	0774, *empbp*	1973, *hlb*	**1917, *map***
17	0125, Carboxylase	2367, *hlgB*	**0121, Putative transporter**
18	2033, Anhydrid	**2407, Ni-transport**	0116, *sirB*
19	1379, Putative	0124, HpcH/HpaI	0126, Hypothetical
20	2012, Dehydratase	**2364, *sbi***	0138, *deoD*

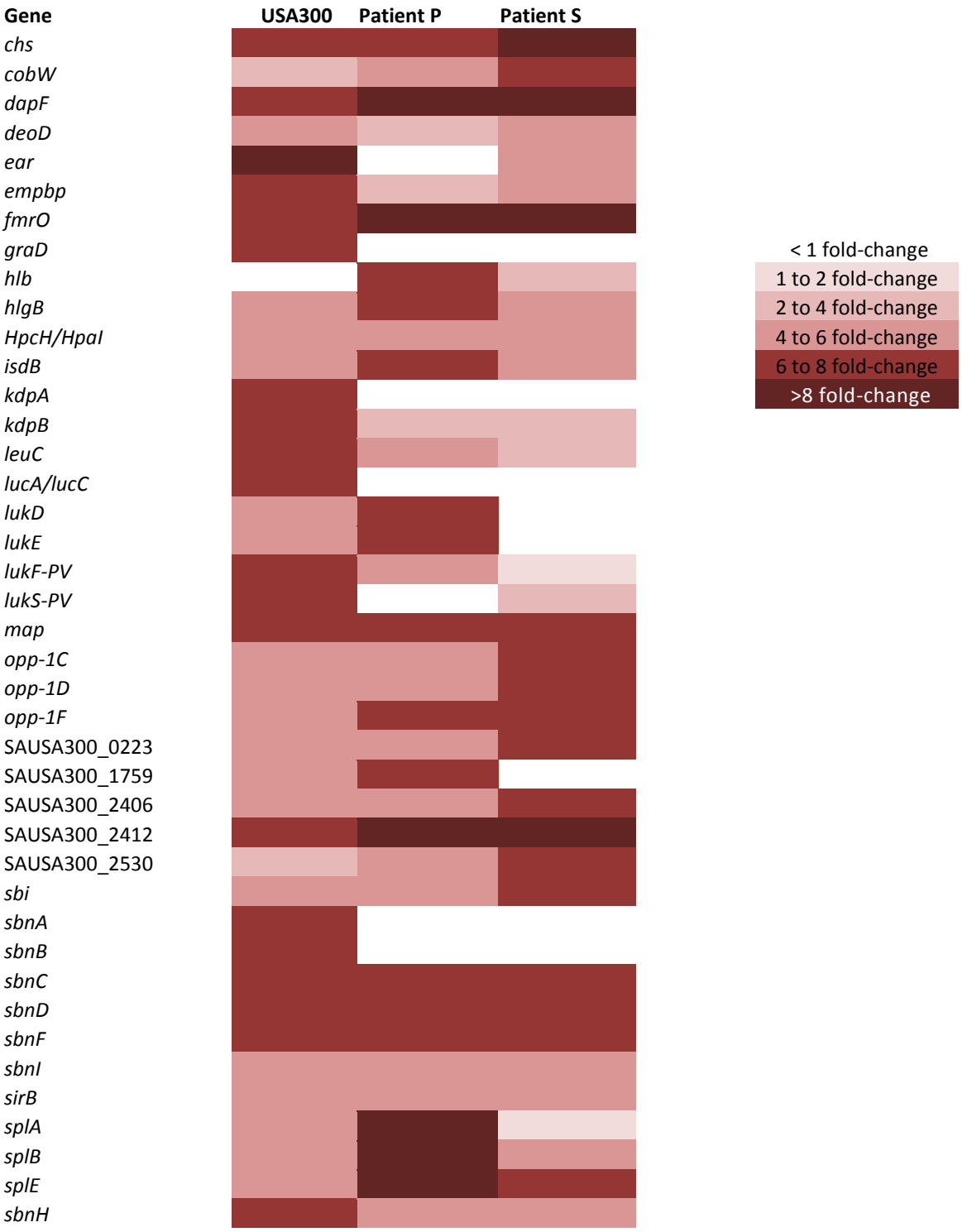

Figure 60: **Upregulated genes with large fold changes in expression *in vivo***

Heat map analysis of upregulated genes *in vivo* compared with *in vitro* in USA300 JE2 (Rsp^+) (left), Patient P nasal isolate (Rsp^+) (centre), Patient S nasal isolate (Rsp^+) (right).

Most genes, for which gene expression is upregulated during infection (Fig. 60), are upregulated in all three strains, but SAUSA300_0118 (Cys synthase A), SAUSA300_0119 (Cyclodeaminase), SAUSA_0122 (LucA/LucC) and SAUSA300_2034 (KdpA) are not transcribed in the clinical isolates (Fig. 60). Six genes (*ear*, *hlb*, *lukS-PV*, *lukF-PV*, SAUSA300_1759, *splA*) show no transcription changes in one strain, while upregulation is present in the other two strains (Fig. 60). However, overall transcriptional trends among this small set of upregulated genes is comparable.

Similar to the congruence observed in upregulated genes, downregulated genes in all three tested strains exhibit similar signatures (Table 14). Ten genes, which are downregulated in USA300, are not transcribed in the clinical nasal isolates. All other genes are downregulated equally in the three backgrounds (Fig. 61).

Table 15: Comparison of twenty downregulated genes *in vivo* in three strains

Genes found in three *in vivo* transcriptomes of *S. aureus* USA300 and the clinical nasal isolates from Patient P and Patient S during murine infection when compared with broth grown bacteria, ranked according to their expression fold change. Bold letters and the same coloured background indicate appearance of the identical gene in two or more strains (Toxins, metabolism, transcription regulator, immune evasion, hypothetical).

Rank	*S. aureus* USA300 [locus tag #, name]	*S. aureus* Patient P [locus tag #, name]	*S. aureus* Patient S [locus tag #, name]
1	**2463, *ddh***	**0654, *sarX***	**1068, PSM β**
2	**1068, PSM β**	**0172, Hypothetical**	**1067, PSM β**
3	**1067, PSM β**	**2463, *ddh***	**2632, Putative protein**
4	**1062, *argF***	0113, *spa*	**2463, *ddh***
5	**0172, Hypothetical**	**1062, *argF***	2164, Hypothetical
6	1063, *arc*	**2573, *isaB***	2333, nark/T transporter
7	1633, *gap*	**1072, *mraZ***	**1072, *mraZ***
8	1180, Hypothetical	**2632, Putative protein**	2107, mtlA transporter
9	**0065, *sarX***	**0114, accessory regulator SarH**	0171, Cation efflux
10	0067, Usp	**1221, Hypothetical**	1065, Exfoliative toxin A
11	0064, *arcD*	1652, *uspA_2*	**2041, Hypothetical**
12	**2573, *isaB***	2279, *LysR*	2275, gdhII
13	2278, *hutU*	1064, *arcP*	0781, Hypothetical
14	0062, *arcB*	**2041, Hypothetical**	1107, Hypothetical
15	1230, Hypothetical	1073, *mraW*	**1062, *argF***
16	**2132, Uncharacterised**	2166, *alsS*	**0654, *sarX***
17	0803, Cro/Cl regulator	0933, Hypothetical	2398, Putative ABC transporter
18	**0114, accessory regulator SarH**	1984, Hypothetical	1685, Uncharacterised
19	1656, *uspA_1*	2313, *lctP*	**0172, Hypothetical**
20	**1221, Hypothetical**	**2132, Uncharacterised**	2097, Hypothetical

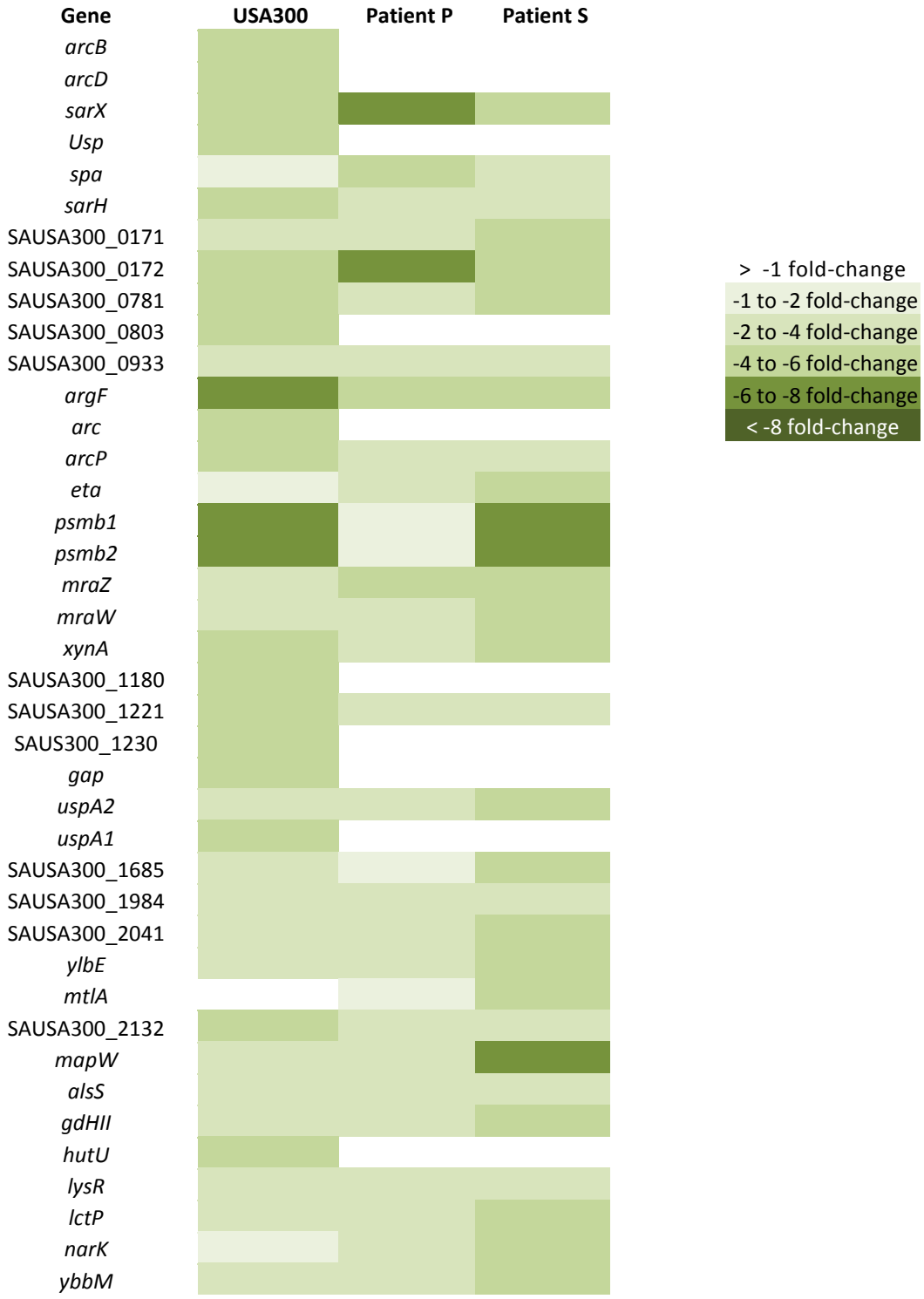

Figure 61: **Downregulated genes with large fold changes in expression *in vivo***

Log_2 fold expression change of downregulated genes *in vivo* compared with *in vitro* in USA300 JE2 (Rsp^+) (left), Patient P nasal isolate (Rsp^+) (centre) and Patient S nasal isolate (Rsp^+) (right).

3.4.2 Functional Profiling of the nasal Clinical Isolates' *in vivo* Transcriptomes

The per-gene analysis demonstrates correlation of *in vivo* transcriptomes between the strains USA300 JE2 and the nasal isolates of Patient P and Patient S. When testing for enrichment in gene sets, grouping according to biological process involvements, results indicate enrichment in metabolic and biosynthetic processes. A pathway upregulated in all tested strains *in vivo* is pathogenesis (Fig. 62), partially driven through upregulation of the *ssp* and *hlg* operon, while oxidation-reduction processes are reduced in all strains.

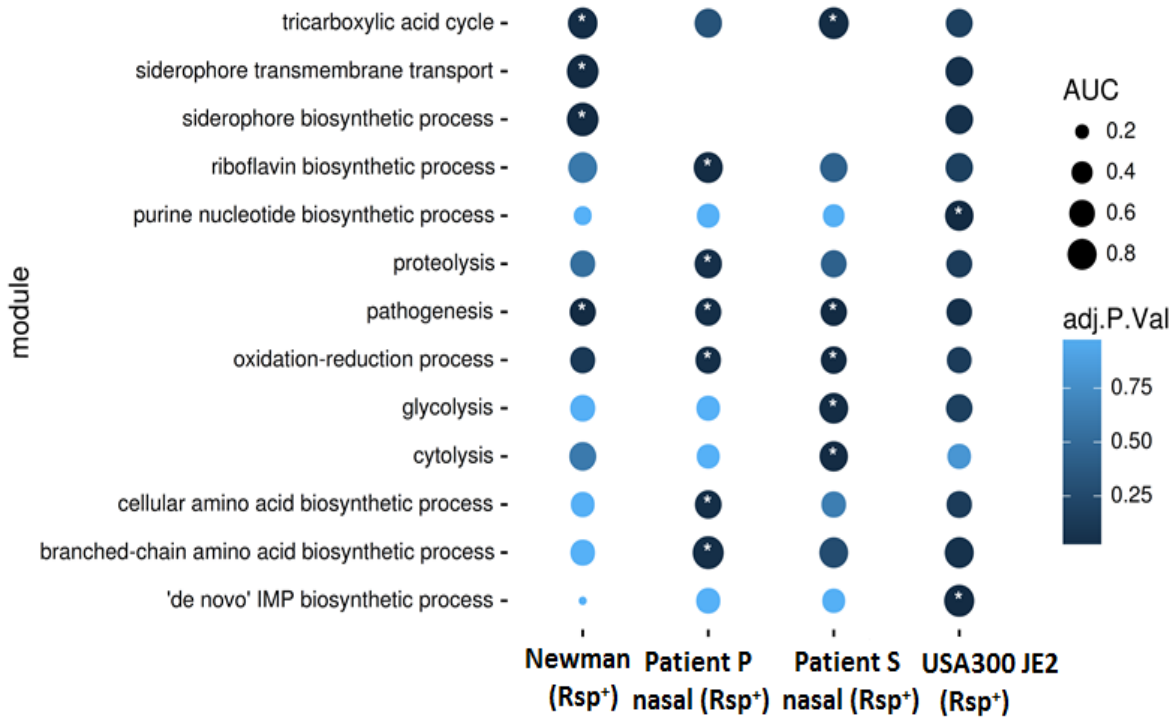

Figure 62: Gene set enrichment analysis for "Biological Process" modules

Genes were grouped according to the predicted biological process they are involved in [Method described in 3.3.5]. The effect size (Area under the curve (AUC) displayed as dot size) and significance (shade of blue) per gene module are displayed for *in vivo* transcriptomes 3 days post infection when compared to *in vitro.* Results for the *S. aureus* strains Newman (Rsp^+) (left) and USA300 JE2 (Rsp^+) (right), as well as the nasal clinical isolates from Patient P (Rsp^+) and S (Rsp^+) (centre) are shown. Significant modules are marked with "*" using a significant cut-off of q=0.05.

When grouped based on their molecular function, only genes encoding for oxidoreductases appear to be significantly downregulated in the clinical isolate obtained from Patient S' nares. Any upregulation of siderophore synthesis or transport as observed in *S. aureus* Newman (Chapter 2, [2.4.6]) is not detected at a significant level in any of the other strains investigated (Fig. 63).

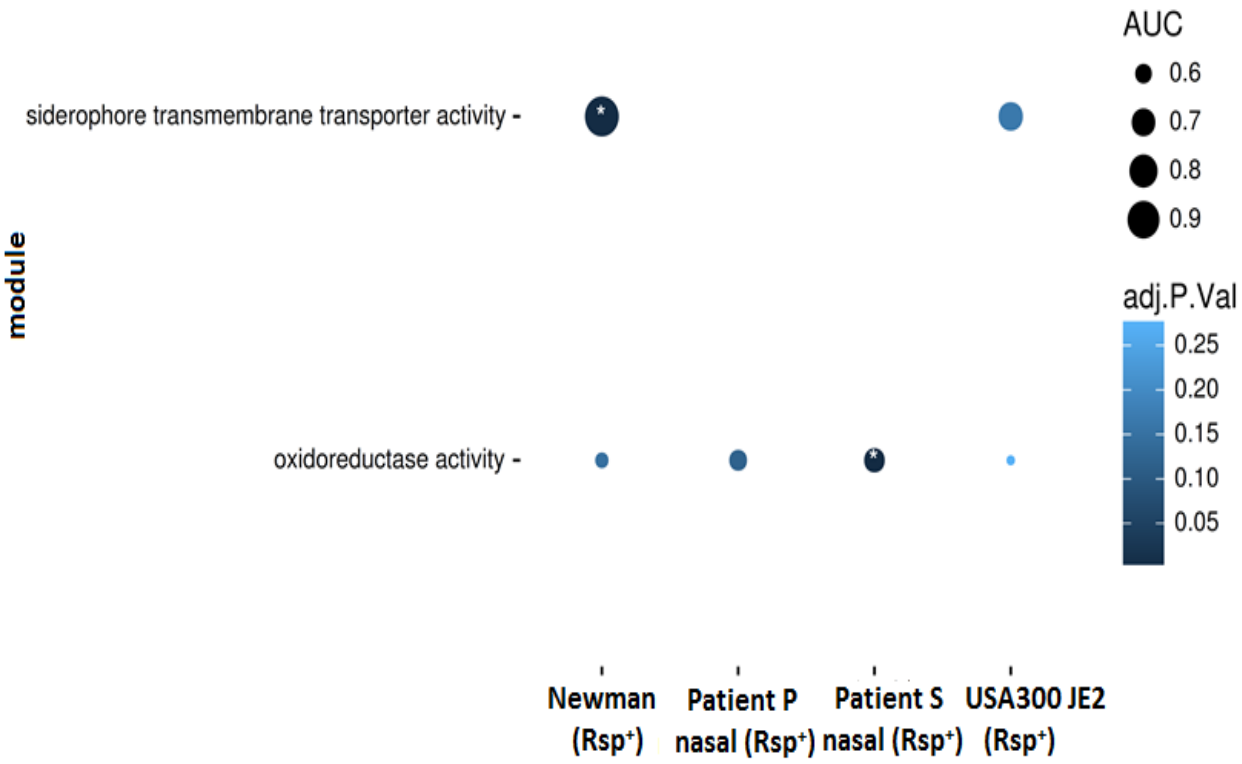

Figure 63: Gene set enrichment analysis for "Molecular Function" modules

Genes were grouped according to their predicted molecular function [Method described in 3.3.5]. The effect size (Area under the curve (AUC) displayed as dot size) and significance (shade of blue) per gene module are displayed for *in vivo* transcriptomes 3 days post infection when compared to *in vitro.* Results for the *S. aureus* strains Newman (Rsp^+) (left) and USA300 JE2 (Rsp^+) (right), as well as the nasal clinical isolates from Patient P (Rsp^+) and S (Rsp^+) (centre) are shown. Significant modules are marked with "*" using a significant cut-off of q=0.05.

As previously observed in *S. aureus* Newman, genes encoding for secreted proteins seem to be upregulated during infection in USA300 JE2 and clinical nasal isolates as well (Fig. 64). Furthermore, USA300 JE2 appears to have enriched gene expression of proteins located at the cell wall, chromosomal DNA and the ribosome within a ribonucleoprotein complex.

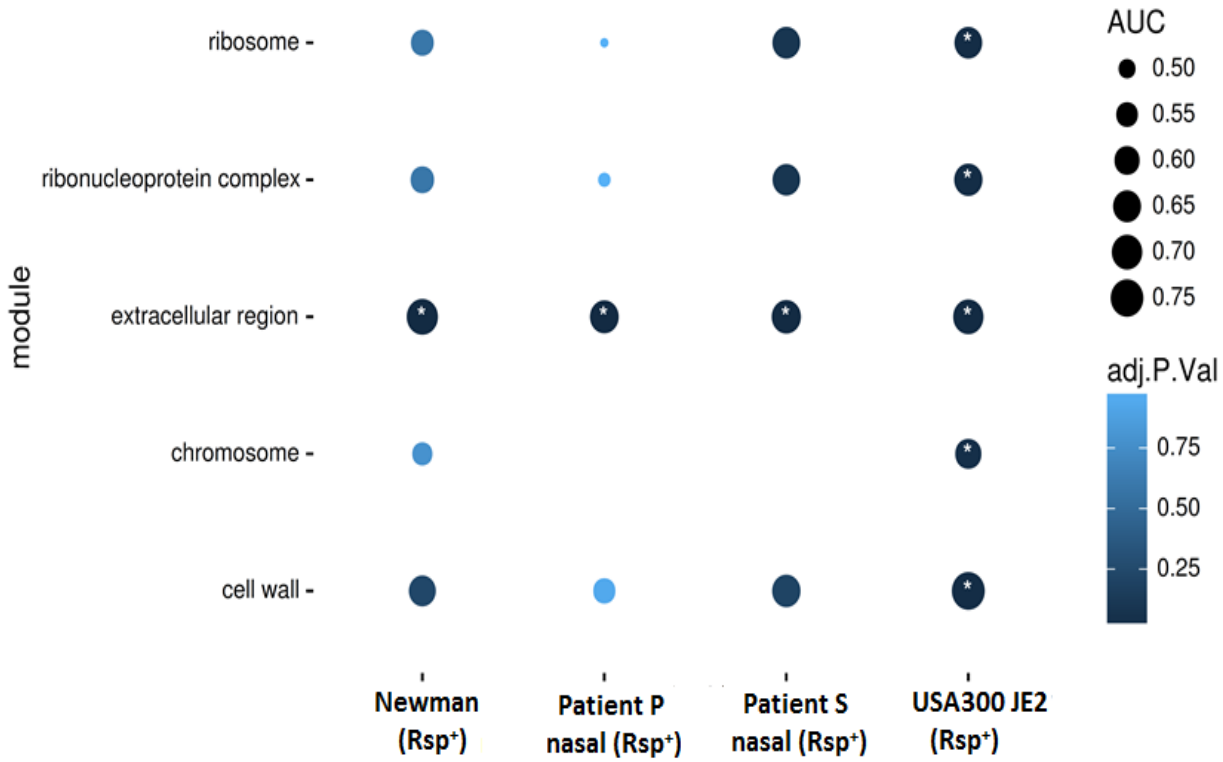

Figure 64: Gene set enrichment analysis for "Cellular Compartment" modules
Genes were grouped according to their predicted subcellular location [Method described in 3.3.5]. The effect size (Area under the curve (AUC) displayed as dot size) and significance (shade of blue) per gene module are displayed for *in vivo* transcriptomes 3 days post infection when compared to *in vitro.* Results for the *S. aureus* strains Newman (Rsp^+) (left) and USA300 JE2 (Rsp^+) (right), as well as the nasal clinical isolates from Patient P (Rsp^+) and S (Rsp^+) (centre) are shown. Significant modules are marked with "*" using a significant cut-off of q=0.05.

To summarize, the functional profiles of the *in vivo* transcriptomes of four different *S. aureus* strains display strain specific signatures and most gene modules are enriched in one or two strains only. The most consistent enrichment during infection across all three strains is found in genes encoding extracellular proteins and proteins involved in pathogenesis or oxidation-reduction mechanisms, underlining the importance of virulence factors and metabolic adaptation in the *in vivo* environment.

3.4.3 Upregulated Genes in an *S. aureus* "*in vivo* core Transcriptome"

When developing a vaccine, interesting antigens are proteins, which are a) expressed during infection and b) essential for the establishment and maintenance of infection. In Chapter 2 [2.4.5] and 3 [3.3.1], I have presented four "*in vivo*" transcriptomes, obtained from *S. aureus* infected murine tissues three days post infection when compared with *in vitro*, for four different bacterial strains. The observed differences indicate that not all genes expressed *in vivo* by one strain are necessarily essential, as their expression might not be detected in another strain during infection, even though the genes are present in the genome. In order to identify genes, whose expression might be essential during infection across different *S. aureus* species, I identified those upregulated in all four *in vivo* transcriptomes. Overlap in these *in vivo* transcriptomes can help us identify genes, which might be present in a strain-independent "*in vivo* core transcriptome". As an approach to define such a core transcriptome, significantly upregulated genes (FDR corrected *p*-value <0.01 and fold change >2) for *S. aureus* USA300 JE2, nasal Patient P, nasal Patient S and Newman were extracted and the overlapping genes between the four strains identified under conditions tested (Fig. 65, full list of genes in Table S5, Supplementary). The numbers of down- and upregulated genes were similar, but which genes were affected differed in all four strains. The largest difference between strains is between *S. aureus* Newman, for which reads were mapped against its specific genome, and the other three strains, for which reads were mapped against the USA300 FPR3757 genome, since the two nasal isolates had no annotated full genome available. The nasal isolates and USA300 JE2 resemble to their *in vivo* transcriptome, having 293 upregulated genes in common. Overall, the nasal isolates

from Patient P and Patient S appear to have only a few genes upregulated in a strain specific way (97 for Patient S and 31 for Patient P).

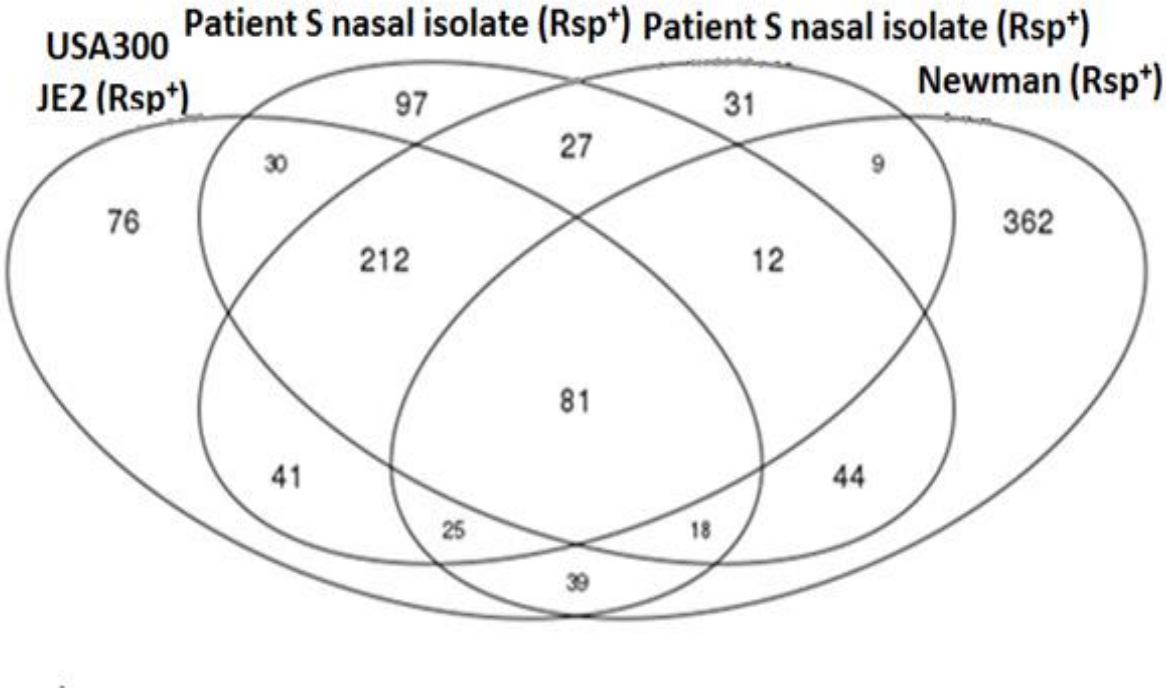

Figure 65: Venn diagram of *in vivo* upregulated genes in four different strains.

Transcriptomes of *S. aureus* strains Newman, USA300 JE2 and the nasal isolates of Patient S and Patient P were characterised *in vivo* in murine tissue compared with broth grown bacteria of the same strain. Reads for *S. aureus* Newman were mapped against the *S. aureus* Newman genome (DNA Database of Japan, accession number: AP009351), all other strains (USA300 JE2, nasal Patient P and S isolates) were mapped against the USA300 FPR3757 genome (NCBI accession NC_007793.1). Overlap of ellipses indicates the number of genes, which are upregulated in more than one strain. The centre shows the number of genes upregulated in all four strains.

I was able to identify 81 genes (Fig. 66 and Table S5, Supplementary), which were significantly upregulated *in vivo* in all four genetic backgrounds. Many of these genes encode known virulence factors, haemolysin gamma for example, some of which have already been investigated as vaccine candidates (152).

Figure 66: Genes, which are upregulated in four different strains during infection

(below) Upregulated genes of *S. aureus* during infection in a murine kidney 3 days post infection when compared to the broth grown inoculum. Only genes, which were upregulated in four strains (Newman, USA 300 FPR3757, Patient P and S nasal isolates) are displayed, shades of red indicate fold-change. Transcriptomes of Patient P and S nasal isolates were mapped to the USA 300 FPR3757 genome (NCBI accession NC_007793.1). References given indicate where this gene has been reported to be upregulated previously in *in vitro* (bacterial cell culture) and/or *ex/in vivo* (human blood/murine tissue) assays.

Gene	Newman	USA300	Patient P	Patient S	Reference
accC					(153)
acuA					(153)
adhE					(154), (155)
arcC					/
asnC					/
cap5F					(156)
cobBC					(153)
cobW					(125)
crtN					(113)
ctaA					/
cysG					/
dnaJ					(157)
drp35					(157), (155)
epiA					/
epiF					(153)
fhuB					/
fmhA					(113)
fmtC					(157)
fmtC					(104)
glpD					(113) , (153)
glpK					/
glpT					/
hlgβ					(153)
isdG					(153)
lexA					(153)
lpl7nm					(158)

malC		(153)
mnhB	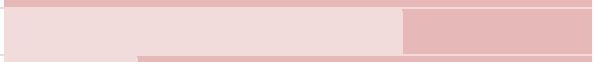	(153)
mnhD		(153)
msa		(153)
msrR		(157)
msrR		(156)
ndh2		(113), (153)
norC		(113), (153)
norQ		(157)
nrdG		(158)
opuCB		(113), (153)
opuCC		(113) , (153)
pabC		(158), (125)
panC		/
pheA		/
queA		/
rdgB		(157)
rimI		(157)
rpoE1		(159)
sak		/
SAUSA300_0303		(158)
SAUSA300_0309		(153)
SAUSA300_0311		(113)
SAUSA300_0353		(104)
SAUSA300_0587		(153)
SAUSA300_0652		/
SAUSA300_0824		(153)
SAUSA300_0920		/
SAUSA300_1057		(104), (160)
SAUSA300_1086		(153)
SAUSA300_1204		(113)
SAUSA300_1236	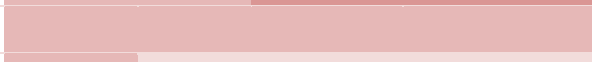	/
SAUSA300_1352		(157)
SAUSA300_1519	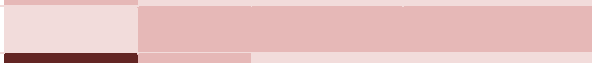	(155)
SAUSA300_1744		(113)
SAUSA300_1806		(113)
SAUSA300_2131		(153)
SAUSA300_2163	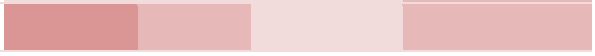	(113)

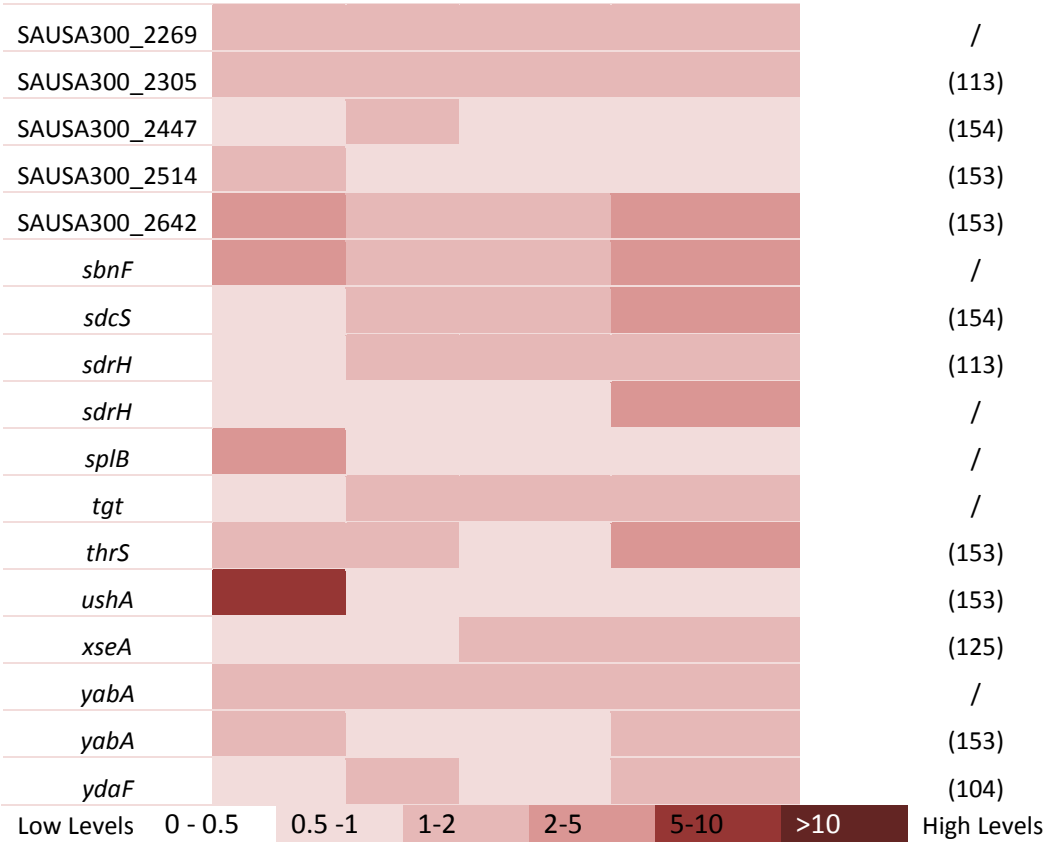
SAUSA300_2269
SAUSA300_2305
SAUSA300_2447
SAUSA300_2514
SAUSA300_2642
sbnF
sdcS
sdrH
sdrH
splB
tgt
thrS
ushA
xseA
yabA
yabA
ydaF
/
(113)
(154)
(153)
(153)
/
(154)
(113)
/
/
/
(153)
(153)
(125)
/
(153)
(104)
Low Levels
0 - 0.5
0.5 -1
1-2
2-5
5-10
>10
High Levels

3.4.4 The Effect of *rsp* Mutation in invasive Isolates on the *in vivo* Transcriptome

After the establishment of *in vivo* RNA extraction and an analysis pipeline for *S. aureus* transcriptomes, its applicability to other settings outside *in vivo* vs *in vitro* comparisons was tested. The transcription regulator *rsp* was found to be mutated in bloodstream isolates from two patients (P and S) who suffered from septicaemia (58). Patients carried the same strain in their nares, but with intact *rsp*. This and the additional observations described [Chapter 1] indicated that the nasal and blood strains of both patients might exhibit phenotypic differences during infection. To test this, mice were infected with the carriage strain from the nares of Patient P and Patient S (Rsp^+) and the blood isolate (Rsp^-) [1.3.3]. In addition, a USA300 transposon mutant for *rsp* (NE1304, Rsp^-) and USA300 JE2 (Rsp^+) were used as inoculum [1.3.3]. The *in vivo* transcriptomes from bacteria obtained from murine kidneys were compared in respect to their *rsp* status. The Rsp regulated non-coding RNA "SSR42" was annotated manually in these experiment, to detect its transcripts during infection in mutants and wild types, as previous transcriptional analysis [Chapter 1, 1.4.5] has indicated, that its abundancy is influenced by Rsp.

3.4.4.1 rsp Mutation affects the S. aureus in vivo Transcriptome only minimally

The *in vivo* transcriptome in murine tissue during infection of three *S. aureus* strains (USA300, Patient P and S) carrying a mutation in *rsp* was defined and compared to the wild type *in vivo* transcriptome of the same strains [1.3.3]. In all three backgrounds, only a few genes were expressed differentially in the mutant (Rsp^-) as compared to the wild type (Rsp^+): In the *S. aureus* strain USA300, only twelve genes were differentially expressed in the Rsp^- USA300 NE1304 when compared to the Rsp^+ USA300 JE2 as background (Supplementary Figure S7). Patient P displayed differential gene expression in just eight genes (Supplementary Figure S8) and Patient S instead had 84 genes affected significantly in their transcription by the *rsp* mutation ((Supplementary Figure S9).

3.4.4.2 Comparison of the Rsp regulon of S. aureus clinical isolates and USA300 in vivo

The gene expression of *rsp* mutants *in vivo* during infection in murine tissues varied little compared to their *rsp* wild types in three genetic backgrounds (Chapter 3, [USA300, 3.4.4.1; Patient P, 3.4.4.2 and Patient S, 3.4.4.3]). When comparing the genes, which differ significantly in the Rsp^- strains compared to the Rsp^+ bacteria, strain specific differences appear (Table 16 and 17). In case of the upregulated genes, there are only four genes upregulated in the Patient S blood isolate and the USA300 NE1304 strain. Three of them belong to the cysteine protease operon *sspABC* and the other is the nickel binding subunit of urease (*ureC*). Overall, the effect of Rsp inactivation seems to be strain specific (Fig. 67).

Table 16: Significantly upregulated genes in *rsp* mutants *in vivo* when compared with *rsp* wild type *in vivo*

Upregulated genes in three *in vivo* transcriptomes in murine tissue during infection of *S. aureus* USA300 NE1304 (Rsp^-) and the clinical blood isolates from Patient P (Rsp^-) and Patient S (Rsp^-) when compared to their Rsp^+ counterparts. Ranking occured according to gene expression fold change. Data for Patient P is shown in brackets, as expression of this gene does not reach the 2-fold change cut-off. Bold letters and same coloured background indicate appearance of the identical gene in USA 300 and Patient S (Protease, metabolism).

Position	*S. aureus* USA300 [locus tag #, name]	*S. aureus* Patient P [locus tag #, name]	*S. aureus* Patient S [locus tag #, name]
1	1106, Lipoprotein	(0548, *sdrE)*	**0951, *sspA***
2	1055, *efb*	-	**0949, *sspC***
3	1052, *efb-c*	-	**0950, *sspB***
4	**0949, *sspC***	-	2572, *aur*
5	0274, Hypothetical	-	2164, *map-w*
6	1766, *epiB*	-	0155, *cap5D*
7	**0950, *sspB***	-	0158, *cap5G*
8	**2240, *ureC***	-	1786, *ecsA*
9	1056, *scc*	-	0156, *cap5E*
10	2306, *hrtA*	-	0166, *cap5O*
11	**0951, *sspA***	-	**2240, *ureC***
12	2440, *fnbB*	-	1976, *dapE*
13	-	-	1922, *sak*
14	-	-	0108, Hydratase
15	-	-	0165, *cap5N*

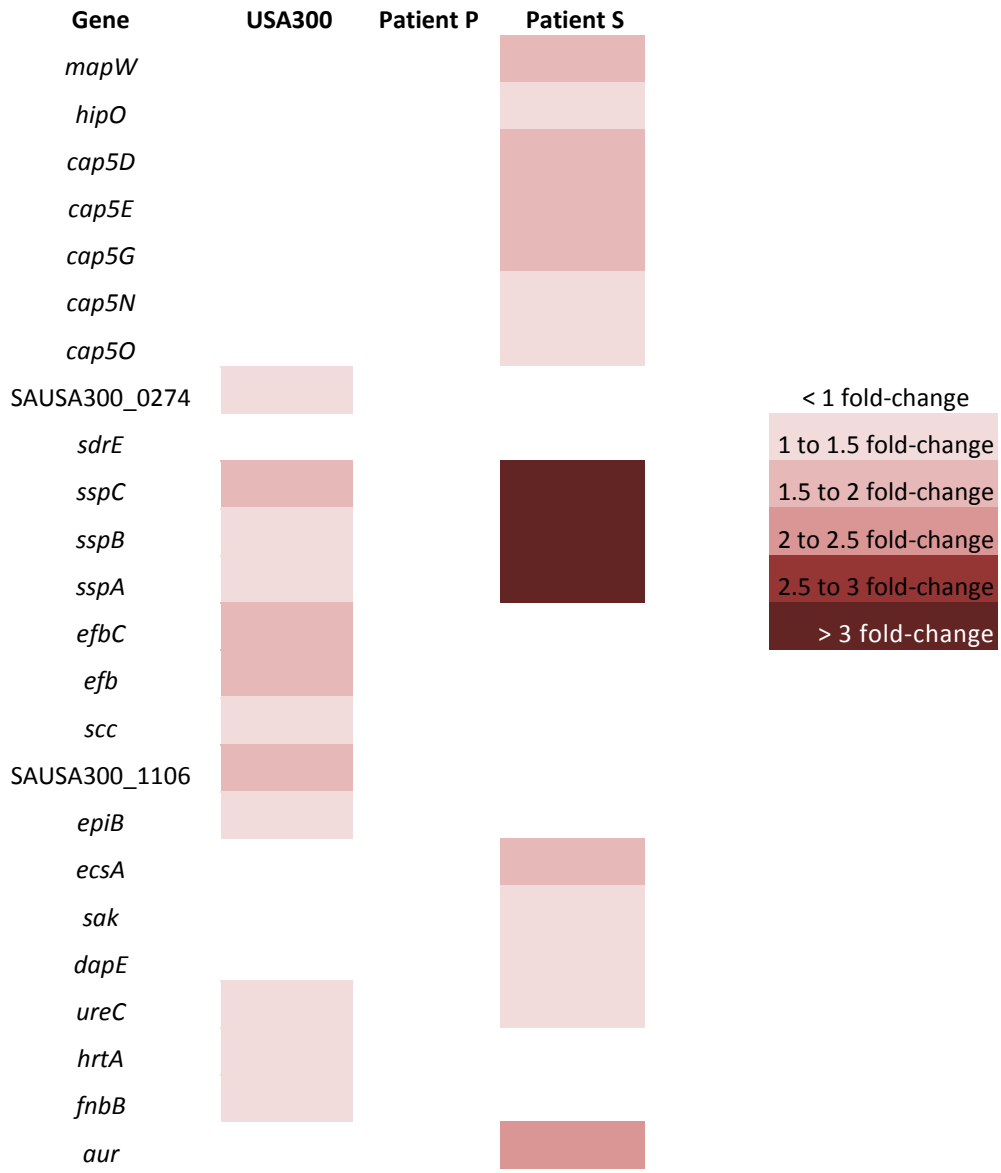

Figure 67: Genes upregulated in Rsp$^-$ *in vivo* when compared with Rsp$^+$ *in vivo*

Expression of 15 upregulated genes in *rsp* mutants *in vivo* in USA300 NE1304 (Rsp$^-$) (left column), Patient P blood isolate (Rsp$^-$) (central column) and Patient S blood isolate (Rsp$^-$) (right column) when compared with *rsp* wild types USA300 JE2 (Rsp$^+$), Patient P nasal isolate (Rsp$^+$) and Patient S nasal isolate (Rsp$^+$), respectively. Shades of red indicate fold-change.

Similar numbers of genes (41 in Patient S, 7 in Patient P and 4 in USA300) were significantly downregulated in an Rsp-dependent manner *in vivo* compared to those that were significantly upregulated (42 in Patient S, 12 in USA300) (Table 17).

Table 17: Significantly downregulated genes in *rsp* mutants *in vivo* when compared with *rsp* wild type *in vivo*

Downregulated genes in three *in vivo* transcriptomes in murine tissue during infection of *S. aureus* USA300 NE1304 (Rsp^-) and the clinical blood isolates from Patient P (Rsp^-) and Patient S (Rsp^-) when compared to their Rsp^+ counterparts. Ranking occured according to gene expression fold change. Bold letters and the same coloured background indicate appearance of the identical gene in two or more strains (Non-coding RNA, Adhesion).

Position	*S. aureus* USA300 [locus tag #, name]	*S. aureus* Patient P [locus tag #, name]	*S. aureus* Patient S [locus tag #, name]
1	**ncRNA, SSR42**	**ncRNA, SSR42**	**ncRNA, SSR42**
2	**0774, *empbp***	1757, *splB*	2440, *fnbB*
3	2326, *rsp*	1758, *splA*	**0774, *empbp***
4	0395, *ssl1*	1755, *splD*	0396, *set7*
5	-	1756, *splC*	2365, *hlgA*
6	-	2056, Hypothetical	2366, *hlgC*
7	-	1754, *splE*	0223, Hypothetical
8	-	-	2367, *hlgB*
9	-	-	1542, *hrcA*
10	-	-	2521, Hypothetical
11	-	-	0815, *ear*
12	-	-	2519, *cobW*
13	-	-	1917, *map*
14	-	-	2441, *fnbA*
15	-	-	1060, *ssl13*

Only three coding genes are affected in the USA300 strain and six in the Patient P isolate. In contrast, the strain isolated from Patient S shows more Rsp-dependent downregulation (41 genes). In all three strains, the non-coding RNA SSR42, which is expressed in an Rsp-dependent way (59) is the most reduced transcript detected (Fig. 68). In two strains, USA300 and Patient S, the adhesion protein Empbp

(secretory extracellular matrix and plasma binding protein), reported to be involved in *S. epidermidis* biofilm formation (161), is downregulated.

The other two genes significantly affected in USA300 are *rsp* itself – which expression is found reduced in all three strains– and a *ssl1*, a gene encoding for a matrix metalloproteinase inhibitor (162). In the clinical blood isolate from Patient P (Rsp^-) members of the serine protease operon *splABCDE* are expressed to a lesser extent than in Patient P's nasal isolate (Rsp^+). Genes found downregulated in Patient S' blood isolate range over a wide scale of biological functions from adhesion proteins (*fnbA* and *B*, *empbp*, *efb* and *efb-c*), toxins (*ssl13* and *hlg*) and immune evasion proteins (*spa* and *sbi*) to transcription regulators (*hrcA* and *saeRS*). To conclude, the *rsp* mutation appears to have a strain specific effect on gene expression under these experimental conditions (Fig. 68).

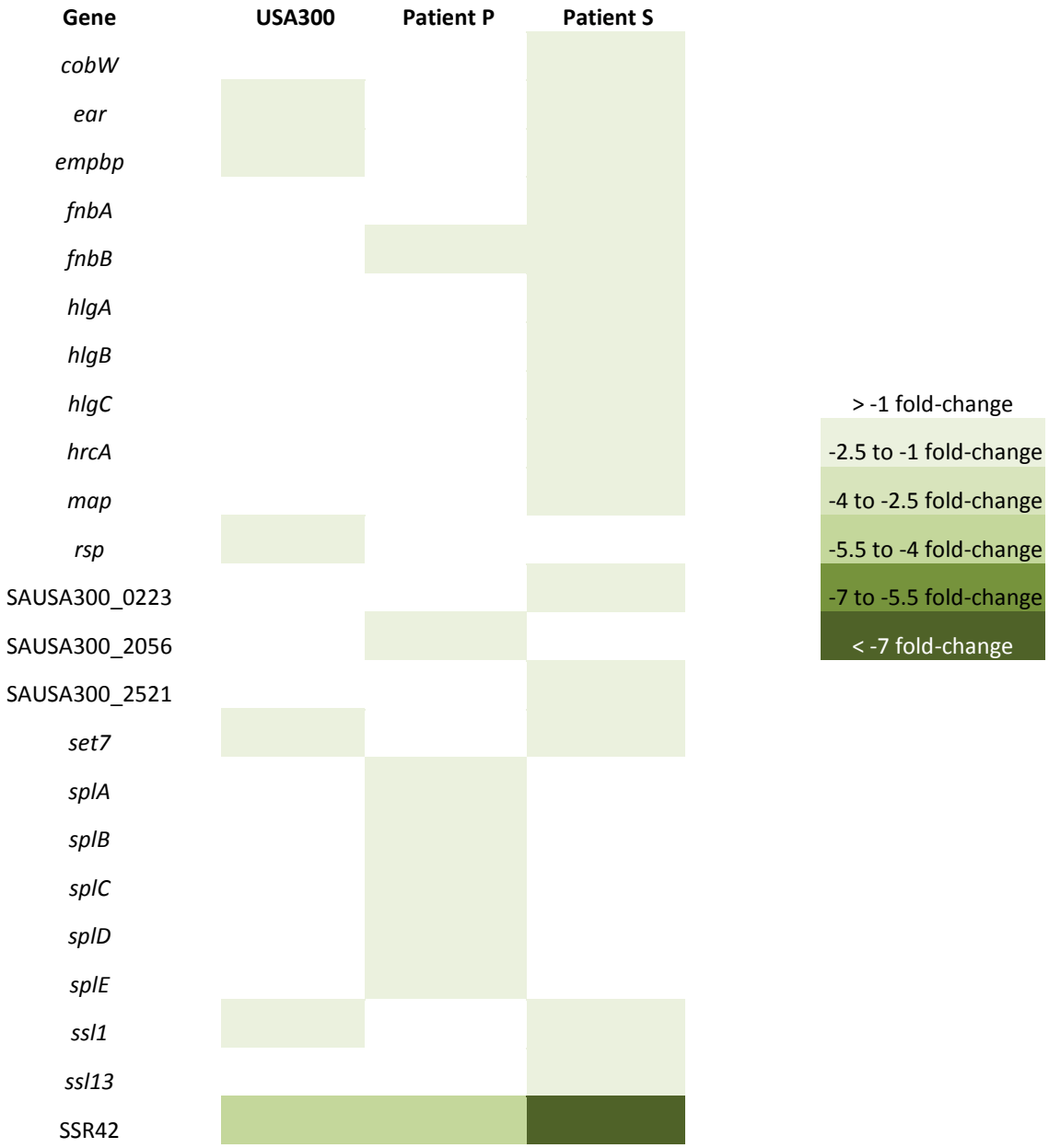

Figure 68: Downregulated genes in Rsp$^-$ *in vivo* when compared with Rsp$^+$ *in vivo*

Gene expression of 15 downregulated genes in *rsp* mutants *in vivo* in USA300 NE1304 (Rsp$^-$) (left column), Patient P blood isolate (Rsp$^-$) (central column) and Patient S blood isolate (Rsp$^-$) (right column) when compared to *in vivo rsp* wild type USA300 JE2 (Rsp$^+$), Patient P nasal isolate (Rsp$^+$) and Patient S (Rsp$^+$) nasal isolate, respectively.

The lack of similarity in gene expression is not only observed for the significantly up- and downregulated genes, but for the overall results of the per-gene analysis, when comparing results for USA300 with the clinical isolates. There is no significant correlation of *in vivo* transcriptomes from USA300 NE1304 (Rsp^-) and from blood isolates from Patient P and Patient S (Rsp^-) (Fig. 69, Pearson coefficient: -0.0191 for both). In conclusion, the effect of *rsp* mutation on the *in vivo* transcriptome at the time point measured is not comparable between the laboratory strain USA300 and the clinical isolates P and S.

A

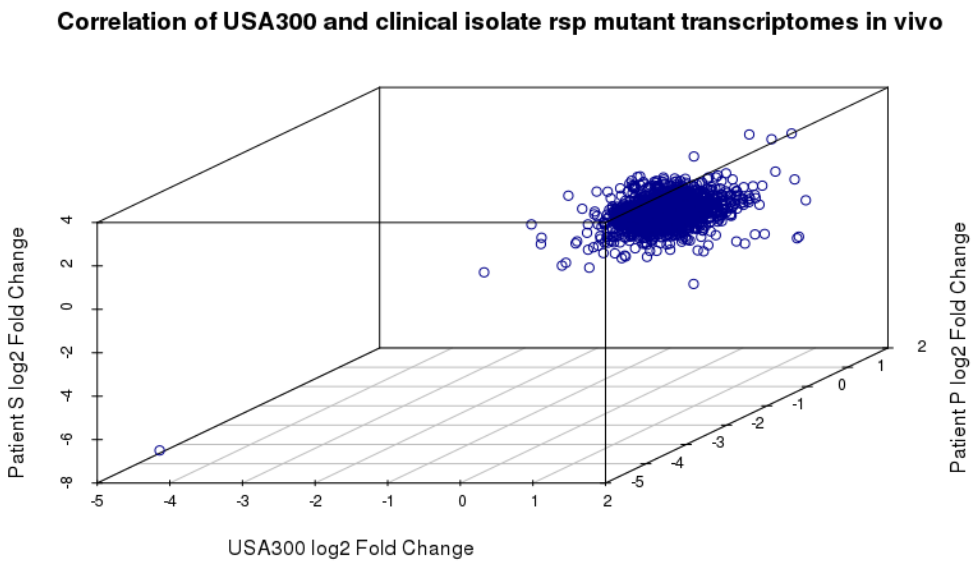

B

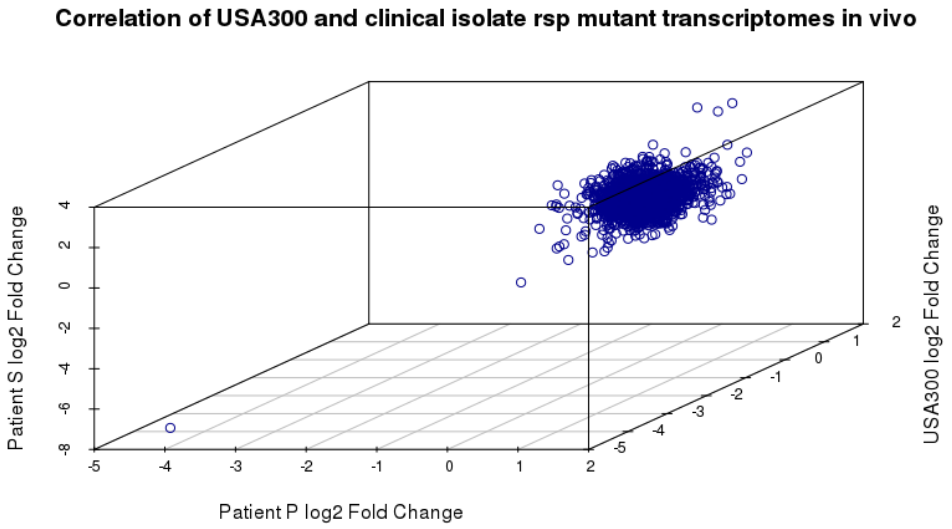

Figure 69: **Correlation of USA300 Rsp$^-$ and clinical isolate Rsp$^-$ transcriptomes *in vivo***

A: Correlation of log_2 fold change expression between USA300 NE1304 (Rsp$^-$) (x-axis), Patient P blood isolate (Rsp$^-$) (y-axis) and Patient S blood isolate (Rsp$^-$) (z-axis) during infection compared to the *rsp* wild types USA300 JE2 (Rsp$^+$), Patient P nasal isolate (Rsp$^+$) and Patient S nasal isolate (Rsp$^+$), respectively. **B:** The perspective is changed with Patient P Rsp$^-$ on the x-axis and USA300 Rsp$^-$ on the y-axis

However, when comparing transcriptomes of *rsp* mutants Patient P (Rsp^-) and Patient S (Rsp^-) *in vivo*, they are remarkably similar (Fig. 70, Pearson coefficient: 0.862) and have a positive correlation. This correlation indicates that, despite the genetically distinct background of the two strains (Fig. 7), the overall effect *rsp* mutation has on gene expression during infection is similar. However, there is no significant fold change in expression on a single gene level.

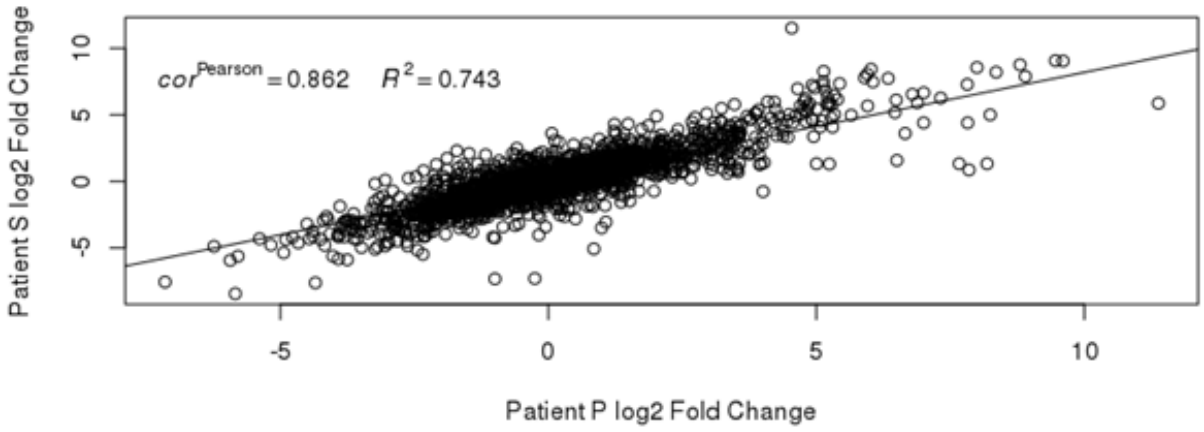

Figure 70: Correlation between Patient P and S Rsp^- *in vivo* transcriptomes

Correlation of log_2 fold change expression between Patient P blood isolate (Rsp^-, x-axis) and Patient S blood isolate (Rsp^-, y-axis) during infection when compared with the Rsp^+ nasal isolates during infection. The Pearson correlation coefficient ($cor^{Pearson}$) and the R square value (R^2) are displayed.

3.4.4.5 The transcriptomic effect of rsp mutation in vivo and in vitro does not correlate

Mutation of the transcription regulator *rsp* causes transcriptional changes *in vitro* (Chapter 1, [1.4.5]) and *in vivo* (Chapter 3, [3.4.4.1-4]). In order to identify correlation between the *rsp* mutation effect observed *in vitro* and *in vivo*, transcriptional changes are plotted for USA300 (Supplementary Figure S10), Patient P (Supplementary Figure S11) and Patient S (Supplementary Figure S12). The *in vivo* and *in vitro* transcriptomes do not correlate in any of the three strains (Pearson correlation: USA300 = -0.00568, Patient P = 0.00481, Patient S = 0.013).

3.4.5 Functional Profiling of transcriptomes of *rsp* mutants *in vivo*

As there was no dominant group of genes identified to be significantly influenced by *rsp* mutation *in vivo* for the time point studied, three days post intravenous infection, grouping of genes into modules was used to identify expression enrichment above the single gene level and significantly up- or downregulated modules were identified. When grouped according to their annotated involvement in biological processes, twelve modules were found to be enriched (Fig. 71).

Figure 71: Gene set enrichment analysis for "Biological Process" modules

Genes were grouped according to the predicted biological process they are involved in. The effect size (Area under the curve (AUC) displayed as dot size) and significance (shade of red) per gene module are displayed for *in vivo* transcriptomes 3 days post infection of the *S. aureus* Rsp$^-$ strains Patient P blood isolate (left), Patient S blood isolate (centre) and USA300 NE1304 (right) when compared with their Rsp$^+$ counterparts Patient P nasal isolate (Rsp$^+$), Patient S (Rsp$^+$) and USA300 JE2 (Rsp$^+$). Significant modules are marked with "*" using a significant cut-off of q=0.05.

Two modules (translation and pathogenesis) are enriched in USA300 NE1304 Rsp$^-$, five in the blood isolate of Patient P Rsp$^-$ (different amino acid synthesis related pathways) and six in Patient S' Rsp$^-$ bacteraemic strain (stress response, protein folding, pathogenesis, cytolysis pathways and lipopolysaccharide synthesis) when compared with their respective Rsp$^+$ strains *in vivo*. However, none of these modules is significant in all three strains and only the "pathogenesis" set is found in USA300 NE1304 Rsp$^-$ and Patient S Rsp$^-$.

The same variation of enrichment between strains is found when comparing genes grouped according to their predicted molecular function (Figure 72).

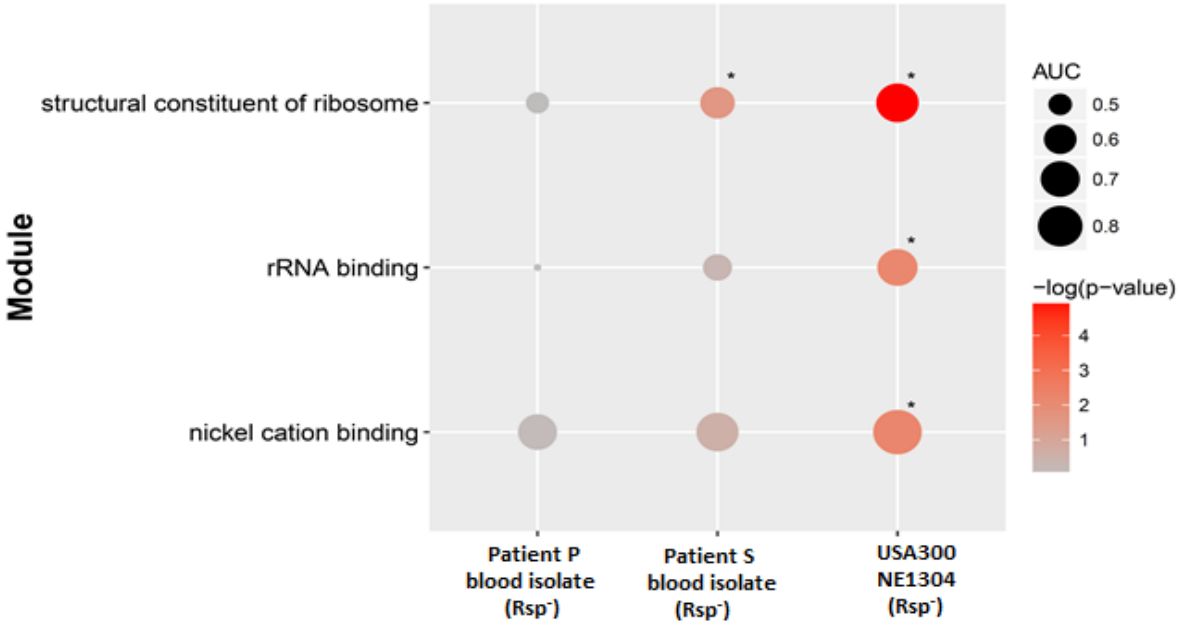

Figure 72: Gene set enrichment analysis for "Molecular Function" modules
Modules displayed are enriched *in vivo* when genes are grouped according to their molecular function. The effect size (Area under the curve (AUC) displayed as dot size) and significance (shade of red) per gene module are displayed for *in vivo* transcriptomes 3 days post infection of the *S. aureus* Rsp$^-$ strains Patient P blood isolate (left), Patient S blood isolate (centre) and USA300 NE1304 (right) when compared with their Rsp$^+$ counterparts Patient P nasal isolate (Rsp$^+$), Patient S (Rsp$^+$) and USA300 JE2 (Rsp$^+$). Significant modules are marked with "*" using a significant cut-off of q=0.05.

Only one module is represented in two strains, the "structural constituent of ribosome" in strain USA300 NE1304 Rsp$^-$ and Patient P blood isolate (Rsp$^-$) (Fig. 72). The Patient P blood isolate (Rsp$^-$) does not have any other module enhanced and Patient S blood isolate (Rsp$^-$) does not display any enrichment at all.

Finally, grouping of genes according to their predicted cellular location reveals an effect of enrichment induced by the *rsp* mutation commonly found in all three strains (Fig. 73).

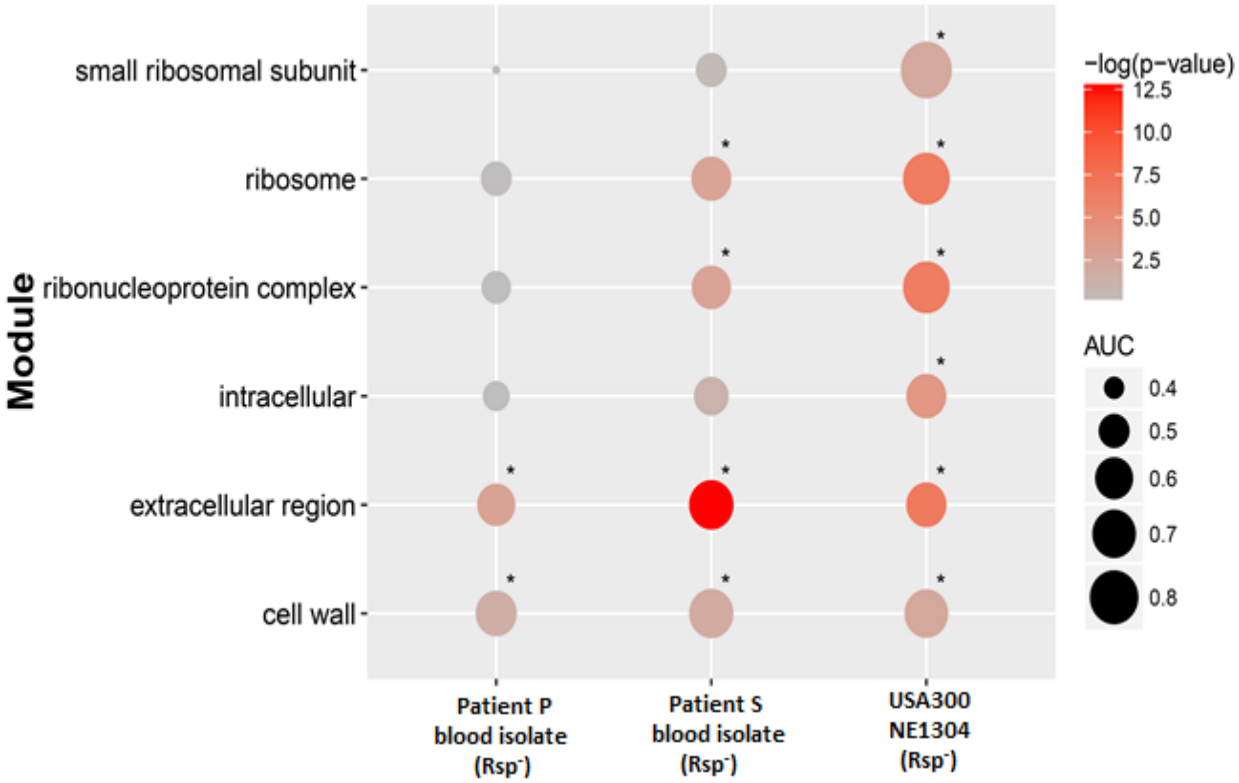

Figure 73: Gene set enrichment analysis for "Cellular Compartment" modules
Modules shown are enriched *in vivo* when genes are grouped according to subcellular location. The effect size (Area under the curve (AUC) displayed as dot size) and significance (shade of red) per gene module are displayed for *in vivo* transcriptomes 3 days post infection of the *S. aureus* Rsp$^-$ strains Patient P blood isolate (left), Patient S blood isolate (centre) and USA300 NE1304 (right). Significant modules are marked with "*" using a significant cut-off of q=0.05.

Two modules were found to be enriched in all three strains when grouping gene expression according to the cellular location (Fig. 73) of their protein products: genes encoding for extracellular and cell wall adjacent. Ribosomal and ribonucleoprotein complex proteins are expressed differently in the Patient S blood isolate (Rsp^-) and USA300 NE1304 (Rsp^-), whereas the modules of intracellular and small ribosomal subunit proteins are only effected in USA300 NE1304 (Rsp^-).

3.4.6 *In vivo* expressed Antigens

A vaccine should contain antigens that are universally expressed in all strains during the infection it aims to prevent. Genes identified in a "core transcriptome" of four genetically different *S. aureus* strains provide a pool of potential antigens, as they might be expressed during infection and thereby be recognized by components of the immune system. Furthermore, the antigen should be accessible to the host' immune system. In intact and often encapsulated bacterial cells, such as *S. aureus*, intracellular and transmembrane proteins might not always be accessible to host recognition. Thus, membrane bound and secreted proteins are usually preferred as vaccine candidates. Conservation across strains is important to assure a wide range of protection. *In vivo* expressed antigens from the described "core transcriptome" (Chapter 3, [3.4.4]) were considered vaccine candidates when they were found to be conserved (>95% of amino acid identity) in most strains (>95%) and secreted or membrane bound according to bioinformatic prediction [3.3.5].

The following seven candidates were identified using these selection criteria.

Table 18: List of *in vivo* expressed antigen candidates

Locus tag	Gene name
SAUSA300_0303	Putative liporotein
SAUSA300_0417	Tandem lipoprotein
SAUSA300_1236	Hypothetical protein
SAUSA300_1757	Serine Protease SplB
SAUSA300_1922	Sak, staphylokinase
SAUSA300_1985	SdrH , serine-aspartate repeat-containing protein
SAUSA300_2367	HlgB, Gamma haemolysin

3.5 Discussion

In this chapter, the RNA extraction and sequencing pipeline established in Chapter 2 was successfully applied to further *S. aureus* strains [1.3.3]: Two strains isolated from nares and bloodstream of two different patients (designated "P" and "S") and the laboratory strain USA300. *In vivo* transcriptomes of these strains (USA300 JE2 (Rsp^+), Patient P nasal (Rsp^+) and Patient S nasal (Rsp^+)) were characterised regarding their differences when compared with *in vitro* transcriptomes. One aspect of the study described, was to identify single genes [3.4.1] and gene modules [3.4.2] differentially transcribed in an infected murine kidney compared to the inoculum used for the infection. Another objective was to identify genes, which are co-upregulated in all four genetic backgrounds tested (Chapter 3, [3.4.3]). The identified genes were considered an "*in vivo* core transcriptome", commonly upregulated during infection in murine tissue independent of the *S. aureus* strain. An additional aim of this study was to test for transcriptional changes *in vivo* during infection in murine tissue caused by mutation of the transcription regulator Rsp. Single genes (Chapter 2, [3.4.4]) and sets [3.4.5] differentially regulated in mutants (Rsp^-) when compared to wild types (Rsp^+) *in vivo* were identified.

An ultimate goal of this thesis is to identify implications of transcriptional changes – *in vitro* and *in vivo* – on vaccine design and in particular the selection of antigens. In Chapter 3 [3.4.6], potential candidates were identified based on an "*in vivo* core transcriptome" [3.4.3], their conservation across *S. aureus* strains and subcellular location. This provides a starting point to choose a sophisticated vaccine composition and to elaborate a basis for a formulation strategy.

3.5.1 The *in vivo* Transcriptome of Nasal Clinical Isolates can be characterised

The established *in vivo* RNA extraction and analysis method was successfully applied to another strain (*S. aureus* USA300) and clinical isolates from the nares of two patients. Expression changes in several genes were found *in vivo* compared to the inoculum for all three strains tested (696 – 858 upregulated and 798 – 901 downregulated).

All three strains show most upregulation in iron uptake (SbnC and F) and immune evasion (Chs, Sbi and Map) involved proteins. As soluble iron accessibility is limited in the blood and tissue of the host, alternative strategies are needed by the pathogen to acquire this metal. *S. aureus* uses SbnC and F to synthesize siderophores under iron depleted conditions (163, 164). SbnC and F respond to low cellular heme concentrations and its operon (*sbnABCDEFGHI*) is required for the synthesis of staphyloferrin B, one of the two siderophores *S. aureus* synthesises (165). Expression of both genes is increased in blood and serum (14, 166).

Regarding the immune evasion proteins: the adhesion protein Map (an MHC class II analogue protein) (81) has been hypothesized to influence T-cell mediated responses. Second, the second immunoglobulin-binding protein (Sbi) is an immunoglobulin G Fc region binding protein, similar to Protein A. Sbi also interacts with the C3 protein of the complement cascade when secreted, leading to futile activation of the alternative pathway. In blood, Sbi promotes survival and opsonophagocytic escape (82). Third, the chemotaxis inhibition protein CHIPS (or Chs) binds to the anaphylatoxin C5a receptor (C5aR) and formylated peptide receptor (FPR), preventing activation of these receptors and inhibiting chemotaxis (167).

All commonly upregulated genes encode for proteins whose functions appear to be crucial during infection. The genes, which are downregulated in all three strains are comprised of genes encoding for metabolic enzymes (Ddh and ArgF), a hypothetical protein (SAUSA300_0172) and the transcription regulator SarX.

D-lactate dehydrogenase (Ddh) catalyses conversions between lactate and pyruvate and is produced to a certain extent upon nitric oxide exposure (168) and ArgF is an ornithine carbamoyltransferase involved in the synthesis of L-arginine (169). Neither has been reported to have a direct effect on virulence in animal models. The transcription regulator SarX instead represses the quorum sensing and virulence regulator *agr* (170). It positively regulates biofilm formation via the *icaADBC* operon (171). Its deactivation might thereby shift the bacteria to a planktonic state with activation of *agr* and less biofilm formation. As *agr* has been reported to be expressed during infection, finding *sarX* downregulated was expected (132, 133).

When looking at the gene set enrichment analysis (Chapter 3, [3.4.2]), we find the pathogenesis, oxidation-reduction pathways and the extracellular region module enriched across all three strains tested in Chapter 3. This indicates that there is consistent upregulation *in vivo* in genes grouped according to their involvement in pathogenesis or their location in the cellular compartment. For all other modules, the genetic background seems to play an important role.

Inosine monophosphate and purine biosynthesis genes are upregulated in USA300 *in vivo* compared to *in vitro*, as well as genes encoding for proteins predicted to be located at ribosomes, chromosomal DNA and the cell wall. Inosine monophosphate

and the ribonucleotide reductase subunit 2 have been found to bind human plasminogen upon secretion (172), possibly explaining this enrichment.

In Patient P, genes in the modules of cellular amino acid synthesis (including the branched amino acid subgroup), riboflavin synthesis and pathogenesis processes are upregulated and this metabolic changes might be a response to the altered environment, while enhanced expression of pathogenesis factors probably helps to maintain infection (140). The downregulation of genes encoding redox proteins instead is unexpected, especially since riboflavin synthesis seems to be upregulated. Riboflavin is a co-factor for oxido-reductase enzymes (173) and co expression might be expected. Lastly, in Patient S the same module is downregulated as well, together with genes encoding for proteins of the Krebs cycle and glycolysis, probably indicating a state of reduced respiratory metabolism and an increase of anaerobic fermentation (174). Representatives of the cytolytic reservoir are also downregulated. However, a few genes of that module (for example the *Hlg* subunits encoding for gamma haemolysin) are upregulated and the enrichment of cytolysis downregulation is just partial. However, for Patient S, the only upregulated modules are the pathogenesis set and the aforementioned extracellular region.

To conclude, the *in vivo* transcriptomes in murine kidney during infection as compared to broth conditions, characterised for *S. aureus* USA300 JE2, Patient P' and S' nasal clinical isolates comply with *a priori* expectations. They correlate largely, despite genetic differences of the strains used. In the single gene analysis, most upregulation in all strains is seen in iron uptake and immune evasion associated proteins. In an iron-depleted environment such as murine tissue with a host immune system actively engaging against the pathogen, this was to be expected. Strongest

downregulation in all backgrounds is seen in metabolic enzymes and transcription regulators, in particular SarX. As the latter is a repressor of *agr* and other virulence factors, this finding confirms credibility of the results.

In the modular analysis, downregulation of redox processes in two strains seems counterintuitive, but upregulation of pathogenesis processes and extracellular proteins is credible.

Overall, these results prove that an *in vivo* transcriptome can be characterised for various *S. aureus* strains, using the presented method and that in depth characterisation and identification of strain specific effects is possible. In addition, this analysis also allows prediction of essential genes for infection, as they are expected to be upregulated in all strains during the infective state. The "core transcriptome" presented here indicates such genes, which might make good vaccine targets. Further analysis of the biochemical function and/or their role in infection of these genes and the proteins they encode could help us understand more about their suitability as vaccines, as well as about the pathogenesis of *S. aureus* in bacteraemia and sepsis.

3.5.2 Identification of an Infection "core Transcriptome"

Various approaches have been made to identify "core genes" or a "core genome" of *S. aureus*, mostly through whole genome comparison, conservation studies and the comparison of similar genes in genetically distant strains (119, 175). In this chapter, instead of trying to identify a "core genome", I identified genes with common altered expression during infection in murine tissue compared to *in vitro* conditions, calling it an "*in vivo core* transcriptome" for the conditions tested. In particular, I extracted genes, which were commonly upregulated *in vivo* in four different *S. aureus* strains. The aim of this was to identify which genes, repressed in a broth culture, are expressed upon exposure to an infection environment. The overlap is small: Only 81 genes of the 600 to 900 genes upregulated in each particular strain (USA300, Newman, Patient P and Patient S) overlap. As only differentially expressed and upregulated genes are captured with strict cut-offs, the "core transcriptome" presented here may represent a group of genes required for *in vivo* adaptation. However, this hypothesis needs to be confirmed experimentally. Other techniques, such as Real Time PCR or – once available – prokaryotic single cell expression analysis could confirm these results. Proteomic and functional assays should be applied to complement this data.

3.5.3 Few Rsp-dependent transcriptional Changes can be detected *in vivo*

Naturally occurring mutations in a transcription regulator named *rsp* have been shown to alter gene transcription of *S. aureus in vitro* (Chapter 1, [1.4.5]). In this Chapter, effects of the *rsp* mutation were investigated *in vivo* (Chapter 3, [3.4.4]). Bacterial gene expression of clinical blood isolates (Rsp^-) was compared to Rsp^+ nasal isolates, using RNA obtained from murine kidneys three days post intravenous infection. An *rsp* transposon mutant of USA300 was compared to its wild type (Rsp^+) in the same way, in order to identify transcriptional changes attributable to the mutation of the transcription regulator.

In USA300 (Chapter 3, [3.4.4.1]), only twelve genes were found to be differentially expressed in the transposon mutant when compared to its wild type. Among these were some adhesins (*efb, ecb, fnbPB*) and extracellular proteases (*sspA, sspB, sspC*). Secreted extracellular fibrinogen-binding protein (Efb), like Sbi, degrades C3 without causing C3b surface deposition on the bacteria. It does so by binding plasminogen simultaneously to C3/C3b, degrading C3/C3b in a futile way – without causing C3b mediated phagocytosis (85). The generated plasmin binds and cleaves C3a and thereby supresses an anaphylatoxin mediated pro-inflammatory response. Efb also inhibits neutrophil adherence and platelet aggregation by binding fibrinogen (176, 177). The extracellular complement-binding protein (Ecb) inhibits complement activation by binding C3d and attracting factor H, a complement cascade inhibitor, to the staphylococcal surface (178). It contributes to virulence together with Efb (179). Fibronectin binding protein (FnbPB) mediates adherence to platelets without inducing aggregation (180), it can also bind plasminogen simultaneously (181) and

confer adherence of *Staphylococci* to host cells (182, 183) and facilitates biofilm formation (184).

The serine proteases V8 (SspA) is activated by aureolysin and activates the cysteine protease staphopain B (SspB) in a cascade like manner. The latter is then regulated by its inhibitor staphostatin (SspC) (185). These proteases/protease inhibitors are required for growth and survival *in vivo*, resistance against antimicrobial peptides, abscess formation and organ invasion (186). They also contribute to immune evasion by inhibiting neutrophil activation and chemotaxis (187).

Due to its transposon insertion in *rsp* in USA300 NE1304, fewer transcripts of the transcription regulator and its regulated non-coding RNA SSR42 are found than in the wild type. The other downregulated genes, encoding the enterotoxin Ssl1 and Empbp (secretory extracellular matrix and plasma binding protein), are supposed to be involved in immune evasion through matrix metalloproteinase inhibition (162) and Empbp in biofilm formation (161).

In Patient P (Chapter 3, [3.4.4.2]), no genes were upregulated in the blood isolate. SSR42 had repeatedly less transcripts in the *rsp* mutant than in the wild type and transcripts for *rsp* were not detected at all, due to the premature stop codon in the blood isolate. The serine SplA, B, C, D and E were all downregulated in the blood isolates compared to the nasal strain. For the Spl proteases, a similar mechanism of relevance for dissemination during disease and regulation of secreted toxins has been proposed (127).

For Patient S (Chapter 3, [3.4.4.3]), changes are observed in the transcriptome of the blood isolated *rsp* mutant, when compared to the wild type nasal isolate. Among the

upregulated genes, we find mainly survival and immune invasion involved proteins, such as the above described proteases SspA (V8 protease), SspB (Staphopain) and aureolysin. Staphylokinase, which dissolves fibrin clots via plasminogen binding and plasmin activation and which protects the bacterium against alpha-defensins, is also found (188). The capsular polysaccharide biosynthesis machinery of *S. aureus* is upregulated as well, indicating further immune evasion in *rsp* mutants through the staphylococcal capsule (189). However, some *S. aureus* strains are acapsular, but whether the isolates from Patient S can produce a capsule or not has not been investigated in this thesis. Thus, no conclusion about its contribution to immune evasion in this model can be made.

In summary, per-gene analysis reveals small differences between Rsp^- strain gene expression and Rsp^+ counterparts *in vivo* during infection (Chapter 3, [3.4.4.4]). There is little overlap between all strains: Only SSR42, the non-coding RNA, is present in lower abundance in all isolates *in vivo*, confirming its dependency on Rsp functionality. In USA300 NE1304 and the Patient S blood isolate, the *sspABC* operon and *ureC*, a nickel binding urease subunit show increased expression. Downregulated in both strains is the secretory extracellular matrix and plasma binding protein (Empbp). However, whether this effect is Rsp-dependent cannot be said for certain, though it can be hypothesized, as Patient S and USA300 wild type and mutant are genetically separated through just one mutation, whereas the Patient P *rsp* mutant has seven further genetic differences to its wild type. However, there is no correlation between the *in vivo* transcriptome of USA300 and either of the clinical strains overall, making the overlap in significantly up-and downregulated genes appear to be rather coincidental. The *in vivo* transcriptomes of Patient P's and

S' blood isolates instead correlate to a high degree. The Rsp effect might consequently be more pronounced in these clinical isolates, where the mutation was initially observed.

Another question addressed in this Chapter is, whether the effect of mutating the *rsp* transcription regulator had *in vitro* on RNA transcription (Chapter 1, [1.4.5]), is reproducible under *in vivo* conditions. The answer for the experimental conditions chosen here is no (Chapter 3, [3.4.4.5]), as there is no correlation between the *in vivo* and *in vitro* transcriptomes of *rsp* mutants in any of the tested genetic backgrounds. It might be hypothesized that Rsp affects transcription during a different stage of infection, for example earlier or later than measured here. For this, its expression could be measured at different time points during infection using, for example, RNA-Seq or Real Time PCR.

The functional grouping of genes into sets demonstrated the strain specificity of the *rsp* mutation effect. Molecular functions and biological processes enriched in USA300 are related to translation, pathogenesis, rRNA binding, ribosome structure or binding of nickel. In Patient P, biosynthetic pathways of lysine and other amino acids are enriched, whereas in Patient S stress response, protein folding, cytolysis, lipopolysaccharide biosynthesis and again pathogenesis pathways are significantly altered. However, when grouped according to their predicted subcellular location, expression of extracellular and cell wall proteins is enhanced in all three strains. Proteins located at the ribosome and within ribonucleoprotein complexes are significantly altered in USA300 and Patient S. Intracellular and small ribosome subunit proteins are only affected in USA300.

In summary, the functional grouping paints a similar picture regarding gene expression differences between mutant and wild type like the *in vitro* vs *in vivo* comparison. Secreted proteins appear to be affected the most – once by exposure to infection conditions and again if *rsp* is mutated.

3.5.4 Antigens which are expressed *in vivo*

In order to conclude implications for vaccine design, based on the results of this Chapter, genes that are significantly upregulated *in vivo*, when compared to broth culture, were identified. They were selected based on their significant appearance (*q*-value < 0.01) within the upregulated (fold change > 2) subset of all four characterised infection transcriptomes of this thesis. The strict cut-off values were chosen in order to minimalize false positive results. The presented eight candidates are all predicted to be secreted during infection and conserved. Gamma haemolysin is already being investigated as a vaccine compound and has shown promising results (152). A member of the Sdr family, SdrG has also been used successfully in a combination vaccine (100). Some of these antigens (SAUSA300_0303, _0417 and _1236) have not received much attention, yet, which is promising regarding intellectual property. On the other hand, these antigens need to be studied further before using them in a vaccine formulation. Functional assays, further expression studies, immune recognition experiments (pre-existing antibodies in human serum e.g.) and antigenicity tests are recommendable. They could also give indications as to how a vaccine containing such an antigen should be formulated and which immune response could be obtained. In short, while they might make good candidates based on the knowledge accessible to us now, further experiments are required to confirm their aptitude.

Chapter 4:
The influence of vaccination on the bacterial *in vivo* transcriptome

4.1 Introduction

4.1.1 The V710 Vaccine – a Case Study

There is an unmet need for an *S. aureus* vaccine, in particular to prevent postoperative infections (49, 190, 191). Efforts have been made to develop a preventive *S. aureus* vaccine and a well-known example is the V710 vaccine Merck Sharp & Dohme manufactured. It consists of an alum adjuvanted protein formulation of a surface bound iron uptake molecule "IsdB" (33). IsdB is part of an iron sequestering complex, the so-called "Iron surface determinants" (Isd), which facilitates the uptake of heme-bound iron via the bacterial membrane in iron-limited conditions (40). Although *isdB* was upregulated during infection (39) and recognized by IgG antibodies from patients surviving *S. aureus*, it was not possible to reproduce the protective effect of the vaccine (45), despite an immunisation-associated increase in anti-IsdB antibodies, observed in animal models in humans (33). Instead of protecting patients from *S. aureus* infection, more infection-associated deaths were observed. No mechanistic explanation for this vaccine failure has been found, but some suggestions have been made (30). One possibility concerns the adoption of a more virulent phenotype by bacteria in vaccinated humans. One can hypothesise that IsdB immunisation might influence bacterial gene expression during infection of vaccinated individuals through anti-IsdB antibodies (192) via exertion of selective pressure on IsdB presenting bacteria (Fig. 74), and these transcriptional changes could be detected using the *in vivo* transcriptome analysis which I had established [Chapter 2]. Specific IsdA and/or IsdB antibodies label cells presenting these surface proteins and induce phagocytosis and killing of the labelled bacteria. Bacterial cells

expressing less IsdA and/or IsdB would be labelled less and probably have greater chances of escaping phagocytosis. However, the Isd surface proteins play an important role in bacterial iron uptake (193) and this role would have to be replaced by other iron uptake pathways. We might therefore find other iron uptake surface proteins upregulated in bacteria during infection of IsdA/B immunised mice.

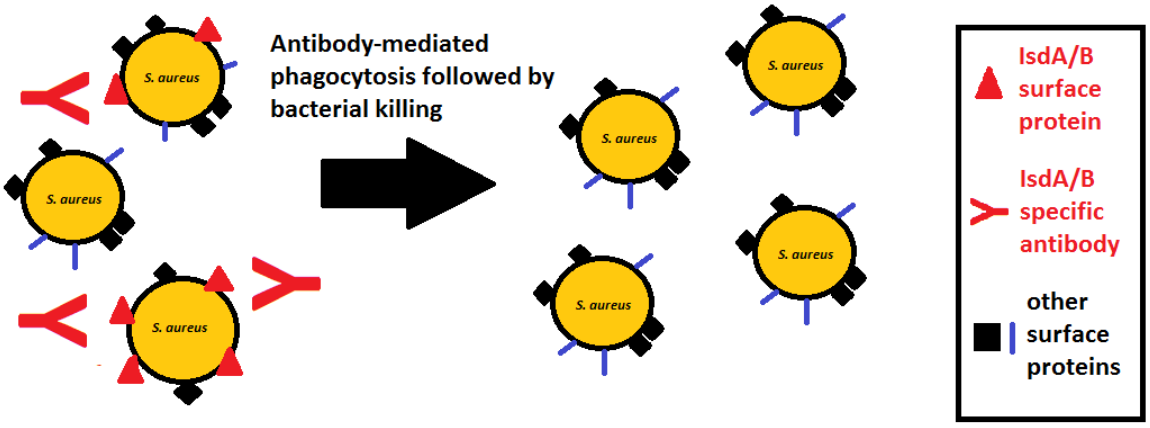

Figure 74: Model describing the speculative effect of vaccine induced antibodies on *S. aureus in vivo*.

Speculative model of the influence vaccine induced host antibodies might have on analysed *S. aureus* population and its transcriptome *in vivo*. Host antibodies directed against IsdA or IsdB surface compounds label bacteria and thereby induce phagocytosis. Labelled bacteria experience more phagocytosis and are lysed more in the phagolysosome of phagocytes than unlabelled bacteria, which do not express IsdA/IsdB. Therefore, bacteria, which do not express IsdA/IsdB, but use alternative iron-uptake pathways and present other iron-uptake surface proteins, have a selective advantage during infection in the immunised host.

4.1.2 Experimental Approach

Immunisation with the *S. aureus* proteins IsdA and IsdB, haemoglobin receptors of the iron-regulated surface determinant group "Isd" (193), has been reported to reduce bacterial loads in the murine kidney infection model. For example, after an intramuscular injection of IsdB protein with Freund's adjuvant, bacterial loads were reduced by up to three $\log_{10}$ in an intravenous infection model (194). This phenomenon was associated with decreased mortality in the mouse model (195). In this chapter, I investigate whether Isd vaccines have an effect on bacterial transcription. I performed these experiments in collaboration with investigators from GSK, Italy. In this experiment, IsdA and IsdB protein formulations (20 μg with 200 μg alum adjuvant) are administered as part of a pre-established vaccination mouse model. Control groups include an adjuvant only (200 μg alum adjuvant) and a placebo (PBS buffer) group.

Within this vaccination model, we first determine whether the reported effect of bacterial tissue load reduction through the IsdB containing vaccine (V710) can be reproduced with our IsdB vaccine formulation in the context of alum adjuvants. Experiments performed by GSK using this formulation had previously produced a reduction of renal bacterial load of one log (unpublished internal results). This reduction is less than the published effects (194, 195), where higher doses of protein or boosts had been given and Freund's adjuvant was used instead of alum. However, our intention is both to use a clinically deployable adjuvant and to induce an immune response, which nevertheless allows sufficient bacterial load for RNA extraction. Furthermore, we aim to reduce the usage of animals to a minimum and avoid

experiments for the purpose of model establishment. For this reason, we selected GSK's established model.

IsdA is another member of the Isd operon, which has been tested as a vaccine candidate and for which less reduction in bacterial load has been reported (~ one log_{10}) when mice are immunized with a protein formulation (192). In the GSK murine vaccination model a reduction of ~0.5 log_{10} is observed (unpublished company internal data).

4.2 Research Questions and Objectives

4.2.1 Research Question

Does IsdA or IsdB protein immunisation of the host alter bacterial transcription during infection?

4.2.2 Research Objective

To describe the bacterial transcriptional response to host immunisation

4.3 Materials & Methods

4.3.1 Experimental Remarks

All experiments described in this chapter were performed in the laboratories of GSK Vaccines, Via Fiorentina 1, Siena, Italy as part of a collaboration with Dr. Fabio Bagnoli. Dr. Clarissa Pozzi supervised all experimental steps. Trained staff from Siena Biotech S.P.A performed all animal experiments, as required by the regulations of GSK Vaccines. I attended the harvest of infected tissues and their preparation, carried out further tissue processing, bacterial enumeration, RNA extraction (Supplementary Figure S1), quality control (Supplementary Figure S2) and computational analysis.

4.3.2 Reagents, Materials and Primers

Reagents and primers used in Chapter 4 of this work have been described in sections 2.3.1 and 2.3.2.

4.3.3 Immunization of Mice

32 mice were divided into four treatment groups. The experiment was carried out twice using a homologous prime-boost regime.

Table 19: Vaccination treatment groups

8 mice per group

Group #	Treatment	Function
1	20 µg IsdA protein + 200 µg alum	Experimental group 1
2	20 µg IsdB protein + 200 µg alum	Experimental group 2
3	200 µg alum only	Control (adjuvant effect)
4	PBS	Control (placebo)

Dr. Clarissa Pozzi (GSK Vaccines) prepared vaccines and control formulations. Briefly, the *S. aureus* proteins IsdA and IsdB were heterologously expressed in *E. coli* and purified. 20 µg/mouse of IsdA or IsdB protein with 200 µg/mouse alum in 100 µl total volume were given intramuscularly – 50 µl per leg (Group 1/2). Group 3 received 200 µg/mouse alum in 100 µl intramuscularly total – 50 µl per leg. Group 4 received 100 µl of sterile PBS in a similar manner. Trained staff of Siena Biotech S.P.A administered vaccines and controls according to the following homologous vaccination regimen (prime – boost):

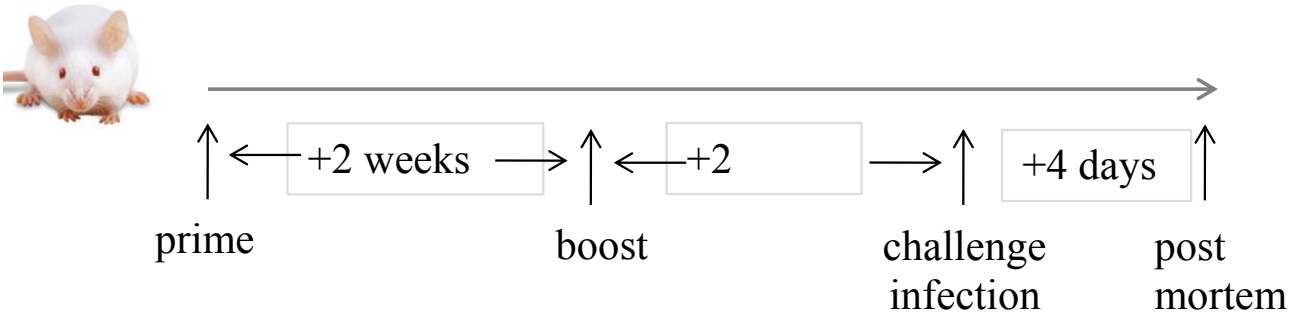

Figure 75: Vaccination schedule

Vaccination schedule for IsdA/IsdB vaccination, followed by intravenous bacterial challenge and sacrifice of mice 4 days post infection.

4.3.4 Bacterial Strains and Bacterial Culture Conditions

All bacterial strains used in this thesis are listed in Table S1 (Supplementary). In this chapter, *S. aureus* Newman was grown in TSB overnight cultures at 180 rpm shaking and 37 °C. The following day, 500 µl of overnight culture were used to inoculate 50 ml TSB in a 250 ml Erlenmeyer. When an OD_{600} of 0.8 was reached, 10 ml of culture were spun (3000 xg, 10 min). The pellet was washed with 10 ml sterile PBS and then taken up in 20 ml sterile PBS.

4.3.5 Murine Sepsis Model

Female BALB/c mice, 12 weeks of age, were administered *S. aureus* Newman intravenously through the lateral tail vein by staff from Siena Biotech S.P.A. with 10^7 CFU/mouse (100 µl). An aliquot of each inoculum was treated with RNAprotect Bacteria (Qiagen) according to manufacturer's instructions. Animals were sacrificed by cervical dislocation of the neck four days post infection and permanent cessation of circulation confirmed.

4.3.6 Tissue Harvest and bacterial Ribonucleic Acid (RNA) Preservation

Murine spleens, kidneys and livers were harvested from infected animals by staff from Siena Biotech S.P.A. Left kidneys were visually inspected for superficial abscesses, which, if present, were removed carefully with a scalpel and submerged into RNAlater (Ambion). Right kidneys were sliced longitudinally (in a coronal plane) and quickly submerged into RNAlater. All tissues in RNA preservation reagent were left at 4 °C overnight, as recommended by the manufacturer, before storage at -80 °C. Left kidneys without abscesses were used to confirm successful infection and estimate bacterial titres via plating on HBA (Oxoid).

4.3.7 Bacterial RNA Extraction and general Quality Assessment

Bacterial RNA was extracted from infected murine kidneys and kidney abscesses as described in sections 2.3.5 to 2.3.7. Quality of obtained RNA was assessed as described in sections 2.3.8, 2.3.9 and 2.3.10. Preparation of cDNA libraries, RNA Sequencing and quality control of results was performed as described in section 2.3.11 (Supplementary Figures S1 and S2).

4.3.8 Computational Analysis

Transcriptomes were analysed as described in section 2.3.12 (gene-by-gene expression analysis) and 2.3.13 (GSEA). Transcriptomes were grouped according to treatment mice had received

- PBS – control 1
- Alum adjuvant only – control 2
- IsdA vaccine – experimental group 1
- IsdB vaccine – experimental group 2

Contrasts were performed between the groups in order to assess association between vaccination regimen and post-infection bacterial transcription.

4.3.9 Statistical Analysis

Statistical analysis of RNA sequencing results performed in this chapter were described in Chapter 2 [2.3.14]. The statistical comparison of bacterial loads in the murine kidney was performed using a Mann-Whitney test.

4.4 Results

4.4.1 The Effect of Vaccination on bacterial Load in murine Kidneys

In this experiment, we immunised mice with *S. aureus* IsdA and IsdB as protein formulations with alum as an adjuvant [4.3.3] and alum only or PBS formulations were given as controls. All treatments were given in a homologous prime-boost regime two weeks apart. Mice were then challenged with *S. aureus* Newman two weeks post boost vaccination. Tissue harvest and bacterial enumeration (Fig. 76) occurred four days post infection.

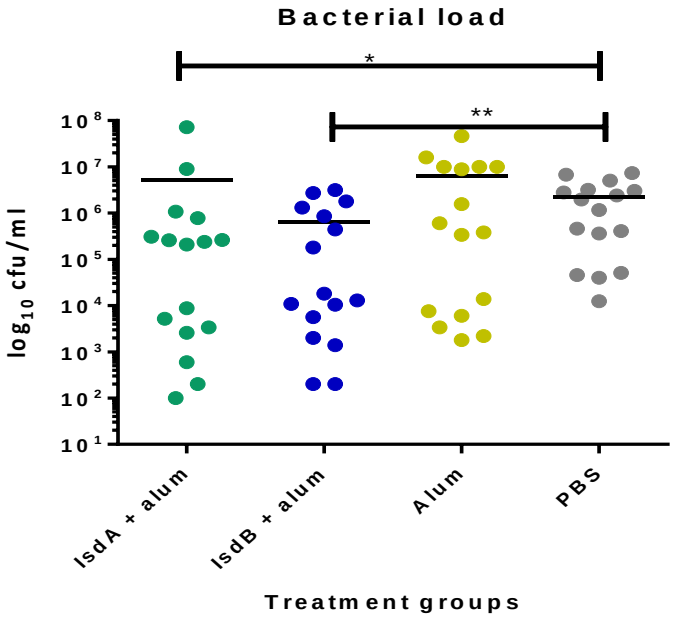

Figure 76: Bacterial load in the right murine kidney four days post infection.

Mice were pre-treated with a homologous prime-boost scheme of A) IsdA protein with alum (green, left group), B) IsdB protein with alum (blue, second left), C) alum only (yellow, second right) and PBS (grey, right group) and then challenged with *S. aureus* Newman. Four days post infection right kidneys were harvested and bacterial load measured is displayed. Significance of differences in groups was tested using a Mann-Whitney test. * indicated a p-value below 0.05 (here: 0.0189) and ** a p-value below 0.01 (here: p=0.0065).

As shown in Figure 76, large variance in bacterial loads within groups is observed. This compromises experimental power in experiments designed to assess vaccine efficacy. However, the significant difference in bacterial load between the IsdA and IsdB vaccinated groups compared to the PBS control group (Mann-Whitney test, p=0.0189/p=0.0065, respectively) appears similar to the previously reported effects of the vaccines (192). Differences between these vaccinated groups and the other, alum vaccinated control group were modest and not significant (p=0.130/p=0.126, respectively). These results are comparable with results previously obtained by GSK (unpublished internal data).

4.4.2 The Effect of Vaccination on *S. aureus in vivo* Transcription

S. aureus infected tissue samples (whole kidneys and single abscesses) from vaccinated animals [4.3.3] were used to extract bacterial RNA [4.3.7]. Two approaches were used: bacterial RNA from whole kidneys was extracted for sequencing, if animals had evidence of infection in the right kidney at a bacterial load of 10^5 CFU/g or higher (Chapter 2, [2.4.1]). Additionally, in some animals where single abscesses on the surface of kidneys were visible, these were excised individually. The number of total tissues (whole kidneys and abscesses) used for extraction, and libraries obtained which passed the established quality control protocol [Chapter 2, 2.4.2; Supplementary Figure S2], are listed below (Table 20).

Table 20: Tissues extracted for bacterial RNA from the different treatment groups

Group	# of tissues extracted	# of transcriptomes obtained
1 – IsdA + alum vaccinated	9 (incl. 2 abscesses)	5 (incl. 2 abscesses)
2 – IsdB + alum vaccinated	7	3
3 – Alum vaccinated	10 (incl. 2 abscesses)	7 (incl. 2 abscesses)
4 – PBS vaccinated	15 (incl. 3 abscesses)	5 (incl. 3 abscesses)

As kidney abscesses and whole kidneys had yielded similar transcriptomic bacterial profiles and exhibited no significant differences in gene-by-gene comparison [Chapter 2, 2.4.3, Figure 38], abscess and whole kidney samples were grouped for analysis. A principal component analysis was performed to summarise major patterns in transcription. Figure 77 shows that transcriptional profiles for IsdA and IsdB pre-treatment seem to cluster, with a few alum pre-treated profiles among them. The PBS treated control tissues appear to separate more distinguishably from the other groups.

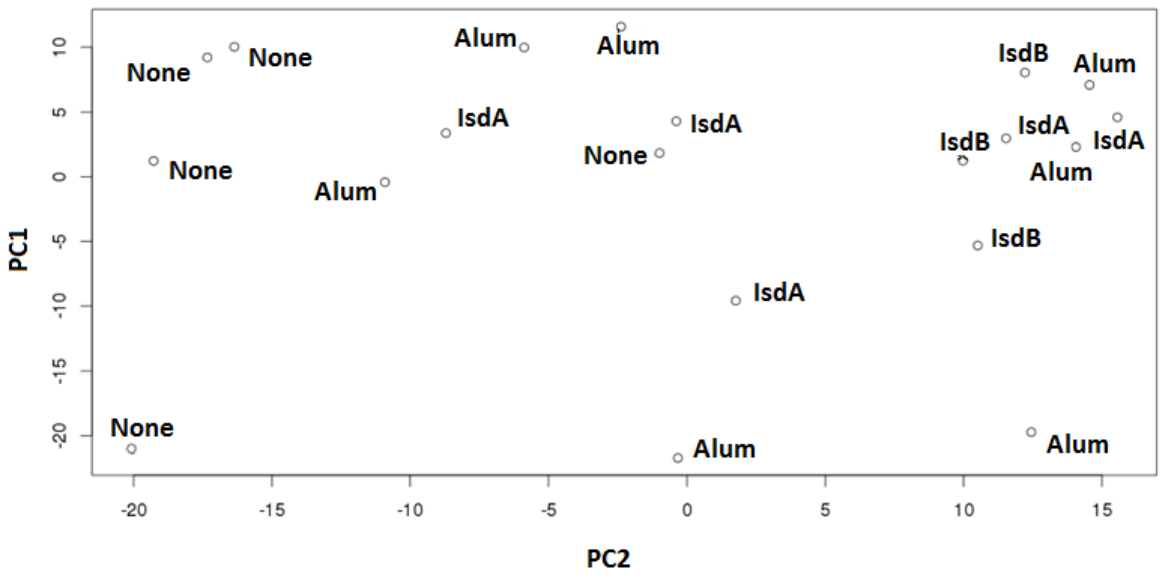

Figure 77: PCA of bacterial *in vivo* transcriptomes from vaccinated mice

Principal component analysis of the bacterial *in vivo* transcriptomes when compared to *in vitro* in mice pre-treated with IsdA + alum vaccination ("IsdA"), IsdB + alum vaccination ("IsdB"), adjuvant only vaccination ("Alum") or PBS buffer mock vaccination ("None").

Figrue 77 indicates that alum adjuvant injection may alter bacterial transcriptional profiles relative to PBS injection. When compared in a gene-by-gene analysis [4.3.7], 184 genes were found to be differentially expressed in bacteria when mice had received an injection of alum compared to PBS buffer (Table S6, Supplementary). However, this was not the primary focus of this work - rather, here I focus on the impact of IsdA and IsdB protein vaccination with alum as an adjuvant. In order to exclude potential adjuvant induced effects, the experimental groups (IsdA and IsdB vaccination) were compared to the alum vaccinated control group. The PBS treated results were omitted from further analysis.

A per-gene analysis compared samples from IsdA and IsdB vaccinated animals to alum only vaccinated animals [4.3.8] using statistical analysis as described [4.3.9]. Bacteria recoverd from IsdA vaccinated groups show positive transcriptional correlation with bacteria recovered from IsdB vaccinated groups ($cor^{Pearson}$ = 0.826, Figure 78). However, no single gene was found to be significantly up- or downregulated in either the IsdA or IsdB vaccinated group when compared to the alum-vaccinated group using FDR based control for false discovery and a significance cut-off of q=0.05.

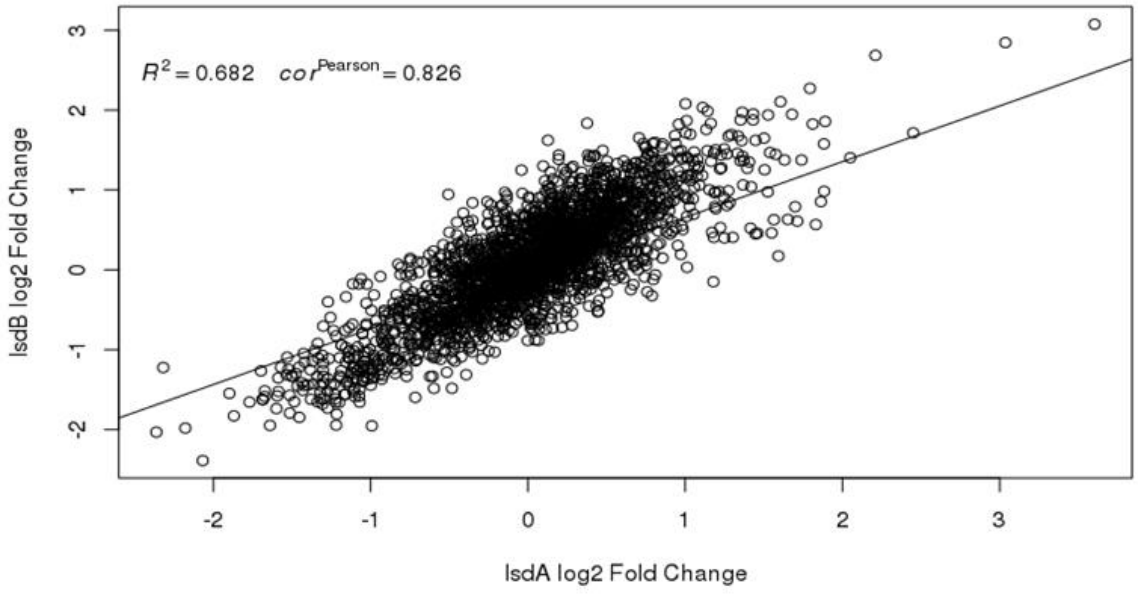

Figure 78: Correlation of bacterial expression changes *in vivo* during infection in murine kidneys in between IsdA and IsdB vaccinated mice

Correlation of log_2 fold change expression in bacterial transcription, during infection when compared with broth grown bacteria, in IsdA + alum vaccinated mice (x-axis) compared with IsdB + alum vaccinated mice (y-axis). The Pearson correlation coefficient ($cor^{Pearson}$) and the R square value (R^2) are displayed, the black line indicates regression.

4.4.3 Functional Profiling of a Vaccination Effect on the *in vivo* Transcriptome of *S. aureus*

Grouping genes according to their biological process involvement, molecular function or subcellular location can increase sensitivity of detection of changes and show differences, which would otherwise be overlooked (196). First, *S. aureus* Newman genes were clustered according to their involvement in biological processes (Fig. 79), their molecular function or cellular compartment as previously described [2.3.13] and bacterial transcriptomes during infection in IsdA and IsdB vaccinated groups compared to the alum only vaccinated group as explained above [4.3.8].

Figure 79: Gene set enrichment analysis for "Biological Process" modules
Gene expression of *S. aureus* Newman *in vivo* when compared with *in vitro* in IsdA or IsdB vaccinated mice was analysed. Genes were grouped according to the predicted biological process they are involved in. The effect size (Area under the curve (AUC) displayed as dot size) and significance (shade of blue) per gene module are displayed for *in vivo* transcriptomes four days post infection of mice immunised with IsdA (left column) or IsdB (right column) with the *S. aureus* strain Newman. Significant modules are marked with "*" using a significant cut-off of q=0.05.

Bacteria infecting mice with previous vaccination against IsdA show cluster specific alterations (Figures 77-79, left column). Unexpectedly, no significant changes are found in IsdB immunised groups when compared to the alum control (Figures 77-79, right column).

Two clusters of genes are significantly upregulated in the IsdA vaccinated group: The siderophore biosynthetic cluster (identical with the siderophore transmembrane transport group) and the nucleic acid phosphodiester bond hydrolysis cluster. The rRNA processing cluster has significantly decreased expression in the IsdA vaccinated group (Figure 80).

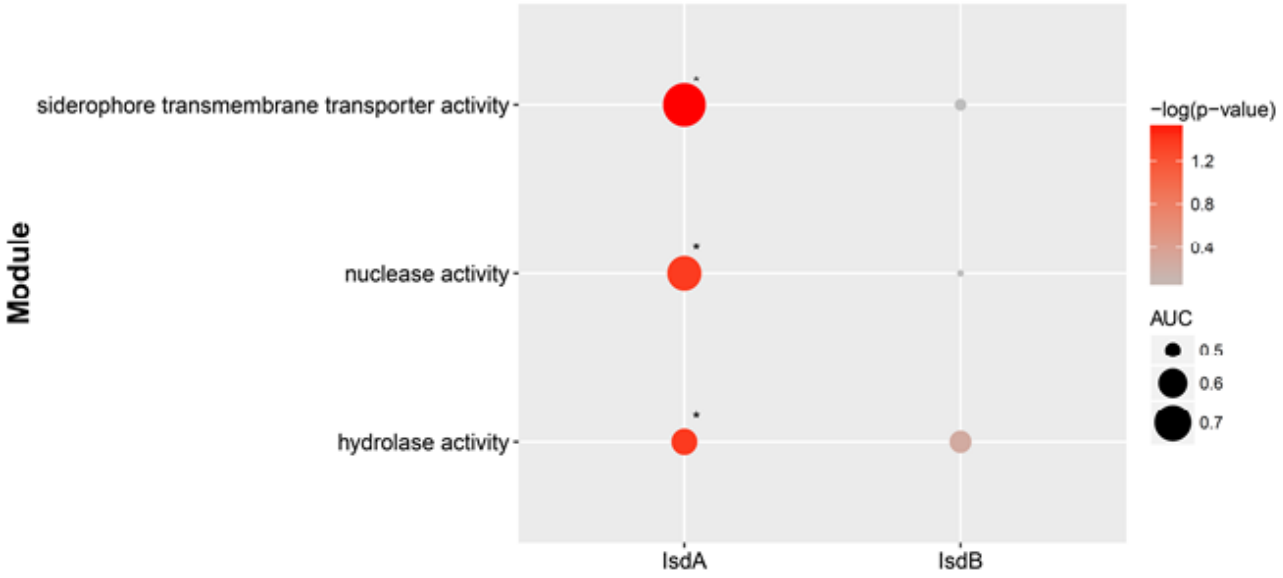

Figure 80: Gene set enrichment analysis for "Molecular Function" modules
Gene expression of *S. aureus* Newman *in vivo* in IsdA + alum or IsdB + alum vaccinated mice when compared with Alum only immunised mice was analysed. Genes were grouped according to their predicted molecular function. The effect size (area under the curve (AUC) displayed as dot size) and the –log(*p*-value) (shade of red) per gene module are displayed for *in vivo* transcriptomes four days post infection of mice immunised with IsdA (left column) or IsdB (right column) with the *S. aureus* strain Newman. Significant modules are marked with "*"using a significant cut-off of q=0.05.

In the gene sets grouped according to their predicted molecular function, the siderophore transporter activity appears again to be increased in the IsdA pre-treated group (Figure 80) and hydrolase and nuclease activities were also found to be enriched. Furthermore, in the IsdB immunised group no differences to the control group was found.

In a GSEA, where genes were grouped according to their subcellular location, only genes encoding for secreted proteins were upregulated in the IsdA immunised group when compared to the alum vaccinated control (Figure 81).

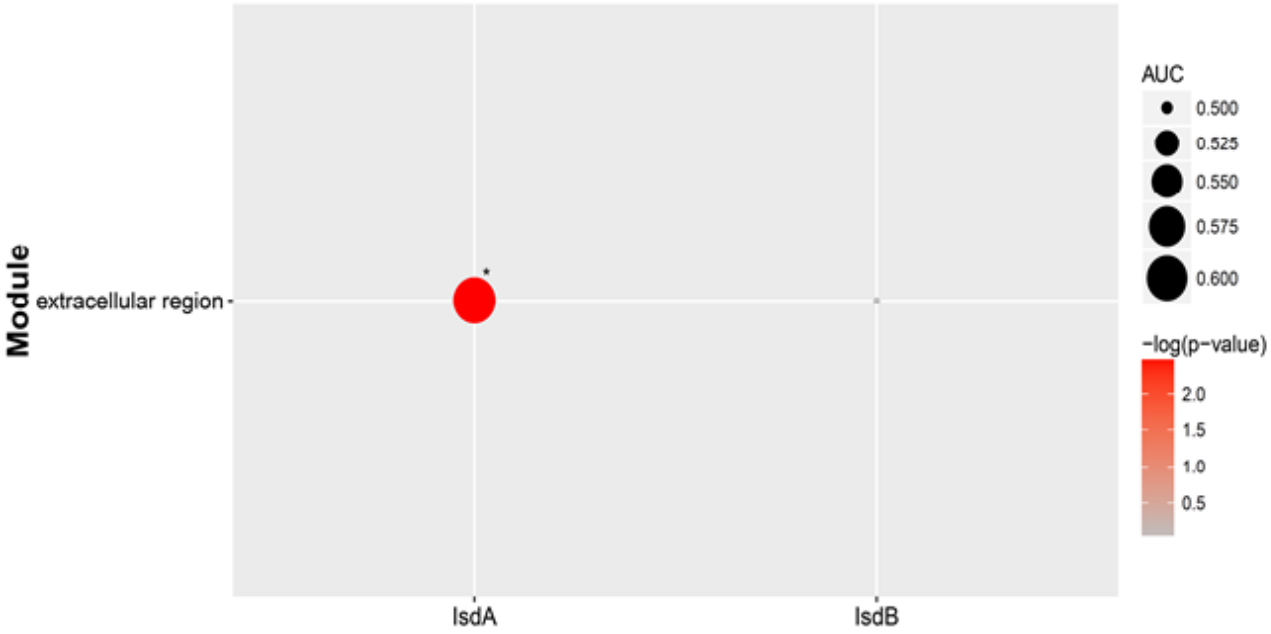

Figure 81: Gene set enrichment analysis for "Cellular Compartment" modules
Gene expression of *S. aureus* Newman *in vivo* in IsdA + alum or IsdB + alum vaccinated mice when compared with Alum only immunised mice was analysed. Genes were grouped according to their predicted subcellular location. The effect size (Area under the curve (AUC) displayed as dot size) and significance (shade of red) per gene module are displayed for *in vivo* transcriptomes four days post infection of mice immunised with IsdA (left column) or IsdB (right column) with the *S. aureus* strain Newman. Significant modules are marked with "*"using a significant cut-off of q=0.05.

In addition to the above described clustering of genes, grouping was also performed according to differential transcription tendencies previously described. This method had been described and applied earlier in this thesis (Chapter 2, [2.3.13] and [2.4.6], respectively). Using this method, an overlap of differential gene expression between bacteria from the IsdA pre-treated group and *in vitro* knockout mutants of the staphylococcal *fur* iron response transcription regulator is seen (Supplementary Figure S13, page 268). This effect is not observed in IsdB pre-treated samples, where no module enrichment is observed.

4.5 Discussion

The objective of this chapter was to investigate the impact of adjuvanted vaccination against iron uptake proteins (IsdA and IsdB), which have previously been investigated as potential human *S. aureus* vaccine candidates (33, 192) on the *in vivo* transcription of *S. aureus* during infection. A subsidiary objective was to investigate whether the *in vivo* RNA extraction technique could be reproduced successfully in different physical settings. Lastly, the speculation of whether a "vaccination escape" effect – a transcriptional response to evade a specific immune response - on bacterial transcription exists, was tested. This is potentially problematic as an objective since highly effective vaccination is associated with large decreases in bacterial load; these protected animals cannot be assessed using bacterial RNA-Seq due to low bacterial RNA yields. Testing this successfully requires identification of experimental conditions in which the vaccine exerts a selective force, but one of sufficiently weak nature that vaccine efficacy does not make the impacted population unobservable due to the limits of sensitivity of the assay technique used.

In respect of the first two objectives defined above, the experiment was successful: the method was reproduced in another laboratory on tissue samples from mice, which had had received a treatment before infection (Chapter 4, [4.4.2]). In addition, differential gene expression was characterised and the vaccination impact quantified (Chapter 4, [4.4.3]).

The experiment used two different control conditions: Vaccination with alum alone, and vaccination with PBS buffer. The transcriptomes for the control groups differed when compared to each other: Bacteria recovered from mice vaccinated with alum adjuvant showed a different gene expression profile compared with bacteria recovered from mice, which had received PBS buffer injections. This indicated an "adjuvant effect" of alum on bacterial gene expression in this model. In this work, we have identified this effect, but not performed mechanistic experiments to identify the basis of this response, which remains to be characterised. We used the adjuvant only control group as the reference group for IsdA + alum and IsdB + alum immunised groups.

Using protein formulations with alum, as previously observed by collaborators in GSK Siena, the change in bacterial load in kidney following immunisation of mice with IsdA and IsdB was modest and large variation in bacterial loads found. Reduction of bacterial load was significant for immunised mice as compared to the PBS buffer immunised control group. For comparison with the alum-vaccinated group, neither vaccine demonstrated a significant reduction of bacterial loads in individual experiments of the size performed. However, the results are compatible with the expected bacterial tissue load reduction of ~ 0.5 $\log_{10}$ CFU/g for IsdA and ~ 1 $\log_{10}$ CFU/g for IsdB vaccinated mice (192). The number of animals with bacterial loads $>10^5$ in the left kidney were similar for IsdA/alum and alum only vaccinated animals (9 vs. 10), as were the number of successful (i.e. with yield above the cut-offs set for RNA-Seq using quality control metrics) extractions (5 vs. 7). By contrast, successful extractions were fewer for IsdB vaccinated animals,

compatible with the lower bacterial densities recovered from IsdB vaccinated animals (Chapter 4, [4.4.2]).

Analysis methods based on detection of differential gene expression at single gene level did not yield any significant results when comparing IsdA or IsdB vaccinated groups to the alum vaccinated group (Chapter 4, [4.4.2]). Only grouping of genes into functional and locational clusters as part of a GSEA resulted in detection of expression alterations in IsdA vaccinated samples (Chapter 4, [4.4.3]). Interestingly, the most affected cluster identified is that of siderophore biosynthesis and membrane transport, and the effect was dominated by upregulation of the siderophores Staphyloferrin A and B (Fig. S4, page 258). This result is intriguing and would be compatible with the original hypothesis that vaccination triggers bacterial transcriptional adaptation during infection: It was previously hypothesized, that immunisation with Isd surface proteins might affect expression of iron uptake pathway related proteins (Chapter 4, 4.1.1, Fig. 74). Siderophores are iron-chelating molecules and the two *S. aureus* siderophores known are Staphyloferrin A (197) and B (165), which have been reported to aid bacterial iron uptake through binding of heme released from host erythrocytes during infection. *S. aureus* can also take up heme through the Isd system, the iron-responsive surface determinant system (198). The proteins used for vaccination in this experiment (IsdA and IsdB) are part of this system, so a mechanistic connection between immunisation and differential gene expression iron uptake pathways might be hypothesized (Chapter 4, 4.1.1, Fig. 74).

Besides, when grouping genes according to transcriptional tendencies observed in published data, similarities in the IsdA vaccinated group to *fur* regulated

transcription appear. *fur* has been reported to regulate responses to low iron environments and regulate IsdA and B expression directly (199). Genes which are found downregulated in *S. aureus* during infection of IsdA vaccinated mice are also found to be differentially regulated upon mutation of the transcription regulator *fur* (Chapter 4: [4.4.3.], Supplementary Figure S13, (200)). However, these conclusions need to be verified in further experiments

To conclude, these results indicate that vaccine induced differences in gene expression can be detected using the *in vivo* transcriptome method [Chapter 2]. However, at the time point measured in the mouse model, grouped analysis such as gene set enrichment analysis is required to achieve statistical significance. In addition, the fact that only kidneys with high bacterial loads (> 10^5 CFU/g tissue) yield sufficient amounts of RNA introduces a potential bias. However, the transcriptional differences in bacteria infecting IsdA vaccinated mice indicate possible transcriptional adaptation of the bacteria to the presence of IsdB antibodies through upregulation of alternative iron uptake pathways (Chapter 4, 4.4.3, Figures 79 and 80) in a similar manner to previously published upregulation of alternative metabolic pathways (201). In summary, there are indications for potentially vaccine induced bacterial compensatory behaviour, which could be investigated using alternative techniques such as Real Time PCR methods, immunohistochemical assays and studies of deletion mutants.

Final Discussion

In this thesis, several aspects of *S. aureus* pathogenesis are studied in four chapters:

In the first chapter, the effect of mutation in the *S. aureus* transcription regulator *rsp* on bacterial behaviour is characterised. Despite not presenting altered growth *in vitro*, *rsp* mutants exhibit differences *in vivo*: When injected intravenously, mice infected with Rsp^- strains develop less severe disease symptoms, reduced lethality and weight loss during the first three days of infection compared to mice infected with the respective Rsp^+ strains. Mutations in *rsp* also execute global changes in gene expression and protein production *in vitro*, leading to differential enzyme activity in the bacterial supernatant when comparing Rsp^+ and Rsp^- strains. The Rsp-dependent phenotypic changes lead to altered interaction with the human complement system while maintaining the ability to survive, proliferate and cause disseminated infection within the human body. Rsp loss-of-function stands as an example of how genetic variation affects key regulatory pathways, thereby influencing disease progression and clinical outcome.

The second chapter describes the development and optimization of an RNA extraction method for bacterial samples isolated from infected murine tissue. Per-gene analysis with these samples showed reproducible *in vivo* transcriptomes for *S. aureus* during murine infection in the kidney and spleen. Genes for well-known and characterised proteins such as haemolytic toxins (Hlg, LukD) and virulence factors such as serine proteases (Spl) were found among the most upregulated during

infection and genes encoding proteins involved in the cell metabolism were among the most downregulated. Main biological processes affected during infection were iron-uptake and pathogenesis processes, as well as the citric acid cycle and expression of extracellular proteins was increased. A large proportion of genes affected encode unstudied hypothetical proteins or hypothetical membrane proteins, whose functions are unknown. These might be important during infection and therefore interesting therapeutic targets, otherwise unrecognized.

In the third chapter, *in vivo* transcriptomes of *S. aureus* clinical isolates (previously described in Chapter 1) and another strain (USA300) are studied, using the method described in Chapter 2. All three strains show most expression upregulation *in vivo* compared to *in vitro* in iron uptake (SbnC and F) and immune evasion (Chs, Sbi and Map) involved proteins and most downregulation in metabolic enzymes (Ddh and ArgF), the transcription regulator SarX and a hypothetical protein. Genes, which are co-upregulated in four genetic backgrounds (two clinical isolates – Patient P an S - and two laboratory strains – USA300 and Newman) were identified were considered an "*in vivo* core transcriptome", commonly upregulated during infection in a strain independent manner. The "core transcriptome" indicates genes, which might make good vaccine targets, due to characteristics they have in common. Further analysis of their biochemical function and/or their role in infection could help us understand more about the pathogenesis of *S. aureus* in bacteraemia and sepsis.

A third objective of Chapter 3 was to study effects of *rsp* mutation *in vivo*. Per-gene analysis reveals only small differences between Rsp^- gene expression and their Rsp^+ strains *in vivo* during infection, while grouped analysis indicates that secreted proteins are affected *in vivo* if *rsp* is mutated.

In the fourth chapter, the impact of adjuvanted vaccination against iron uptake proteins (IsdA and IsdB) on the *in vivo* transcription of *S. aureus* was measured. While an effect of the alum adjuvant was found on bacterial gene expression, IsdA or IsdB protein vaccination did not yield significantly altered gene expression at single gene level. However, grouping of genes resulted in an effect of IsdA protein vaccination of the host on bacterial siderophore biosynthesis and membrane transport protein expression, and the effect was dominated by upregulation of the siderophores Staphyloferrin A and B. In addition, genes, which are found downregulated in *S. aureus* during infection of IsdA vaccinated mice, are also found to be downregulated upon mutation of the transcription regulator *fur*, which regulates iron uptake in *S. aureus*. The proteins used for vaccination in this experiment (IsdA and IsdB) are parts of the bacterial iron uptake system, so a mechanistic connection might be hypothesized. In summary, my work indicates potentially vaccine induced bacterial compensatory behaviour, which needs to be investigated further in order to be verified.

Conclusions

This thesis describes the phenotypic characterisation of the effects of a mutation found in invasive *S. aureus* isolates in the transcription factor *rsp*. The mutants, obtained from patients' bloodstream, do not grow differentially *in vitro*, nor is they survival in human blood *ex vivo* affected. However, in a murine sepsis model *rsp* mutant infected mice show less disease symptoms and succumb less to infection than wild type infected mice. The effect was not due to differences in abscess formation or bacterial survival in the mouse, as bacterial loads in murine tissue were unaltered and histological analysis showed similar tissue lesions caused by *rsp* mutants and wild types. Furthermore, inactivation of Rsp led to transcriptomic and protein expression changes, which caused differential enzyme activities in the supernatant from these mutants. The supernatant of *rsp* mutants interacted more with complement system proteins from the alternative pathway than supernatant from the wild type, possibly activating it in a futile way and thereby evading detection. I conclude that Rsp repressed extracellular proteins might represent suitable vaccine antigen candidates, as our results indicate that *S. aureus* uses them to evade an inflammatory host response and disease symptoms while maintaining its capability to infect the host.

In addition to the *in vitro* characterisation of the above-mentioned clinical isolate, a method to extract bacterial RNA from infected murine tissues in sufficient quality for sequencing was developed and applied to identify *in vivo* transcriptomes of two *S. aureus* laboratory strains and two clinical isolates. Commonly upregulated genes in these four strains were identified, defining an "*in vivo* core transcriptome", which

might be crucial for *S. aureus* pathogenesis. Based on these results I proposed a selection of new potential vaccine antigen candidates.

Moreover, the presented method was used to investigate effects of mutations in the *rsp* transcription regulator on transcription *in vivo* during infection in mice. Here, similar tendencies of expression changes caused by the mutation are observed when genes are grouped. Inactivation of the "*repressor of secreted proteins" (*Rsp*)* leads to an increase in extracellular protein expression, corroborating the applicability of the method.

Finally, the method was applied to describe the bacterial transcriptional response to host immunisation. Indications for different bacterial transcriptional response to IsdA and IsdB vaccination were found, which can now be studied using complimentary methods.

In conclusion, the presented method is an innovative way to study *S. aureus* pathogenesis and technique represents, together with complementary strategies, an initial step in vaccine development by providing a pool of conservatively selected antigens on a rational base.

References

1. Kloos W SK. Staphylococcus. Bergey's Manual of Systematic Bacteriology. 1986.
2. Eriksen NH, Espersen F, Rosdahl VT, Jensen K. Carriage of Staphylococcus aureus among 104 healthy persons during a 19-month period. Epidemiology and infection. 1995 Aug;115(1):51-60. PubMed PMID: 7641838. Pubmed Central PMCID: 2271555.
3. Hu L, Umeda A, Kondo S, Amako K. Typing of Staphylococcus aureus colonising human nasal carriers by pulsed-field gel electrophoresis. Journal of medical microbiology. 1995 Feb;42(2):127-32. PubMed PMID: 7869348.
4. von Eiff C, Becker K, Machka K, Stammer H, Peters G. Nasal carriage as a source of Staphylococcus aureus bacteremia. Study Group. The New England journal of medicine. 2001 Jan 04;344(1):11-6. PubMed PMID: 11136954.
5. Wertheim HF, Melles DC, Vos MC, van Leeuwen W, van Belkum A, Verbrugh HA, et al. The role of nasal carriage in Staphylococcus aureus infections. The Lancet Infectious diseases. 2005 Dec;5(12):751-62. PubMed PMID: 16310147.
6. Bode LG, Kluytmans JA, Wertheim HF, Bogaers D, Vandenbroucke-Grauls CM, Roosendaal R, et al. Preventing surgical-site infections in nasal carriers of Staphylococcus aureus. The New England journal of medicine. 2010 Jan 07;362(1):9-17. PubMed PMID: 20054045.
7. Kluytmans J, van Belkum A, Verbrugh H. Nasal carriage of Staphylococcus aureus: epidemiology, underlying mechanisms, and associated risks. Clinical microbiology reviews. 1997 Jul;10(3):505-20. PubMed PMID: 9227864. Pubmed Central PMCID: 172932.
8. Verkaik NJ, de Vogel CP, Boelens HA, Grumann D, Hoogenboezem T, Vink C, et al. Anti-staphylococcal humoral immune response in persistent nasal carriers and noncarriers of Staphylococcus aureus. J Infect Dis. 2009 Mar 01;199(5):625-32. PubMed PMID: 19199541.
9. Crum NF. The emergence of severe, community-acquired methicillin-resistant Staphylococcus aureus infections. Scandinavian journal of infectious diseases. 2005;37(9):651-6. PubMed PMID: 16126565.
10. Young DM, Harris HW, Charlebois ED, Chambers H, Campbell A, Perdreau-Remington F, et al. An epidemic of methicillin-resistant Staphylococcus aureus soft tissue infections among medically underserved patients. Archives of surgery. 2004 Sep;139(9):947-51; discussion 51-3. PubMed PMID: 15381611.
11. Turnidge JD, Kotsanas D, Munckhof W, Roberts S, Bennett CM, Nimmo GR, et al. Staphylococcus aureus bacteraemia: a major cause of mortality in Australia and New Zealand. The Medical journal of Australia. 2009 Oct 05;191(7):368-73. PubMed PMID: 19807625.
12. Thammavongsa V, Kim HK, Missiakas D, Schneewind O. Staphylococcal manipulation of host immune responses. Nature reviews Microbiology. 2015 Sep;13(9):529-43. PubMed PMID: 26272408. Pubmed Central PMCID: 4625792.

13. Liu GY. Molecular pathogenesis of Staphylococcus aureus infection. Pediatric research. 2009 May;65(5 Pt 2):71R-7R. PubMed PMID: 19190527. Pubmed Central PMCID: 2919328.
14. Malachowa N, DeLeo FR. Staphylococcus aureus survival in human blood. Virulence. 2011 Nov-Dec;2(6):567-9. PubMed PMID: 21971187. Pubmed Central PMCID: 3260549.
15. Bestebroer J, Poppelier MJ, Ulfman LH, Lenting PJ, Denis CV, van Kessel KP, et al. Staphylococcal superantigen-like 5 binds PSGL-1 and inhibits P-selectin-mediated neutrophil rolling. Blood. 2007 Apr 01;109(7):2936-43. PubMed PMID: 17132726.
16. Laarman A, Milder F, van Strijp J, Rooijakkers S. Complement inhibition by gram-positive pathogens: molecular mechanisms and therapeutic implications. Journal of molecular medicine. 2010 Feb;88(2):115-20. PubMed PMID: 20062962. Pubmed Central PMCID: 2832872.
17. Bera A, Herbert S, Jakob A, Vollmer W, Gotz F. Why are pathogenic staphylococci so lysozyme resistant? The peptidoglycan O-acetyltransferase OatA is the major determinant for lysozyme resistance of Staphylococcus aureus. Mol Microbiol. 2005 Feb;55(3):778-87. PubMed PMID: 15661003.
18. Pelz A, Wieland KP, Putzbach K, Hentschel P, Albert K, Gotz F. Structure and biosynthesis of staphyloxanthin from Staphylococcus aureus. The Journal of biological chemistry. 2005 Sep 16;280(37):32493-8. PubMed PMID: 16020541.
19. Karavolos MH, Horsburgh MJ, Ingham E, Foster SJ. Role and regulation of the superoxide dismutases of Staphylococcus aureus. Microbiology. 2003 Oct;149(Pt 10):2749-58. PubMed PMID: 14523108.
20. Cosgrove K, Coutts G, Jonsson IM, Tarkowski A, Kokai-Kun JF, Mond JJ, et al. Catalase (KatA) and alkyl hydroperoxide reductase (AhpC) have compensatory roles in peroxide stress resistance and are required for survival, persistence, and nasal colonization in Staphylococcus aureus. Journal of bacteriology. 2007 Feb;189(3):1025-35. PubMed PMID: 17114262. Pubmed Central PMCID: 1797328.
21. Richardson AR, Dunman PM, Fang FC. The nitrosative stress response of Staphylococcus aureus is required for resistance to innate immunity. Mol Microbiol. 2006 Aug;61(4):927-39. PubMed PMID: 16859493.
22. Surewaard BG, Deniset JF, Zemp FJ, Amrein M, Otto M, Conly J, et al. Identification and treatment of the Staphylococcus aureus reservoir in vivo. The Journal of experimental medicine. 2016 Jun 27;213(7):1141-51. PubMed PMID: 27325887. Pubmed Central PMCID: 4925027.
23. Lehar SM, Pillow T, Xu M, Staben L, Kajihara KK, Vandlen R, et al. Novel antibody-antibiotic conjugate eliminates intracellular S. aureus. Nature. 2015 Nov 19;527(7578):323-8. PubMed PMID: 26536114.
24. Dantes R, Mu Y, Belflower R, Aragon D, Dumyati G, Harrison LH, et al. National burden of invasive methicillin-resistant Staphylococcus aureus infections, United States, 2011. JAMA internal medicine. 2013 Nov 25;173(21):1970-8. PubMed PMID: 24043270.
25. Lee BY, Singh A, David MZ, Bartsch SM, Slayton RB, Huang SS, et al. The economic burden of community-associated methicillin-resistant Staphylococcus aureus (CA-MRSA). Clin Microbiol Infect. 2013 Jun;19(6):528-36. PubMed PMID: 22712729. Pubmed Central PMCID: 3463640.

26. Bamberger DM, Boyd SE. Management of Staphylococcus aureus infections. American family physician. 2005 Dec 15;72(12):2474-81. PubMed PMID: 16370403.
27. Fowler VG, Jr., Olsen MK, Corey GR, Woods CW, Cabell CH, Reller LB, et al. Clinical identifiers of complicated Staphylococcus aureus bacteremia. Archives of internal medicine. 2003 Sep 22;163(17):2066-72. PubMed PMID: 14504120.
28. Mitchell DH, Howden BP. Diagnosis and management of Staphylococcus aureus bacteraemia. Internal medicine journal. 2005 Dec;35 Suppl 2:S17-24. PubMed PMID: 16271058.
29. Lowy FD. Antimicrobial resistance: the example of Staphylococcus aureus. The Journal of clinical investigation. 2003 May;111(9):1265-73. PubMed PMID: 12727914. Pubmed Central PMCID: 154455.
30. Fowler VG, Jr., Proctor RA. Where does a Staphylococcus aureus vaccine stand? Clin Microbiol Infect. 2014 May;20 Suppl 5:66-75. PubMed PMID: 24476315. Pubmed Central PMCID: 4067250.
31. Proctor RA. Challenges for a universal Staphylococcus aureus vaccine. Clinical infectious diseases : an official publication of the Infectious Diseases Society of America. 2012 Apr;54(8):1179-86. PubMed PMID: 22354924.
32. Lowy FD. Staphylococcus aureus infections. The New England journal of medicine. 1998 Aug 20;339(8):520-32. PubMed PMID: 9709046.
33. Fowler VG, Allen KB, Moreira ED, Moustafa M, Isgro F, Boucher HW, et al. Effect of an investigational vaccine for preventing Staphylococcus aureus infections after cardiothoracic surgery: a randomized trial. Jama. 2013 Apr 03;309(13):1368-78. PubMed PMID: 23549582.
34. Skurnik D, Merighi M, Grout M, Gadjeva M, Maira-Litran T, Ericsson M, et al. Animal and human antibodies to distinct Staphylococcus aureus antigens mutually neutralize opsonic killing and protection in mice. The Journal of clinical investigation. 2010 Sep;120(9):3220-33. PubMed PMID: 20739753. Pubmed Central PMCID: 2929724.
35. Proctor RA. Is there a future for a Staphylococcus aureus vaccine? Vaccine. 2012 Apr 19;30(19):2921-7. PubMed PMID: 22115633.
36. McCarthy AJ, Lindsay JA. Genetic variation in Staphylococcus aureus surface and immune evasion genes is lineage associated: implications for vaccine design and host-pathogen interactions. BMC Microbiol. 2010 Jun 15;10:173. PubMed PMID: 20550675. Pubmed Central PMCID: 2905362.
37. Thammavongsa V, Missiakas DM, Schneewind O. Staphylococcus aureus degrades neutrophil extracellular traps to promote immune cell death. Science. 2013 Nov 15;342(6160):863-6. PubMed PMID: 24233725. Pubmed Central PMCID: 4026193.
38. Berends ET, Horswill AR, Haste NM, Monestier M, Nizet V, von Kockritz-Blickwede M. Nuclease expression by Staphylococcus aureus facilitates escape from neutrophil extracellular traps. Journal of innate immunity. 2010;2(6):576-86. PubMed PMID: 20829609. Pubmed Central PMCID: 2982853.
39. Pancari G, Fan H, Smith S, Joshi A, Haimbach R, Clark D, et al. Characterization of the mechanism of protection mediated by CS-D7, a monoclonal antibody to Staphylococcus aureus iron regulated surface determinant B (IsdB). Front Cell Infect Microbiol. 2012;2:36. PubMed PMID: 22919628. Pubmed Central PMCID: 3417506.

40. Mazmanian SK, Skaar EP, Gaspar AH, Humayun M, Gornicki P, Jelenska J, et al. Passage of heme-iron across the envelope of Staphylococcus aureus. Science. 2003 Feb 07;299(5608):906-9. PubMed PMID: 12574635.
41. Lambris JD, Ricklin D, Geisbrecht BV. Complement evasion by human pathogens. Nature reviews Microbiology. 2008 Feb;6(2):132-42. PubMed PMID: 18197169. Pubmed Central PMCID: 2814840.
42. Alonzo F, 3rd, Torres VJ. The bicomponent pore-forming leucocidins of Staphylococcus aureus. Microbiol Mol Biol Rev. 2014 Jun;78(2):199-230. PubMed PMID: 24847020. Pubmed Central PMCID: 4054254.
43. Ventura CL, Malachowa N, Hammer CH, Nardone GA, Robinson MA, Kobayashi SD, et al. Identification of a novel *Staphylococcus aureus* two-component leukotoxin using cell surface proteomics. PloS one. 2010;5(7):e11634. PubMed PMID: 20661294. Pubmed Central PMCID: 2905442.
44. Bubeck Wardenburg J, Bae T, Otto M, Deleo FR, Schneewind O. Poring over pores: alpha-hemolysin and Panton-Valentine leukocidin in Staphylococcus aureus pneumonia. Nature medicine. 2007 Dec;13(12):1405-6. PubMed PMID: 18064027.
45. Joshi A, Pancari G, Cope L, Bowman EP, Cua D, Proctor RA, et al. Immunization with Staphylococcus aureus iron regulated surface determinant B (IsdB) confers protection via Th17/IL17 pathway in a murine sepsis model. Hum Vaccin Immunother. 2012 Mar;8(3):336-46. PubMed PMID: 22327491. Pubmed Central PMCID: 3426080.
46. Gillet Y, Issartel B, Vanhems P, Fournet JC, Lina G, Bes M, et al. Association between Staphylococcus aureus strains carrying gene for Panton-Valentine leukocidin and highly lethal necrotising pneumonia in young immunocompetent patients. Lancet. 2002 Mar 02;359(9308):753-9. PubMed PMID: 11888586.
47. Inoshima I, Inoshima N, Wilke GA, Powers ME, Frank KM, Wang Y, et al. A Staphylococcus aureus pore-forming toxin subverts the activity of ADAM10 to cause lethal infection in mice. Nature medicine. 2011 Sep 18;17(10):1310-4. PubMed PMID: 21926978. Pubmed Central PMCID: 3192248.
48. Rose HR, Holzman RS, Altman DR, Smyth DS, Wasserman GA, Kafer JM, et al. Cytotoxic Virulence Predicts Mortality in Nosocomial Pneumonia Due to Methicillin-Resistant Staphylococcus aureus. J Infect Dis. 2015 Jun 15;211(12):1862-74. PubMed PMID: 25298028. Pubmed Central PMCID: 4836718.
49. Chen LF, Arduino JM, Sheng S, Muhlbaier LH, Kanafani ZA, Harris AD, et al. Epidemiology and outcome of major postoperative infections following cardiac surgery: risk factors and impact of pathogen type. American journal of infection control. 2012 Dec;40(10):963-8. PubMed PMID: 22609237. Pubmed Central PMCID: 3535474.
50. Laabei M, Uhlemann AC, Lowy FD, Austin ED, Yokoyama M, Ouadi K, et al. Evolutionary Trade-Offs Underlie the Multi-faceted Virulence of Staphylococcus aureus. PLoS biology. 2015;13(9):e1002229. PubMed PMID: 26331877. Pubmed Central PMCID: 4558032.
51. Nozohoor S, Heimdahl A, Colque-Navarro P, Julander I, Soderquist B, Mollby R. Virulence factors of Staphylococcus aureus in the pathogenesis of endocarditis. A comparative study of clinical isolates. Zentralblatt fur Bakteriologie : international journal of medical microbiology. 1998 May;287(4):433-47. PubMed PMID: 9638873.

52. Traber KE, Lee E, Benson S, Corrigan R, Cantera M, Shopsin B, et al. agr function in clinical *Staphylococcus aureus* isolates. Microbiology. 2008 Aug;154(Pt 8):2265-74. PubMed PMID: 18667559.
53. Shopsin B, Drlica-Wagner A, Mathema B, Adhikari RP, Kreiswirth BN, Novick RP. Prevalence of agr dysfunction among colonizing Staphylococcus aureus strains. J Infect Dis. 2008 Oct 15;198(8):1171-4. PubMed PMID: WOS:000259891800012. English.
54. Soong G, Paulino F, Wachtel S, Parker D, Wickersham M, Zhang DN, et al. Methicillin-Resistant Staphylococcus aureus Adaptation to Human Keratinocytes. Mbio. 2015 Mar-Apr;6(2). PubMed PMID: WOS:000355312400087. English.
55. Tuchscherr L, Loffler B. Staphylococcus aureus dynamically adapts global regulators and virulence factor expression in the course from acute to chronic infection. Current genetics. 2016 Feb;62(1):15-7. PubMed PMID: 26123224.
56. Tuchscherr L, Medina E, Hussain M, Volker W, Heitmann V, Niemann S, et al. Staphylococcus aureus phenotype switching: an effective bacterial strategy to escape host immune response and establish a chronic infection. EMBO molecular medicine. 2011 Mar;3(3):129-41. PubMed PMID: 21268281. Pubmed Central PMCID: 3395110.
57. Kalinka J, Hachmeister M, Geraci J, Sordelli D, Hansen U, Niemann S, et al. Staphylococcus aureus isolates from chronic osteomyelitis are characterized by high host cell invasion and intracellular adaptation, but still induce inflammation. Int J Med Microbiol. 2014 Nov;304(8):1038-49. PubMed PMID: 25129555.
58. Young BC, Golubchik T, Batty EM, Fung R, Larner-Svensson H, Votintseva AA, et al. Evolutionary dynamics of Staphylococcus aureus during progression from carriage to disease. Proc Natl Acad Sci U S A. 2012 Mar 20;109(12):4550-5. PubMed PMID: 22393007. Pubmed Central PMCID: 3311376.
59. Das S, Lindemann C, Young BC, Muller J, Osterreich B, Ternette N, et al. Natural mutations in a Staphylococcus aureus virulence regulator attenuate cytotoxicity but permit bacteremia and abscess formation. Proc Natl Acad Sci U S A. 2016 May 31;113(22):E3101-10. PubMed PMID: 27185949. Pubmed Central PMCID: 4896717.
60. Everitt RG, Didelot X, Batty EM, Miller RR, Knox K, Young BC, et al. Mobile elements drive recombination hotspots in the core genome of Staphylococcus aureus. Nat Commun. 2014 May 23;5:3956. PubMed PMID: 24853639. Pubmed Central PMCID: 4036114.
61. Lei MG, Cue D, Roux CM, Dunman PM, Lee CY. Rsp inhibits attachment and biofilm formation by repressing fnbA in Staphylococcus aureus MW2. Journal of bacteriology. 2011 Oct;193(19):5231-41. PubMed PMID: 21804010. Pubmed Central PMCID: 3187379.
62. Holden MT, Feil EJ, Lindsay JA, Peacock SJ, Day NP, Enright MC, et al. Complete genomes of two clinical Staphylococcus aureus strains: evidence for the rapid evolution of virulence and drug resistance. Proceedings of the National Academy of Sciences of the United States of America. 2004 Jun 29;101(26):9786-91. PubMed PMID: 15213324. Pubmed Central PMCID: 470752.
63. Fey PD, Endres JL, Yajjala VK, Widhelm TJ, Boissy RJ, Bose JL, et al. A Genetic Resource for Rapid and Comprehensive Phenotype Screening of Nonessential Staphylococcus aureus Genes. Mbio. 2013 Jan-Feb;4(1). PubMed PMID: WOS:000315814300027. English.

64. Tenover FC, Goering RV. Methicillin-resistant Staphylococcus aureus strain USA300: origin and epidemiology. The Journal of antimicrobial chemotherapy. 2009 Sep;64(3):441-6. PubMed PMID: 19608582.
65. van der Maten E, de Jonge MI, de Groot R, van der Flier M, Langereis JD. A versatile assay to determine bacterial and host factors contributing to opsonophagocytotic killing in hirudin-anticoagulated whole blood. Sci Rep. 2017 Feb 08;7:42137. PubMed PMID: 28176849. Pubmed Central PMCID: 5296863.
66. Langford DJ, Bailey AL, Chanda ML, Clarke SE, Drummond TE, Echols S, et al. Coding of facial expressions of pain in the laboratory mouse. Nat Methods. 2010 Jun;7(6):447-9. PubMed PMID: 20453868.
67. Bremell T, Lange S, Yacoub A, Ryden C, Tarkowski A. Experimental Staphylococcus aureus arthritis in mice. Infect Immun. 1991 Aug;59(8):2615-23. PubMed PMID: 1855981. Pubmed Central PMCID: 258064.
68. Allen ER, van Diemen P, Yamaguchi Y, Lindemann C, Soilleux E, Rollier C, et al. MRI Based Localisation and Quantification of Abscesses following Experimental S. aureus Intravenous Challenge: Application to Vaccine Evaluation. PLoS One. 2016;11(5):e0154705. PubMed PMID: 27228181. Pubmed Central PMCID: 4881890.
69. Bolger AM, Lohse M, Usadel B. Trimmomatic: a flexible trimmer for Illumina sequence data. Bioinformatics. 2014 Aug 1;30(15):2114-20. PubMed PMID: 24695404. Pubmed Central PMCID: 4103590.
70. Langmead B, Trapnell C, Pop M, Salzberg SL. Ultrafast and memory-efficient alignment of short DNA sequences to the human genome. Genome Biol. 2009;10(3). PubMed PMID: WOS:000266544500005. English.
71. Anders S, Pyl PT, Huber W. HTSeq-a Python framework to work with high-throughput sequencing data. Bioinformatics. 2015 Jan 15;31(2):166-9. PubMed PMID: WOS:000347832300003. English.
72. Shilov IV, Seymour SL, Patel AA, Loboda A, Tang WH, Keating SP, et al. The paragon algorithm, a next generation search engine that uses sequence temperature values and feature probabilities to identify peptides from tandem mass spectra. Mol Cell Proteomics. 2007 Sep;6(9):1638-55. PubMed PMID: WOS:000249237200014. English.
73. Zhang J, Xin L, Shan BZ, Chen WW, Xie MJ, Yuen D, et al. PEAKS DB: De Novo Sequencing Assisted Database Search for Sensitive and Accurate Peptide Identification. Mol Cell Proteomics. 2012 Apr;11(4). PubMed PMID: WOS:000302786500005. English.
74. Love MI, Huber W, Anders S. Moderated estimation of fold change and dispersion for RNA-seq data with DESeq2. Genome Biol. 2014;15(12). PubMed PMID: WOS:000346609500022. English.
75. Rice K. A Decision-Theoretic Formulation of Fisher's Approach to Testing. Am Stat. 2010 Nov;64(4):345-9. PubMed PMID: WOS:000286451800010. English.
76. Bourgon R, Gentleman R, Huber W. Independent filtering increases detection power for high-throughput experiments. P Natl Acad Sci USA. 2010 May 25;107(21):9546-51. PubMed PMID: WOS:000278054700015. English.
77. Benjamini Y, Hochberg Y. Controlling the False Discovery Rate - a Practical and Powerful Approach to Multiple Testing. J Roy Stat Soc B Met. 1995;57(1):289-300. PubMed PMID: WOS:A1995QE45300017. English.

78. Cheng AG, Kim HK, Burts ML, Krausz T, Schneewind O, Missiakas DM. Genetic requirements for Staphylococcus aureus abscess formation and persistence in host tissues. Faseb J. 2009 Oct;23(10):3393-404. PubMed PMID: WOS:000270354300017. English.
79. Alami SY, Kelly FC, Race GJ. Pathogenicity of staphylococci: with special reference to the persitence of infection in mice. The American journal of pathology. 1968 Oct;53(4):577-89. PubMed PMID: 5677139. Pubmed Central PMCID: 2013414.
80. Cheng AG, DeDent AC, Schneewind O, Missiakas D. A play in four acts: Staphylococcus aureus abscess formation. Trends in microbiology. 2011 May;19(5):225-32. PubMed PMID: 21353779. Pubmed Central PMCID: 3087859.
81. Lee LY, Miyamoto YJ, McIntyre BW, Hook M, McCrea KW, McDevitt D, et al. The Staphylococcus aureus Map protein is an immunomodulator that interferes with T cell-mediated responses. The Journal of clinical investigation. 2002 Nov;110(10):1461-71. PubMed PMID: 12438444. Pubmed Central PMCID: 151818.
82. Smith EJ, Visai L, Kerrigan SW, Speziale P, Foster TJ. The Sbi protein is a multifunctional immune evasion factor of Staphylococcus aureus. Infect Immun. 2011 Sep;79(9):3801-9. PubMed PMID: 21708997. Pubmed Central PMCID: 3165492.
83. O'Riordan K, Lee JC. Staphylococcus aureus capsular polysaccharides. Clinical microbiology reviews. 2004 Jan;17(1):218-34. PubMed PMID: 14726462. Pubmed Central PMCID: 321462.
84. Jusko M, Potempa J, Kantyka T, Bielecka E, Miller HK, Kalinska M, et al. Staphylococcal proteases aid in evasion of the human complement system. Journal of innate immunity. 2014;6(1):31-46. PubMed PMID: 23838186. Pubmed Central PMCID: 3972074.
85. Koch TK, Reuter M, Barthel D, Bohm S, van den Elsen J, Kraiczy P, et al. Staphylococcus aureus proteins Sbi and Efb recruit human plasmin to degrade complement C3 and C3b. PLoS One. 2012;7(10):e47638. PubMed PMID: 23071827. Pubmed Central PMCID: 3469469.
86. Sharp JA, Echague CG, Hair PS, Ward MD, Nyalwidhe JO, Geoghegan JA, et al. Staphylococcus aureus surface protein SdrE binds complement regulator factor H as an immune evasion tactic. PLoS One. 2012;7(5):e38407. PubMed PMID: 22675461. Pubmed Central PMCID: 3364985.
87. Laarman AJ, Ruyken M, Malone CL, van Strijp JA, Horswill AR, Rooijakkers SH. Staphylococcus aureus metalloprotease aureolysin cleaves complement C3 to mediate immune evasion. J Immunol. 2011 Jun 1;186(11):6445-53. PubMed PMID: 21502375.
88. Corrigan RM, Miajlovic H, Foster TJ. Surface proteins that promote adherence of Staphylococcus aureus to human desquamated nasal epithelial cells. BMC Microbiol. 2009;9:22. PubMed PMID: 19183486. Pubmed Central PMCID: 2642834. Epub 2009/02/03. eng.
89. Morrison JM, Miller EW, Benson MA, Alonzo F, 3rd, Yoong P, Torres VJ, et al. Characterization of SSR42, a novel virulence factor regulatory RNA that contributes to the pathogenesis of a *Staphylococcus aureus* USA300 representative. J Bacteriol. 2012 Jun;194(11):2924-38. PubMed PMID: 22493015. Pubmed Central PMCID: Pmc3370614. Epub 2012/04/12. eng.

90. Konieczna I, Zarnowiec P, Kwinkowski M, Kolesinska B, Fraczyk J, Kaminski Z, et al. Bacterial Urease and its Role in Long-Lasting Human Diseases. Curr Protein Pept Sc. 2012 Dec;13(8):789-806. PubMed PMID: WOS:000313564400008. English.
91. Stockland AE, San Clemente CL. Multiple forms of lactate dehydrogenase in Staphylococcus aureus. Journal of bacteriology. 1969 Oct;100(1):347-53. PubMed PMID: 4310081. Pubmed Central PMCID: 315398.
92. Richardson AR, Libby SJ, Fang FC. A nitric oxide-inducible lactate dehydrogenase enables Staphylococcus aureus to resist innate immunity. Science. 2008 Mar 21;319(5870):1672-6. PubMed PMID: WOS:000254172300043. English.
93. Traber KE, Lee E, Benson S, Corrigan R, Cantera M, Shopsin B, et al. agr function in clinical Staphylococcus aureus isolates. Microbiol-Sgm. 2008 Aug;154:2265-74. PubMed PMID: WOS:000258860200009. English.
94. Li T, He L, Song Y, Villaruz AE, Joo HS, Liu Q, et al. AraC-Type Regulator Rsp Adapts Staphylococcus aureus Gene Expression to Acute Infection. Infect Immun. 2016 Mar;84(3):723-34. PubMed PMID: 26712209. Pubmed Central PMCID: 4771356.
95. Stryjewski ME, Kanafani ZA, Chu VH, Pappas PA, Harding T, Drew LA, et al. Staphylococcus aureus bacteremia among patients with health care-associated fever. The American journal of medicine. 2009 Mar;122(3):281-9 e2. PubMed PMID: 19272489.
96. Koziel J, Maciag-Gudowska A, Mikolajczyk T, Bzowska M, Sturdevant DE, Whitney AR, et al. Phagocytosis of Staphylococcus aureus by macrophages exerts cytoprotective effects manifested by the upregulation of antiapoptotic factors. PLoS One. 2009;4(4):e5210. PubMed PMID: 19381294. Pubmed Central PMCID: 2668171.
97. Thwaites GE, Gant V. Are bloodstream leukocytes Trojan Horses for the metastasis of Staphylococcus aureus? Nature reviews Microbiology. 2011 Mar;9(3):215-22. PubMed PMID: 21297670.
98. Prajsnar TK, Hamilton R, Garcia-Lara J, McVicker G, Williams A, Boots M, et al. A privileged intraphagocyte niche is responsible for disseminated infection of Staphylococcus aureus in a zebrafish model. Cellular microbiology. 2012 Oct;14(10):1600-19. PubMed PMID: 22694745. Pubmed Central PMCID: 3470706.
99. Burman JD, Leung E, Atkins KL, O'Seaghdha MN, Lango L, Bernado P, et al. Interaction of human complement with Sbi, a staphylococcal immunoglobulin-binding protein: indications of a novel mechanism of complement evasion by Staphylococcus aureus. The Journal of biological chemistry. 2008 Jun 20;283(25):17579-93. PubMed PMID: 18434316. Pubmed Central PMCID: 2649420.
100. Anderson AS, Miller AA, Donald RG, Scully IL, Nanra JS, Cooper D, et al. Development of a multicomponent Staphylococcus aureus vaccine designed to counter multiple bacterial virulence factors. Hum Vaccin Immunother. 2012 Nov 01;8(11):1585-94. PubMed PMID: 22922765. Pubmed Central PMCID: 3601133.
101. Attia AS, Cassat JE, Aranmolate SO, Zimmerman LJ, Boyd KL, Skaar EP. Analysis of the Staphylococcus aureus abscess proteome identifies antimicrobial host proteins and bacterial stress responses at the host-pathogen interface. Pathog Dis. 2013 Oct;69(1):36-48. PubMed PMID: 23847107. Pubmed Central PMCID: 3877740.

102. Diep BA, Phung Q, Date S, Arnott D, Bakalarski C, Xu M, et al. Identifying potential therapeutic targets of methicillin-resistant Staphylococcus aureus through in vivo proteomic analysis. J Infect Dis. 2014 May 15;209(10):1533-41. PubMed PMID: 24280367. Pubmed Central PMCID: 3997574.
103. Windmuller N, Witten A, Block D, Bunk B, Sproer C, Kahl BC, et al. Transcriptional adaptations during long-term persistence of Staphylococcus aureus in the airways of a cystic fibrosis patient. Int J Med Microbiol. 2015 Jan;305(1):38-46. PubMed PMID: 25439320.
104. Chaffin DO, Taylor D, Skerrett SJ, Rubens CE. Changes in the Staphylococcus aureus transcriptome during early adaptation to the lung. PLoS One. 2012;7(8):e41329. PubMed PMID: 22876285. Pubmed Central PMCID: 3410880.
105. Nagalakshmi U, Waern K, Snyder M. RNA-Seq: a method for comprehensive transcriptome analysis. Current protocols in molecular biology. 2010 Jan;Chapter 4:Unit 4 11 1-3. PubMed PMID: 20069539.
106. Mutz KO, Heilkenbrinker A, Lonne M, Walter JG, Stahl F. Transcriptome analysis using next-generation sequencing. Current opinion in biotechnology. 2013 Feb;24(1):22-30. PubMed PMID: 23020966.
107. Fu X, Fu N, Guo S, Yan Z, Xu Y, Hu H, et al. Estimating accuracy of RNA-Seq and microarrays with proteomics. BMC Genomics. 2009 Apr 16;10:161. PubMed PMID: 19371429. Pubmed Central PMCID: 2676304.
108. Bottomly D, Walter NA, Hunter JE, Darakjian P, Kawane S, Buck KJ, et al. Evaluating gene expression in C57BL/6J and DBA/2J mouse striatum using RNA-Seq and microarrays. PLoS One. 2011 Mar 24;6(3):e17820. PubMed PMID: 21455293. Pubmed Central PMCID: 3063777.
109. Sirbu A, Kerr G, Crane M, Ruskin HJ. RNA-Seq vs dual- and single-channel microarray data: sensitivity analysis for differential expression and clustering. PLoS One. 2012;7(12):e50986. PubMed PMID: 23251411. Pubmed Central PMCID: 3518479.
110. Chaves-Moreno D, Wos-Oxley ML, Jauregui R, Medina E, Oxley AP, Pieper DH. Exploring the transcriptome of Staphylococcus aureus in its natural niche. Sci Rep. 2016 Sep 19;6:33174. PubMed PMID: 27641137. Pubmed Central PMCID: 5027550.
111. Xu Y, Maltesen RG, Larsen LH, Schonheyder HC, Le VQ, Nielsen JL, et al. In vivo gene expression in a Staphylococcus aureus prosthetic joint infection characterized by RNA sequencing and metabolomics: a pilot study. BMC Microbiol. 2016 May 05;16:80. PubMed PMID: 27150914. Pubmed Central PMCID: 4858865.
112. Malachowa N, Kobayashi SD, Sturdevant DE, Scott DP, DeLeo FR. Insights into the Staphylococcus aureus-host interface: global changes in host and pathogen gene expression in a rabbit skin infection model. PLoS One. 2015;10(2):e0117713. PubMed PMID: 25719526. Pubmed Central PMCID: 4342162.
113. Date SV, Modrusan Z, Lawrence M, Morisaki JH, Toy K, Shah IM, et al. Global gene expression of methicillin-resistant Staphylococcus aureus USA300 during human and mouse infection. J Infect Dis. 2014 May 15;209(10):1542-50. PubMed PMID: 24286981.
114. Pfaffl MW. A new mathematical model for relative quantification in real-time RT-PCR. Nucleic acids research. 2001 May 1;29(9):e45. PubMed PMID: 11328886. Pubmed Central PMCID: 55695.

115. He S, Wurtzel O, Singh K, Froula JL, Yilmaz S, Tringe SG, et al. Validation of two ribosomal RNA removal methods for microbial metatranscriptomics. Nat Methods. 2010 Oct;7(10):807-12. PubMed PMID: 20852648.
116. Yamaguchi KD, Ruderman DL, Croze E, Wagner TC, Velichko S, Reder AT, et al. IFN-beta-regulated genes show abnormal expression in therapy-naive relapsing-remitting MS mononuclear cells: gene expression analysis employing all reported protein-protein interactions. Journal of neuroimmunology. 2008 Mar;195(1-2):116-20. PubMed PMID: 18279974.
117. Becker C, Hammerle-Fickinger A, Riedmaier I, Pfaffl MW. mRNA and microRNA quality control for RT-qPCR analysis. Methods. 2010 Apr;50(4):237-43. PubMed PMID: 20079844.
118. Vermeulen J, De Preter K, Lefever S, Nuytens J, De Vloed F, Derveaux S, et al. Measurable impact of RNA quality on gene expression results from quantitative PCR. Nucleic acids research. 2011 May;39(9):e63. PubMed PMID: 21317187. Pubmed Central PMCID: 3089491.
119. Bosi E, Monk JM, Aziz RK, Fondi M, Nizet V, Palsson BO. Comparative genome-scale modelling of Staphylococcus aureus strains identifies strain-specific metabolic capabilities linked to pathogenicity. Proc Natl Acad Sci U S A. 2016 Jun 28;113(26):E3801-9. PubMed PMID: 27286824. Pubmed Central PMCID: 4932939.
120. Giannoukos G, Ciulla DM, Huang K, Haas BJ, Izard J, Levin JZ, et al. Efficient and robust RNA-seq process for cultured bacteria and complex community transcriptomes. Genome Biol. 2012;13(3):R23. PubMed PMID: 22455878. Pubmed Central PMCID: 3439974.
121. Haas BJ, Chin M, Nusbaum C, Birren BW, Livny J. How deep is deep enough for RNA-Seq profiling of bacterial transcriptomes? BMC Genomics. 2012 Dec 27;13:734. PubMed PMID: 23270466. Pubmed Central PMCID: 3543199.
122. Stec-Niemczyk J, Pustelny K, Kisielewska M, Bista M, Boulware KT, Stiennicke HR, et al. Structural and functional characterization of SplA, an exclusively specific protease of Staphylococcus aureus. Biochem J. 2009 May 1;419:555-64. PubMed PMID: WOS:000265901500004. English.
123. Reed SB, Wesson CA, Liou LE, Trumble WR, Schlievert PM, Bohach GA, et al. Molecular characterization of a novel Staphylococcus aureus serine protease operon. Infection and Immunity. 2001 Mar;69(3):1521-7. PubMed PMID: WOS:000167090200039. English.
124. Saliba AE, Westermann AJ, Gorski SA, Vogel J. Single-cell RNA-seq: advances and future challenges. Nucleic acids research. 2014 Aug;42(14):8845-60. PubMed PMID: 25053837. Pubmed Central PMCID: 4132710.
125. Garzoni C, Francois P, Huyghe A, Couzinet S, Tapparel C, Charbonnier Y, et al. A global view of Staphylococcus aureus whole genome expression upon internalization in human epithelial cells. BMC Genomics. 2007;8:171. PubMed PMID: 17570841. Pubmed Central PMCID: 1924023. Epub 2007/06/16. eng.
126. Ishii K, Adachi T, Yasukawa J, Suzuki Y, Hamamoto H, Sekimizu K. Induction of virulence gene expression in Staphylococcus aureus by pulmonary surfactant. Infect Immun. 2014 Apr;82(4):1500-10. PubMed PMID: 24452679. Pubmed Central PMCID: 3993393.
127. Paharik AE, Salgado-Pabon W, Meyerholz DK, White MJ, Schlievert PM, Horswill AR. The Spl Serine Proteases Modulate Staphylococcus aureus Protein

Production and Virulence in a Rabbit Model of Pneumonia. mSphere. 2016 Sep-Oct;1(5). PubMed PMID: 27747296. Pubmed Central PMCID: 5061998.
128. Kochan I. The role of iron in bacterial infections, with special consideration of host-tubercle bacillus interaction. Current topics in microbiology and immunology. 1973;60:1-30. PubMed PMID: 4197776.
129. Corbin BD, Seeley EH, Raab A, Feldmann J, Miller MR, Torres VJ, et al. Metal chelation and inhibition of bacterial growth in tissue abscesses. Science. 2008 Feb 15;319(5865):962-5. PubMed PMID: 18276893.
130. Black MB, Parks BB, Pluta L, Chu TM, Allen BC, Wolfinger RD, et al. Comparison of microarrays and RNA-seq for gene expression analyses of dose-response experiments. Toxicological sciences : an official journal of the Society of Toxicology. 2014 Feb;137(2):385-403. PubMed PMID: 24194394.
131. Mooney M, Bond J, Monks N, Eugster E, Cherba D, Berlinski P, et al. Comparative RNA-Seq and microarray analysis of gene expression changes in B-cell lymphomas of Canis familiaris. PLoS One. 2013;8(4):e61088. PubMed PMID: 23593398. Pubmed Central PMCID: 3617154.
132. Yarwood JM, Schlievert PM. Quorum sensing in Staphylococcus infections. The Journal of clinical investigation. 2003 Dec;112(11):1620-5. PubMed PMID: 14660735. Pubmed Central PMCID: 281656.
133. Heyer G, Saba S, Adamo R, Rush W, Soong G, Cheung A, et al. Staphylococcus aureus agr and sarA functions are required for invasive infection but not inflammatory responses in the lung. Infect Immun. 2002 Jan;70(1):127-33. PubMed PMID: 11748173. Pubmed Central PMCID: 127645.
134. Blevins JS, Elasri MO, Allmendinger SD, Beenken KE, Skinner RA, Thomas JR, et al. Role of sarA in the pathogenesis of Staphylococcus aureus musculoskeletal infection. Infect Immun. 2003 Jan;71(1):516-23. PubMed PMID: 12496203. Pubmed Central PMCID: 143404.
135. von Eiff C, Heilmann C, Proctor RA, Woltz C, Peters G, Gotz F. A site-directed Staphylococcus aureus hemB mutant is a small-colony variant which persists intracellularly. Journal of bacteriology. 1997 Aug;179(15):4706-12. PubMed PMID: 9244256. Pubmed Central PMCID: 179315.
136. Cuaron JA, Dulal S, Song Y, Singh AK, Montelongo CE, Yu W, et al. Tea tree oil-induced transcriptional alterations in Staphylococcus aureus. Phytotherapy research : PTR. 2013 Mar;27(3):390-6. PubMed PMID: 22619070. Pubmed Central PMCID: 3593976.
137. Kenny JG, Ward D, Josefsson E, Jonsson IM, Hinds J, Rees HH, et al. The Staphylococcus aureus response to unsaturated long chain free fatty acids: survival mechanisms and virulence implications. PLoS One. 2009;4(2):e4344. PubMed PMID: 19183815. Pubmed Central PMCID: 2629846.
138. Petek M, Baebler S, Kuzman D, Rotter A, Podlesek Z, Gruden K, et al. Revealing fosfomycin primary effect on Staphylococcus aureus transcriptome: modulation of cell envelope biosynthesis and phosphoenolpyruvate induced starvation. BMC Microbiol. 2010 Jun 01;10:159. PubMed PMID: 20515462. Pubmed Central PMCID: 2887449.
139. Dastgheyb SS, Otto M. Staphylococcal adaptation to diverse physiologic niches: an overview of transcriptomic and phenotypic changes in different biological environments. Future microbiology. 2015;10(12):1981-95. PubMed PMID: 26584249. Pubmed Central PMCID: 4946774.

140. Novick RP. Autoinduction and signal transduction in the regulation of staphylococcal virulence. Mol Microbiol. 2003 Jun;48(6):1429-49. PubMed PMID: 12791129.
141. Liang X, Zheng L, Landwehr C, Lunsford D, Holmes D, Ji Y. Global regulation of gene expression by ArlRS, a two-component signal transduction regulatory system of Staphylococcus aureus. Journal of bacteriology. 2005 Aug;187(15):5486-92. PubMed PMID: 16030243. Pubmed Central PMCID: 1196029.
142. Ji Q, Zhang L, Sun F, Deng X, Liang H, Bae T, et al. Staphylococcus aureus CymR is a new thiol-based oxidation-sensing regulator of stress resistance and oxidative response. The Journal of biological chemistry. 2012 Jun 15;287(25):21102-9. PubMed PMID: 22553203. Pubmed Central PMCID: 3375533.
143. Ibarra JA, Perez-Rueda E, Carroll RK, Shaw LN. Global analysis of transcriptional regulators in Staphylococcus aureus. BMC Genomics. 2013 Feb 26;14:126. PubMed PMID: 23442205. Pubmed Central PMCID: 3616918.
144. Steinhuber A, Goerke C, Bayer MG, Doring G, Wolz C. Molecular architecture of the regulatory Locus sae of Staphylococcus aureus and its impact on expression of virulence factors. Journal of bacteriology. 2003 Nov;185(21):6278-86. PubMed PMID: 14563862. Pubmed Central PMCID: 219404.
145. Cheung AL, Projan SJ. Cloning and sequencing of sarA of Staphylococcus aureus, a gene required for the expression of agr. Journal of bacteriology. 1994 Jul;176(13):4168-72. PubMed PMID: 8021198. Pubmed Central PMCID: 205618.
146. Chen PR, Bae T, Williams WA, Duguid EM, Rice PA, Schneewind O, et al. An oxidation-sensing mechanism is used by the global regulator MgrA in Staphylococcus aureus. Nature chemical biology. 2006 Nov;2(11):591-5. PubMed PMID: 16980961.
147. Cassat J, Dunman PM, Murphy E, Projan SJ, Beenken KE, Palm KJ, et al. Transcriptional profiling of a Staphylococcus aureus clinical isolate and its isogenic agr and sarA mutants reveals global differences in comparison to the laboratory strain RN6390. Microbiology. 2006 Oct;152(Pt 10):3075-90. PubMed PMID: 17005987.
148. Yu CS, Chen YC, Lu CH, Hwang JK. Prediction of protein subcellular localization. Proteins. 2006 Aug 15;64(3):643-51. PubMed PMID: 16752418.
149. Goldberg T, Hecht M, Hamp T, Karl T, Yachdav G, Ahmed N, et al. LocTree3 prediction of localization. Nucleic acids research. 2014 Jul;42(Web Server issue):W350-5. PubMed PMID: 24848019. Pubmed Central PMCID: 4086075.
150. Gardy JL, Laird MR, Chen F, Rey S, Walsh CJ, Ester M, et al. PSORTb v.2.0: expanded prediction of bacterial protein subcellular localization and insights gained from comparative proteome analysis. Bioinformatics. 2005 Mar 01;21(5):617-23. PubMed PMID: 15501914.
151. Zhou M, Boekhorst J, Francke C, Siezen RJ. LocateP: genome-scale subcellular-location predictor for bacterial proteins. BMC Bioinformatics. 2008 Mar 27;9:173. PubMed PMID: 18371216. Pubmed Central PMCID: 2375117.
152. Delfani S, Mohabati Mobarez A, Imani Fooladi AA, Amani J, Emaneini M. Protection of mice against Staphylococcus aureus infection by a recombinant protein ClfA-IsdB-Hlg as a vaccine candidate. Medical microbiology and immunology. 2016 Feb;205(1):47-55. PubMed PMID: 26155981.

153. Malachowa N, Whitney AR, Kobayashi SD, Sturdevant DE, Kennedy AD, Braughton KR, et al. Global changes in Staphylococcus aureus gene expression in human blood. PloS one. 2011 Apr 15;6(4):e18617. PubMed PMID: 21525981. Pubmed Central PMCID: 3078114.
154. Schlag S, Nerz C, Birkenstock TA, Altenberend F, Gotz F. Inhibition of staphylococcal biofilm formation by nitrite. Journal of bacteriology. 2007 Nov;189(21):7911-9. PubMed PMID: 17720780. Pubmed Central PMCID: 2168742.
155. Pietiainen M, Francois P, Hyyrylainen HL, Tangomo M, Sass V, Sahl HG, et al. Transcriptome analysis of the responses of Staphylococcus aureus to antimicrobial peptides and characterization of the roles of vraDE and vraSR in antimicrobial resistance. BMC genomics. 2009 Sep 14;10:429. PubMed PMID: 19751498. Pubmed Central PMCID: 2748101.
156. Beenken KE, Dunman PM, McAleese F, Macapagal D, Murphy E, Projan SJ, et al. Global gene expression in Staphylococcus aureus biofilms. Journal of bacteriology. 2004 Jul;186(14):4665-84. PubMed PMID: 15231800. Pubmed Central PMCID: 438561.
157. Palazzolo-Ballance AM, Reniere ML, Braughton KR, Sturdevant DE, Otto M, Kreiswirth BN, et al. Neutrophil microbicides induce a pathogen survival response in community-associated methicillin-resistant Staphylococcus aureus. Journal of immunology. 2008 Jan 1;180(1):500-9. PubMed PMID: 18097052.
158. Chang W, Small DA, Toghrol F, Bentley WE. Global transcriptome analysis of Staphylococcus aureus response to hydrogen peroxide. Journal of bacteriology. 2006 Feb;188(4):1648-59. PubMed PMID: 16452450. Pubmed Central PMCID: 1367260.
159. Nobre LS, Saraiva LM. Effect of combined oxidative and nitrosative stresses on Staphylococcus aureus transcriptome. Applied microbiology and biotechnology. 2013 Mar;97(6):2563-73. PubMed PMID: 23389340.
160. . !!! INVALID CITATION !!!
161. Christner M, Franke GC, Schommer NN, Wendt U, Wegert K, Pehle P, et al. The giant extracellular matrix-binding protein of Staphylococcus epidermidis mediates biofilm accumulation and attachment to fibronectin. Mol Microbiol. 2010 Jan;75(1):187-207. PubMed PMID: 19943904.
162. Koymans KJ, Bisschop A, Vughs MM, van Kessel KP, de Haas CJ, van Strijp JA. Staphylococcal Superantigen-Like Protein 1 and 5 (SSL1 & SSL5) Limit Neutrophil Chemotaxis and Migration through MMP-Inhibition. International journal of molecular sciences. 2016 Jul 05;17(7). PubMed PMID: 27399672. Pubmed Central PMCID: 4964448.
163. Dale SE, Doherty-Kirby A, Lajoie G, Heinrichs DE. Role of siderophore biosynthesis in virulence of Staphylococcus aureus: identification and characterization of genes involved in production of a siderophore. Infect Immun. 2004 Jan;72(1):29-37. PubMed PMID: 14688077. Pubmed Central PMCID: 343950. Epub 2003/12/23. eng.
164. Laakso HA, Marolda CL, Pinter TB, Stillman MJ, Heinrichs DE. A Heme-responsive Regulator Controls Synthesis of Staphyloferrin B in Staphylococcus aureus. The Journal of biological chemistry. 2016 Jan 1;291(1):29-40. PubMed PMID: 26534960. Pubmed Central PMCID: 4697164.

165. Cheung J, Beasley FC, Liu S, Lajoie GA, Heinrichs DE. Molecular characterization of staphyloferrin B biosynthesis in Staphylococcus aureus. Mol Microbiol. 2009 Nov;74(3):594-608. PubMed PMID: 19775248.
166. Oogai Y, Matsuo M, Hashimoto M, Kato F, Sugai M, Komatsuzawa H. Expression of virulence factors by Staphylococcus aureus grown in serum. Applied and environmental microbiology. 2011 Nov;77(22):8097-105. PubMed PMID: 21926198. Pubmed Central PMCID: 3208999.
167. Postma B, Poppelier MJ, van Galen JC, Prossnitz ER, van Strijp JA, de Haas CJ, et al. Chemotaxis inhibitory protein of Staphylococcus aureus binds specifically to the C5a and formylated peptide receptor. J Immunol. 2004 Jun 1;172(11):6994-7001. PubMed PMID: 15153520.
168. Fuller JR, Vitko NP, Perkowski EF, Scott E, Khatri D, Spontak JS, et al. Identification of a lactate-quinone oxidoreductase in Staphylococcus aureus that is essential for virulence. Front Cell Infect Microbiol. 2011;1:19. PubMed PMID: 22919585. Pubmed Central PMCID: 3417369.
169. Nuxoll AS, Halouska SM, Sadykov MR, Hanke ML, Bayles KW, Kielian T, et al. CcpA regulates arginine biosynthesis in Staphylococcus aureus through repression of proline catabolism. PLoS pathogens. 2012;8(11):e1003033. PubMed PMID: 23209408. Pubmed Central PMCID: 3510247.
170. Manna AC, Cheung AL. Expression of SarX, a negative regulator of agr and exoprotein synthesis, is activated by MgrA in Staphylococcus aureus. Journal of bacteriology. 2006 Jun;188(12):4288-99. PubMed PMID: 16740935. Pubmed Central PMCID: 1482969.
171. Cue D, Lei MG, Lee CY. Activation of sarX by Rbf is required for biofilm formation and icaADBC expression in Staphylococcus aureus. Journal of bacteriology. 2013 Apr;195(7):1515-24. PubMed PMID: 23354746. Pubmed Central PMCID: 3624532.
172. Molkanen T, Tyynela J, Helin J, Kalkkinen N, Kuusela P. Enhanced activation of bound plasminogen on Staphylococcus aureus by staphylokinase. FEBS letters. 2002 Apr 24;517(1-3):72-8. PubMed PMID: 12062412.
173. Juarez O, Nilges MJ, Gillespie P, Cotton J, Barquera B. Riboflavin is an active redox cofactor in the Na+-pumping NADH: quinone oxidoreductase (Na+-NQR) from Vibrio cholerae. The Journal of biological chemistry. 2008 Nov 28;283(48):33162-7. PubMed PMID: 18832377. Pubmed Central PMCID: 2586278.
174. Wright JS, 3rd, Jin R, Novick RP. Transient interference with staphylococcal quorum sensing blocks abscess formation. Proc Natl Acad Sci U S A. 2005 Feb 01;102(5):1691-6. PubMed PMID: 15665088. Pubmed Central PMCID: 547845.
175. Ben Zakour NL, Sturdevant DE, Even S, Guinane CM, Barbey C, Alves PD, et al. Genome-wide analysis of ruminant Staphylococcus aureus reveals diversification of the core genome. Journal of bacteriology. 2008 Oct;190(19):6302-17. PubMed PMID: 18567666. Pubmed Central PMCID: 2566005.
176. Shannon O, Flock JI. Extracellular fibrinogen binding protein, Efb, from Staphylococcus aureus binds to platelets and inhibits platelet aggregation. Thrombosis and haemostasis. 2004 Apr;91(4):779-89. PubMed PMID: 15045140.
177. Ko YP, Liang X, Smith CW, Degen JL, Hook M. Binding of Efb from Staphylococcus aureus to fibrinogen blocks neutrophil adherence. The Journal of biological chemistry. 2011 Mar 18;286(11):9865-74. PubMed PMID: 21247890. Pubmed Central PMCID: 3059020.

178. Amdahl H, Jongerius I, Meri T, Pasanen T, Hyvarinen S, Haapasalo K, et al. Staphylococcal Ecb protein and host complement regulator factor H enhance functions of each other in bacterial immune evasion. J Immunol. 2013 Aug 15;191(4):1775-84. PubMed PMID: 23863906.
179. Jongerius I, von Kockritz-Blickwede M, Horsburgh MJ, Ruyken M, Nizet V, Rooijakkers SH. Staphylococcus aureus virulence is enhanced by secreted factors that block innate immune defenses. Journal of innate immunity. 2012;4(3):301-11. PubMed PMID: 22327617. Pubmed Central PMCID: 3357151.
180. Heilmann C, Niemann S, Sinha B, Herrmann M, Kehrel BE, Peters G. Staphylococcus aureus fibronectin-binding protein (FnBP)-mediated adherence to platelets, and aggregation of platelets induced by FnBPA but not by FnBPB. J Infect Dis. 2004 Jul 15;190(2):321-9. PubMed PMID: 15216468.
181. Pietrocola G, Nobile G, Gianotti V, Zapotoczna M, Foster TJ, Geoghegan JA, et al. Molecular Interactions of Human Plasminogen with Fibronectin-binding Protein B (FnBPB), a Fibrinogen/Fibronectin-binding Protein from Staphylococcus aureus. The Journal of biological chemistry. 2016 Aug 26;291(35):18148-62. PubMed PMID: 27387503. Pubmed Central PMCID: 5000064.
182. Heying R, van de Gevel J, Que YA, Moreillon P, Beekhuizen H. Fibronectin-binding proteins and clumping factor A in Staphylococcus aureus experimental endocarditis: FnBPA is sufficient to activate human endothelial cells. Thrombosis and haemostasis. 2007 Apr;97(4):617-26. PubMed PMID: 17393025.
183. Herman-Bausier P, El-Kirat-Chatel S, Foster TJ, Geoghegan JA, Dufrene YF. Staphylococcus aureus Fibronectin-Binding Protein A Mediates Cell-Cell Adhesion through Low-Affinity Homophilic Bonds. Mbio. 2015 May 26;6(3):e00413-15. PubMed PMID: 26015495. Pubmed Central PMCID: 4447249.
184. McCourt J, O'Halloran DP, McCarthy H, O'Gara JP, Geoghegan JA. Fibronectin-binding proteins are required for biofilm formation by community-associated methicillin-resistant Staphylococcus aureus strain LAC. FEMS microbiology letters. 2014 Apr;353(2):157-64. PubMed PMID: 24628034.
185. Shaw L, Golonka E, Potempa J, Foster SJ. The role and regulation of the extracellular proteases of Staphylococcus aureus. Microbiology. 2004 Jan;150(Pt 1):217-28. PubMed PMID: 14702415.
186. Kolar SL, Ibarra JA, Rivera FE, Mootz JM, Davenport JE, Stevens SM, et al. Extracellular proteases are key mediators of Staphylococcus aureus virulence via the global modulation of virulence-determinant stability. MicrobiologyOpen. 2013 Feb;2(1):18-34. PubMed PMID: 23233325. Pubmed Central PMCID: 3584211.
187. Laarman AJ, Mijnheer G, Mootz JM, van Rooijen WJ, Ruyken M, Malone CL, et al. Staphylococcus aureus Staphopain A inhibits CXCR2-dependent neutrophil activation and chemotaxis. The EMBO journal. 2012 Aug 29;31(17):3607-19. PubMed PMID: 22850671. Pubmed Central PMCID: 3433787.
188. Bokarewa MI, Jin T, Tarkowski A. Staphylococcus aureus: Staphylokinase. The international journal of biochemistry & cell biology. 2006;38(4):504-9. PubMed PMID: 16111912.
189. Nanra JS, Buitrago SM, Crawford S, Ng J, Fink PS, Hawkins J, et al. Capsular polysaccharides are an important immune evasion mechanism for Staphylococcus aureus. Hum Vaccin Immunother. 2013 Mar;9(3):480-7. PubMed PMID: 23249887. Pubmed Central PMCID: 3891703.

190. Kanafani ZA, Arduino JM, Muhlbaier LH, Kaye KS, Allen KB, Carmeli Y, et al. Incidence of and preoperative risk factors for Staphylococcus aureus bacteremia and chest wound infection after cardiac surgery. Infection control and hospital epidemiology. 2009 Mar;30(3):242-8. PubMed PMID: 19199534.
191. Fowler VG, Jr., O'Brien SM, Muhlbaier LH, Corey GR, Ferguson TB, Peterson ED. Clinical predictors of major infections after cardiac surgery. Circulation. 2005 Aug 30;112(9 Suppl):I358-65. PubMed PMID: 16159846.
192. Kim HK, DeDent A, Cheng AG, McAdow M, Bagnoli F, Missiakas DM, et al. IsdA and IsdB antibodies protect mice against Staphylococcus aureus abscess formation and lethal challenge. Vaccine. 2010 Aug 31;28(38):6382-92. PubMed PMID: 20226248. Pubmed Central PMCID: 3095377.
193. Torres VJ, Pishchany G, Humayun M, Schneewind O, Skaar EP. Staphylococcus aureus IsdB is a hemoglobin receptor required for heme iron utilization. Journal of bacteriology. 2006 Dec;188(24):8421-9. PubMed PMID: 17041042. Pubmed Central PMCID: 1698231.
194. Stranger-Jones YK, Bae T, Schneewind O. Vaccine assembly from surface proteins of Staphylococcus aureus. Proc Natl Acad Sci U S A. 2006 Nov 07;103(45):16942-7. PubMed PMID: 17075065. Pubmed Central PMCID: 1636558.
195. Kuklin NA, Clark DJ, Secore S, Cook J, Cope LD, McNeely T, et al. A novel Staphylococcus aureus vaccine: iron surface determinant B induces rapid antibody responses in rhesus macaques and specific increased survival in a murine S. aureus sepsis model. Infect Immun. 2006 Apr;74(4):2215-23. PubMed PMID: 16552052. Pubmed Central PMCID: 1418914.
196. Subramanian A, Tamayo P, Mootha VK, Mukherjee S, Ebert BL, Gillette MA, et al. Gene set enrichment analysis: a knowledge-based approach for interpreting genome-wide expression profiles. Proc Natl Acad Sci U S A. 2005 Oct 25;102(43):15545-50. PubMed PMID: 16199517. Pubmed Central PMCID: 1239896.
197. Beasley FC, Vines ED, Grigg JC, Zheng Q, Liu S, Lajoie GA, et al. Characterization of staphyloferrin A biosynthetic and transport mutants in Staphylococcus aureus. Mol Microbiol. 2009 May;72(4):947-63. PubMed PMID: 19400778. Epub 2009/04/30. eng.
198. Grigg JC, Ukpabi G, Gaudin CF, Murphy ME. Structural biology of heme binding in the Staphylococcus aureus Isd system. Journal of inorganic biochemistry. 2010 Mar;104(3):341-8. PubMed PMID: 19853304.
199. Xiong A, Singh VK, Cabrera G, Jayaswal RK. Molecular characterization of the ferric-uptake regulator, fur, from Staphylococcus aureus. Microbiology. 2000 Mar;146 (Pt 3):659-68. PubMed PMID: 10746769.
200. Johnson M, Sengupta M, Purves J, Tarrant E, Williams PH, Cockayne A, et al. Fur is required for the activation of virulence gene expression through the induction of the sae regulatory system in Staphylococcus aureus. Int J Med Microbiol. 2011 Jan;301(1):44-52. PubMed PMID: 20705504. Pubmed Central PMCID: 2994983.
201. Sadykov MR, Thomas VC, Marshall DD, Wenstrom CJ, Moormeier DE, Widhelm TJ, et al. Inactivation of the Pta-AckA pathway causes cell death in Staphylococcus aureus. Journal of bacteriology. 2013 Jul;195(13):3035-44. PubMed PMID: 23625849. Pubmed Central PMCID: 3697545.

202. Fey PD, Endres JL, Yajjala VK, Widhelm TJ, Boissy RJ, Bose JL, et al. A genetic resource for rapid and comprehensive phenotype screening of nonessential *Staphylococcus aureus* genes. mBio. 2013;4(1):e00537-12. PubMed PMID: 23404398. Pubmed Central PMCID: 3573662.
203. Baba T, Bae T, Schneewind O, Takeuchi F, Hiramatsu K. Genome sequence of Staphylococcus aureus strain Newman and comparative analysis of staphylococcal genomes: polymorphism and evolution of two major pathogenicity islands. Journal of bacteriology. 2008 Jan;190(1):300-10. PubMed PMID: 17951380. Pubmed Central PMCID: 2223734.

Supplementary

Protocol: Extraction of S. *aureus* Ribonucleic Acid (RNA) from infected murine Kidneys and Spleens

Risks from Chemicals used:

- Chaotropic salts (Guanidinium isothiocyanate)
- β – Mercaptoethanol

- β – Mercaptoethanol contaminated waste (liquids or plastics) need to be stored and discarded separately in a labelled container ("β – Mercaptoethanol contaminated liquids" or "β – Mercaptoethanol contaminated plastics, <1 % β – Mercaptoethanol")

Objective

Extracting *S. aureus* RNA from murine tissues (kidney or spleen) after intravenous challenge of mice.

Reagents and Materials

Reagent/Material	Company	Catalogue #
40 µm cell strainer, medical grade	BD	352340
β – Mercaptoethanol , molecular biological grade	Calbiochem	444203
Ethanol, pure, molecular biological grade	Sigma	E7023
FastPrep120 (or later version) (**for kidneys only)**	MP	-
Plastic pipettes, individually wrapped, (2 ml, 5 ml, 10 ml)	Appleton Woods	CC114 CC116 CC117
Horse Blood Agar (HBA) Plates	Oxoid	PB0114
Infected murine kidneys, abscesses and/or spleens	-	-
Lysing Matrix B-tubes (**for kidneys only)**	MP	11462410
Lysostaphin, >500 units/mg	Sigma-	L7386 1MG
Phosphate Buffer Saline (PBS), liquid, sterile	Sigma	D-8537
PPE, especially gloves (change frequently to avoid RNase contamination)	-	-
Proteinase K, 2ml, >600mAU/ml	Qiagen	19131
RNAprotect Bacteria Reagent	Qiagen	76506
RNase-free DNase Set	Qiagen	79254
RNase free water, HyClone, Molecular Biology	GE	SH30538.02
RNasin Recombinant Ribonuclease Inhibitor	Promega	N2111
RNase*Zap* RNase Inhibitor surface decontamination	Invitrogen	AM9780
RNeasy Midi Kit	Qiagen	75144
Thermomixer	Eppendorf	-
TRIS - EDTA buffer	Qiagen	19046
Triton-X100 1% solution	Thermo Fisher	HFH10

Method

Clean workspace with Microsol and RNAZap, decontaminate pipettes, and make sure to touch everything with gloves hereafter. Use RNAse free barrier filter tips for all subsequent manipulations. **Do not** touch the pipette ejector on the side of the tube (the tubes used should – if possible – be shorter than the pipette tip to avoid this). If tubes are too big, use stripettes or disposable plastic pipettes.

Day -2

- Prepare *S. aureus* stockplate and overnight culture according to J193

Day -1 and Day 0

- Carry out *S. aureus* challenge of mice
- Keep the inoculum used in the challenge, plate and aliquot for inoculum enumeration (-4 to -6 dilution) on Horse Blood Agar Plates
- Spin down the inoculum culture rest at 3000 rpm for 10 min
- Take up the pellet in 2 ml RNA Bacteria Protect (Qiagen), incubate 5 min at room temperature
- Split into aliquots (end concentration should be ~1 x 10^8 CFU/pellet) and spin down (5000 xg, 10 min)
- Remove supernatant and store at -80°C until tissue extraction (used as positive control for *S. aureus* RNA)

Day 1

- Count inoculum plate growth and calculate exact CFU/mouse and CFU/inoculum aliquot stored at -80°C

Day 3

- Harvest kidneys and/or spleens at desired time point, emerge organs to be extracted in 2 ml RNAlater solution **IMMEDIATELY** and store overnight at 4°C
- To enumerate CFU before infection use right kidney for plating and left for extraction, for spleens, cut off a small piece (before emerging the larger piece into RNAlater) and plate (-1 to -3 of the spleen and -2 to -4 of the kidney disrupted in PBS using a spiral plater)

Day 4

- Discard RNAlater solution in which tissues were emerged and "dry" kidneys and spleens on a (clean) towel, before storing them at -80°C until tissue extraction

Day of extraction

- Prepare a clean hood, a spillage tray, pipettes and pipette boy (cleaned with RNAzap according to instructions) and the following buffer in advance:
  - Add β – Mercaptoethanol to RLT buffer [10 µl/ml] (Qiagen)
  - Have 50 µg/ml Lysostaphin in TE on ice, add 500 U/ml RNasin immediately before use
  - Prepare DNase by adding RDD buffer (20 µl + 140 µl)
  - Prepare disruption buffer : 0.15 % Triton – X 100 using prediluted 10 % stock in PBS
  - Precool Centrifuges to **4°C,** prepare tubes (50 ml, 15 ml, 2 ml) and label
  - take one inoculum out and let it thaw on ice
- Take out kidneys and spleens, store on ice and process as soon as possible Allocate 2 ml disruption buffer in M-tubes for each kidney or spleen, add kidneys/spleens and disrupt using "RNA_2" protocol for frozen tissue (work quickly!)
- Store on ice afterwards and pass through a 40 µm cell strainer into a 50 ml tube standing in ice.
- Wash cell strainer with 1 ml PBS twice, taking up remainings from the M-tubes, too, keep tubes on ice!
- Spin all samples, including the inoculum at 3200 xg, 10 min, **4°C** (allow centrifuge to warm back up to RT after this run)
- Add 500 U/ml RNasin to Lysostaphin (18.75 µl per 1.5 ml Lysostaphin aliquot)
- Take up pellets in 1 ml TE while standing on ice, transfer to a 2 ml microcentrifuge tube
- Spin all samples at 3200 xg, 10 min, 4°C

- Take up pellets in 400 µl Lysostaphin/RNasin in TE, incubate for 20 min at 37°C with 300 rpm shaking (Thermomixer)
- Add 40 µl Proteinase K to the mixture; continue incubation for another 10 min.
- **For kidneys ONLY:** Transfer samples to a Lysing Matrix B tube and process 2 x 45s (level 6.5) in the FastPrep120 (store samples on ice for 5 min between the two procedures!!)
- Spin all samples (including spleens) at 3200 xg, 10 min, 4°C
- Transfer supernatant to a 15 ml tube containing 2 ml RLT buffer
- Wash kidney B-tube beads with 1 ml TE buffer per tube
- Spin the B-tubes again at 3200 xg, 10 min, 4°C
- Add the B-tubes
- supernatant to the rest of the 15 ml tube, vortex
- Proceed following the RNeasy Midi Kit instructions:
    - Add 1.4 ml absolute Ethanol, mix by shaking
    - Apply to a RNeasy column, spin 5 min at 3200 xg
    - Wash with 2 ml RW1, spin 5 min, 3200 xg
    - Add 160 µl of DNase mix, incubate 15 min RT
    - Add 2 ml RW1, incubate another 5min, RT before spinning it at 3200 xg, 5 min
    - Add 2.5 ml RPE to the column, spin at 3200 xg, 2 min
    - Add another 2.5 ml RPE, spin at 3200 xg, 10 min
    - Put column into a fresh elution tube (be careful not to touch the used tube with the column tip!!)
    - Add 250 µl of RNase free water, incubate 5 min RT, elute 3 min at 3200 xg
    - Repeat last elution step, transfer the eluted RNA to a 1.5 ml microcentrifuge tube (MUST be RNase free!)
    - Store at -80°C immediately, aliquot if downstream process allows lower amounts

Supplementary Figures

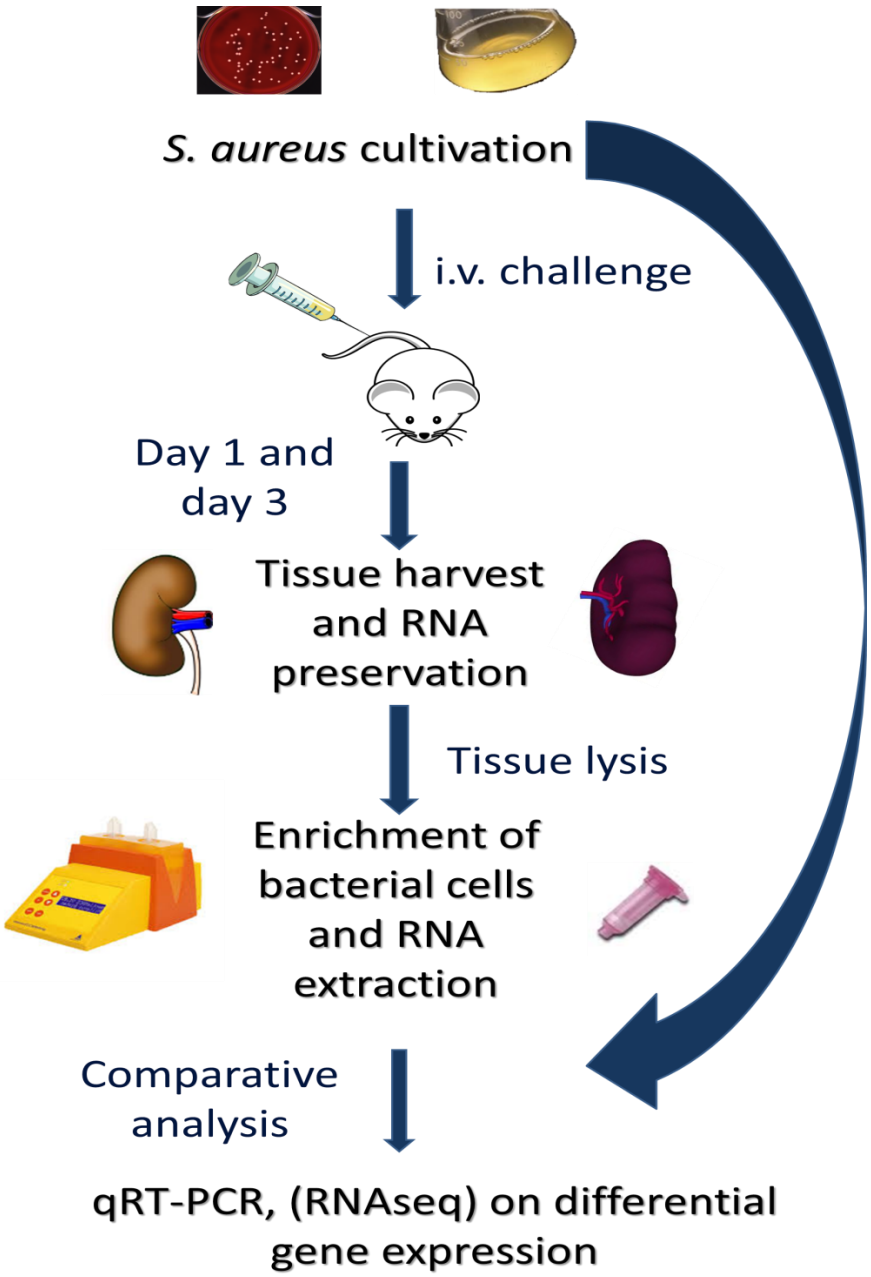

Figure S1: Overview of method. *S. aureus* are grown in broth and then used for IV. challenge (Balb/c mice). On day 1 (early stage of infection) and day 3 (mid stage/beginning of tissue abscess establishment) spleens, kidneys and visible abscesses are harvested, followed by RNA preservation. Tissue lysis and separation of bacterial cells precedes RNA extraction and purification. Qualitative control of RNA is performed using Real Time PCR. Differential gene expression is analysed using Next Generation Sequencing.

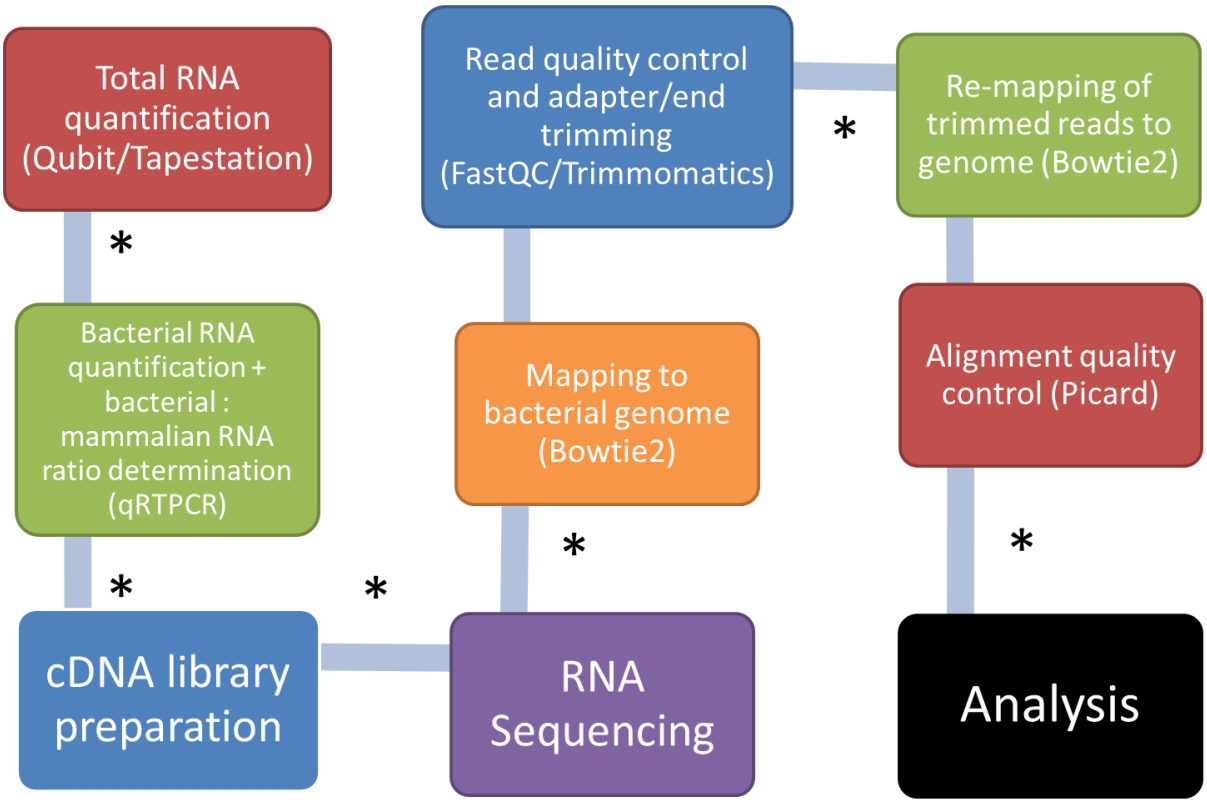

Figure S2: Flowchart of quality assessment. Method/packages applied are given in brackets. cDNA library preparation and RNA Sequencing were performed by the High Throughput Genomic Core, Oxford. Checkpoints, were samples had to pass a certain quality standard are marked with an asterisk "*".

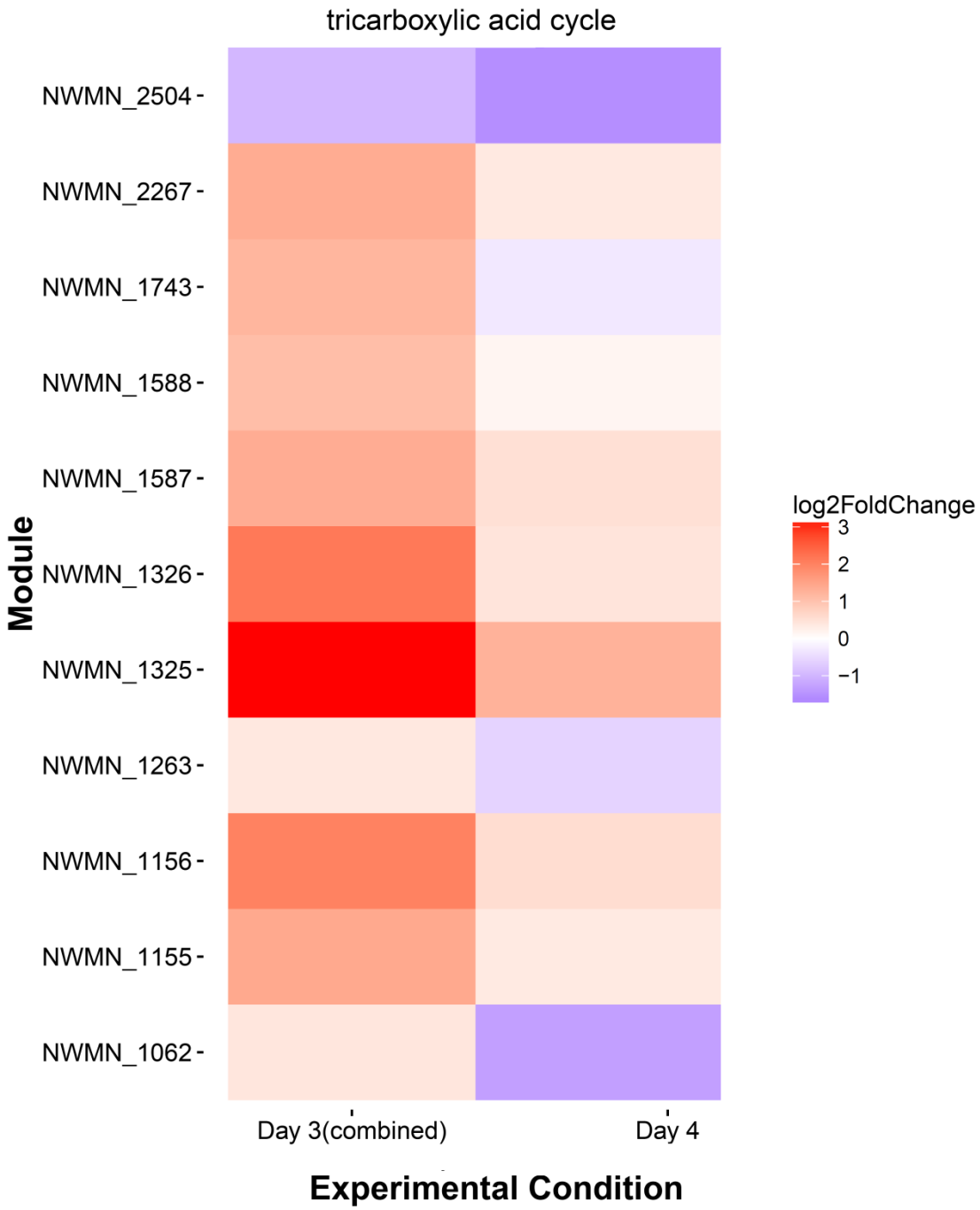

Figure S3: Per gene effect in the biological process cluster "tricarboxylic acid cycle" in *S. aureus* Newman *in vivo* when compared with *in vitro* grown bacteria. Red shades indicate upregulation, blue shades downregulation. Column 1 (Day 3(combined)) shows results for samples from two experimental replicates obtained three days post infection combined. Column 2 shows results of *in vivo* transcriptomes obtained four days post infection as comparison.

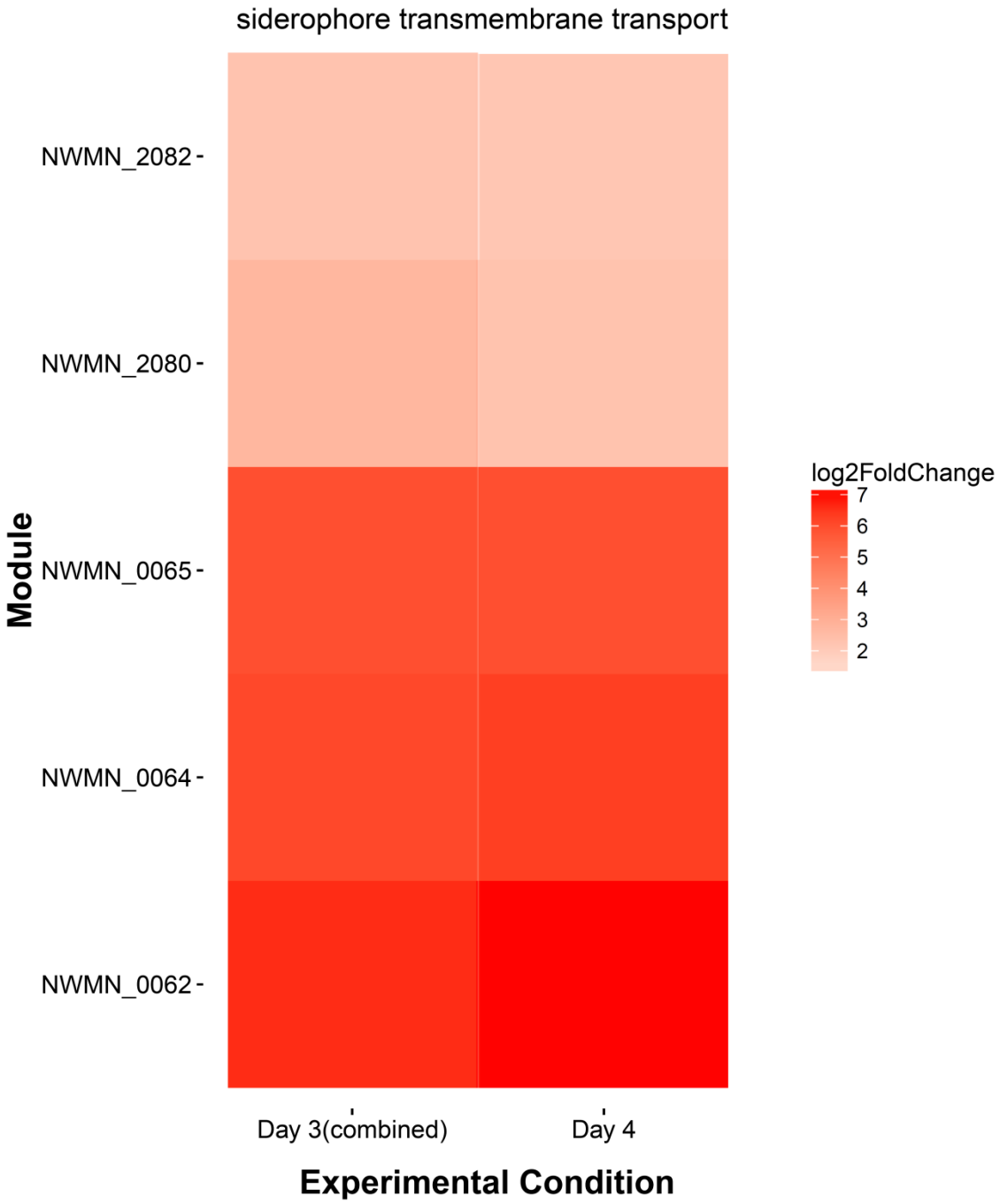

Figure S4: Per gene effect in the biological process cluster "siderophore transmembrane transport/biosynthetic process" in *S. aureus* Newman *in vivo* when compared with *in vitro* grown bacteria. Red shades indicate upregulation, blue shades downregulation. Column 1 (Day 3(combined)) shows results for samples from two experimental replicates obtained three days post infection combined. Column 2 shows results of *in vivo* transcriptomes obtained four days post infection as comparison.

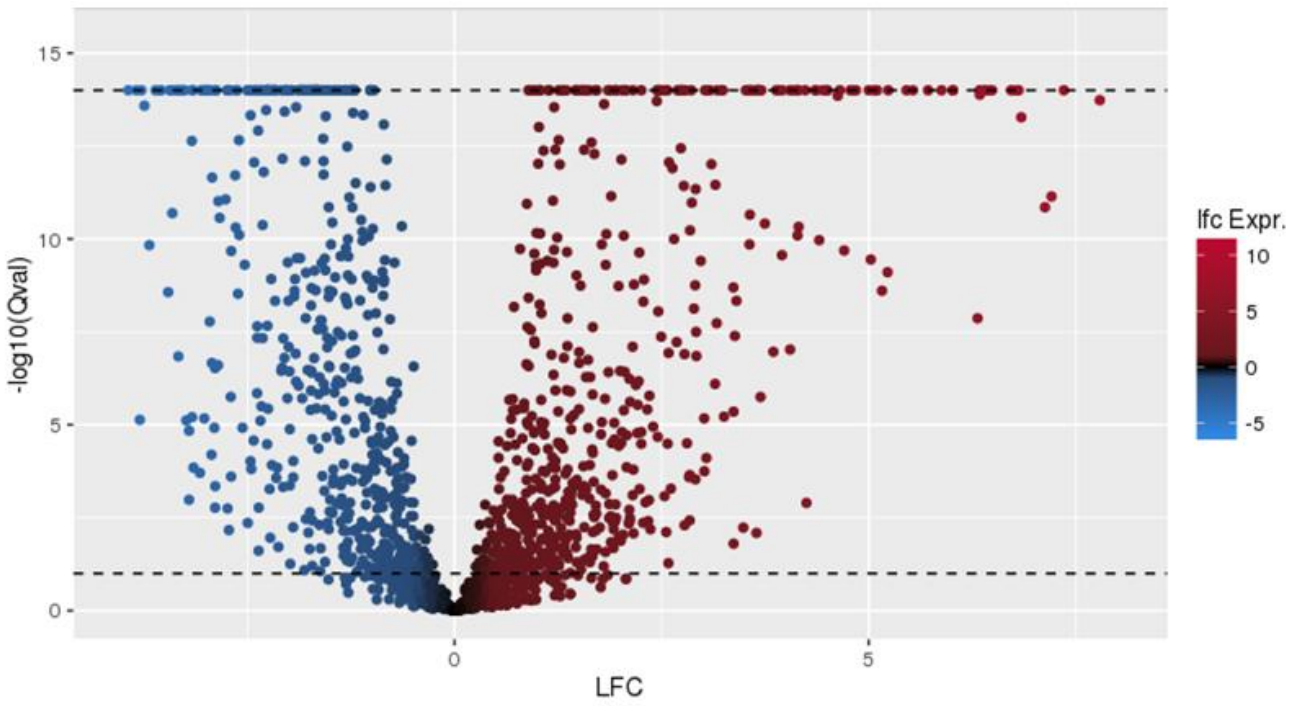

Figure S5: Up- and downregulated genes in Patient P nasal isolate (Rsp$^+$) *in vivo* when compared with *in vitro* grown bacteria

Volcano plot of up- (red, on the right) and down- (blue, on the left) regulated genes in *S. aureus* Patient P nasal isolate (Rsp$^+$) during infection in mice when compared with *in vitro* grown bacteria. Log_2 fold change (LFC, x-axis) is plotted against the *q*-value ($-log_{10}$(Qval), y-axis). Genes with q-value<10^{-14} are plotted at q=10^{-14} to improve visibility of significantly affected genes.

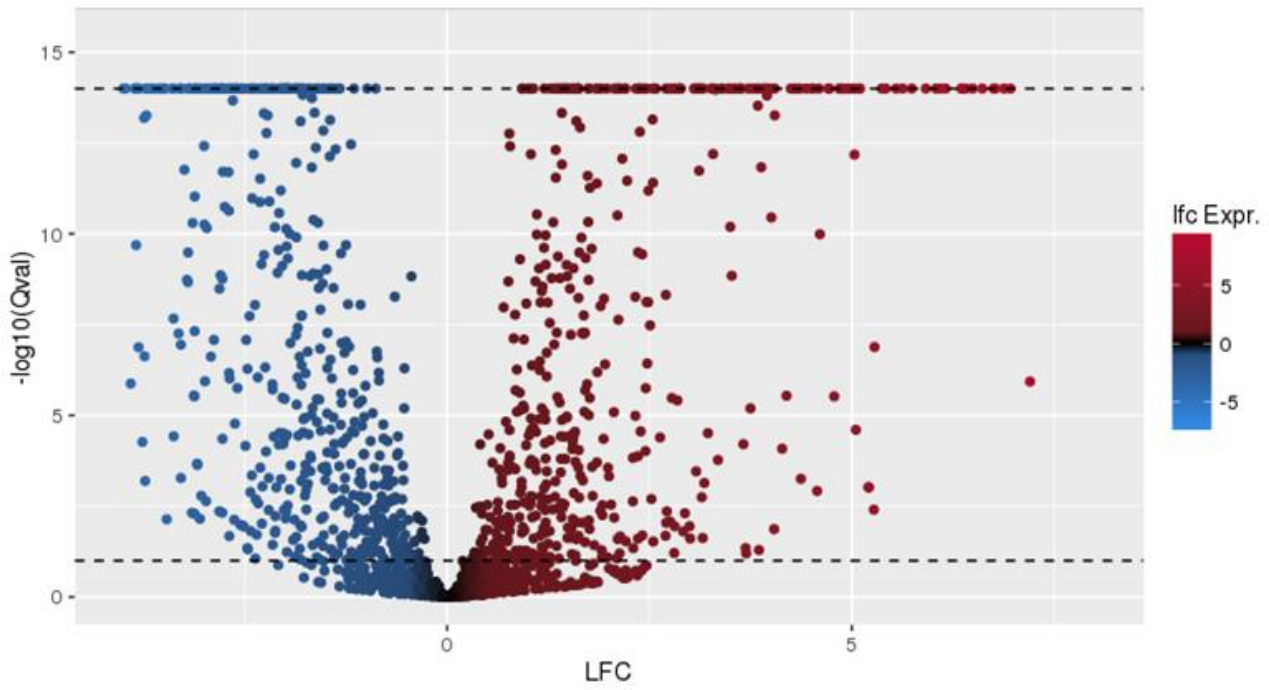

Figure S6: Up- and downregulated genes in Patient S nasal isolate (Rsp$^+$) *in vivo* when compared with *in vitro* grown bacteria

Volcano plot of up- (red, on the right) and down- (blue, on the left) regulated genes in *S. aureus* Patient S nasal isolate (Rsp$^+$) during infection in mice when compared with *in vitro* grown bacteria. Log_2 fold change (LFC, x-axis) is plotted against the *q*-value ($-log_{10}$(Qval), y-axis). Genes with q-value<10^{-14} are plotted at q=10^{-14} to improve visibility of significantly affected genes.

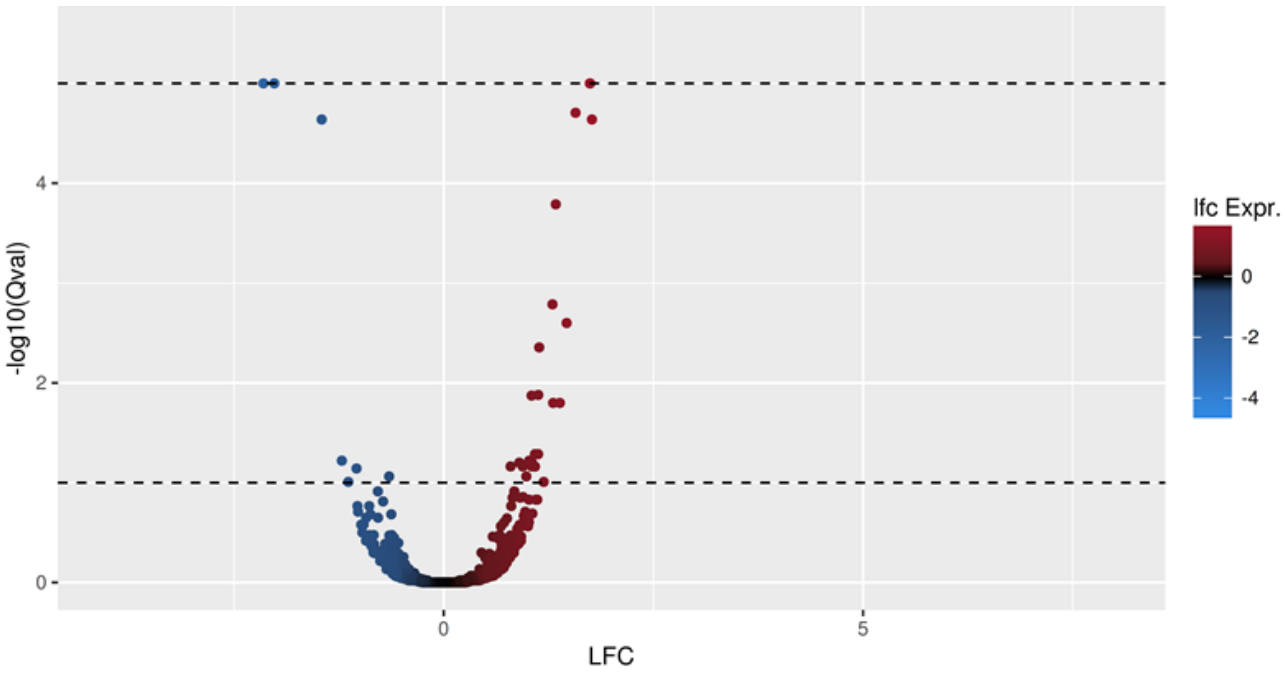

Figure S7: Up- and downregulated genes in USA300 NE1304 (Rsp$^-$) *in vivo* when compared with USA300 JE2 (Rsp$^+$) *in vivo*

Volcano plot of up- (red, on the right) and down- (blue, on the left) regulated genes in *S. aureus* USA300 NE1304 (Rsp$^-$) during infection in mice when compared with USA300 JE2 (Rsp$^+$) expression *in vivo*. Log_2 fold change (LFC, x-axis) is plotted against the *q*-value (-log_{10}(Qval), y-axis). Genes with q-value<10^{-14} are plotted at q=10^{-14} to improve visibility of significantly affected genes.

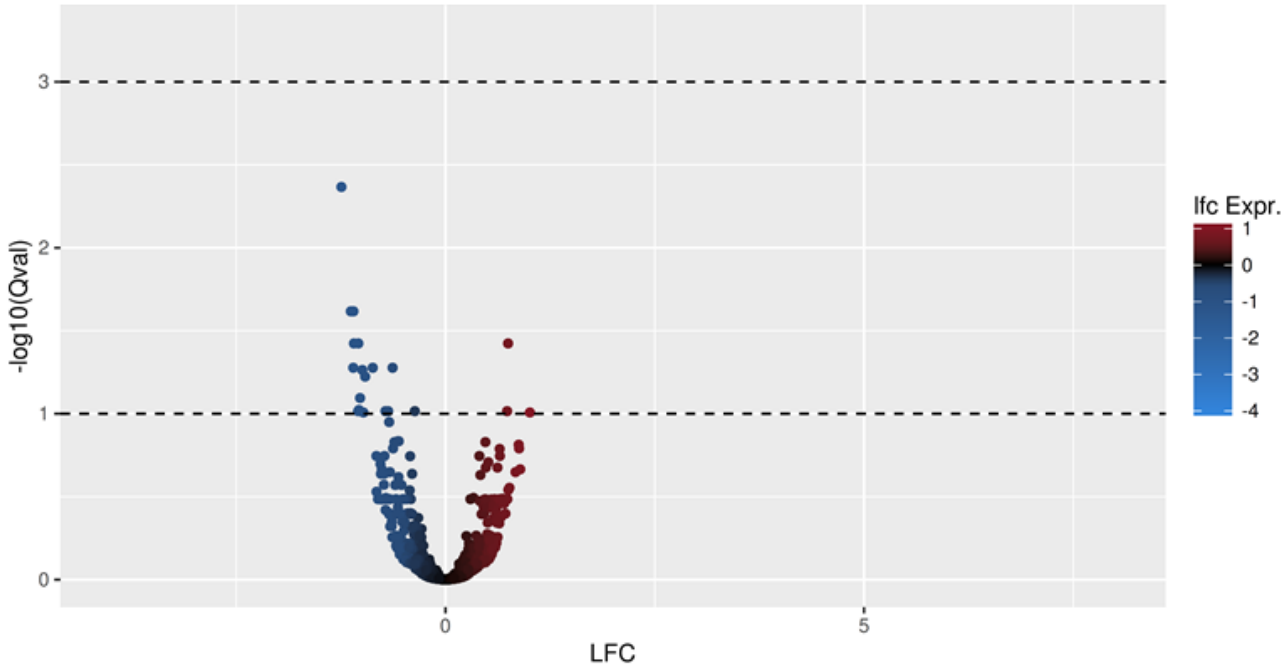

Figure S8: Up- and downregulated genes in Patient P blood isolate (Rsp$^-$) *in vivo* when compared with Patient P nasal isolate (Rsp$^+$) *in vivo*

Volcano plot of up- (red, on the right) and down- (blue, on the left) regulated genes in *S. aureus* Patient P blood isolate (Rsp$^-$) during infection in mice when compared with Patient P nasal isolate (Rsp$^+$) expression *in vivo*. Log_2 fold change (LFC, x-axis) is plotted against the *q*-value ($-log_{10}$(Qval), y-axis). Genes with q-value<10^{-14} are plotted at q=10^{-14} to improve visibility of significantly affected genes.

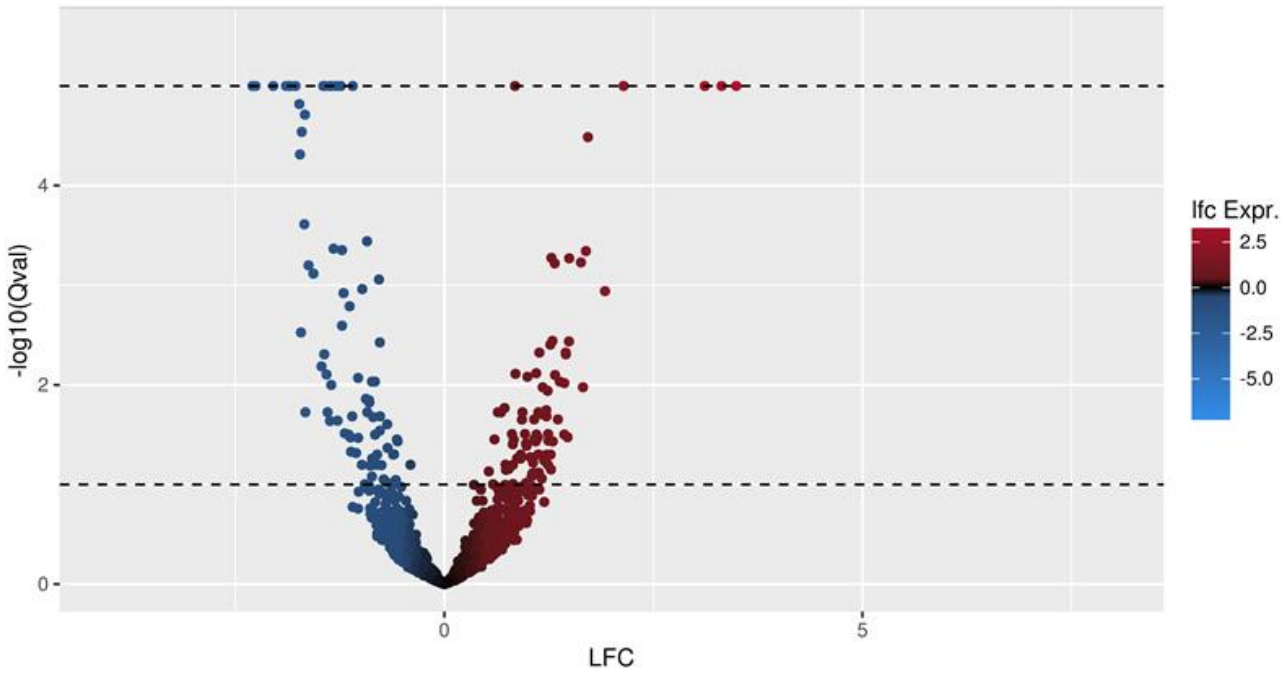

Figure S9: Up- and downregulated genes in Patient S blood isolate (Rsp$^-$) *in vivo* when compared with Patient S nasal isolate (Rsp$^+$) *in vivo*

Volcano plot of up- (red, on the right) and down- (blue, on the left) regulated genes in *S. aureus* Patient S blood isolate (Rsp$^-$) during infection in mice when compared with Patient S nasal isolate (Rsp$^+$) expression *in vivo*. Log_2 fold change (LFC, x-axis) is plotted against the *q*-value ($-log_{10}$(Qval), y-axis). Genes with q-value<10^{-14} are plotted at q=10^{-14} to improve visibility of significantly affected genes.

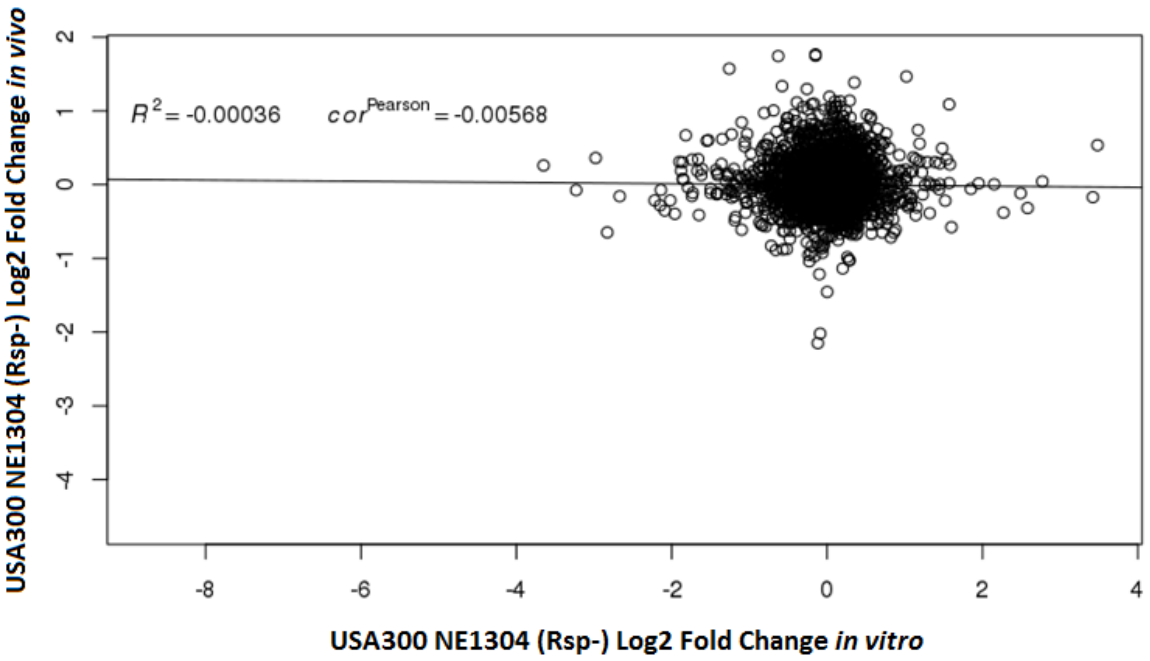

Figure S10: Correlation between the transcriptomes of USA300 NE1304 (Rsp$^-$) *in vivo* and *in vitro* when compared to USA300 JE2 (Rsp$^+$)

Correlation of $\log_2$ fold change expression between USA300 NE1304 (Rsp$^-$, x-axis) *in vivo* during infection in murine kidney and *in vitro* grown bacteria when compared to *rsp* wild type USA300 JE2 (Rsp$^+$). The Pearson correlation coefficient (cor^{Pearson}) and the R square value (R^2) are displayed.

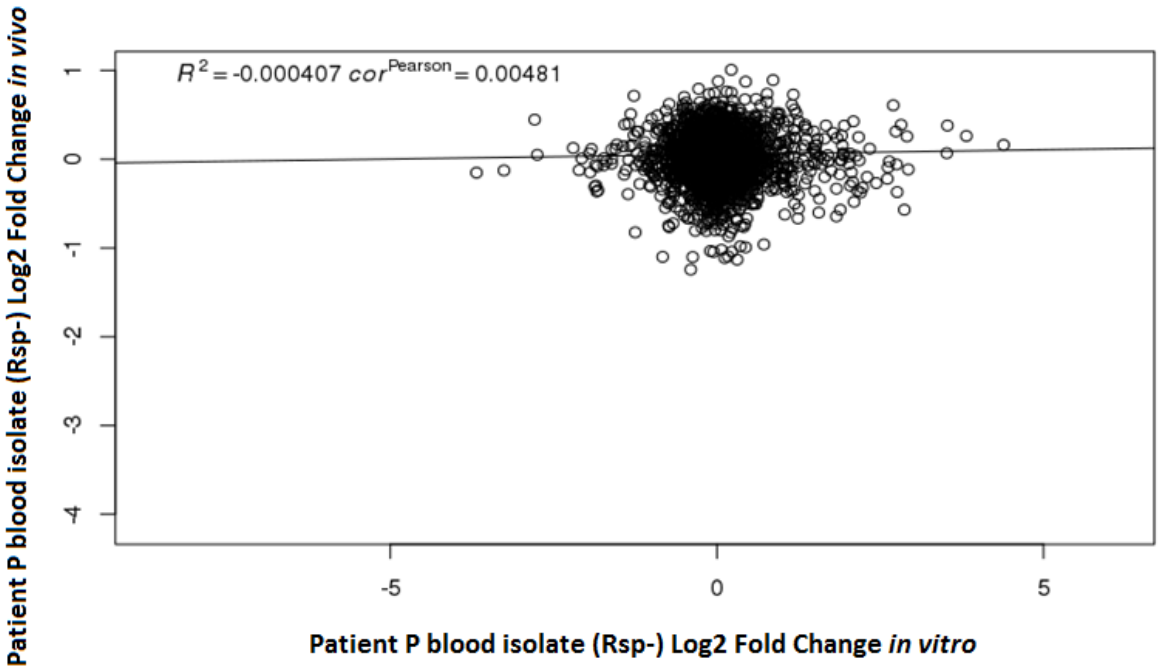

Figure S11: Correlation between the transcriptomes of Patient P blood isolate (Rsp^-) *in vivo* and *in vitro* when compared to Patient P nasal isolate (Rsp^+)

Correlation of log_2 fold change expression between Patient P blood isolate (Rsp^-, x-axis) *in vivo* during infection in murine kidney and *in vitro* grown bacteria when compared to *rsp* wild type Patient P nasal isolate (Rsp^+). The Pearson correlation coefficient ($cor^{Pearson}$) and the R square value (R^2) are displayed.

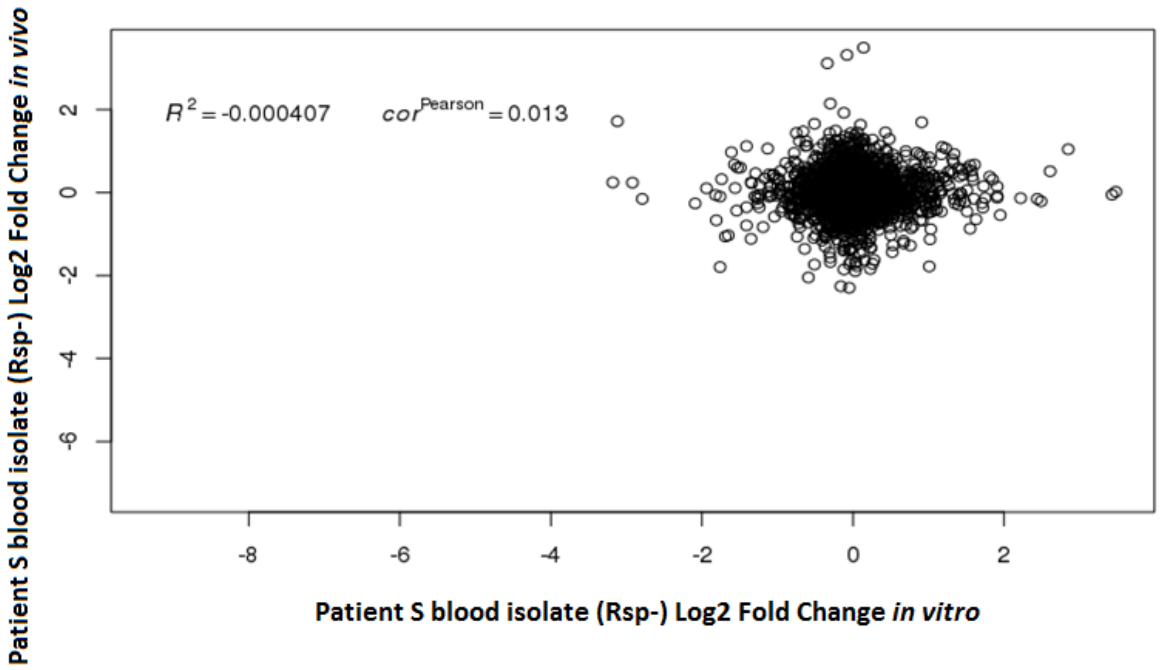

Figure S12: Correlation between the transcriptomes of Patient S blood isolate (Rsp^-) *in vivo* and *in vitro* when compared to Patient S nasal isolate (Rsp^+)

Correlation of log_2 fold change expression between Patient S blood isolate (Rsp^-, x-axis) *in vivo* during infection in murine kidney and *in vitro* grown bacteria when compared to *rsp* wild type Patient S nasal isolate (Rsp^+). The Pearson correlation coefficient ($cor^{Pearson}$) and the R square value (R^2) are displayed.

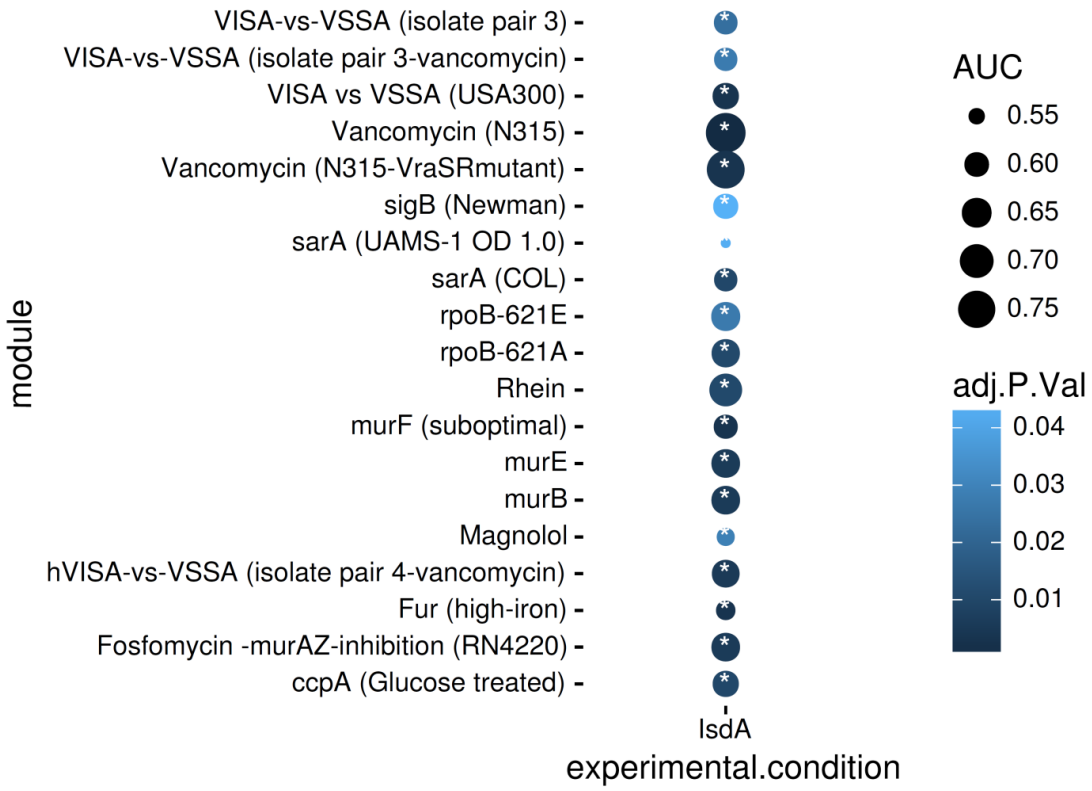

Figure S13: **Gene set enrichment analysis of the *S. aureus in vivo* transcriptome using microarray effect based gene modules (downregulation)**

List of *S. aureus* Newman gene clusters downregulated *in vivo* during infection in an IsdA + alum immunised mice when compared to the transcriptome of bacteria infecting alum only immunised mice. Genes were grouped in clusters according to the conditions under which they are found to be downregulated. [Methods are described in 4.3.8 and 4.3.9]. The size of the circle represents the area under the curve (AUC) of the Receiver Operator Curve (ROC), the shade of blue indicates the adjusted *p*-value and significant modules are indicated with an asterisk.

Supplementary Tables

Table S1: Bacterial Strains used in this thesis

Strain	Description	Source
Proteus mirabilis		
Clinical isolate	Urease positive Clinical isolate	JR hospital, Oxford, United Kingdom
Escherichia coli		
Clinical isolate	Urease negative Clinical isolate	JR hospital, Oxford, United Kingdom
Staphylococcus aureus		
JE2	USA300, Rsp^+. Derivative of LAC, which was cured of three plasmids.	(202)
NE1304	NE1304, Rsp^-, JE2 transposon insertion mutant within *rsp* gene, locus ID – SAUSA300_2326	(202)
Newman	Isolated from human infection	(203)
Clinical isolates of *Staphylococcus aureus*		
Patient P nasal isolate	Rsp^+ (Reference genome C1360)	(58)
Patient P bloodstream isolate	Rsp^-, (Reference genome C11585)	(58)
Patient S nasal isolate	Rsp^+ (Reference genome C24365)	(59)
Patient P bloodstream isolate	Rsp^- (Reference genome C24366)	This publication

Table S2: Average sequence similarity of toxins and adhesins encoded by the Patient S strain as compared to published *S. aureus* genomes

Gene	Sequence similarity [%]
ebpS	96.64613
icaA	99.27361
icaB	99.19817
icaC	97.151
icaD	98.69281
icaR	99.10873
cap8A	98.94419
cap8B	97.114
cap8C	98.82353
cap8D	97.64254
cap8E	99.41691
cap8F	98.28829
cap8G	99.2
capH	98.88889
cap8I	99.21147
cap8J	99.64158
cap8K	99.11219
cap8L	99.25373
cap8M	98.92473
cap8N	98.31081
cap8O	98.89153
cap8P	99.06463
geh	98.36224
sspB	97.20812
sspC	98.18182
adsA	96.2915
chp	100
scn	100
isdA	97.0892
isdB	95.15059
isdC	97.36842
isdD	98.79294
isdE	99.43117
isdF	99.07121
isdG	98.76543
srtB	99.18367
sak	99.79675
esaA	98.84488
esaB	100

essA	100
essB	99.25094
esxA	99.65986
hly	99.16667
hla	99.16667
hld	99.27536
hlgA	99.67742
hlgC	95.99156
eta	98.52321
seb	100

Table S3: Scoring system used for mice challenged intravenously with *S. aureus*

	Description	Score
Appearance	Normal	0
	General lack of grooming	1
	Coat staring, ocular and nasal discharges	2
	Piloerection, hunched up	3 – endpoint
Behavior	Normal	0
	Slight change; either less or more active than usual	1
	Agitated, alert, isolated or significantly less mobile	2
	Vocalisation, self-mutilation, unusual aggression or stillness	3 - endpoint
Mouse grimace score	Orbital tightening	0-1-2
	Nose and/or cheek bulge	0-1-2
	Ear position	0-1-2
Arthropathy	Normal	0
	Decreased movements	1
	Decreased movements and either swelling of joints or nodose tail	2
	Decrease movements and retracted limb	3 - endpoint
Total score		0-24

Table S4: Twenty up- and down-regulated genes in rsp mutants in vitro

In vitro transcriptomes of USA300 NE1304 (Rsp^-), Patient P and S blood isolates (Rsp^-), Patient P and S nasal isolates (Rsp^+). Twenty genes, which were up- and downregulated in all three genetic backgrounds, are listed below.

Upregulated in Rsp^- vs Rsp^+			**Downregulated in Rsp^- vs Rsp^+**		
Gene*	**Fold change**	**Product**	**Gene***	**Fold change**	**Product**
0693	6.00	putative lipoprotein	2493	0.56	conserved hypothetical protein
0692	5.82	conserved hypothetical protein	2311	0.56	conserved hypothetical protein
0409	5.10	conserved hypothetical protein	*entB*	0.55	isochorismatase
1056	4.53	conserved hypothetical protein	*sdrC*	0.55	SdrC protein
efb	4.23	fibrinogen binding protein	*grpE*	0.54	co-chaperone GrpE
saeR	4.06	DNA-binding response regulator SaeR	*hrcA*	0.53	heat-inducible transcription repressor
saeS	4.00	sensor histidine kinase SaeS	2310	0.53	conserved hypothetical protein
1918	3.36	truncated beta-hemolysin	*arsR*	0.51	arsenical resistance operon repressor
hlgA	3.34	gamma-hemolysin component A	2245	0.49	staphylococcal accessory regulator R
ureC	3.23	urease, alpha subunit	0372	0.48	putative lipoprotein
0108	3.20	Antigen, 67 kDa	*fadA*	0.48	(putative) acyl-CoA acetyltransferase FadA
efb	3.18	fibrinogen-binding protein	*fadD*	0.47	acyl-CoA dehydrogenase FadD
ureB	3.16	urease, beta subunit	0226	0.46	3-hydroxyacyl-CoA dehydrogenase
0274	3.12	conserved hypothetical protein	*arcA*	0.46	arginine deiminase
0278	3.10	conserved hypothetical protein	*fadE*	0.45	acyl-CoA synthetase FadE
0273	3.03	putative membrane protein	0229	0.44	putative acyl-CoA transferase FadX
hlgC	3.01	gamma-hemolysin component C	2453	0.44	ABC transporter, ATP-binding protein
2524	3.01	conserved hypothetical protein	2306	0.44	ABC transporter, ATP-binding protein
0272	2.87	conserved hypothetical protein	2307	0.30	ABC transporter, permease protein
0238	2.85	transcriptional antiterminator, BglG family	0179	0.26	putative D-isomer specific 2-hydroxyacid dehydrogenase
lukA(G)	2.83	leukocidin LukA (G)	*SSR42*	0.004	small stable RNA 42

Table S5: Genes upregulated *in vivo* during infection in four *S. aureus* strains

Transcriptomes *in vivo* during infection of four *S. aureus* strains (USA300 JE2 (Rsp^+), Patient P nasal strain (Rsp^+), Patient S nasal strain (Rsp^+) and Newman (Rsp^+) were compared with transcriptomes of broth grown bacteria from the same strain. Genes, which were found to be upregulated in all four strains during infection when compared *in vitro* are listed below.

Locus Tag	Log_2 Fold Change				Description
USA300	Newman	USA300	P	S	
SAUSA300_1757	8.82	1.32	1.47	1.33	serine protease SplB
SAUSA300_0151	6.84	1.11	1.84	2.63	bifunctional acetaldehyde-CoA/alcohol dehydrogenase
SAUSA300_0123	6.45	3.33	3.04	4.30	IucC family siderophore biosynthesis protein
SAUSA300_0848	6.27	2.42	1.12	1.39	hypothetical protein
SAUSA300_0228	5.29	2.16	1.54	4.00	acyl-CoA synthetase FadE
SAUSA300_1234	4.86	2.05	2.19	2.52	30S ribosomal protein S14
SAUSA300_2550	4.61	2.18	1.75	1.82	anaerobic ribonucleotide reductase, small subunit
SAUSA300_2367	4.44	2.32	1.41	2.41	gamma-hemolysin component B
SAUSA300_0404	4.42	2.15	1.68	3.81	superantigen-like protein
SAUSA300_0129	4.23	2.43	2.26	2.70	acetoin reductase
SAUSA300_1035	4.17	2.18	2.73	4.82	heme-degrading monooxygenase IsdG
SAUSA300_0311	4.14	1.72	1.34	3.21	PfkB family carbohydrate kinase
SAUSA300_0157	4.07	2.71	2.17	3.50	capsular polysaccharide biosynthesis protein Cap5F
SAUSA300_2642	4.02	2.06	2.11	4.42	hypothetical protein
SAUSA300_0195	4.02	1.53	1.82	2.16	transcriptional regulator
SAUSA300_1767	3.98	3.49	1.56	4.10	lantibiotic epidermin biosynthesis protein EpiA
SAUSA300_2519	3.83	3.23	3.25	4.16	putative cobalamin synthesis protein
SAUSA300_0594	3.75	2.22	2.65	3.20	alcohol dehydrogenase
SAUSA300_1207	3.71	2.85	2.40	4.20	hypothetical protein
SAUSA300_2553	3.68	2.83	2.53	6.61	precorrin-2 dehydrogenase
SAUSA300_1275	3.31	2.18	1.21	2.62	peptide ABC transporter permease
SAUSA300_2286	3.28	1.67	1.53	1.69	hypothetical protein
SAUSA300_0577	3.27	2.38	1.45	2.32	hypothetical protein
SAUSA300_1922	3.27	3.84	3.35	5.10	staphylokinase
SAUSA300_2307	3.20	1.89	1.16	3.45	ABC transporter permease
SAUSA300_1846	3.11	3.62	3.78	4.10	hypothetical protein
SAUSA300_2625	3.04	2.03	2.20	2.92	PadR family transcriptional regulator
SAUSA300_2567	2.94	1.83	2.21	3.84	carbamate kinase
SAUSA300_0620	2.94	1.64	1.81	2.84	ABC transporter ATP-binding protein
SAUSA300_2392	2.88	1.57	1.14	3.17	glycine betaine/carnitine/choline ABC transporter

SAUSA300_0303	2.87	2.45	1.79	3.72	hypothetical protein
SAUSA300_0178	2.84	3.52	3.35	3.97	hypothetical protein
SAUSA300_2239	2.82	1.56	2.13	1.62	urease subunit beta
SAUSA300_0343	2.74	2.21	1.80	3.29	acetyltransferase
SAUSA300_0393	2.67	2.25	2.20	3.29	hypothetical protein
SAUSA300_1204	2.65	3.45	4.01	5.54	hypothetical protein
SAUSA300_0662	2.64	1.59	1.70	1.68	acetyltransferase
SAUSA300_0083	2.64	1.93	1.62	4.21	hypothetical protein
SAUSA300_2609	2.63	1.74	1.66	1.59	imidazoleglycerol-phosphate dehydratase
SAUSA300_0634	2.63	2.01	1.60	1.57	ferrichrome transport permease fhuB
SAUSA300_2607	2.57	3.10	2.56	3.66	carboxamide isomerase
SAUSA300_2003	2.54	5.59	4.07	3.47	ribosomal-protein-alanine acetyltransferase
SAUSA300_2514	2.46	1.23	1.10	1.47	hypothetical protein
SAUSA300_1308	2.45	1.40	1.58	2.06	DNA-binding response regulator
SAUSA300_0416	2.43	2.01	1.95	4.65	tandem lipoprotein
SAUSA300_1738	2.37	2.48	3.01	4.78	putative lipoprotein
SAUSA300_0222	2.35	1.35	1.20	1.48	hypothetical protein
SAUSA300_2217	2.32	1.52	1.24	1.33	putative drug transporter
SAUSA300_0417	2.30	2.06	1.84	1.97	tandem lipoprotein
SAUSA300_1448	2.27	1.16	1.37	3.12	FUR family transcriptional regulator
SAUSA300_2391	2.26	1.49	1.63	2.88	glycine betaine/carnitine/choline ABC transporter
SAUSA300_1236	2.25	3.24	2.47	3.88	hypothetical protein
SAUSA300_2533	2.24	1.63	1.80	1.69	pantoate--beta-alanine ligase
SAUSA300_1257	2.24	4.51	3.41	3.11	peptide methionine sulfoxide reductase regulator MsrR
SAUSA300_2269	2.19	2.72	2.53	3.01	hypothetical protein
SAUSA300_0339	2.18	1.88	1.86	2.66	hypothetical protein
SAUSA300_2356	2.17	2.87	4.18	5.92	fmhA protein
SAUSA300_1504	2.17	2.62	2.46	2.93	putative competence protein ComGA
SAUSA300_0794	2.13	1.64	1.67	2.24	TOPRIM domain-containing protein
SAUSA300_0379	2.12	6.41	6.09	5.70	alkyl hydroperoxide reductase subunit F
SAUSA300_0512	2.12	1.61	2.64	2.65	PilT domain-containing protein
SAUSA300_2243	2.06	1.59	1.22	2.66	urease accessory protein UreG
SAUSA300_1762	2.03	1.34	1.41	1.79	lantibiotic epidermin immunity protein F
SAUSA300_1024	1.99	2.17	3.54	2.48	phosphopantetheine adenylyltransferase
SAUSA300_1733	1.98	3.13	2.88	2.91	hypothetical protein
SAUSA300_0796	1.97	1.78	1.46	2.77	ABC transporter ATP-binding protein
SAUSA300_2498	1.97	4.20	4.61	6.13	squalene synthase
SAUSA300_0106	1.97	1.15	1.42	1.98	putative drug transporter
SAUSA300_0105	1.95	2.40	3.00	3.75	M20/M25/M40 family peptidase
SAUSA300_1591	1.95	1.27	1.23	1.66	adenine phosphoribosyltransferase

SAUSA300_1255	1.95	3.33	2.02	2.60	oxacillin resistance-related FmtC protein
SAUSA300_1905	1.88	3.50	1.99	2.03	hypothetical protein
SAUSA300_0572	1.87	1.76	1.56	1.50	mevalonate kinase
SAUSA300_0946	1.84	1.76	1.58	1.44	oxoglutarate decarboxylase
SAUSA300_1806	1.83	2.37	1.73	3.33	putative iron-sulfur cluster-binding protein
SAUSA300_0538	1.80	2.09	2.40	3.18	NAD-dependent epimerase/dehydratase family protein
SAUSA300_2419	1.80	3.05	3.01	3.79	hypothetical protein
SAUSA300_1306	1.77	2.06	1.98	2.86	2-oxoglutarate dehydrogenase E1 component
SAUSA300_2447	1.76	2.28	1.97	1.45	hypothetical protein
SAUSA300_2223	1.76	2.02	1.28	3.40	molybdopterin-guanine dinucleotide biosynthesis protein B
SAUSA300_1139	1.75	3.16	3.46	2.45	succinyl-CoA synthetase subunit alpha
SAUSA300_1071	1.75	3.32	2.43	6.33	hypothetical protein
SAUSA300_0725	1.72	2.39	3.41	4.45	hypothetical protein
SAUSA300_0841	1.72	1.79	1.04	4.65	hypothetical protein
SAUSA300_0420	1.71	3.96	3.94	6.84	hypothetical protein
SAUSA300_1680	1.69	2.96	3.24	3.83	acetoin utilization protein AcuA
SAUSA300_0264	1.69	1.58	1.63	1.76	ribose transporter RbsU
SAUSA300_1086	1.64	1.44	1.51	4.17	hypothetical protein
SAUSA300_0210	1.59	2.19	2.09	2.78	maltose ABC transporter permease
SAUSA300_2513	1.58	1.48	1.21	2.51	hypothetical protein
SAUSA300_0907	1.55	3.46	3.17	2.31	GTP pyrophosphokinase
SAUSA300_1514	1.54	1.94	1.71	4.38	ferric uptake regulation protein
SAUSA300_2176	1.54	1.69	1.38	1.48	cobalt transporter ATP-binding subunit
SAUSA300_1288	1.53	1.92	1.73	1.77	dihydrodipicolinate synthase
SAUSA300_0369	1.52	1.73	1.59	2.44	hypothetical protein
SAUSA300_0728	1.50	4.29	2.71	5.04	hypothetical protein
SAUSA300_0920	1.47	2.97	3.20	3.84	hypothetical protein
SAUSA300_0147	1.44	1.57	1.14	1.26	5' nucleotidase family protein
SAUSA300_1944	1.44	2.13	1.59	2.54	phi77 ORF026-like protein phage transcriptional activator
SAUSA300_2517	1.39	1.13	1.11	1.22	amidohydrolase family protein
SAUSA300_1104	1.39	1.28	1.47	3.30	phosphopantothenate-cysteine ligase
SAUSA300_0825	1.38	2.13	1.34	3.40	2-nitropropane dioxygenase family oxidoreductase
SAUSA300_1021	1.38	2.25	2.04	1.08	hypothetical protein
SAUSA300_1192	1.33	4.16	3.33	5.04	glycerol kinase
SAUSA300_0767	1.33	2.38	3.26	2.87	hypothetical protein
SAUSA300_2339	1.28	1.34	1.10	1.26	hypothetical protein
SAUSA300_1193	1.28	2.50	1.59	4.62	aerobic glycerol-3-phosphate dehydrogenase
SAUSA300_0824	1.27	3.08	2.93	4.60	hypothetical protein
SAUSA300_1896	1.26	1.64	1.86	1.77	prephenate dehydratase

SAUSA300_1720	1.25	1.53	1.07	1.75	hypothetical protein
SAUSA300_1544	1.20	1.86	1.91	2.53	GTP-binding protein LepA
SAUSA300_1243	1.18	2.05	3.17	3.92	exonuclease SbcC
SAUSA300_1451	1.17	1.74	2.08	2.52	short chain dehydrogenase/reductase family oxidoreductase
SAUSA300_0700	1.17	1.99	1.73	3.12	hypothetical protein
SAUSA300_1618	1.14	3.11	1.84	1.78	hemA concentration negative effector hemX
SAUSA300_0839	1.13	3.95	3.06	2.01	hypothetical protein
SAUSA300_1187	1.13	2.72	2.09	2.15	hypothetical protein
SAUSA300_0553	1.11	2.39	1.69	2.24	hypothetical protein
SAUSA300_2292	1.10	1.32	1.16	1.78	isopentenyl pyrophosphate isomerase
SAUSA300_1519	1.09	2.78	2.70	3.12	hypothetical protein
SAUSA300_0630	1.07	2.39	2.42	3.66	ABC transporter ATP-binding protein
SAUSA300_1641	1.06	1.63	1.20	2.05	citrate synthase
SAUSA300_0381	1.05	2.98	1.32	4.19	putative NAD(P)H-flavin oxidoreductase
SAUSA300_2163	1.04	2.09	1.14	2.25	hypothetical protein
SAUSA300_1985	1.04	3.55	3.33	2.64	serine-aspartate repeat-containing protein SdrH
SAUSA300_2314	1.01	1.49	1.48	1.58	hypothetical protein

Table S6: Differential gene expression in vivo in S. aureus infecting mice immunised with alum vs mice immunised with PBS buffer

S. aureus Newman gene expression during infection of mice immunised with an alum adjuvant was compared with bacterial gene expression during infection of mic immunised with a placebo (PBS buffer). Genes found to be differentially expressed are listed below.

Locus Tag	*p*-value (adjusted)	Fold Change	Description
NWMN_0017	0.05	0.68	DNA-binding response regulator
NWMN_0023	0.01	0.39	ribosomal RNA large subunit methyltransferase H
NWMN_0055	0.00	0.20	peptidoglycan-binding protein LysM
NWMN_0061	0.04	2.16	ornithine cyclodeaminase
NWMN_0080	0.00	0.29	purine nucleoside phosphorylase
NWMN_0081	0.02	0.41	tetracycline resistance MFS efflux pump
NWMN_0082	0.02	0.42	2-deoxyribose-5-phosphate aldolase
NWMN_0083	0.00	0.30	phosphopentomutase
NWMN_0094	0.04	0.42	bifunctional acetaldehyde-CoA/alcohol dehydrogenase
NWMN_0103	0.04	2.35	capsular polysaccharide biosynthesis protein
NWMN_0104	0.05	2.07	capsular polysaccharide biosynthesis protein
NWMN_0105	0.01	2.80	capsular polysaccharide biosynthesis protein
NWMN_0112	0.05	1.80	hypothetical protein
NWMN_0125	0.03	0.45	hypothetical protein
NWMN_0133	0.03	0.48	PTS glucose EIICBA component
NWMN_0167	0.02	0.38	acetyl-CoA acetyltransferase
NWMN_0176	0.01	0.36	L-lactate dehydrogenase
NWMN_0177	0.00	0.42	PTS glucose transporter subunit IIB
NWMN_0196	0.01	0.34	antiholin-like protein LrgA
NWMN_0202	0.00	0.35	ribokinase
NWMN_0219	0.01	0.39	virulence factor EsxA
NWMN_0229	0.01	2.03	hypothetical protein
NWMN_0258	0.00	0.30	N-acetylmannosamine kinase
NWMN_0260	0.01	0.45	N-acetylmannosamine-6-phosphate 2-epimerase
NWMN_0322	0.00	0.23	PTS ascorbate transporter subunit IIC
NWMN_0323	0.05	0.36	PTS lactose transporter subunit IIB
NWMN_0324	0.02	0.33	PTS ascorbate transporter subunit IIA
NWMN_0325	0.00	0.28	hypothetical protein
NWMN_0357	0.00	0.43	30S ribosomal protein S6
NWMN_0359	0.00	0.35	30S ribosomal protein S18
NWMN_0366	0.04	0.44	membrane protein
NWMN_0371	0.00	0.41	alkyl hydroperoxide reductase subunit F
NWMN_0372	0.00	0.36	alkyl hydroperoxide reductase subunit C

NWMN_0395	0.02	2.70	hypothetical protein
NWMN_0396	0.01	2.38	hypothetical protein
NWMN_0429	0.00	0.23	N-acetylmuramoyl-L-alanine amidase
NWMN_0439	0.04	0.49	trehalose-6-phosphate hydrolase
NWMN_0443	0.02	0.50	hypothetical protein
NWMN_0467	0.05	1.63	stage V sporulation protein B
NWMN_0470	0.02	1.54	RNA-binding protein S1
NWMN_0489	0.00	2.13	membrane protein
NWMN_0507	0.02	0.41	30S ribosomal protein S12
NWMN_0522	0.05	2.00	FMN-dependent NADPH-azoreductase
NWMN_0551	0.02	0.65	phosphate acetyltransferase
NWMN_0570	0.01	3.12	hypothetical protein
NWMN_0584	0.02	1.77	alpha/beta hydrolase
NWMN_0596	0.04	1.85	cation:proton antiporter
NWMN_0623	0.03	0.46	membrane protein
NWMN_0628	0.02	1.95	DNA-binding response regulator
NWMN_0634	0.00	0.21	peptidase M23
NWMN_0665	0.01	0.39	hypothetical protein
NWMN_0669	0.04	0.50	PTS fructose transporter subunit IIC
NWMN_0671	0.04	1.73	hypothetical protein
NWMN_0703	0.04	2.18	iron ABC transporter permease
NWMN_0705	0.03	1.73	hypothetical protein
NWMN_0742	0.04	1.68	phosphoglycerate kinase
NWMN_0747	0.00	0.34	protein-export membrane protein SecG
NWMN_0761	0.00	0.50	cold-shock protein
NWMN_0765	0.00	4.06	hypothetical protein
NWMN_0778	0.02	2.62	topiosmerase
NWMN_0779	0.01	2.45	thioredoxin
NWMN_0787	0.02	0.53	cysteine desulfurase
NWMN_0853	0.00	0.44	3-oxoacyl-ACP synthase III
NWMN_0896	0.00	0.25	hypothetical protein
NWMN_0922	0.00	0.30	mannosyl-glycoprotein endo-beta-N-acetylglucosamidase
NWMN_0929	0.00	0.51	quinol oxidase subunit 1
NWMN_0930	0.02	0.60	quinol oxidase subunit 2
NWMN_0946	0.01	1.70	hypothetical protein
NWMN_0955	0.04	0.52	hypothetical protein
NWMN_0960	0.01	0.44	pyruvate dehydrogenase E1 component subunit beta
NWMN_0961	0.01	0.48	dihydrolipoyllysine-residue acetyltransferase component of pyruvate dehydrogenase complex
NWMN_0991	0.00	0.44	50S ribosomal protein L32
NWMN_1040	0.00	2.70	iron-regulated surface determinant protein B
NWMN_1043	0.02	2.60	hypothetical protein
NWMN_1044	0.05	2.28	heme uptake system protein IsdE

NWMN_1066	0.05	1.57	fibrinogen-binding protein
NWMN_1070	0.02	1.81	fibrinogen-binding protein
NWMN_1088	0.03	0.40	division/cell wall cluster transcript repressor MraZ
NWMN_1089	0.00	0.24	ribosomal RNA small subunit methyltransferase H
NWMN_1090	0.00	0.40	cell division protein FtsL
NWMN_1091	0.03	0.51	penicillin-binding protein
NWMN_1118	0.02	0.51	3-demethylubiquinone-9 3-methyltransferase
NWMN_1141	0.05	0.65	3-ketoacyl-ACP reductase
NWMN_1156	0.01	0.51	succinyl-CoA ligase subunit alpha
NWMN_1163	0.00	0.47	ATP-dependent protease subunit HslV
NWMN_1175	0.04	0.59	ribosome maturation factor RimP
NWMN_1182	0.01	0.53	30S ribosomal protein S15
NWMN_1207	0.04	0.50	glycerol transporter
NWMN_1251	0.00	0.51	LexA repressor
NWMN_1276	0.03	0.42	DNA repair protein MucB
NWMN_1298	0.01	2.79	phosphate ABC transporter permease
NWMN_1299	0.00	3.74	phosphate ABC transporter permease
NWMN_1300	0.00	4.55	phosphate-binding protein
NWMN_1327	0.01	2.03	two-component system sensor histidine kinase
NWMN_1328	0.05	1.81	DNA-binding response regulator
NWMN_1332	0.02	1.60	serine protease
NWMN_1352	0.02	0.47	sulfite reductase subunit alpha
NWMN_1382	0.00	0.32	DNA-binding protein HU
NWMN_1384	0.05	0.73	GTPase Der
NWMN_1414	0.01	0.44	oligo-1,6-glucosidase
NWMN_1475	0.01	0.50	iron transporter
NWMN_1476	0.05	0.55	hypothetical protein
NWMN_1485	0.03	2.17	HrcA family transcriptional regulator
NWMN_1504	0.00	2.83	hypothetical protein
NWMN_1505	0.02	2.35	iron transporter
NWMN_1547	0.02	0.48	50S ribosomal protein L27
NWMN_1549	0.02	0.50	50S ribosomal protein L21
NWMN_1564	0.01	0.61	porphobilinogen deaminase
NWMN_1566	0.02	0.60	glutamyl-tRNA reductase
NWMN_1572	0.00	0.52	50S ribosomal protein L20
NWMN_1573	0.01	0.52	50S ribosomal protein L35
NWMN_1574	0.05	0.65	translation initiation factor IF-3
NWMN_1582	0.04	1.76	formamidopyrimidine-DNA glycosylase
NWMN_1583	0.04	1.54	DNA polymerase I
NWMN_1585	0.01	2.49	sensor histidine kinase
NWMN_1613	0.02	0.57	30S ribosomal protein S4
NWMN_1650	0.02	0.46	hypothetical protein
NWMN_1689	0.01	0.42	hypothetical protein
NWMN_1710	0.05	2.04	hypothetical protein

NWMN_1730	0.01	0.46	hypothetical protein
NWMN_1831	0.00	0.30	non-heme ferritin
NWMN_1872	0.00	2.40	membrane protein
NWMN_1921	0.01	0.35	transcriptional regulator
NWMN_1940	0.00	0.41	hypothetical protein
NWMN_1971	0.03	1.83	serine-protein kinase RsbW
NWMN_1972	0.01	2.05	anti-sigma-B factor antagonist
NWMN_1979	0.05	2.50	hypothetical protein